Synthesis of Ruthenium and Rhodium Complexes for Their Use as Anti-Cancer Agents and Catalysts

Aida Maryam Binti Haji Basri

Submitted in accordance with the requirements for the degree of

Doctor of Philosophy

The University of Leeds

School of Chemistry

July 2014

The candidate confirms that the work submitted is her own and that appropriate credit has been given where reference has been made to the work of others.

This copy has been supplied on the understanding that it is copyright material and that no quotation from the thesis may be published without proper acknowledgement.

The right of Aida Maryam Binti Haji Basri to be identified as Author of this work has been asserted by her in accordance with the Copyright, Designs and Patents Act 1988.

Acknowledgements

In the name of Allah, the Most Gracious and the Most Merciful.
Alhamdulillah, all praises to Allah for the Strengths and His shower of Blessings.

I would like to thank Paddy McGowan for your huge support, guidance and advices all throughout the course. Thank you for believing in me, and giving me the confidence in my work, allowing me to develop many skills that I didn't think I would have. It has been a great pleasure to have you as my supervisor. I would also like to thank Roger Phillips and his group who has welcomed me to the ICT in Bradford, giving me the chance to handle the biological work on my own. Special thanks to Rianne Lord for the initial training in cell work and for being a great teacher to me both in chemistry and biology. My thank you also goes to Charlotte Willans and Mike Chapman from lab 1.32 for the GC and for the initial help in catalytic work.

To Chris Pask, who has never hesitated to spend his time in helping me with all my questions and problems, and the endless proof-readings, thank you so much! I would also like to thank Ian Blakeley, Simon Barrett and Tanya Marinko-Covell for sample analysis and data characterisation, and to Helena Shepherd for X-ray crystallography. Also, thank you to Jamie Gould for the help with powder diffraction data, and to Carlo Sambiagio for helping me throughout the catalytic work. A lot of thanks goes to everyone in the McGowan group, past and present members - Andrew, Steph, Felix, Andrea, Rianne, Carlo and Laura, who have made the lab a very enjoyable place, and to the Halcrow group - Jonathan, Laurence, Tom, Amedeo and Raf. Thank you also to Paddy McGowan, University of Leeds and Ministry of Education, Brunei Darussalam for the funding.

A special big thank you goes to my family in Brunei, especially to my beloved parents, who have never failed to support and encouraged me towards getting the degree. I love you! To "Bruleeds", I enjoyed every moment I have spent with all of you in the UK, and I hope to see you all in Brunei. Last but not least, I wish to thank Zaaim Jamahat, for always being there for me, especially in the last few months whilst I was writing up, despite the distance and the 7 hours of time difference. Thank you!

Abstract

This thesis is concerned with the synthesis and characterisation of a series of functionalised *bis*-picolinamide ruthenium and rhodium dihalide complexes that have the potential to be developed as anti-cancer agents and catalysts. Their structural characterisations and, anti-cancer and catalytic activities were explored and investigated.

There are more than thirty novel *bis*-picolinamide ruthenium dihalide complexes [RuX$_2$L$_2$] and six *bis*-picolinamide rhodium dihalide complexes [RhX$_2$L$_2$] (where X is chloride or iodide, and L is the functionalised bidentate picolinamide ligand) synthesised and fully characterised. X-ray crystallography showed the picolinamide ligands are bonded in *N,N-* and *N,O-* coordination modes to the metal centre. Three different geometries were seen for the dichloride complexes which were *cis-cis-cis, cis-trans-cis* and *trans-trans-trans*, whereas only the *trans* geometry was seen for the diiodide complexes. UV-Vis solution studies of the Ru complexes have shown no visible changes in the spectra over a range of days and temperature. Powder diffraction of Ru dichloride gave inconclusive data, however Ru diiodide complexes showed evidence of *trans* structural stability. As Ru(III) complexes are not amendable to study by NMR, Rh analogues were prepared to analyse their structural characterisation. The results have shown that there is a possible mixture of three different isomers within the Rh dichloride complexes, whereas the Rh diiodide only showed *trans* isomer, confirming that the diiodide complexes both for Ru and Rh are stable in structure conformations.

There has been much interest in developing new metal-based anti-cancer complexes since the successful discovery of cisplatin. Ru-based complexes have become one of the most promising groups of complexes, having cytotoxic properties but not significantly affecting normal healthy cells. *Bis*-picolinamide Ru dihalide complexes were tested against a variety of cancer cell lines to determine the cytotoxicity. It was found that the cytotoxicity increases when changing the halide ligands from dichloride

to diiodide, and when the substituents on the phenyl ring of the ligands are *meta* or *para* chloro or bromo substituents. Complexes **4.8** and **4.13** are the two most promising anti-cancer complexes, which are potent both under normoxic and hypoxic conditions. Following the cytotoxicity studies, selected complexes were examined for hydrolysis and hydrophobicity. The most cytotoxic Ru dichloride complex hydrolyses more and undergoes the fastest hydrolysis, which is in contrast with Ru diiodide complexes, by which the most cytotoxic complex undergoes the least hydrolysis. There are very few correlations observed between the cytotoxicity and log P values of the Ru dichloride complexes, suggesting that the cell uptake mechanism may not relate to their cytotoxic anti-cancer activities.

The ongoing research on catalytic transfer hydrogenation reaction is targeted towards metal catalysts that can favour high activity under mild operating conditions. Several *bis*-picolinamide Ru and Rh dihalide complexes were studied as catalysts in the reduction of benzaldehyde. The complexes that were selected for the studies have several components that can be used to investigate their structural-activity relationships. In general, the diiodide analogues of the catalysts are more active than the dichloride analogues. In combination of the dihalide ligands with the appropriate functionalised picolinamide ligands can improve their catalytic activities. There is a contrasting activity seen between Ru and Rh catalysts, whereby their catalytic activities are affected by different components of the catalysts. Ru catalyst may be largely affected by the different functionalised picolinamide ligands, whereas Rh catalysts have showed difference in activities when changing the X ligands.

Contents

List of Abbreviations

δ	Chemical Shift
η	Hapticity
μ_B	Bohr magneton
μ_{eff}	Effective magnetic moment
°C	Degrees Celsius
Å	Angstrom
A	Adenine
A2780	Human ovarian carcinoma cell line
A2780cis	Human ovarian carcinoma cisplatin resistant cell line
Ampy	Amidopyridine
ATH	Asymmetric transfer hydrogenation
Azpy	Azopyridine
bip	Biphenyl
bpy	Bipyridine
br.	Broad
$CDCl_3$	Deuteurated chloroform
CNS	Central Nervous System
COSY	Correlation Spectroscopy
Cp	Cyclopentadienyl
CTR1	Copper Transporter 1
d/dd/ddd/dtd	doublet/ doublet of doublets/ doublet of doublet of doublets/ doublet of triplet of doublets
Da	Dalton
dGMP	deoxyguanosine monophosphate
DHA	Dihydroanthracene
DMSO	Dimethylsulfoxide
DNA	Deoxyribonucleic acid
DPEN	Diphenylethylenediamine
dppf	1,1'-Bis(diphenylphosphino)ferrocene

en	Ethylenediamine
EPR	Electron paramagnetic resonance spectroscopy
ESI-MS	Electrospray ionisation mass spectrometry
et al.	"*et alia*", "and others"
Et_3N	Triethylamine
G	Guanine
GC	Gas Chromatography
HIF-1	Hypoxia-inducible factor 1 (HIF-1
HT-29	Human Colon Adenocarcinoma
IC_{50}	50% growth inhibition concentration
ICR	Imidazolium[*trans*-tetrachlorobis(imidazole)-ruthenate(III)
Impy	Imidazopyridine
in situ	on site
in vacuo	in vacuum
in vitro	in glass
in vivo	within the living
IPA	Isopropanol
IR	Infrared
J	coupling constant
K	Kelvin
Log P	Partition Coefficient
m	multiplet (for NMR), medium (for IR)
m/z	mass to charge ratio
MeOH/MeOD	Methanol/Deuteurated methanol
MTT	3-(4,5-dimethylthiazol-2-yl)-2,5-diphenyltetrazolium bromide
NADP	Nicotinamide adenine dinucleotide phosphate
NAMI-A	New Anti-Metastatic Inhibitor-A
NHC	N-heterocyclic carbene
NMR	Nuclear Magnetic Resonance
p	Probability
p-cym	*para*-Cymene

PBS	Phosphate Buffer Saline
ppm	parts per million
PXRD	Powder X-Ray Diffraction
Py	Pyridine
ROS	Reactive oxygen species
RPMI	Roswell Park Memorial Institute
SAR	Structural-Activity Relationship
t/td	triplet/ triplet of doublets
THF	Tetrahydrofuran
TLC	Thin Layer Chromatography
TPA	*Trans* platinum amino
TPZ	Tirapazamine
Trx-R	Thioredoxin Reductase
Ts	tosyl
Ts-DPEN	*N*-1,2-diphenylethylenediamine
s.u.s	standard uncertainties
s	singlet (for NMR), strong (for IR)
SRB	Sulforhodamine B
UV-Vis	Ultraviolet-visible
w	weak (for IR)

List of Publications

Z. Almodares, S. J. Lucas, B. D. Crossley, A. M. Basri, C. M. Pask, A. J. Hebden, R. M. Phillips, and P. C. McGowan, 'Rhodium, Iridium, and Ruthenium Half-Sandwich Picolinamide Complexes as Anticancer Agents', *Inorg. Chem.*, **2014**, 53, 727-736

A. Rodríguez-Bárzano, R. M. Lord, A. M. Basri, R. M. Phillips, A. J. Blacker and P. C. McGowan, **2014**, *Manuscript submitted*

S. J. Lucas, R. M. Lord, A. M. Basri, R. M. Phillips, A. J. Blacker and P. C. McGowan, **2014**, *Manuscript submitted*

A. M. Basri, F. D. Janeway, C. M. Pask, R. M. Phillips and P. C. McGowan, **2014**, *Manuscript submitted*

A. M. Basri, A. Rodriguez-Barzano, F. D. Janeway, S. J. Lucas, R. M. Phillips and P. C. McGowan, **2014**, *Manuscript in preparation*

CHAPTER 1

Introduction

1   Introduction

This chapter introduces various metal complexes as anti-cancer agents, including platinum, titanium, ruthenium and rhodium that have been found to be active against cancer cells. Cisplatin is the most successful anti-cancer drug, however there were several side effects found and modification of these complexes are required with the aim to have better anti-cancer activity and fewer side effects. Budotitane has successfully entered Phase I clinical trials, but has shown to undergo rapid dissociation and failed to progress to Phase II. NAMI-A and KP1019 are the two most promising ruthenium-based anti-cancer complexes with very low toxicities which are currently in the Phase II clinical trials. Previous works reported by Tocher *et al*, Sheldrick *et al*, Sadler *et al* and McGowan *et al*, on organometallic ruthenium anti-cancer complexes having bioactive ligands, and the coordination chemistry of ruthenium complexes and their ligands reported by Mestroni *et al*, Alessio *et al*, Keppler *et al*, Bhattachrya *et al*, Reedijk *et al* and McGowan *et al* are also discussed in this chapter.

1.1   Cancer

Cancer remains the main cause of mortality worldwide, according to the statistics of the World Health Organisation reported in February 2008.[1, 2] It is defined as a class of diseases in which cells undergo uncontrollable growth, leading to their ability to invade the surrounding normal healthy tissues. It develops mainly due to the growing adoption of unhealthy lifestyles.[3] Initiation and progression of cancer depends on both external factors in the environment (biological, physical and chemical carcinogens) and factors within the cell (hormones, immune conditions and genetic mutations).[4]

Cancer mortality can be decreased dramatically by early diagnosis and providing effective treatments. These cells are less likely to spread to other normal tissue regions if detected at an earlier stage, and so the more favourable the diagnosis for the individual. Surgical removal of the original cancer cell may not always be a successful treatment as microscopic spread can occur.[5] If these cancer cells are left untreated, these will result in localised recurrence of the cancer and eventually spread to the healthy living cells in the body (metastasis). Research is constantly

ongoing in order to develop treatments against different types of cancer of different stages.

1.2 Metal complexes as Anti-Cancer Agents

For years, metals have had a very important role in medicine. They are classified into two forms, which can either be a nutrient that is essential for maintaining a healthy life, or simply toxic. Even though metals can appear to be toxic at minimal dosage levels, they may not be equally dangerous for all organisms at all levels.[6] They can be used as invaluable diagnostic tools in the medical profession, which uses a variety of radioactive element techniques to discover the inner structures of the human body without the need for invasive procedures. It has also been proven that toxic metal complexes can kill tumours at certain body locations.

Cisplatin, which contains platinum, is one of the many exciting and valuable drugs found from research into metals for therapeutic agents.[7-10] Other metal-based medicines include silvadene, a silver-based drug that has antimicrobial properties,[11-13] and the iron complex sodium nitroprusside which is used as a cardiovascular drug (**Figure 1.1**).[14] These metal-based drugs have been successfully developed and more studies are performed to design new metal-based drugs from different complexes that could lead to a wide range of therapeutic applications.

Cisplatin   Sodium nitroprusside

Silvadene
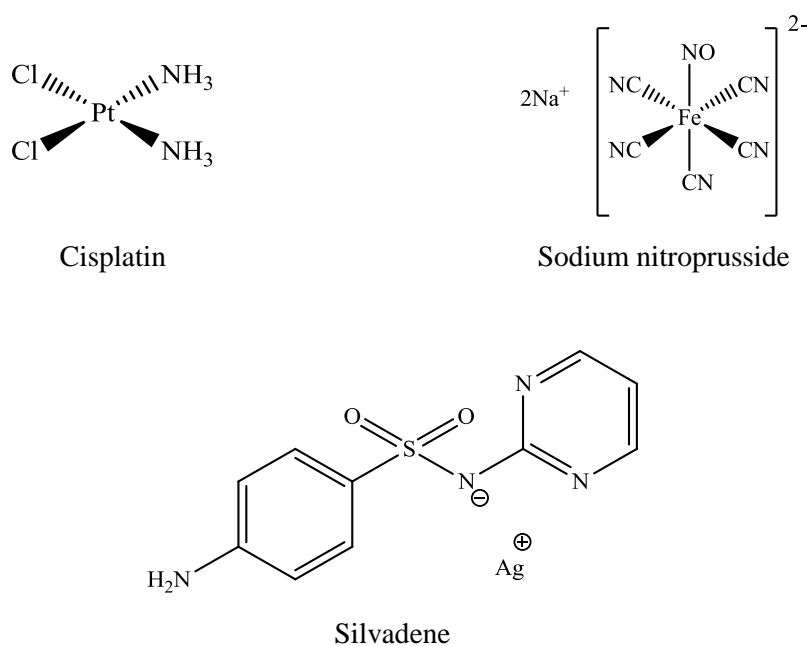
Figure 1.1 Examples of successfully developed metal-based medicines

The search of metal-based complexes which are active towards cancer cells with mild toxicity and fewer side-effects, are still developing. Cisplatin has been used for the treatment of various cancers. The ruthenium-based complex, NAMI-A, has successfully finished Phase I clinical trial and is currently in Phase II clinical trial.[15] The titanium-based complex, budotitane, failed to progress further due to its rapid dissociation upon interaction with water molecules. These complexes are discussed further in detail.

1.3   Platinum-based anti-cancer complexes

Cisplatin or *cis*-diamminedichloroplatinum(II) is a platinum-based anti-cancer complex which continues to be the most successful drug used for the treatment of several cancers, including testicular, ovarian, bladder, cervical, head and neck and small-cell lung cancers, either as a first-line treatment or in combination with other anti-cancer drugs. The anti-cancer activity of cisplatin was discovered in 1965 by Rosenberg when it was found to inhibit bacterial cell division from the effect of an electromagnetic field.[16] It was the first metal-based drug to enter clinical trials in 1971 after its anti-cancer activity was demonstrated in a mouse model, and was approved by the Food and Drug Administration for use as an anti-cancer drug in 1978.

Cisplatin is a neutral complex which has square planar coordination geometry. The *cis* configuration is responsible for its anti-cancer activity. It has two amine ligands which are inert to substitution under biological conditions, and two labile *cis* chloride groups which undergo hydrolysis in the cells resulting in a positively charged complex. **Scheme 1.1** shows the chemical structure of cisplatin and its hydrolysis.[17-23]
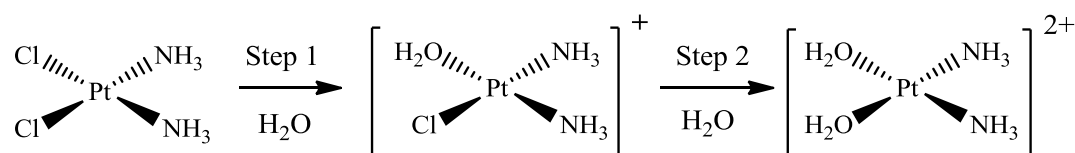
Scheme 1.1 *Structure of cisplatin and its mechanism of hydrolysis in the cell*

Blood plasma, having a high chloride concentration (~100mM), prevents the hydrolysis of cisplatin until it enters the cell by either passive diffusion[24] or a copper transporter CTR1.[25, 26] The very low chloride concentration in the cells (~3mM) facilitates the hydrolysis of cisplatin, making it an active electrophile which then reacts with the nucleophilic sites in the cell, where DNA is the most preferential and cytotoxic target.[10] Electrostatic attraction and covalent bonding of the positively charged complex to DNA, specifically the N7 atoms of the imidazole rings of guanine and adenine bases (**Figure 1.2**) are believed to be its mechanism of action.[27]
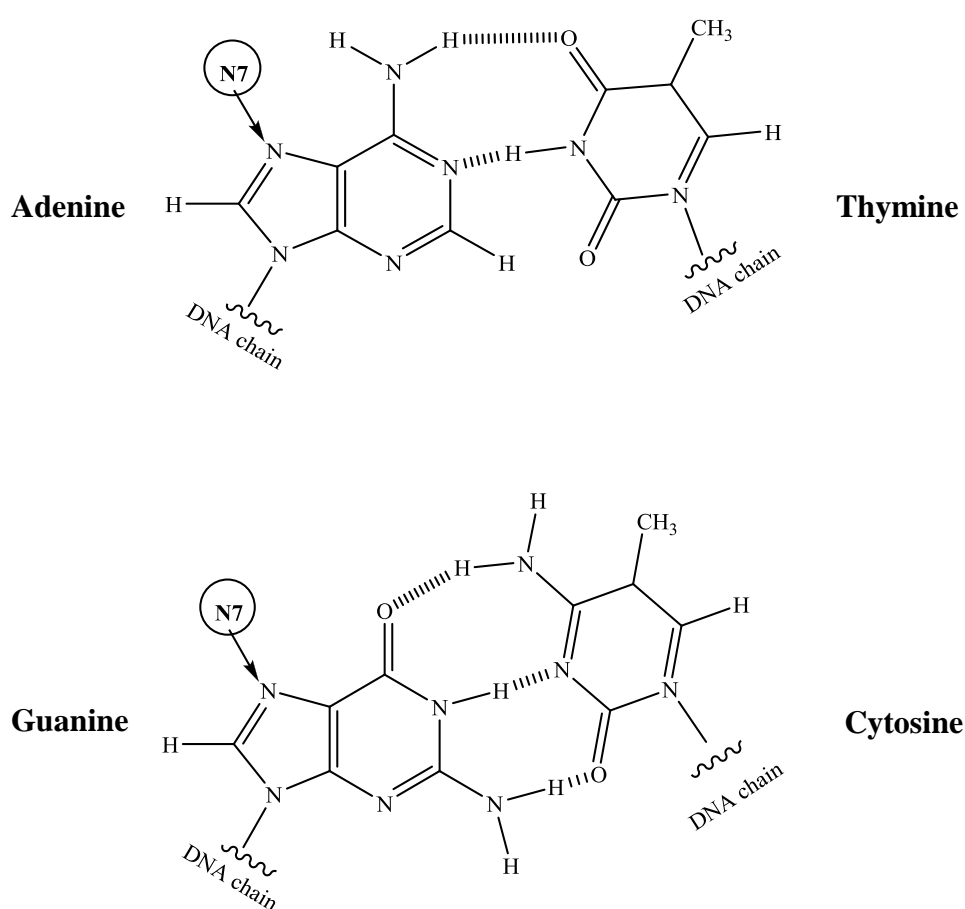
Figure 1.2 *Cisplatin coordinates to the N7 atoms of the imidazole rings of guanine and adenine DNA bases* [28]

There are three different types of aquated cisplatin crosslinking to DNA (**Figure 1.3**).[29] DNA monoadducts are formed when one molecule of water is lost from the aquated cisplatin, which then tends to react and form crosslinks. Intrastrand crosslinks are formed when two chloride ligands of the aquated cisplatin are replaced by purine nitrogen atoms on adjacent bases of the same DNA strand. These crosslinks are referred to as 1,2-d(GpG) crosslinks and almost all cisplatin DNA crosslinks are of this type.[30-33] Additional DNA crosslinks include the interstrand crosslinks. All cisplatin crosslinks to DNA lead to the disruption of its helical structure that cannot be identified by repair enzymes, hence trigger a series of events leading to the inhibition of DNA replication[34, 35] which is responsible for the anti-cancer activity of cisplatin.
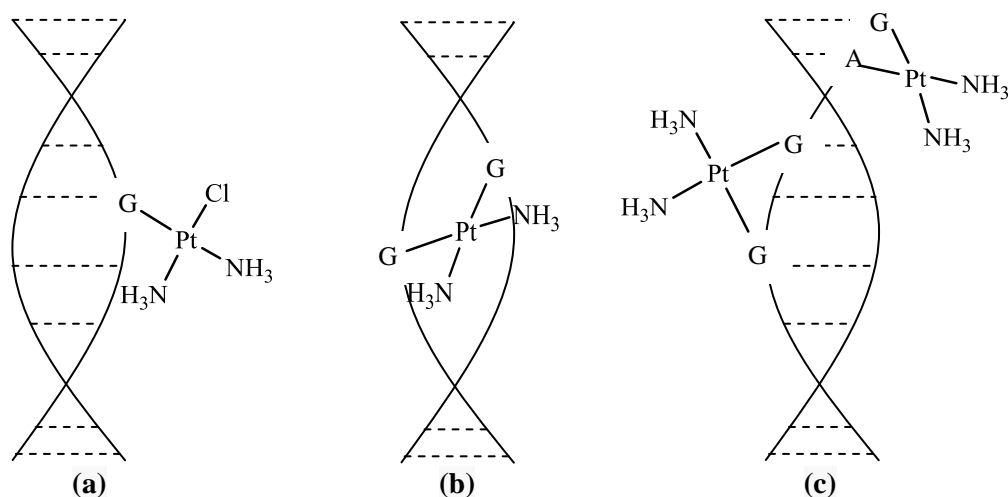
Figure 1.3 Cisplatin-DNA crosslinking. (a) DNA monoadducts; (b) Intrastrand crosslinks; (c) Interstrand crosslinks [29]

Since only a small fraction, approximately 1% of intracellular cisplatin is bound to DNA,[36, 37] much research has been carried out, and is still ongoing, into the mechanism of action of cisplatin in killing cancer cells. Another study has revealed that cisplatin prevents tubulin to form microtubules, leading to the blocking of cell division in living cells and eventually, cell apoptosis.[38] Despite the success of cisplatin towards the death of cancer cells, cancer treatment with cisplatin is associated with toxicities ranging from mild to severe adverse effects such as nephrotoxicity and ototoxicity. It has also been shown that cancer cells are able to develop resistance towards cisplatin through changes in the cell environment.[39-42]

These include drug transport that leads to a decrease of intracellular cisplatin accumulation, an increase in drug detoxification systems, an increase in DNA repair system, changes in tolerance mechanisms from damage of DNA and changes in cell death pathways to apoptosis.

Due to the drawbacks, a second generation of platinum-based anti-cancer agents was introduced (**Figure 1.4**). Carboplatin [*cis*-diammine-1,1-cyclobutane dicarboxylate platinum(ll)] was first introduced into the clinic in 1989 [43, 44] and used for the treatment of advanced ovarian cancer in combination with other approved chemotherapeutic agents.[45-47] The two chloride leaving groups of cisplatin are replaced by a bidentate dicarboxylate ligand, which leads to less side effects and less toxicity, being more lipophilic when compared with cisplatin.

(a)   (b)
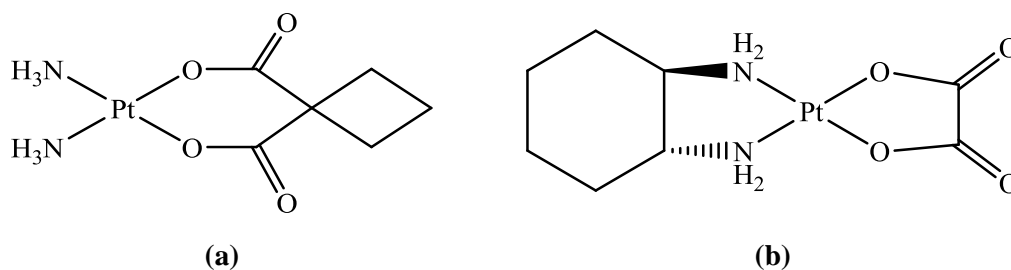
Figure 1.4 Second generation platinum-based anti-cancer agents (a) carboplatin (b) oxaliplatin

Carboplatin reacts with DNA in a similar way to cisplatin. It undergoes hydrolysis and forms adducts with DNA.[48] The difference between the activity of the drugs is the variation in their aquation rates to release the active Pt(II) that contributes to cancer cell death.[49] A study has also been presented that carbonate may play an important role in the activation of carboplatin to produce platinum-carbonato and – hydroxo complexes.[50] **Scheme 1.2** shows the reaction of carboplatin with carbonate.
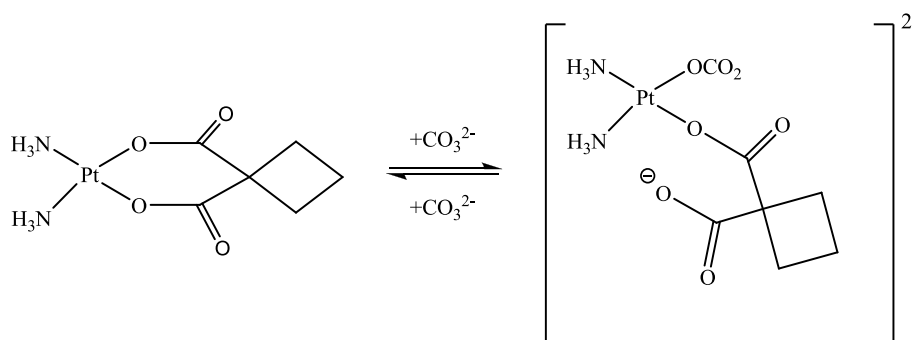
Scheme 1.2 Reaction of carboplatin with carbonate ions

Oxaliplatin was first synthesised in the late 1970s and is the third successful derivative of platinum based anti-cancer drugs and entered the clinic in 1994.[51, 52] It has an oxalate ligand which hydrolyses, and diaminocyclohexane (DACH) as the inert ligand. The mechanism of action is similar to cisplatin and carboplatin, by undergoing hydrolysis and forming crosslinks with guanine or adenine bases of DNA. Oxaliplatin has the potential to treat cisplatin-resistant cancer cells and is also active against colorectal cancer cells for which it is now used for treatment in combination with 5-fluorouracil.[53] It has been tested against ovarian cancer cell lines, and was found to be more potent than cisplatin, in which the fewer DNA adducts by oxaliplatin induce early secondary DNA strand breaks and huge apoptosis of cancer cells.[54] The difference that occurs with oxalipatin when compared to cisplatin and carboplatin is rather the effect that the drug gives rather than the mechanism of action. Oxaliplatin gives lower toxicity and has shown the absence of nephrotoxicity and a decrease in ototoxicity, which were present in treatments with cisplatin and carboplatin against cancer cells.

1.4   Titanium-based anti-cancer complexes

The titanium (IV) complex, *cis*-[(CH$_3$CH$_2$O)$_2$(bzac)$_2$Ti(IV)] (Budotitane), as shown in **Figure 1.5**, was the first non-platinum complex that entered clinical trials after it has shown promising anti-cancer activity *in vivo* on three different transplantable tumour systems, which are the transplantable murine ascitic-colorectal MAC 15A, the TD-osteosarcoma of the rat, and the intramuscularly transplanted murine sarcoma 180.[55-57]
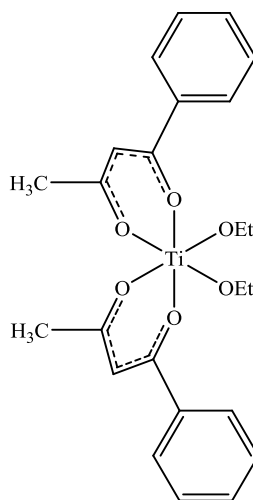
Figure 1.5 Budotitane

Budotitane undergoes hydrolysis in a similar manner to cisplatin. However, there were problems with the complex displaying low solubility and stability in aqueous solution. It hydrolyses greatly in water at pH > 5 to form oligomeric $[Ti(bzac)_2O]_2$ which is insoluble, leading to toxicities affecting the liver and kidneys.[58]

The interest in non-platinum complexes was limited and was not explored in detail until 1979, when titanocene dichloride, (Cp_2TiCl_2) was discovered to have anti-cancer activity with no evidence of nephrotoxicity.[59] This has stimulated the interest in investigating various non-platinum complexes that have different mechanisms of action against cancer cells. Metallocenes of the general formula, Cp_2MX_2, where Cp = cyclopentadienyl anion, M = Ti, V, Nb, Mo, and X = halides and pseudo-halides, have been synthesised and investigated to determine their anti-cancer activities. **Figure 1.6** shows the structure of titanocene dichloride. This complex has shown lower toxicity than cisplatin, and was the most active metallocene complex to enter Phase I and Phase II clinical trials.[60, 61]
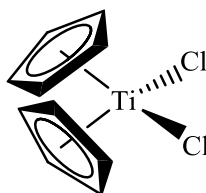
Figure 1.6 Titanocene dichloride

Studies to understand the mechanism of action of titanocene dichloride are still ongoing, with initial studies showing that it undergoes hydrolysis[62] and binds with DNA to form adducts. **Scheme 1.3** shows the three-step reaction for hydrolysis of titanocene dichloride, and studies have shown that the rate of the first hydrolysis is faster than that of the second hydrolysis.[63] Hydrolysis is the activation process before it interacts with DNA, where the chloride ligands dissociate rapidly and are replaced by water molecules forming aqua and hydroxy-titanocene complexes. These complexes are then able to develop titanium-rich compounds during further reaction steps.[63]
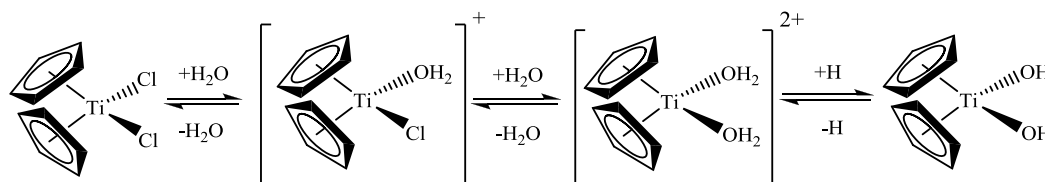
Scheme 1.3 Hydrolysis of Titanocene Dichloride

More recent investigations of titanocene dichloride with DNA have indicated that hydrogen-bond donors of aquated titanocene complexes play an important role in forming stable complexes by interacting with hydrogen-bond acceptors of purine N7 bases or O6 phosphate group, with the latter being the preferred binding site.[64] These interactions are shown in **Figure 1.7**. Titanocene dichloride has anti-proliferative activity against various cell lines *in vitro*, and has shown anti-cancer activity against ovarian cancer cells which are resistant to cisplatin. However, after spending many years in clinical trials, titanocene dichloride was dismissed and its trials were not pursued. It failed to show enough promising results against renal and breast cancer in Phase II clinical trials.[65, 66] There was no response detected for anti-cancer activity with the given dose, and since its mechanistic details are poorly understood, this also impedes its use as an anti-cancer agent.
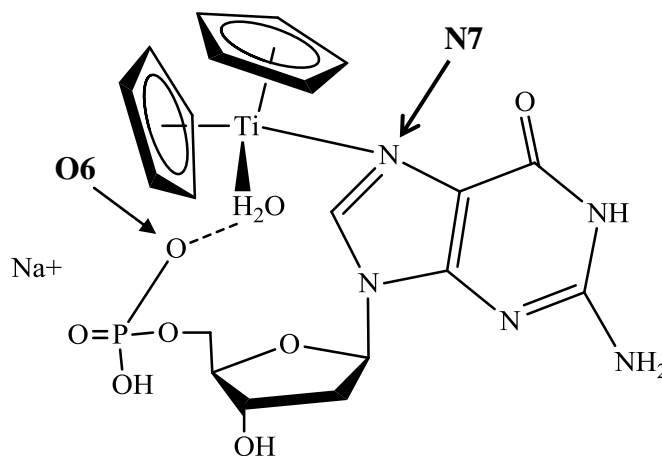
Figure 1.7 The interaction of aquated titanocene complexes with purine N7 and O6 phosphate group of DNA

Despite the failure of titanocene dichloride in the clinical trials, many papers are still published on the mechanism of action and have given a lot of interest to the scientific community. Various modifications of the complex have been synthesised and characterised, in order to improve future novel anti-cancer complexes. Careful selection of groups to functionalise Cp ligands and replacing chloride with hydrophilic ligands are very important for the stability and solubility of these complexes. **Figure 1.8** shows examples of titanium derivatives with functionalised ligands.

R = *o,p*-F, *o,p*-Cl, *o,p*-Br, *p*-NO$_2$

(a)   **(b)**
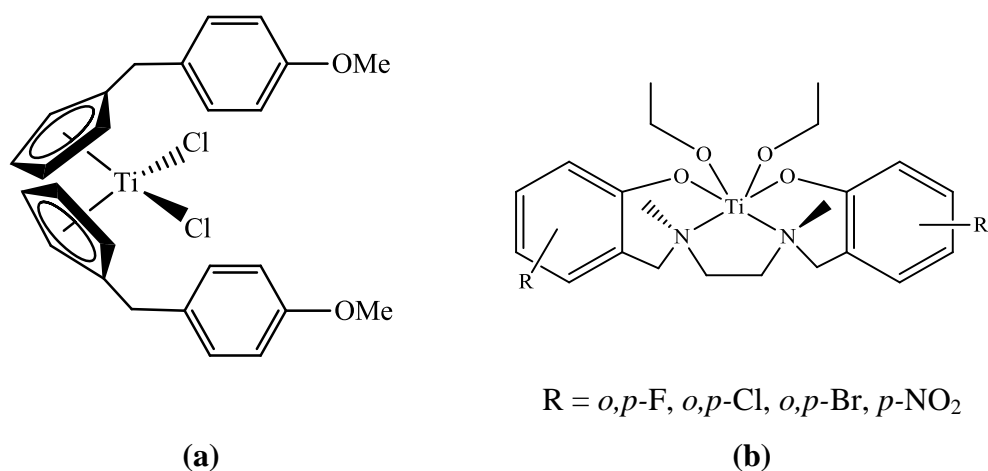
Figure 1.8 Examples of titanium derivatives (a) Titanocene Y; (b) salan-Ti(IV)

Ansa-titanocene dichloride complexes were first synthesised in 1970 as catalysts for olefin polymerisation.[67] It is thought that the C2 bridge between the two Cp groups increase the hydrolytic stability of the complex, and the introduction of two dimethylamino substituents increase the water solubility when compared to titanocene dichloride itself. These complexes were tested on Ehrlich ascites tumours (EAT) in mice and results have shown that they have restored natural killer cell function in mice that prevents the cancer cells from growing thus extending life.[68, 69]

New titanium derivatives have been introduced recently, having [ONNO]-type diamine *bis*(phenolato) salan ligands, where salan = *N,N'-bis*(o-hydroxybenzyl)-1,2-diaminoethane. Salan-Ti(IV) complexes have demonstrated higher hydrolytic stability having hydrolytic half lives in the range of hours,[70, 71] and higher anti-cancer activity towards breast and colon cancer cells *in vitro* and *in vivo*.[69, 72]

Salan-Ti(IV) complexes with halogens on the aromatic rings have been found to be the most promising subgroup, having low IC_{50} values.[73] However, the mechanism of action and cell uptake of these salan-Ti(IV) complexes are not yet well known. Within the McGowan group, much research has focused on functionalised cyclopentadienyl complexes. The Cp rings in these complexes are functionalised with an amino pendant arm that could make the complex become more water soluble and more stable. **Figure 1.9** shows the structure of a functionalised-Cp titanocene dibromide that has been synthesised and characterised. Their cytotoxic properties have shown that they have significantly better activity and stability than non-functionalised counterparts, and have exhibited anti-cancer properties against cisplatin-resistant ovarian cancer cell lines.[74]
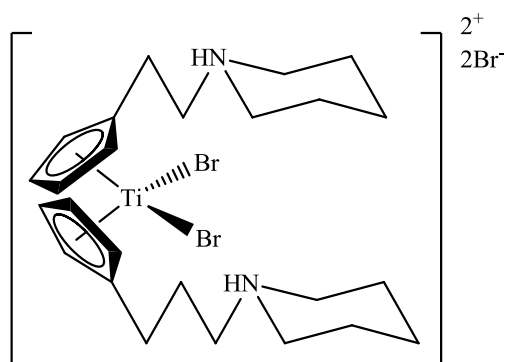
Figure 1.9 *Example of a titanocene derivative functionalised-Cp titanocene dibromide*

1.5   Ruthenium-based anti-cancer complexes

Various metal complexes have been synthesised and tested for cytotoxicity in the search for new metal-based anti-cancer agents with high cytotoxic properties. Among all complexes, ruthenium-based complexes have become one of the most promising groups of complexes, having cytotoxic properties but not significantly affecting normal healthy cells. As illustrated in **Figure 1.10**, ruthenium-based agents appear especially attractive because they exhibit three important properties suitable to biological applications: (1) Ligand exchange, (2) Accessible oxidation states and (3) Iron mimicking.[75]
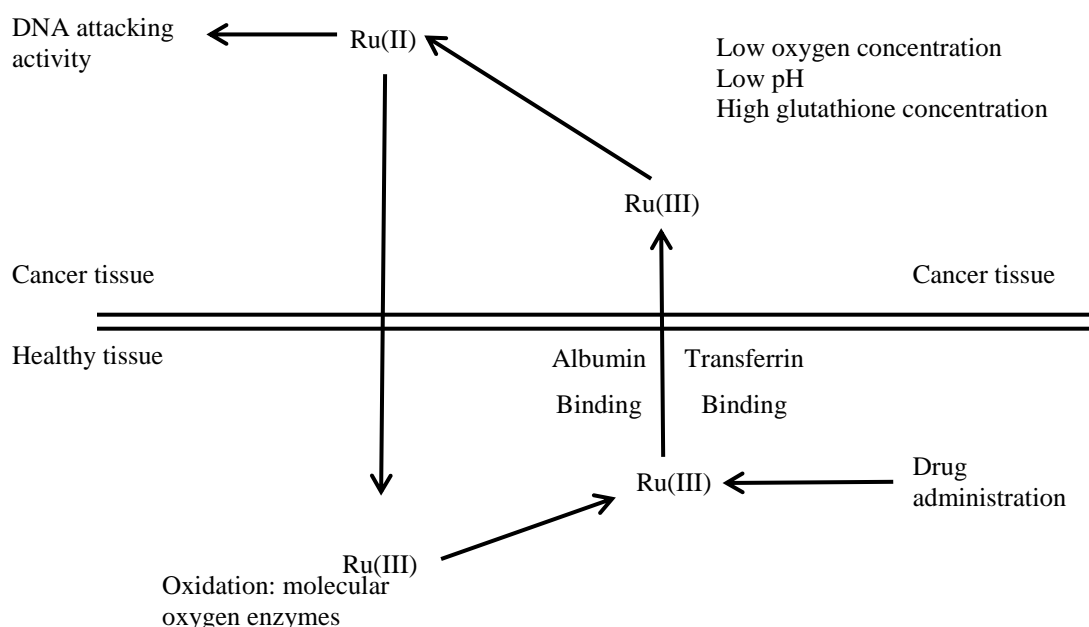
Figure 1.10 *"Activation by reduction" hypothesis of Ru(II)/Ru(III) complexes, adapted from "Ruthenium in Medicine: Current Clinical Uses and Future Prospects"* [75]

(1) Ligand Exchange

Ligand exchange is important to determine the biological activity of a drug. Most metal-based drugs are able to reach their biological target after being modified. Ru(II)/Ru(III) complexes have similar rate of ligand exchange as those Pt(II) complexes, which takes hours at ambient temperature. Ligand exchange rate is dependent on the concentration of the ligand exchange in surrounding solution. Due to this, the drug's activity can be affected as diseases are able to change the concentrations in cells.

(2) Accessible oxidation states

Ru(Il), Ru(III) and Ru(IV) are all accessible under physiological conditions. Ru(III) complexes are biologically inert compared to Ru(II) and (IV) complexes. By varying the ligands in the complexes, the redox potential of a complex is modifiable. Prodrugs which are relatively inert Ru(III) complexes may be administered and then reduced, hence activated, in diseased tissues. Cancer cells are known to have higher metabolic rate, higher levels of glutathione and a lower pH than healthy normal tissues, creating a strongly reducing environment in which Ru(II) is favoured over Ru(III). Ru(II) is more available for binding to cellular components than Ru(III), which gives the advantage of potential drugs to be administered in a +3 oxidation state and reduced *in vivo* to a +2 oxidation state. When the biologically active Ru(II) complexes leave an oxygen poor environment, they can be converted back by biological oxidants to inert Ru(III) complexes. This is called the "activation by reduction" hypothesis, where Ru(III) complexes are basically prodrugs that are activated by reduction when entering cancer cells.

(3) Iron mimicking

Ruthenium has the ability to mimic iron in binding to albumin and transferrin, which are the two iron-carriers that reduce toxicity of ruthenium.[76] Cancer cells are rapidly dividing cells having an increase number in transferrin receptors, and therefore a high requirement for iron molecules. This allows the ruthenium complexes to mimic iron and target cancer cells specifically, which explains the reason of its low toxicity, as the drug targets cancer cells rather than healthy cells.[77, 78] Also, the ability of the cells to release the excess ruthenium is thought to be another reason for their lower toxicity when compared to platinum-based complexes.[78, 79]

Complexation of ruthenium with different ligands has been of much interest in recent years. This is due to its properties of being able to reduce and oxidise, as well as its photophysical and photochemical properties. These properties are directed by the different coordination environment around the central metal ion.[80] In general, ruthenium complexes are well suited for pharmaceutical applications.[81-83] Ruthenium complexes with varying oxidation states have recently displayed good anti-cancer activity and have exhibited remarkably low toxicity compared to cisplatin and its derivatives.

1.5.1 NAMI-A

[Na]*trans*-[RuCl$_4$(Im)(dmso-S)] (NAMI) was first synthesised and found to be active against solid metastasising tumours in mice.[84] At a later stage in pre-clinical experiments, its Na salt was replaced with imidazolium salt, to avoid co-precipitation of DMSO with Na$^+$ during the last phase of complexation.[85]
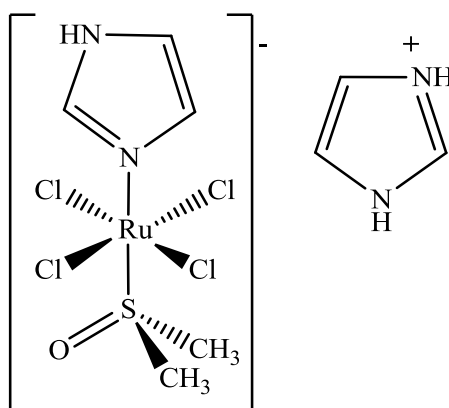
Figure 1.11 NAMI-A

[ImH]*trans*-[RuCl$_4$(Im)(dmso-S)] (NAMI-A) (**Figure 1.11**) has an increased stability towards air oxidation compared to NAMI. It is the most promising ruthenium-based anti-cancer complex and was the first to successfully finish Phase 1 clinical trials. It was found to be inactive against primary cancer cell lines, however, it has the same anti-metastatic properties as NAMI and is more stable towards air oxidation. It has shown a reduction in the formation of lung metastasis of malignant tumours,[86] however, this did not show a relation with the cytotoxicity against tumour cells, which has been suggested that extracellular activity might be involved.

The mechanism of action for NAMI-A is thought to be unique compared to that of platinum-based complexes. It shows several features that might be related for its activity in inhibiting *in vivo* metastases. These include the involvement of biological activities that influence cell functions in cancer cells. NAMI-A interacts rapidly with targets at cell membrane and triggers integrin activation, actin nucleation and microfilament elongation, which relate to adhesion in cancer cells.[87] An important contribution is also caused by the decrease in angiogenic activity, which is an important process involved in metastasis. This has been shown in an

experiment with CAM (Chorio Allantoic Membrane) model that inhibits a number of *in vitro* endothelial cell functions.[88]

In NAMI-A the DMSO ligand, bound through sulfur, is a reasonable π-acceptor and stabilises Ru(II). It also influences its chemical behaviour in aqueous solution, where it undergoes two well-separated steps of hydrolysis, as shown in **Scheme 1.4**. Inert NAMI-A is administered by infusion, which gives a reactive aqua complex in slightly acidic environment by suppressing the hydrolysis of Cl⁻ and slowly dissociating DMSO.[89] At physiological pH, biological reducing agents such as glutathione, reduce NAMI-A to dianionic Ru(II) species (NAMI-AR), which then undergoes a two-step chloride hydrolysis. However, the "activation by reduction" hypothesis is not necessary for NAMI-A. Instead, the anti-metastatic activity of NAMI-A is strictly related to the presence of the DMSO ligand.[90]
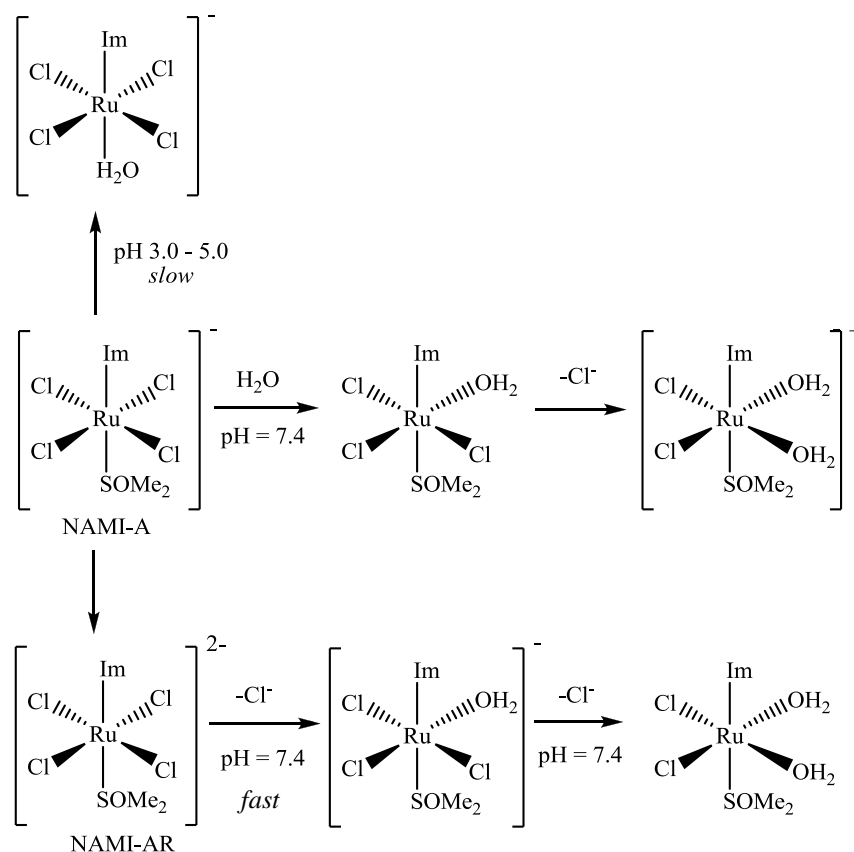
Scheme 1.4 Chemical behaviour of NAMI-A under various conditions

The mechanisms of action of NAMI-A are not fully understood yet, but, aquation is thought to be an important step for it to function, by forming a reactive aqua species *in vivo* that enables it to bind with biomolecules. In a very recent study, the behaviour of NAMI-A, specifically its ligand-exchange processes with human serum albumin (hsA) was investigated using electron paramagnetic resonance spectroscopy (EPR).[91] NAMI-A was found to bind rapidly with the protein side chains, possibly the imidazole ring of histidine, *via* hydrophobic interactions. **Scheme 1.5** shows the main NAMI-A ligand-exchange processes in hsA, which involves the binding of NAMI-A to three distinct proteins following aquated NAMI-A complexes.
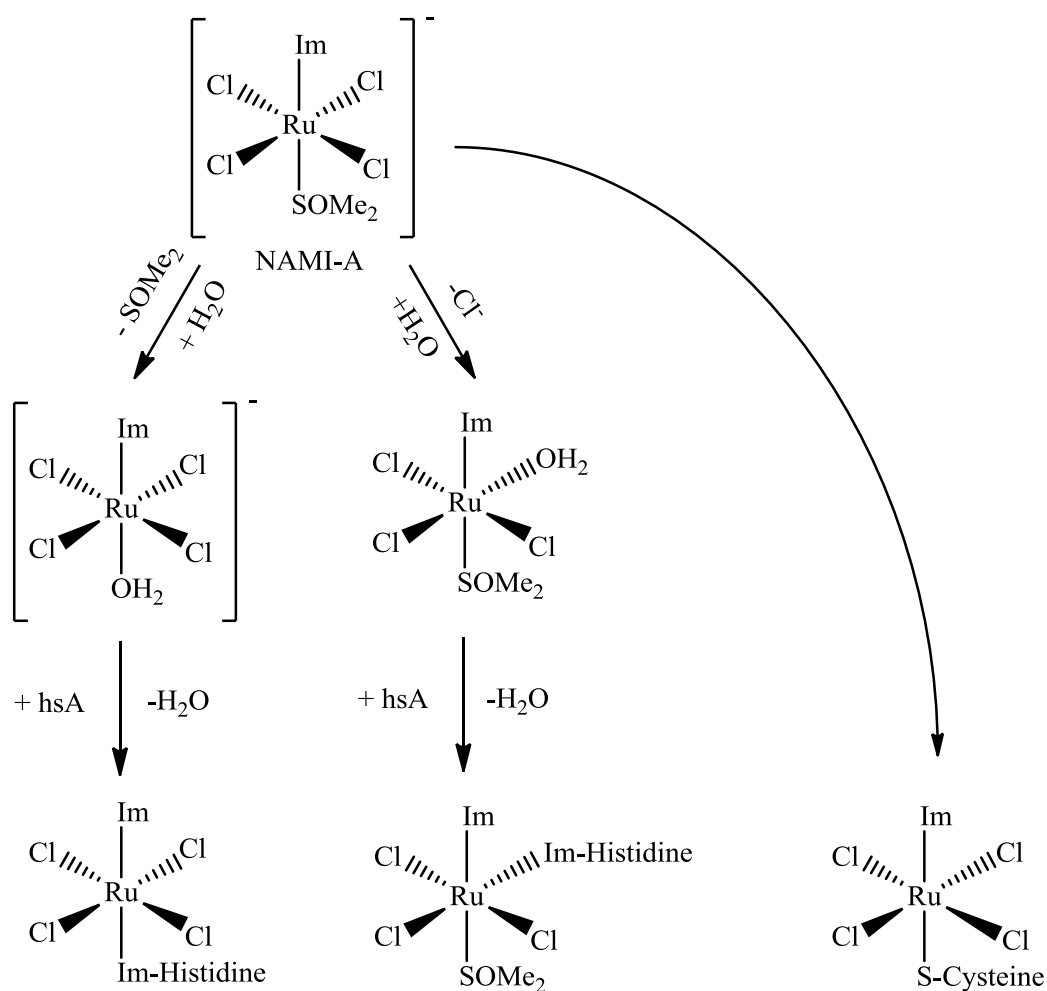
***Scheme 1.5** Aqua NAMI-A complexes binding with protein Histidine and Cysteine*

As DNA is thought to be the primary target for cisplatin, a study on NAMI-A and its interaction with DNA has been carried out.[10] DNA was found not to be the only target for its anti-metastatic activity, but it is likely to interact with DNA once it enters the cancer cells. This has been proven *in vitro* when at equal concentrations of both NAMI-A and cisplatin, the number of Ru-GG and –AG DNA adducts is much lower than cisplatin.[15] The reactive aqua complex formed from hydrolysis of NAMI-A in lower pH subsequently binds to DNA.[92] However, other targets such as plasma proteins and glutathione are thought to be more important than DNA for their anti-cancer activities.

NAMI-A metabolites are released rapidly from cells which is responsible for its low and reversible side effects on kidneys, where high concentration of ruthenium was found, suggesting the main pathway of ruthenium excretion.[93] NAMI-A complexes have been shown to exhibit low cytotoxicity and has efficacy against metastatic tumours and is potentially a very promising drug for clinic use.

1.5.2   KP1019 and ICR

KP1019, indazolium[*trans*-tetrachlorobis(indazole)-ruthenate(III)] is a heterocyclic ruthenium (III) complex, developed by Keppler *et al.*,[94] which contains an octahedral ruthenium (III) centre bound to two indazole ligands trans to each other and four chlorides completing the coordination sphere. The structure is shown in **Figure 1.12**. It has exhibited anti-cancer activity against a wide range of cancer cell lines including colorectal carcinomas, and has been shown to have lower toxicity than other ruthenium-based anti-cancer complexes.
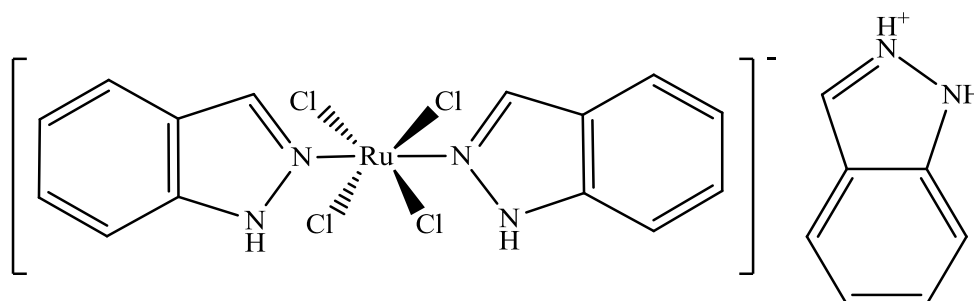
Figure 1.12 KP1019

Many studies have been performed to investigate its mechanism of action and structural-activity relationships. It is thought to have a high binding affinity to

plasma protein transferrin, which transports iron into cells. Since cancer cells have a high requirement for iron and contain a huge number of transferrin receptors, they tend to bind and transport Ru(III) complexes into cells.[76] This increases their concentration in cancer cells giving a higher chance for them to function as anti-cancer complexes. Once Ru(III) enters the cell, the complexes are activated by reduction to Ru(II), due to the hypoxic environment in cancer cells, and then undergoes hydrolysis. The kinetic rates for hydrolysis of KP1019 are highly dependent on pH and the temperature of solution.[95] They hydrolyse by dissociating a chloride to give reactive aqua complexes which show high affinity binding to N7 donor atoms present in DNA bases. A study has also demonstrated that the cytotoxic effects of KP1019 are induced by oxidative stress forming H_2O_2 which can react with macromolecules including DNA and induce oxidation of bases, promutagenic adducts and strand breaks triggering apoptosis.[96]

Initially, KP1019 demonstrated promising anti-cancer activity with limited side effects and lower toxicity in Phase I clinical trials. The ruthenium complex did not cause any serious side effects but showed disease stabilisation up to 10 weeks.[97] It was given as flat dose to patients starting from 25 mg/patient, however, has stopped dose escalation at 600 mg/patient because of drug solubility problems.[98] Due to this, KP1339, the sodium salt of KP1019, with higher water solubility was selected as a lead candidate for further development in the clinical trial.[99] Generally, KP1019 is more potent than KP1339, however studies have shown that both Ru(III) drugs share similar mode of action.[100]

ICR, imidazolium[*trans*-tetrachlorobis(imidazole)-ruthenate(III)] is an imidazole analogue of KP1019, whose structure is shown in **Figure 1.13**. It has a similar structure to NAMI-A and has shown promising anti-cancer activity against various cancer cell lines. Similar to cisplatin, ICR undergo hydrolysis, reacts and binds to DNA bases. However, a study of the interaction between ICR and DNA has shown that freshly prepared solutions of ICR did not show the binding of ICR with DNA, but it did show ICR-DNA binding in aged ICR solutions.[101] This indicates that the Ru(III) complex acts as a prodrug and undergoes intracellular hydrolysis to form the active aqua Ru(II) complex for activation. Similar to KP1019, ICR is also

thought to enter cancer cells by binding with transferrin. The mechanism of action is however still unknown.
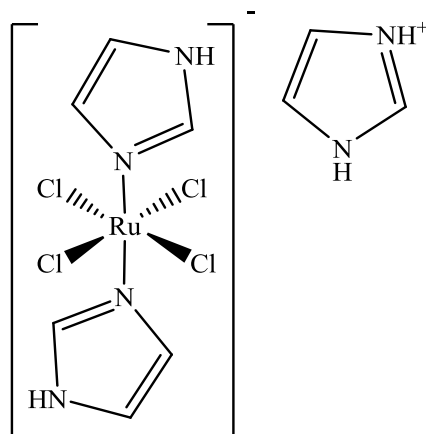
Figure 1.13 *Structure of ICR*

ICR is one of the most active complexes with improved water solubility. The aquation rate constant of ICR was found to be slightly lower than that of cisplatin. ICR undergoes hydrolysis and loses Cl⁻, giving different hydrolysis products depending on the conditions. The hydrolysis pathway of ICR is shown in **Scheme 1.6**. At pH 6-8, the first aquation step involves a rapid deprotonation and hydrolysis of a *trans* Cl⁻ ligand that happens during the transport process in blood. The lower concentration of chloride ions in the cell causes the following aquation to occur, and will produce reactive aqua complexes that can then bind to DNA.
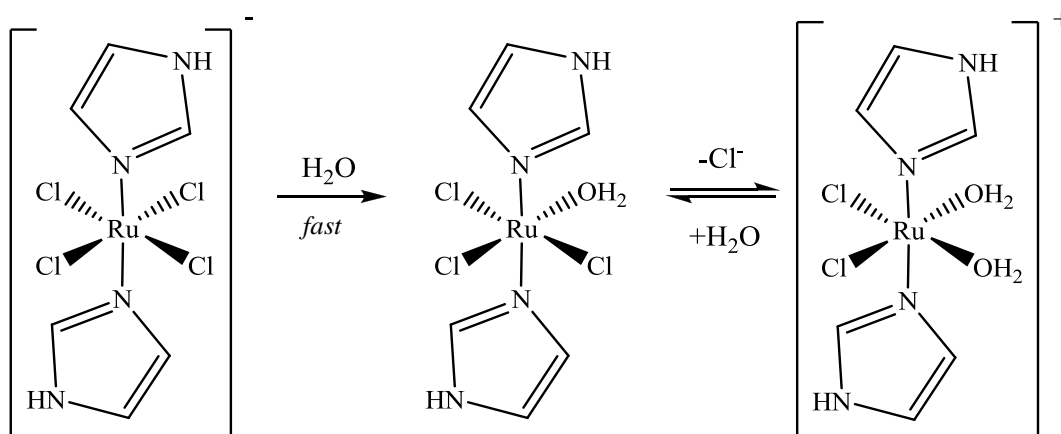
Scheme 1.6 *Hydrolytic pathway of ICR*

1.5.3 Ru(azpy)$_2$Cl$_2$ Anti-Cancer Complexes

The synthesis and chemistry of dichlorobis[2-(phenylazo)pyridine]ruthenium(II) (Ru(azpy)$_2$Cl$_2$) was first reported by Krause and Krause in 1980.[102] They have reported the five possible isomers that could exist with complexes of the type RuCl$_2$L$_2$, and showed the characterisation of three different isomers of Ru(azpy)$_2$Cl$_2$ complexes characterised by IR, NMR, visible spectra, and cyclic voltammetry. The fourth and fifth isomers were later found and reported by Popov *et al.*[103] and Reedijk *et al.*[104] accordingly. The five different structural isomers are as shown in **Figure 1.14** defined by the position of the chloride ligands, pyridine and azo group of the azopyridine ligands whether they are *cis* or *trans* to each other when bonded to the ruthenium metal centre, and each isomers are labelled by the different Greek symbols.
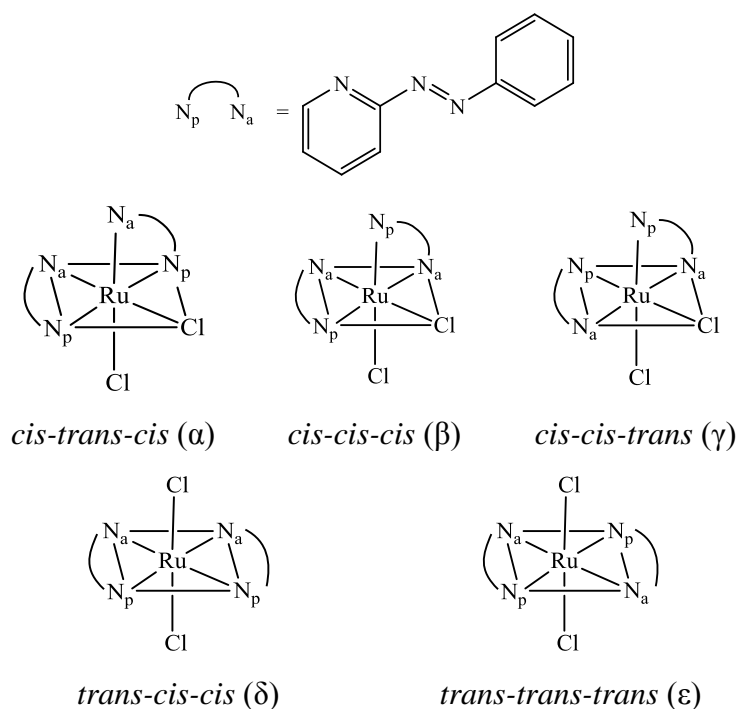
Figure 1.14 *Five possible isomers for Ru(azpy)$_2$Cl$_2$*

Reedijk *et al.* has reported the anti-cancer activities of the Ru(azpy)$_2$Cl$_2$ complexes and has shown the differences in their activities due to different structural isomers.[105] The α-isomer is 10 times more cytotoxic against a series of cancer cell lines, than β and δ-isomer. DNA binding studies have also shown that the α-isomer is sterically less hindered when binding to guanine compared to the β-isomer. These findings indicate that the *cis* geometry is highly important for the anti-cancer activity of (Ru(azpy)$_2$Cl$_2$ complexes specifically the *cis-trans-cis* (α) isomer.

1.5.4 Ruthenium Arene Anti-Cancer Complexes

The field in developing ruthenium arene complexes was started after an enhanced cytotoxicity was observed by coordinating the anti-cancer agent metronidazole [1-β-(hydroxyethyl)-2-methyl-5-nitro-imidazole] to a benzene ruthenium dichloro fragment (**Figure 1.15a**).[106] A typical structure of a half-sandwich ''piano-stool'' [(η^6- arene)Ru(X)(Y)(Z)] complex is shown in **Figure 1.15b**, where the arene forms the seat of the piano stool and the ligands resemble the legs. Ligands X and Y are linked forming a bidentate chelating ligand, which seems to give an advantage for anti-cancer activities.

Ru(II) half-sandwich complexes have a structure that allow variations on the monodentate ligand Z, the bidentate ligand XY and the arene, for tuning the properties of these complexes. The chelating ligand helps to control stability and the kinetics of ligand-exchange. The arene group influences the cell uptake and its interactions towards potential targets. The leaving group Z occupies the biomolecule binding site on metal centre. The main reason for the structure design is the amphiphilic properties of the arene ruthenium unit, where the arene ligand being hydrophobic is balanced by the hydrophilic metal centre. Another important feature is the ability of the Ru-Z bonds to hydrolyse giving aqua ruthenium complex, once it enters the cell with low Cl$^-$ concentration.

(a)   (b)
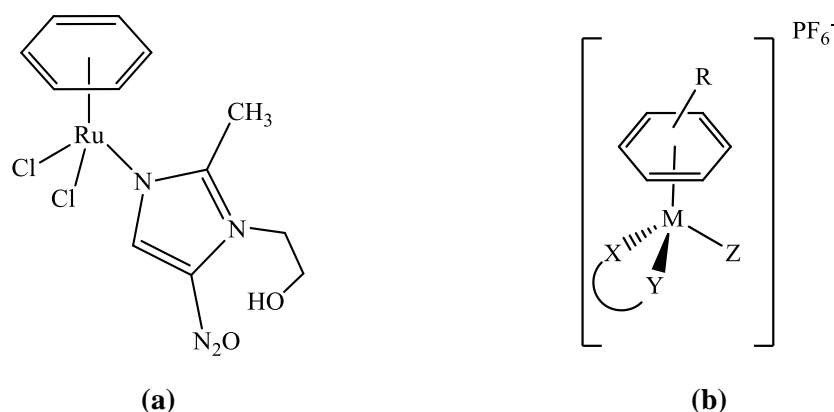
***Figure 1.15** (a) (η^6-benzene) Ruthenium dichloro metronidazole; (b) Typical structure of organometallic anti-cancer complexes containing metal (M), a η^6-(arene), a bidentate ligand (XY) and a halide (Z)*

Sheldrick *et al.* first discovered the biological use of organometallic η^6-arene ruthenium complexes, which take the form of $[(\eta^6\text{-arene})\text{ruthenium(II)(en)X}]^+$ (X = halide, en = ethylenediamine) (**Figure 1.16**).[107] Different arene substituents of the complexes were also shown to exert activity *in vitro* and *in vivo* against a range of cancer cell lines.

p-Cymene (*p*-cym)   Biphenyl (Bip)

R =

5,8,9,10-Tetrahydroanthracene   9,10-Dihydroanthracene (DHA)
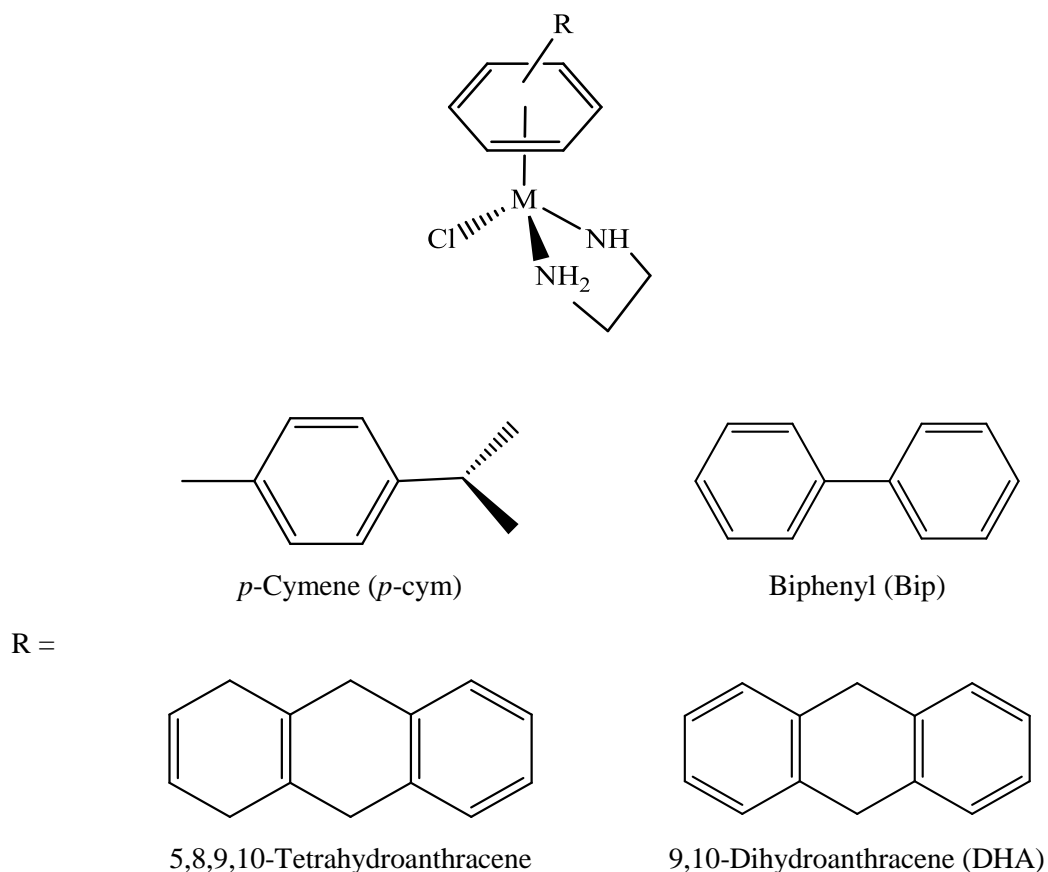
Figure 1.16 *Structures of organometallic η^6-arene ruthenium complexes in the form of $[(\eta^6\text{-arene})ruthenium(II)(en)X]^+$*

Sadler *et al.* have studied organometallic η^6-arene ruthenium complexes in the form of $[(\eta^6\text{-arene})\text{Ru(azpy)I}]^+$ (arene = *p*-cymene or biphenyl, azpy = *N,*-dimethylphenyl- or hydroxyphenyl-azopyridine) (**Figure 1.17**). These complexes were shown to be inert towards ligand substitution in aqueous solution, but are highly cytotoxic to A2780 and A549 cancer cells, due to an increase in reactive oxygen species (ROS), which was suggested by fluorescence-trapping studies in A549 cells.[108]
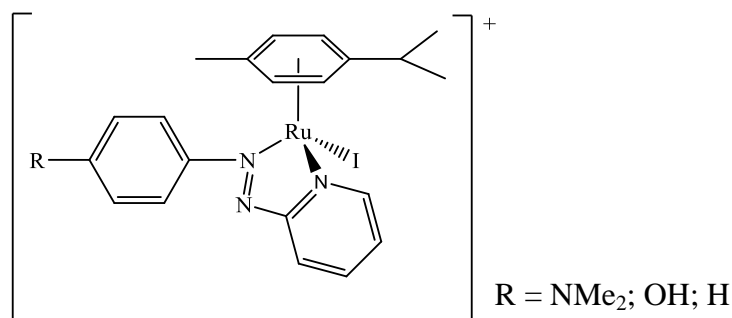
Figure 1.17 *Structures of organometallic η⁶-arene ruthenium complexes in the form of [(η⁶-arene)Ru(azpy)I]⁺*

McGowan *et al.* worked on organometallic η⁶-arene ruthenium complexes.[109] Their studies involved developing a range of ruthenium complexes which incorporate ligands having high degree of flexibility, both sterically and electronically, for the evaluation of cytotoxicity effects (**Figure 1.18**). To this end, the ruthenium arene complexes synthesised involved fragments for H-bonding and aryl groups, which allow DNA interaction as well as affecting increased hydrophobic nature of the compounds.
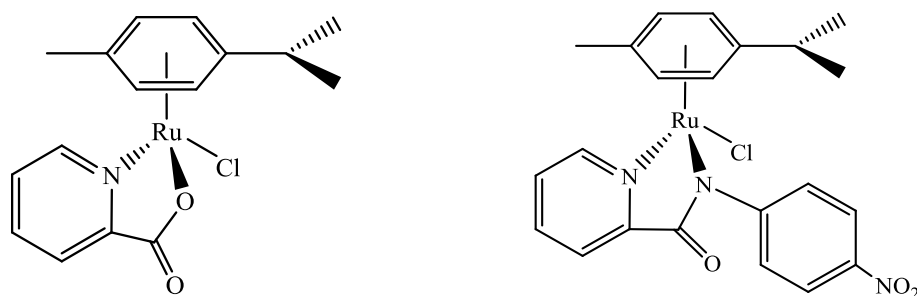
Figure 1.18 *Examples of organometallic η⁶-arene ruthenium complexes*

1.6   Rhodium-based anti-cancer complexes

There have only been few biological investigations on rhodium complexes, until very recently that they are considered to have properties that can make them the potential as anti-cancer agents.[110] By coordinating cytotoxic ligands to the rhodium metal centre, it can lead to the increase in solubility and cell uptake, hence contributing to their anti-cancer activity. Ligand combination and coordination geometry are important in the design of drugs in order to improve their pharmacokinetics and bioavailability.

A variety of rhodium(III) analogues of ruthenium(III) anti-cancer complexes have showed contrasting activities between ruthenium and their rhodium analogues.[111, 112] The 'activation by reduction' mechanism of Ru(III) complexes was found to be unlikely for the Rh(III) analogues which could explain their low in anti-cancer activity. **Figure 1.19** shows the structures of previously reported rhodium anti-cancer complexes. Rh complexes mer,*cis*-[$Cl_3(Me_2SO)(Im)_2Rh(III)$], Na[*trans*-[$Cl_4(Me_2SO)(Im)Rh(III)$] and (Him)*trans*-[$Cl_4(Im)_2Rh(III)$] were found to be inactive against A2780 ovarian cancer cells with IC_{50} values > 200 μM, > 100 μM and > 1000 μM respectively. Whereas mer, *cis*-[$Cl_3(Me_2SO)_2LRh(III)$], where L is either NH_3 or imidazole, showed significant cytotoxic activity against A2780 ovarian cancer cells with IC_{50} value 1.5 ± 0.4 μM and 15.6 ± 2 μM respectively. Both Na[*trans*-[$Cl_4(Me_2SO)(Im)Rh(III)$] and mer, *cis*-[$Cl_3(Me_2SO)_2(Me_2SO)Rh(III)$] have shown to inhibit the growth of the primary MCa mammary tumor implanted in mice and the latter Rh complex have also shown to inhibit metastatic cancer cells in the lungs.

mer, *cis*-[$Cl_3(Me_2SO)_2LRh(III)$]

L = NH_3 or Im

mer,*cis*-[$Cl_3(Me_2SO)(Im)_2Rh$]

Na[*trans*-[$Cl_4(Me_2SO)(Im)Rh(III)$]

(Him)*trans*-[$Cl_4(Im)_2Rh(III)$]
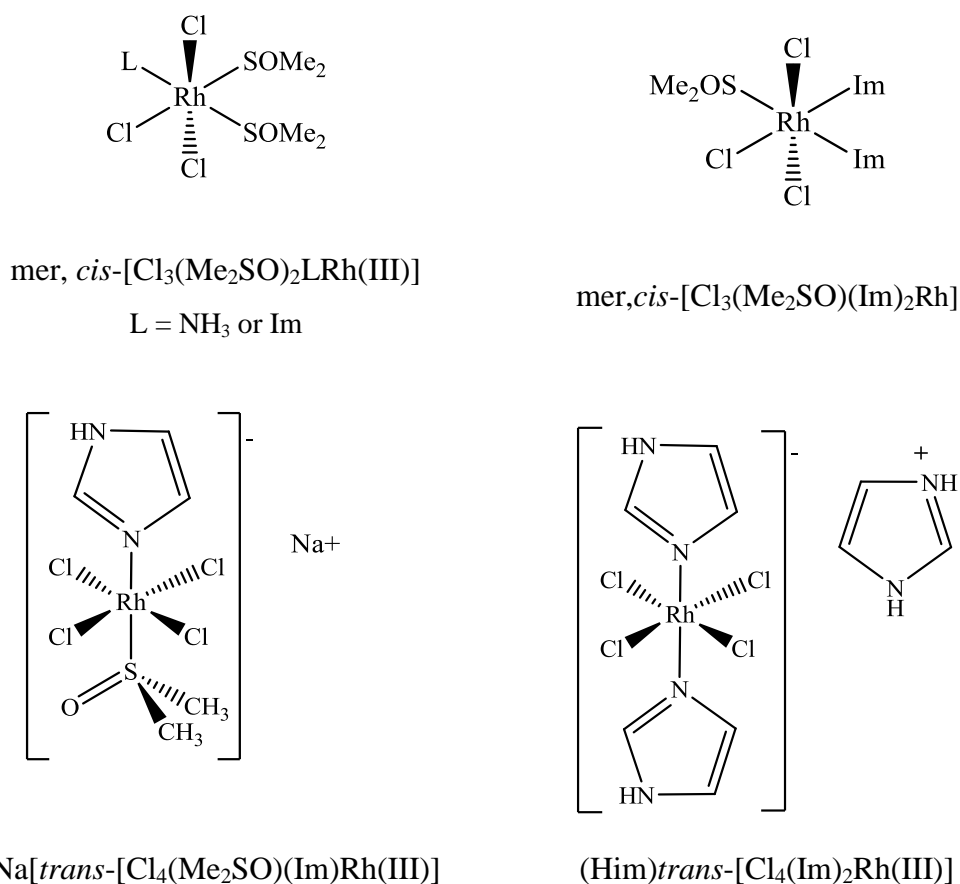
Figure 1.19 Rhodium(III) anti-cancer complexes

Sheldrick *et al.* prepared a series of trichlorido rhodium(III) complexes, $RhCl_3(DMSO)LL$, where LL is either ethylenediamine (en), bipyridine (bpy), 1,10-phenantroline (phen), 1,2-diaminobenzene (dab) or [6]aneS$_2$ ligand (**Figure 1.20**).[113] These complexes have showed high cytotoxicity values against MCF7 breast cancer cells and HT-29 colon cancer cells. Their cytotoxicity increases in the order of en $<$ dab $<$ [6]aneS$_2$ $<$ bpy, showing the importance of the polypyridyl ligands in their anti-cancer activity. They have also reported that the high cell uptake of the complexes along the series, as well as, an increase in kinetic stability may relate to their cytotoxic activity against the different cancer cells.

Y = DMSO

LL = en, bpy, phen,dab, [6]anesS$_2$
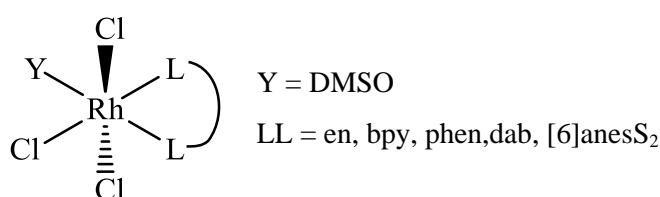
Figure 1.20 *A general structure of trichlorido rhodium(III) complexes*

Dyson *et al* has reported the rhodium analogues of an antimetastatic agent [(η^6-*p*-cym)RuCl$_2$(pta)] (RAPTA-C), as shown in **Figure 1.21a**.[114] Both the dichlorido, [(η^5-C$_5$Me$_5$)RhCl$_2$(pta)], and monochlorido, [(η^5-C$_5$Me$_5$)RhCl(pta)$_2$]$^+$ Rh complexes did not show any activity against a series of human cancer cell lines, with IC$_{50}$ values $>$ 380 μM and $>$ 400 μM respectively. McGowan *et al.* reported [(η^5-C$_5$Me$_5$)RhCl(3-Cl-picolinamide)] (**Figure 1.21b**) which has showed a moderate cytotoxicity with IC$_{50}$ value of 28.8 ± 0.5 μM against A2780 ovarian cancer cells.[115] This complex was also found to be a potent inhibitor of thioredoxin reductase 1 (Trx-R) activity, which may be a potential mechanism of action in its cytotoxic activity.

(a)   (b)
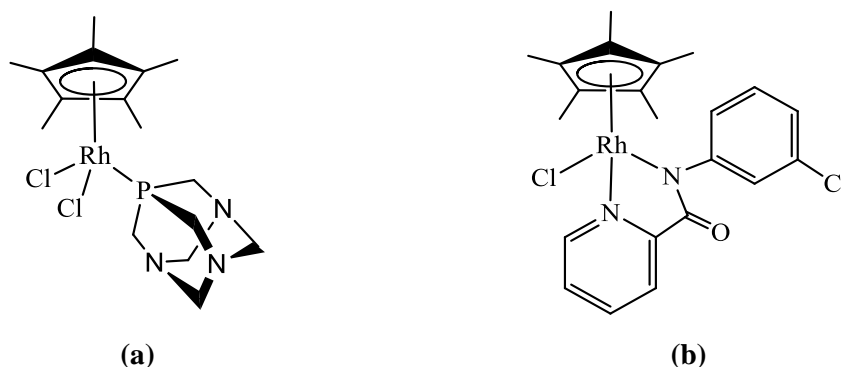
Figure 1.21 *Structure of (a) [(η^5-C$_5$Me$_5$)RhCl$_2$(pta)], and (b) [(η^5-C$_5$Me$_5$)RhCl(3-Cl-picolinamide)]*

1.7   Metal Picolinamide Complexes

Bhattacharya *et al.* have selected a group of picolinamide ligands to obtain ruthenium complexes of the type [Ru(L-R)$_3$]. These complexes were synthesised using RuCl$_3$.3H$_2$O or [RuCl$_2$(DMSO)$_4$] in the presence of triethylamine. **Figure 1.22a** shows the complex reported, in which picolinamide ligands are coordinated to the metal centre through the nitrogens of pyridine and amide, giving an (*N,N*) bonding to ruthenium and leaving the whole complex as neutral.[116] Nair *et al.* have reported structural and electrochemical studies of cyclometalated iridium(III) picolinamide complexes (**Figure 1.22b**). Their electrochemical studies have shown two oxidation peaks, where one occurs due to the metal center with a substantial contribution from the ligands. The second oxidation is due to the ancillary picolinamide ligand.[117] Another Ru(L-R)$_3$ complex that has also been reported in the literature contains picolinic acid as the tris-bidentate ligand bonded to ruthenium centre through nitrogen of pyridine and oxygen of carboxylated group,[118] as shown in **Figure 1.22c**.

(a)   (b)

(c)
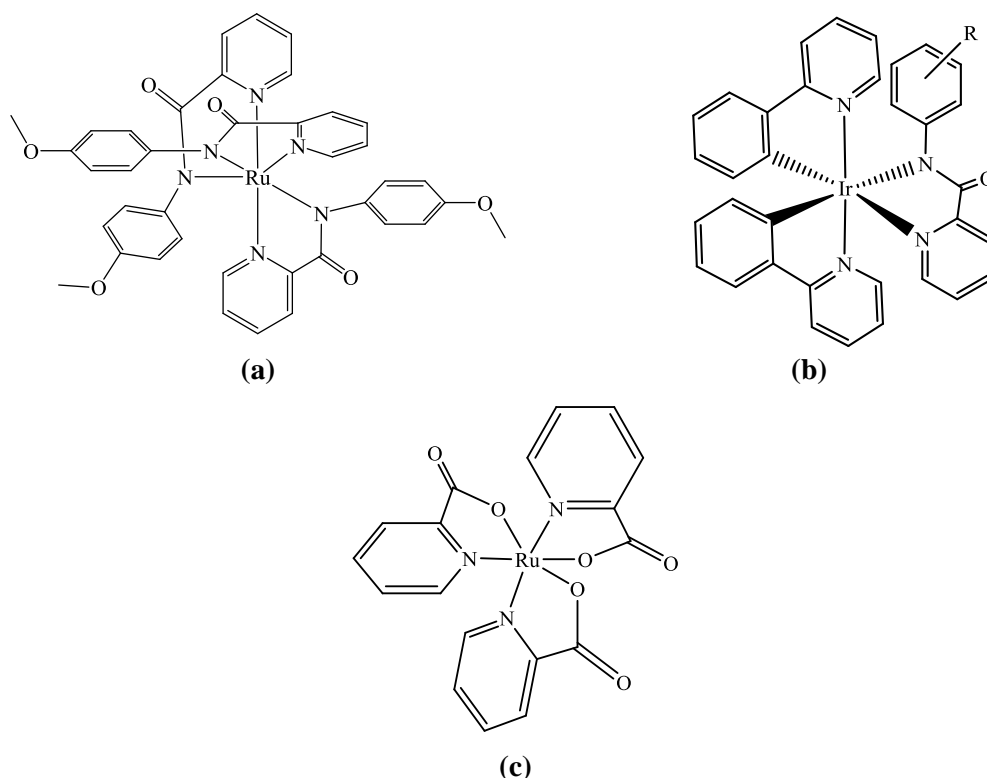
Figure 1.22 (a) *N,N-binding on RuL$_3$ complex* ***(b)*** *Ir(ppy)$_2$L, where L is a picolinamide ligand* ***(c)*** *N,O-binding on Ru(III) Picolinic acid complex*

Several metal picolinamide complexes have also been synthesised within the McGowan group as shown in **Figure 1.23**. Complex **1** was prepared by synthesising a solution of [(Ru(p-cymene))$_2$(μ-Br)$_2$Br$_2$)] in ethanol with an excess of the ligands in the presence of NH$_4$PF$_6$, to give a *tris*-picolinamide with *(N,O)*-coordination to the ruthenium centre, giving the whole complex a +2 charge, and balanced with two PF$_6^-$ counter ions.[119] Complex **2** and **3**, where M is either Ruthenium or Osmium, and arene is either *p*-cymene or a biphenyl ring, have different coordination mode of the picolinamide ligands to show which binding mode, either *N,N-* or *N,O*-coordination, gives a major effect to their anti-cancer activity.[120] Their studies have shown that *N,N*-coordinated complexes are more active than the *N,O*-coordinated complexes in terms of cytotoxicity, hydrolysis and DNA binding. Complex **4**, where M is either iridium or rhodium, have also been reported to have the potential in anti-cancer activity and they were found to be the potent inhibitors of Thioredoxin Reductase 1 (Trx-R) enzymes' activity, which is a good target for anti-cancer treatment.[115]
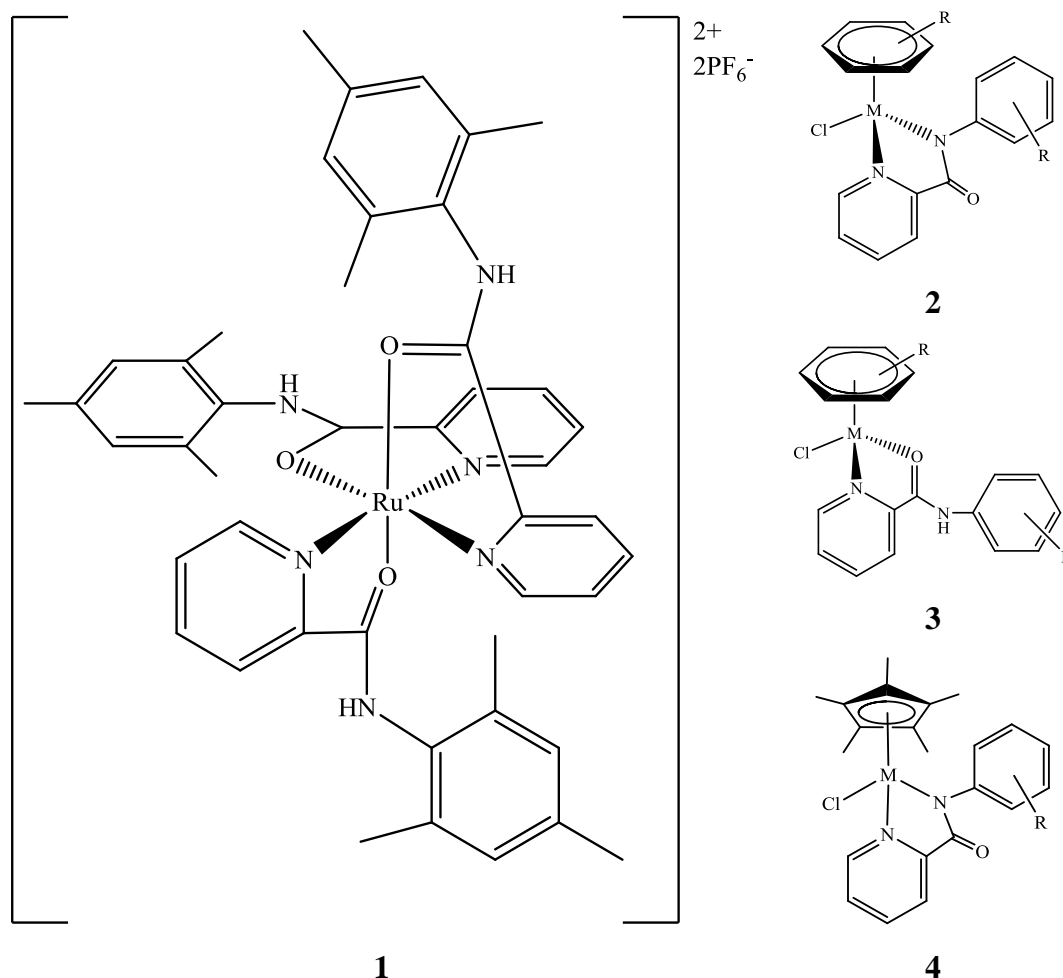
Figure 1.23 *Metal-picolinamide complexes synthesised within the McGowan group*

1.8   Aims of the research project

The aims of this project were to:

- Synthesise and characterise a series of *N*-functionalised picolinamide ligands using IR, NMR, ES-MS, CHN elemental analysis and X-ray crystallisation (Chapter 2)

- Synthesise and characterise a range of novel ruthenium dihalide complexes containing bidentate picolinamide ligands using IR, ES-MS, CHN elemental analysis and X-ray crystallisation (Chapters 3 and 4)

- Synthesise and characterise a library of novel rhodium dihalide complexes containing bidentate picolinamide ligands using IR, NMR, ES-MS, CHN elemental analysis and X-ray crystallisation (Chapter 5)

- Study on the structural isomers of the ruthenium and rhodium dihalide complexes by NMR, UV-Vis and X-ray powder diffraction (Chapters 3-5)

- Investigate the structural-activity relationship of the ruthenium dihalide complexes as anti-cancer agents. The studies include cytotoxicity (IC_{50}), hydrophobicity (Log P) and hydrolysis (Chapters 6 and 7)

- Study the structural-activity relationship of the ruthenium and rhodium dihalide complexes as catalysts against transfer hydrogenation reactions (Chapter 8)

The ruthenium complexes synthesised contain several fragments, which have shown to be important for anti-cancer, as listed below:
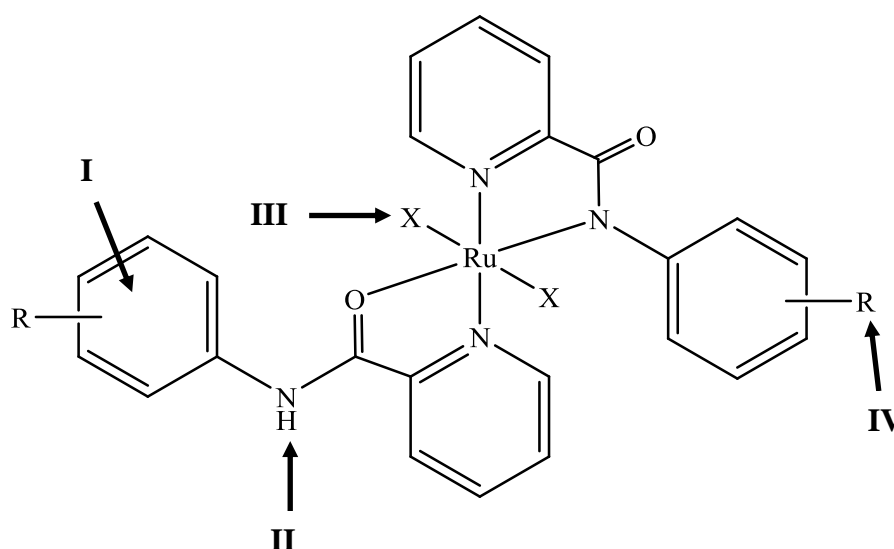
I Planar aromatic groups may cause a potential site π-π stacking with nucelobases within DNA chain (intercalation)

II The acidic amide proton may interact with guanine or other hydrogen acceptor sites on the DNA chain, as a hydrogen bind donor

III The labile halide ligand enables fast hydrolysis at low chloride concentration inside cell, making the complex to form covalent bonds with nucleophilic site on a DNA chain

IV Various substituents on the aromatic phenyl ring increase the hydrophilicity of the complex, also increase the anti-cancer activity of the complex

The rhodium complexes prepared were the analogue of the ruthenium dihalide complexes containing several possible moieties that may be involved in transfer hydrogenation reactions.
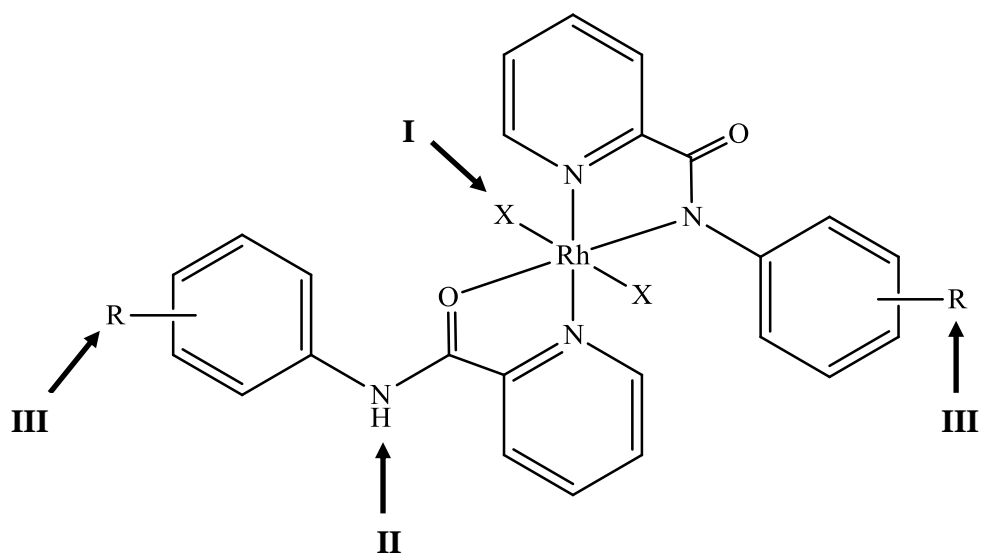
I The labile halide ligand may undergo substitution to generate alkoxide formation

II The NH moiety may be used to deliver a hydroxyl proton to the substrate

III Modifying the substituents on the phenyl ring may increase the catalytic activity of the complex

1.9   References

1.   A. Jemal, F. Bray, M. M. Center, J. Ferlay, E. Ward and D. Forman, *CA-Cancer J. Clin.,* 2011, **61**, 69-90.

2.   J. Ferlay, H. R. Shin, F. Bray, D. Forma, C. D. Mathers and P. D., GLOBOCAN 2008, Lyon, France: International Agency for Research on Cancer.

3.   S. Missailidis, *Anticancer Therapeutics*, John Wiley and Sons Ltd, Chicester, 2008.

4.   M. Hejmadi, *Introduction to Cancer Biology,* Ventus Publishing Aps, 2010.

5.   J. Gabriel, *The Biology of Cancer*, John & Wiley Sons. Ltd, Chichester, 2007.

6.   R. M. Roat-Malone, *Bioinorganic Chemistry: A Short Course*, John Wiley & Sons Inc, 2002.

7.   Z. Guo and P. J. Sadler, *Angew. Chem., Int. Ed.*, 1999, **38**, 1512-1531.

8.   M. A. Jakupec, M. Galanski and B. K. Keppler, *Rev. Physiol. Bioch. Pharm.*, 2003, 1-53.

9.   V. Brabec and J. Kasparkova, *Drug Resist. Update*, 2005, **8**, 131-146.

10.   H. Zorbas and B. K. Keppler, *Chembiochem,* 2005, **6**, 1157-1166.

11.   C. L. Fox, Jr. and S. M. Modak, *Antimicrob. Agents Ch.*, 1974, **5**, 582-588.

12.   H. J. Klasen, *Burns*, 2000, **26**, 131-138.

13.   B. S. Atiyeh, M. Costagliola, S. N. Hayek and S. A. Dibo, *Burns*, 2007, **33**, 139-148.

14.   J. A. Friederich and J. F. Butterworth, *Anesth. Analg.*, 1995, **81**, 152 - 162.

15.   J. M. Rademaker-Lakhai, D. van den Bongard, D. Pluim, J. H. Beijnen and J. H. Schellens, *Clin. Cancer Res.*, 2004, **10**, 3717-3727.

16.   B. Rosenberg, L. Vancamp and T. Krigas, *Nature*, 1965, **205**, 698-699.

17.   L. B., *Cisplatin: Chemistry and Biochemistry of a Leading Anticancer Drug*, Wiley-VCH, Chimica Acta, Zurich, 1999.

18.   Y. Zhang, Z. Guo and X. Z. You, *J. Am. Chem. Soc.*, 2001, **123**, 9378-9387.

19.   J. Reedijk, *Proc. Natl. Acad. Sci.*, 2003, **100**, 3611-3616.

20.   M. A. Fuertes, C. Alonso and J. M. Perez, *Chem. Rev.*, 2003, **103**, 645-662.

21.   A. Sigel and H. Sigel, *Metal Ions in Biological Systems*, Marcel Dekker, New York, Basel, 2004.

22.   D. Wang and S. J. Lippard, *Nat. Rev. Drug Discov.*, 2005, **4**, 307-320.

23.   J. K.-C. Lau and B. Ensing, *Phys. Chem. Ch. Ph.*, 2010, **12**, 10348-10355.

24.   S. Y. Sharp, P. M. Rogers and L. R. Kelland, *Clin. Cancer Res.*, 1995, **1**, 981-989.

25.   S. Ishida, J. Lee, D. J. Thiele and I. Herskowitz, *Proc. Natl. Acad. Sci.*, 2002, **99**, 14298-14302.

26.   J. L. Nitiss, *Proc. Natl. Acad. Sci.*, 2002, **99**, 13963-13965.

27.   D. Payet, F. Gaucheron, M. Sip and M. Leng, *Nucleic Acids Res.*, 1993, **21**, 5846–5851.

28.   P. Pil and S. J. Lippard, *Encyclopedia of Cancer*, Academic Press, San Diego, CA, 1997.

29.   A. M. J. Fichtinger-Schepman, J. L. Van der Veer, J. H. J. Den Hartog, P. H. M. Lohman and J. Reedijk, *Biochem.*, 1985, **24**, 707-713.

30.   D. E. Szymkowski, K. Yarema, J. M. Essigmann, S. J. Lippard and R. D. Wood, *Biochem.*, 1992, **89**, 10772-10776.

31.   J. N. Burstyn, W. J. Heiger-Bernays, S. M. Cohen and S. J. Lippard, *Nucleic Acids Res.*, 2000, **28**, 4237-4243.

32.   K. Stehlikova, H. Kostrhunova, J. Kasparkova and V. Brabec, *Nucleic Acids Res.*, 2002, **30**, 2894-2898.

33.   S. H. Ferlay J, Bray F, Forman D, Mathers CD, Parkin D., Lyon, France: International Agency for Research on Cancer, 2010.

34.   R. B. Ciccarelli, M. J. Solomon, A. Varshavsky and S. J. Lippard, *Biochem.*, 1985, **24**, 7533-7540.

35.   M. A. Barry, C. A. Behnke and A. Eastman, *Biochem. Pharmacol.*, 1990, **40**, 2353-2362.

36.   E. R. Jamieson and S. J. Lippard, *Chem. Rev.*, 1999, **99**, 2467-2498.

37.   F. Yu, J. Megyesi and P. M. Price, *Am. J. Physiol.*, 2008, **295**, F44-52.

38.   A. A. Tulub and V. E. Stefanov, *Int. J. Biol. Macromol.,* 2001, **28**, 191-198.

39.   C. A. Rabik and M. E. Dolan, *Cancer Treat. Rev.*, 2007, **33**, 9-23.

40.   R. P. Perez, *Eur. J. Cancer*, 1998, **34**, 1535-1542.

41.   A. Eastman, *Cancer Treat. Rev.*, 1991, **57**, 233-249.

42.   B. Köberle, M. T. Tomicic, S. Usanova and B. Kaina, *Biochim. Biophys. Acta*, 2010, **1806**, 172-182.

43. T. C. Shea, M. Flaherty, A. Elias, J. P. Eder, K. Antman, C. Begg, L. Schnipper, E. Frei, 3rd and W. D. Henner, *J. Clin. Oncol.*, 1989, **7**, 651-661.

44. A. H. Calvert, D. R. Newell, L. A. Gumbrell, S. O'Reilly, M. Burnell, F. E. Boxall, Z. H. Siddik, I. R. Judson, M. E. Gore and E. Wiltshaw, *J. Clin. Oncol.*, 1989, **7**, 1748-1756.

45. N. Katsumata, *Ann. Oncol.*, 2011, **22**, viii29-viii32.

46. H. G. Meerpohl, *Int. J. Gynecol. Cancer*, 1997, **7**, 18-22.

47. J. Pfisterer, I. Vergote, A. Du Bois and E. Eisenhauer, *Int. J. Gynecol. Cancer*, 2005, **15 Suppl 1**, 36-41.

48. G. Natarajan, R. Malathi and E. Holler, *Biochem. Pharm.*, 1999, **58**, 1625-1629.

49. S. J. Berners-Price, L. Ronconi and P. J. Sadler, *Prog. Nucl. Mag. Res. Sp.*, 2006, **49**, 65-98.

50. A. J. Di Pasqua, J. Goodisman and J. C. Dabrowiak, *Inorg. Chim. Acta*, 2012, **389**, 29-35.

51. J. L. Misset, *Br. J. Cancer*, 1998, **77 Suppl 4**, 4-7.

52. H. Bleiberg, *Br. J. Cancer*, 1998, **77 Suppl 4**, 1-3.

53. B. Stordal, N. Pavlakis and R. Davey, *Cancer Treat. Rev.*, 2007, **33**, 347-357.

54. S. Faivre, D. Chan, R. Salinas, B. Woynarowska and J. M. Woynarowski, *Biochem. Pharm.*, 2003, **66**, 225-237.

55. B. K. Keppler, C. Friesen, H. G. Moritz, H. Vongerichten and E. Vogel, in *Bioinorg. Chem.*, 1991, 97-127.

56. B. K. Keppler, M. E. Heim, H. Flechtner, F. Wingen and B. L. Pool, *Arzneim-Forsch*, 1989, **39**, 706-709.

57. T. Schilling, K. B. Keppler, M. E. Heim, G. Niebch, H. Dietzfelbinger, J. Rastetter and A. R. Hanauske, *Invest. New Drugs*, 1996, **13**, 327-332.

58. T. Pieper, K. Borsky and B. K. Keppler, *Topics in Biological Inorganic Chemistry*, Springer, Berlin, 1999.

59. H. Köpf and P. Köpf-Maier, *Angew. Chem. Int. Ed.*, 1979, **18**, 477-478.

60. C. V. Christodoulou, D. R. Ferry, D. W. Fyfe, A. Young, J. Doran, T. M. Sheehan, A. Eliopoulos, K. Hale, J. Baumgart, G. Sass and D. J. Kerr, *J. Clin. Oncol.*, 1998, **16**, 2761-2769.

61.   A. Korfel, M. E. Scheulen, H. J. Schmoll, O. Grundel, A. Harstrick, M. Knoche, L. M. Fels, M. Skorzec, F. Bach, J. Baumgart, G. Sass, S. Seeber, E. Thiel and W. E. Berdel, *Clin. Cancer Res.*, 1998, **4**, 2701-2708.

62.   J. H. Toney and T. J. Marks, *J. Am. Chem. Soc.*, 1985, **107**, 947-953.

63.   X. Chen and L. Zhou, *J. Mol. Struc-Theochem*, 2010, **940**, 45-49.

64.   C. Deng and L. Zhou, *Inorg. Chim. Acta*, 2011, **370**, 70-75.

65.   G. Lummen, H. Sperling, H. Luboldt, T. Otto and H. Rubben, *Cancer Chem. Pharm.*, 1998, **42**, 415-417.

66.   N. Kröger, U. R. Kleeberg, K. Mross, L. Edler and D. K. Hossfeld, *Onkologie*, 2000, **23**, 60-62.

67.   W. Kaminsky, *Dalton Trans.,* 1998, 1413-1418.

68.   M. C. Valadares, A. L. Ramos, F.-J. K. Rehmann, N. J. Sweeney, K. Strohfeldt, M. Tacke and M. L. S. Queiroz, *Eur. J. Pharm.*, 2006, **534**, 264-270.

69.   T. A. Immel, U. Groth, T. Huhn and P. Öhlschläger, *PLoS one*, 2011, **6**, e17869.

70.   H. Glasner and E. Y. Tshuva, *J. Am. Chem. Soc.*, 2011, **133**, 16812-16814.

71.   S. Meker, C. M. Manna, D. Peri and E. Y. Tshuva, *Dalton Trans.*, 2011, **40**, 9802-9809.

72.   J. Schur, C. M. Manna, A. Deally, R. W. Koster, M. Tacke, E. Y. Tshuva and I. Ott, *Chem. Comm.*, 2013, **49**, 4785-4787.

73.   T. A. Immel, M. Debiak, U. Groth, A. Bürkle and T. Huhn, *ChemMedChem*, 2009, **4**, 738-741.

74.   O. R. Allen, A. L. Gott, J. A. Hartley, J. M. Hartley, R. J. Knox and P. C. McGowan, *Dalton Trans.*, 2007, 5082-5090.

75.   C. S. Allardyce and P. J. Dyson, *Platinum Metals Rev.*, 2001, **45**, 62-69.

76.   M. Pongratz, P. Schluga, M. A. Jakupec, V. B. Arion, C. G. Hartinger, G. Allmaier and B. K. Keppler, *J. Anal. At. Spectrom.*, 2004, **19**, 46-51.

77.   W. Han Ang and P. J. Dyson, *European Journal of Inorganic Chemistry*, 2006, **2006**, 4003-4018.

78.   C. Gabbiani, *Proteins as possible targets for antitumor metal complexes. Biophysical studies of their interactions.*, Firenze University Press, Italy, 2009.

79.   M. A. Jakupec, M. Galanski, V. B. Arion, C. G. Hartinger and B. K. Keppler, *Dalton Trans.*, 2008, 183-194.

80.   S. Nag, R. J. Butcher and S. Bhattacharya, *Eur. J. Inorg. Chem.*, 2007, **2007**, 1251-1260.

81.   A. Martínez, C. K. Rajapakse, B. Naoulou, Y. Kopkalli, L. Davenport and R. Sánchez-Delgado, *J. Biol. Inorg. Chem.*, 2008, **13**, 703-712.

82.   A. I. Ramos, T. M. Braga and S. S. Braga, *Mini-rev. Med. Chem.*, 2012, **12**, 227-235.

83.   C. M. Bastos, K. A. Gordon and T. D. Ocain, *Bioorg. Med. Chem. Lett.*, 1998, **8**, 147-150.

84.   G. Sava, S. Pacor, G. Mestroni and E. Alessio, *Clin. Exp. Metastasis*, 1992, **10**, 273-280.

85.   G. Sava, I. Capozzi, K. Clerici, G. Gagliardi, E. Alessio and G. Mestroni, *Clin. Exp. Metastasis*, 1998, **16**, 371-379.

86.   A. Bergamo, R. Gagliardi, V. Scarcia, A. Furlani, E. Alessio, G. Mestroni and G. Sava, *J. Pharm. Expt. Ther.*, 1999, **289**, 559-564.

87.   G. Sava, F. Frausin, M. Cocchietto, F. Vita, E. Podda, P. Spessotto, A. Furlani, V. Scarcia and G. Zabucchi, *Eur. J. Cancer*, 2004, **40**, 1383-1396.

88.   A. Vacca, M. Bruno, A. Boccarelli, M. Coluccia, D. Ribatti, A. Bergamo, S. Garbisa, L. Sartor and G. Sava, *Br. J. Cancer*, 2002, **86**, 993-998.

89.   G. Sava, A. Bergamo, S. Zorzet, B. Gava, C. Casarsa, M. Cocchietto, A. Furlani, V. Scarcia, B. Serli, E. Iengo, E. Alessio and G. Mestroni, *Eur. J. Cancer*, 2002, **38**, 427-435.

90.   I. Bratsos, S. Jedner, T. Gianferrara and E. Alessio, *Chimia*, 2007, **61**, 692-697.

91.   M. I. Webb and C. J. Walsby, *Dalton Trans.*, 2011, **40**, 1322-1331.

92.   M. Bacac, A. C. G. Hotze, K. v. d. Schilden, J. G. Haasnoot, S. Pacor, E. Alessio, G. Sava and J. Reedijk, *J. Inorg. Biochem.*, 2004, **98**, 402-412.

93.   F. Frausin, V. Scarcia, M. Cocchietto, A. Furlani, B. Serli, E. Alessio and G. Sava, *J. Pharm. Expt. Ther.*, 2005, **313**, 227-233.

94.   B. K. Keppler, M. Henn, U. M. Juhl, M. R. Berger, R. Niebl and F. E. Wagner, in *Ruthenium and Other Non-Platinum Metal Complexes in Cancer Chemotherapy*, eds. E. Baulieu, D. Forman, M. Ingelman-

Sundberg, L. Jaenicke, J. Kellen, Y. Nagai, G. Springer, L. Träger, L. Will-Shahab and J. Wittliff, Springer Berlin Heidelberg, 1989, pp. 41-69.

95. A. Küng, T. Pieper, R. Wissiack, E. Rosenberg and B. K. Keppler, *J. Biol. Inorg. Chem.*, 2001, **6**, 292-299.

96. S. Kapitza, M. A. Jakupec, M. Uhl, B. K. Keppler and B. Marian, *Cancer Lett.*, 2005, **226**, 115-121.

97. C. G. Hartinger, S. Zorbas-Seifried, M. A. Jakupec, B. Kynast, H. Zorbas and B. K. Keppler, *J. Inorg. Biochem.*, 2006, **100**, 891-904.

98. A. Bergamo, C. Gaiddon, J. H. M. Schellens, J. H. Beijnen and G. Sava, *J. Inorg. Biochem.*, 2012, **106**, 90-99.

99. F. Lentz, A. Drescher, A. Lindauer, M. Henke, R. A. Hilger, C. G. Hartinger, M. E. Scheulen, C. Dittrich, B. K. Keppler and U. Jaehde, *Anti-cancer drugs*, 2009, **20**, 97-103.

100. P. Heffeter, K. Bock, B. Atil, M. A. Reza Hoda, W. Korner, C. Bartel, U. Jungwirth, B. K. Keppler, M. Micksche, W. Berger and G. Koellensperger, *J. Biol. Inorg. Chem.*, 2010, **15**, 737-748.

101. H. Depenbrock, S. Schmelcher, R. Peter, B. K. Keppler, G. Weirich, T. Block, J. Rastetter and A. R. Hanauske, *Eur. J. Cancer*, 1997, **33**, 2404-2410.

102. R. A. Krause and K. Krause, *Inorg. Chem.*, 1980, **19**, 2600-2603.

103. A. M. Popov, M. B. Egorova, V. A. Lutovinov and R. I. Dmitrieva, *Zh. Obshch. Khim.*, 1990, **60**, 2169-2170.

104. A. H. Velders, K. van der Schilden, A. C. Hotze, J. Reedijk, H. Kooijman and A. L. Spek, *Dalton Trans.*, 2004, 448-455.

105. A. H. Velders, H. Kooijman, A. L. Spek, J. G. Haasnoot, D. de Vos and J. Reedijk, *Inorg. Chem.*, 2000, **39**, 2966-2967.

106. L. D. Dale, J. H. Tocher, T. M. Dyson, D. I. Edwards and D. A. Tocher, *Anti-cancer Drug Des.*, 1992, **7**, 3-14.

107. W. S. Sheldrick and S. Heeb, *Inorg. Chim. Acta*, 1990, **168**, 93-100.

108. Y. Fu, A. Habtemariam, A. M. Basri, D. Braddick, G. J. Clarkson and P. J. Sadler, *Dalton Trans.*, 2011, **40**, 10553-10562.

109. K. D. Camm, A. El-Sokkary, A. L. Gott, P. G. Stockley, T. Belyaeva and P. C. McGowan, *Dalton Trans.*, 2009, 10914-10925.

110. Y. Geldmacher, M. Oleszak and W. S. Sheldrick, *Inorg. Chim. Acta*, 2012, **393**, 84-102.

111. G. Mestroni, E. Alessio, A. Sessanta o Santi, S. Geremia, A. Bergamo, G. Sava, A. Boccarelli, A. Schettino and M. Coluccia, *Inorg. Chim. Acta*, 1998, **273**, 62-71.

112. S. Pacor, G. Sava, G. Mestroni and E. Alessio, *Pharm. Res.*, 1992, **25, Supplement 1**, 73-74.

113. Y. Geldmacher, K. Splith, I. Kitanovic, H. Alborzinia, S. Can, R. Rubbiani, M. A. Nazif, P. Wefelmeier, A. Prokop, I. Ott, S. Wölfl, I. Neundorf and W. Sheldrick, *J. Biol. Inorg. Chem.*, 2012, **17**, 631-646.

114. A. Dorcier, W. H. Ang, S. Bolaño, L. Gonsalvi, L. Juillerat-Jeannerat, G. Laurenczy, M. Peruzzini, A. D. Phillips, F. Zanobini and P. J. Dyson, *Organometallics*, 2006, **25**, 4090-4096.

115. Z. Almodares, S. J. Lucas, B. D. Crossley, A. M. Basri, C. M. Pask, A. J. Hebden, R. M. Phillips and P. C. McGowan, *Inorg. Chem.*, 2014, **53**, 727-736.

116. A. Das, S.-M. Peng, G.-H. Lee and S. Bhattacharya, *New J. Chem.*, 2004, **28**, 712-717.

117. V. Chandrasekhar, B. Mahanti, P. Bandipalli, K. Bhanuprakash and N. N. Nair, *J. Organomet. Chem.*, 2011, **696**, 2711-2719.

118. M. Carmen Barral, R. Jiménez-Aparicio, E. C. Royer, M. J. Saucedo, F. A. Urbanos, E. Gutiérrez-Puebla and C. Ruíz-valero, *Dalton Trans.*, 1991, **6**, 1609-1613.

119. K. Rafferty, PhD Thesis, University of Leeds, 2008.

120. S. H. van Rijt, A. J. Hebden, T. Amaresekera, R. J. Deeth, G. J. Clarkson, S. Parsons, P. C. McGowan and P. J. Sadler, *J. Med. Chem.*, 2009, **52**, 7753-7764.

CHAPTER 2

Synthesis and Characterisation of Arene Functionalised Picolinamide Ligands

2   Arene Functionalised Picolinamide Ligands

2.1   Introduction

The chemistry of amide ligands is of much interest due to their role in biological activities where the amide bond [-C=O-NH-] is an essential building unit in forming protein structure.[1] It has a high stability towards hydrolysis,[2] which is important for biological systems, as this allows the construction and maintenance of proteins. It has been known for many years that the synthetic routes towards picolinic amide derivatives involve the reaction between amines with either picolinic acid,[3] or pyridine-2-carbonyl chloride.[4, 5] Bhattacharya *et al.* have developed a preparation for high yielding picolinamide ligands adapted from Barnes *et al.*, by a condensation reaction of picolinic acid and the respective aniline with the presence of a base.[6, 7] These ligands have the ability to chelate to the metal centre in two ways, either as neutral *N,O*-donors or as monoanionic *N,N*-donors *via* the loss of amide proton,[8] as shown in **Figure 2.1**.

(a)   (b)
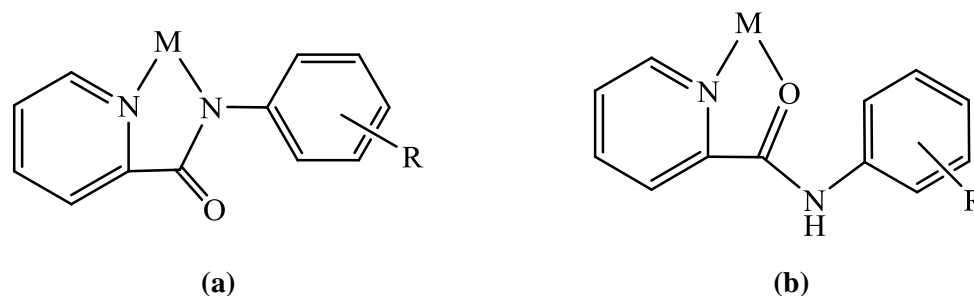
Figure 2.1 (a) monoanionic N,N-donors (b) neutral N,O-donors

N,N-coordination to the metal centre is known to stabilise metal ions in their high oxidation states due to the strong σ-donor effect,[9] while *N,O*-coordination, relatively favours lower oxidation states.[10] Interconversion between these two coordination binding modes is able to influence the chemical properties of the metal centre, as well as biological properties of the complex.

2.2   Picolinamide ligands

The picolinamide ligands used in this work are shown in **Figure 2.2**. Ligands **2.1** -
2.10 and **2.16** were previously synthesised and have been fully characterised within the
McGowan group and will not be reported in detail here.[11, 12] Ligands **2.11** - **2.15** are
novel and have been fully synthesised and characterised.
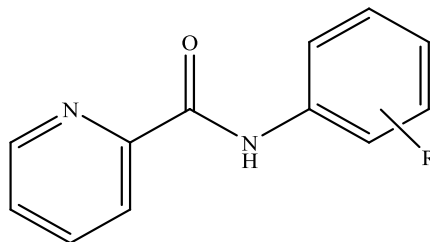
R = H	(**2.1**)	2'-Cl	(**2.6**)	2'-Br	(**2.11**)
2'-F	(**2.2**)	3'-Cl	(**2.7**)	3'-Br	(**2.12**)
4'-F	(**2.3**)	4'-Cl	(**2.8**)	4'-Br	(**2.13**)
2',4'-F	(**2.4**)	2,4'-Cl	(**2.9**)	2,4'-Br	(**2.14**)
2',5'-F	(**2.5**)	2,5'-Cl	(**2.10**)	2,5'-Br	(**2.15**)
				2'-I	(**2.16**)

Figure 2.2 Functionalised picolinamide derivatives 2.1-2.16

These ligands were synthesised according to **Scheme 2.1** by a condensation reaction
between picolinic acid and the relevant aniline in the presence of pyridine and
triphenyl phosphite. The crude product was isolated *via* filtration and washed with
distilled water.

R = F, Cl, Br, I
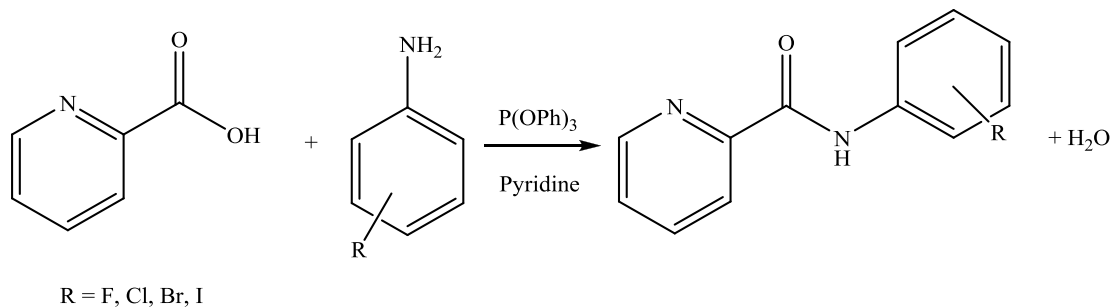
Scheme 2.1 Synthesis of picolinamide ligands

2.3   Characterisation of *N*-Functionalised Picolinamide Ligands

N-functionalised picolinamide ligands were prepared *via* **Scheme 2.1** to obtain ligands **2.11** - **2.15** as pure products in yields ranging from 37-69% and characterised using IR, ^{1}H NMR, ^{13}C{^{1}H} NMR, ES-MS, elemental analysis and single crystal X-Ray diffraction. The NMR and IR spectra for all the picolinamide ligands have very similar patterns. The IR, ^{1}H, ^{13}C{^{1}H}, ^{1}H-^{13}C{^{1}H} NMR spectra for ligand **2.11** are shown as an example of the comparison, in **Section 2.3.1** and **2.3.2**.

2.3.1   IR Data for Ligand 2.11

The IR spectrum for ligand **2.11** is as shown in **Figure 2.3**. It has several bands of different intensities in the 1600-400 cm^{-1} area. Two NH stretches are observed at 3105 and 3281 cm^{-1}, and a strong stretch for the CO group is seen at 1691 cm^{-1}.
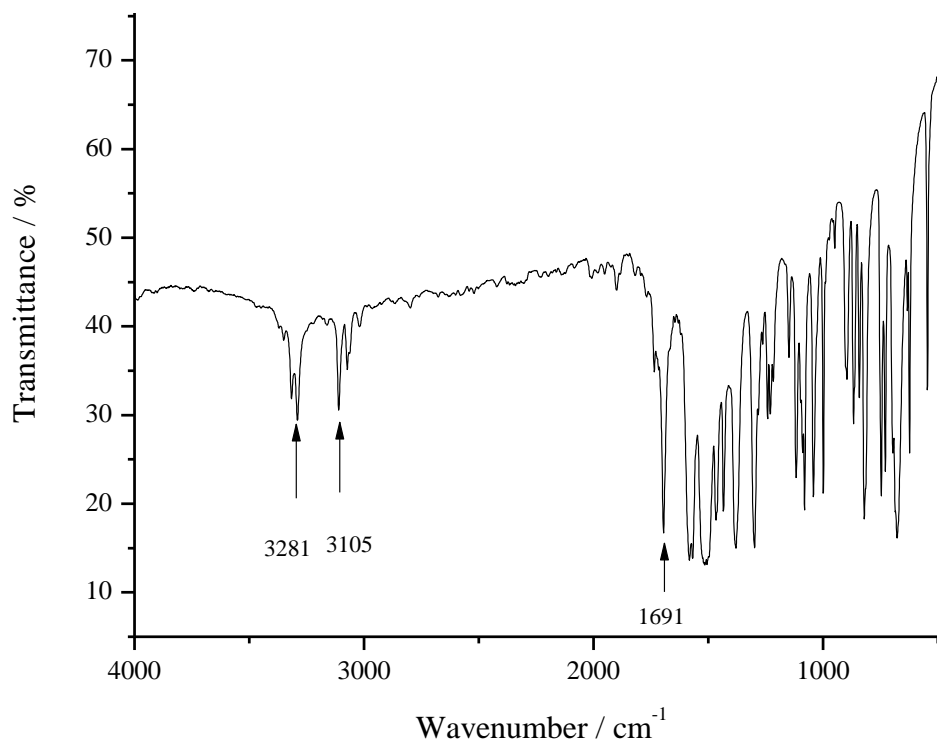
*Figure 2.3 IR spectra of ligand **2.11***

2.3.2   NMR Data for Ligand 2.11

A labelled diagram of ligand **2.11** is shown in **Figure 2.4**. The ^{1}H, ^{13}C{^{1}H} and ^{1}H-^{13}C{^{1}H} NMR spectra are shown in **Figure 2.5**, **Figure 2.6** and **Figure 2.7** respectively, with the chemical shift assignments presented in **Table 2.1**. A broad NH singlet is seen at the downfield region at 10.72 ppm, and signals of doublets and triplets between 7.04 - 8.70 ppm which corresponds to the protons on the pyridine and phenyl rings of the picolinamide. The ^{13}C{^{1}H} NMR spectra shows a C=O signal at 162.28 ppm, and C-Br signal at 113.90 ppm.
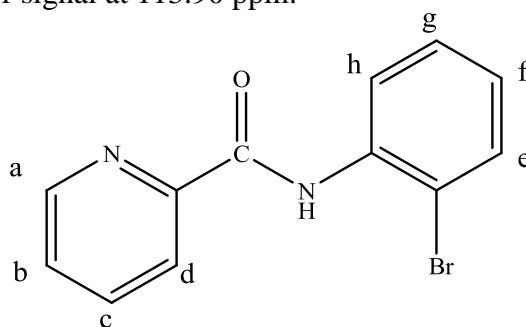
Figure 2.4 *Labelled diagram of ligand **2.11***
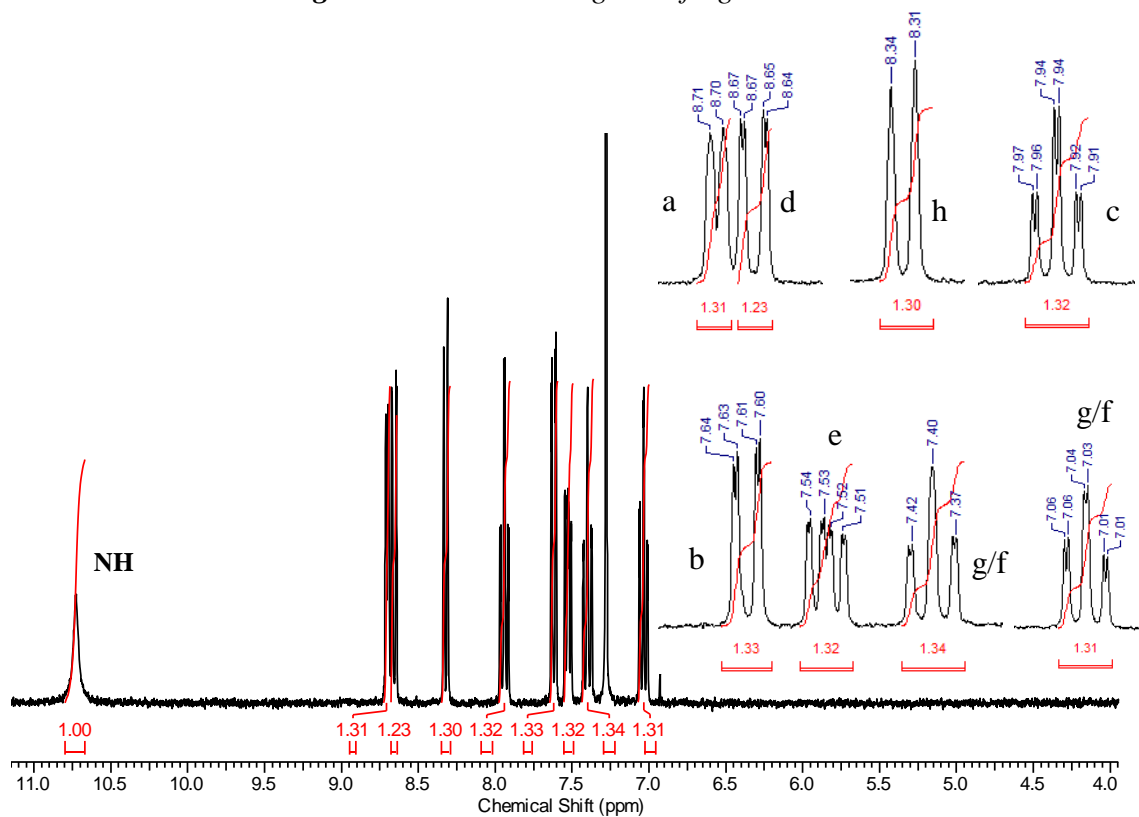
Figure 2.5 *^{1}H NMR spectrum of ligand **2.11** (CDCl$_3$, 300.13 MHz, 300 K)*

Table 2.1 *¹H and ¹³C{¹H} NMR chemical shift assignments for ligand **2.11***

Chemical Shift (δ ppm) ¹H	Splitting Pattern	Assignment	Chemical Shift (δ ppm) ¹³C{¹H}	Assignment
10.72	s	NH	162.28	C=O
8.70	d	a	149.78	Quaternary
8.66	dd	d	148.33	a
8.32	d	h	137.64	c
7.94	td	c	135.94	Quaternary
7.62	dd	e	132.49	e
7.53	ddd	b	128.37	g
7.40	m	g or f	126.62	b
7.04	td	g or f	125.13	f
			122.43	h
			121.41	d
			113.90	C-Br
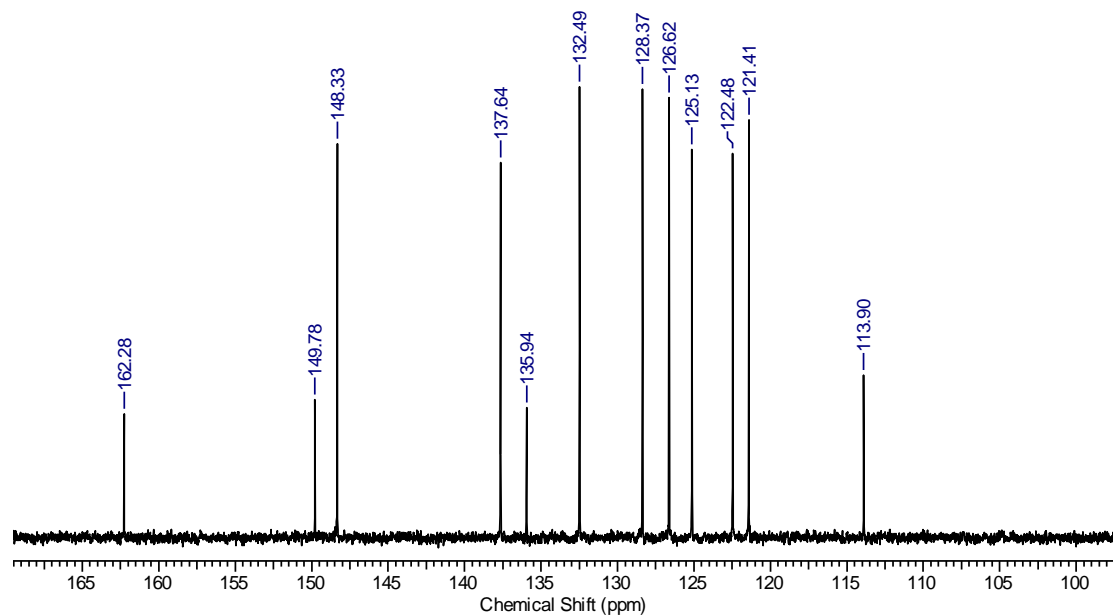
Figure 2.6 *¹³C{¹H} NMR spectrum of ligand **2.11** (CDCl₃, 75.48 MHz, 300K)*
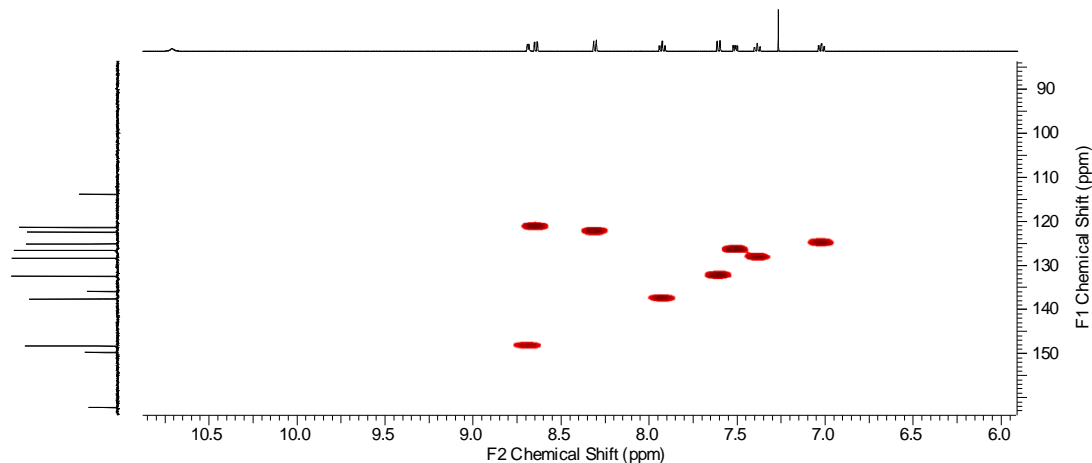
Figure 2.7 *Expanded ^{1}H-$^{13}C\{^{1}H\}$ NMR spectrum of ligand **2.11** (CDCl$_3$, 300K)*

2.3.3 X-ray Crystal Structure for Ligand 2.13

Colourless prisms suitable for X-ray crystallography were obtained from a concentrated methanol solution. Ligand **2.13** crystallised in a triclinic cell and structural solution was performed in the space group $P\,\bar{1}$ with the asymmetric unit containing one molecule. The molecular structure is shown in **Figure 2.8** and selected bond lengths and angles are given in **Table 2.2**. Ligand **2.13** adopts an almost planar configuration, in which C(7)-N(2)-C(6)-C(5) shows a torsion angle between the pyridyl ring and aniline ring of 178.5(6)°. Intramolecular hydrogen bonding exists between N(2)-H and N(1) with bond distance of 2.718(8) Å, and between C(12)-H and O(1) with bond distance of 2.946(9) Å. Ligand **2.13** arranges itself in parallel planes along the *a* axis as shown in **Figure 2.9(a)**, and in alternating direction by 180° when viewed along the *c* axis as shown in **Figure 2.9(b)**. These planes are held together by intermolecular hydrogen bonding between C(8)-H and O(1) with bond distance of 3.279(9) Å (**Figure 2.9(c)**).
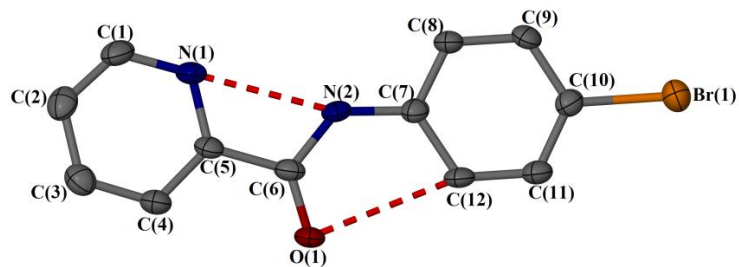
Figure 2.8 Molecular structure of ligand *2.13*. Displacement ellipsoids are at the 50% probability level.

Table 2.2 Selected bond lengths and angles for ligand *2.13* with s.u.s shown in parenthesis

Bond length (Å)		Bond Angle (°)	
C(1)-N(1)	1.378(10)	N(1)-C(5)-C(6)	117.8(6)
N(1)-C(5)	1.375(9)	C(5)-C(6)-O(1)	121.3(6)
C(5)-C(6)	1.513(10)	O(1)-C(6)-N(2)	124.6(6)
C(6)-O(1)	1.257(8)	C(6)-N(2)-C(7)	130.3(6)
C(6)-N(2)	1.378(9)	N(2)-C(7)-C(8)	117.9(6)
N(2)-C(7)	1.427(9)	C(9)-C(10)-Br(1)	118.4(5)
C(7)-C(8)	1.392(10)		
C(10)-Br(1)	1.943(7)		

(a)   (b)   (c)
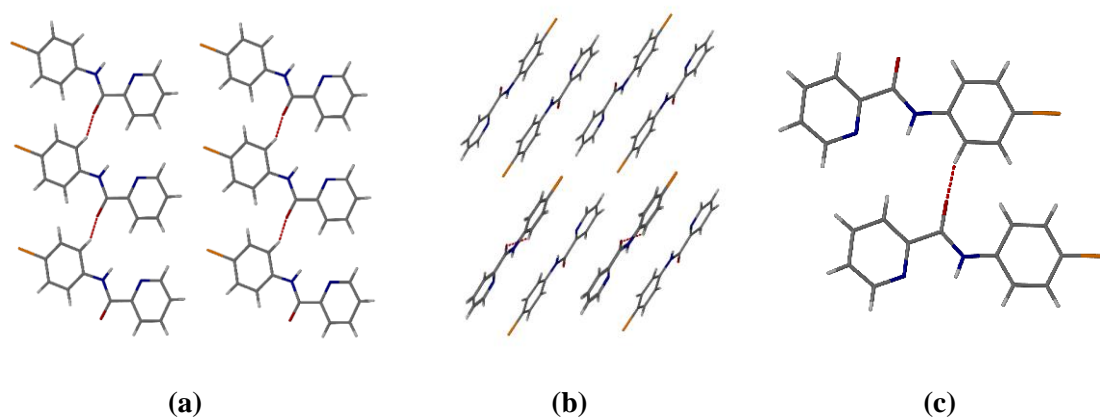
Figure 2.9 Packing diagram of ligand *2.13* viewed along the *(a)* a axis, *(b)* c axis, and *(c)* showing intermolecular hydrogen bond interactions

2.3.4   X-ray Crystal Structure for Ligand 2.15

White needle-like crystals suitable for X-ray crystallography were obtained from a concentrated methanol solution. Ligand **2.15** crystallised in a monoclinic cell and structural solution was performed in the space group *P 21/c* with the asymmetric unit containing one molecule. The molecular structure is shown in **Figure 2.10** and selected bond lengths and angles are given in **Table 2.3**. Similarly as previously synthesised picolinamide ligands, ligand **2.15** adopts an almost planar configuration, in which the torsion angle between the pyridyl ring and aniline ring N(1)-C(5)-C(6)-N(2) is 9.2(16)°. Intramolecular hydrogen bonding exists in ligand **2.15** between N(2)-H and N(1), C(12)-H and O(1), and N(2)-H and Br(1) with bond distances of 2.679(14) Å, 2.888(14) Å, and 3.080(8) Å respectively. **Figure 2.11(a)** and **(b)** show the packing diagrams of ligand **2.15**. When packed, the molecule stacks in a herringbone motif along the *a*-axis, and in layers along the *b*-axis with the molecule alternating direction by 180°. These planes are held together by intermolecular hydrogen bonding between C(4)-H and O(1) with bond distance of 3.323(15) Å (**Figure 2.12**).
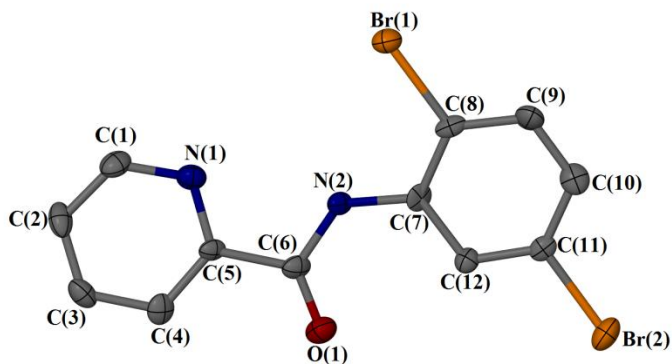
Figure 2.10 *Molecular structure of ligand **2.15**. Displacement ellipsoids are at the 50% probability level.*

Table 2.3 *Selected bond lengths and angles for ligand **2.15** with s.u.s shown in*

parenthesis

Bond	Distance (Å)	Bond	Angle (°)
C(1)-N(1)	1.369(16)	N(1)-C(5)-C(6)	117.5(10)
N(1)-C(5)	1.348(13)	C(5)-C(6)-O(1)	122.7(11)
C(5)-C(6)	1.523(16)	O(1)-C(6)-N(2)	124.9(11)
C(6)-O(1)	1.222(13)	C(6)-N(2)-C(7)	128.6(9)
C(6)-N(2)	1.384(14)	N(2)-C(7)-C(8)	118.2(10)
N(2)-C(7)	1.417(15)	C(7)-C(8)-Br(1)	120.4(9)
C(7)-C(8)	1.414(16)	C(12)-C(11)-Br(2)	116.0(8)
C(8)-Br(1)	1.916(10)		
C(11)-Br(2)	1.910(11)		

(a)	(b)
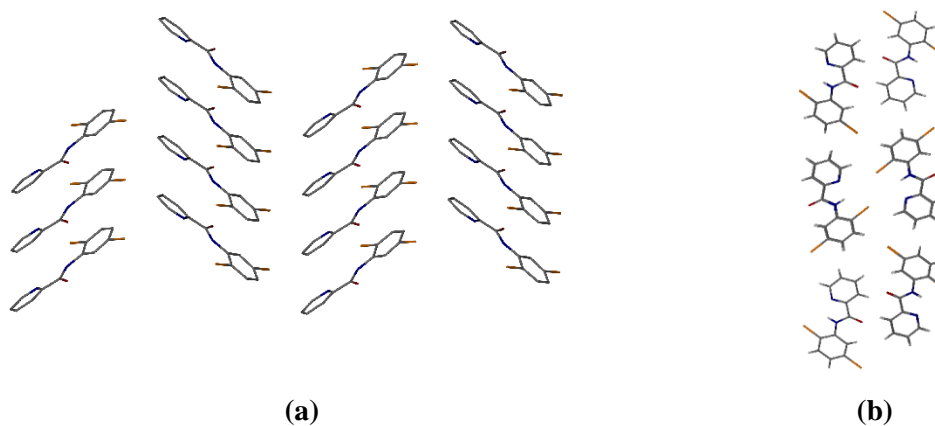
Figure 2.11 *Packing diagram of ligand **2.15** viewed along the (**a**) a axis (**b**) b axis.*

Hydrogen atoms are omitted for clarity.
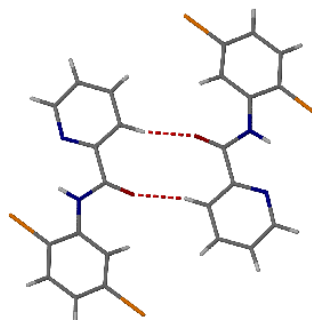
Figure 2.12 *Intermolecular hydrogen bond interactions in ligand **2.15***

2.4   References

1.   B. Alberts, A. Johnson, J. Lewis, M. Raff, K. Roberts and P. Walter, *Molecular Biology of the Cell*, Garland Science, New York, 2007.

2.   B. Testa and J. M. Mayer, *Hydrolysis in Drug and Prodrug Metabolism*, John Wiley & Sons, Switzerland, 2003.

3.   A. P. Swain and S. K. Naegele, *J. Am. Chem. Soc.*, 1957, **79**, 5250-5253.

4.   A. J. Robichaud, D. W. Engers, C. W. Lindsley and C. R. Hopkins, *ACS Chem. Neurosci.*, 2011, **2**, 433-449.

5.   T.-T. Huang, Y.-C. Huang, X.-Y. Qing, Y. Xia, X. Luo, T.-H. Ye and L.-T. Yu, *Molecules*, 2012, **17**, 6317-6330.

6.   S. Dutta, S. Pal and P. K. Bhattacharya, *Polyhedron*, 1999, **18**, 2157-2162.

7.   D. J. Barnes, R. L. Chapman, R. S. Vagg and E. C. Watton, *J. Chem. Eng. Data*, 1978, **23**, 349-350.

8.   D. W. Margerum, *Pure & Appl. Chem.*, 1983, **55**, 23-34.

9.   A. J. Canty and C. V. Lee, *Inorg. Chim. Acta*, 1981, **54**, L205-L206.

10. T. J. Collins, *Acc. Chem. Res.*, 1994, **27**, 279-285.

11. K. Rafferty, Ph.D Thesis, University of Leeds, Leeds, 2008.

12. Z. Almodares, S. J. Lucas, B. D. Crossley, A. M. Basri, C. M. Pask, A. J. Hebden, R. M. Phillips and P. C. McGowan, *Inorg. Chem.*, 2014, **53**, 727-736.

CHAPTER 3

Synthesis and Characterisation of Functionalised *Bis*-Picolinamide Ruthenium Dichloride Complexes

3   Synthesis of Ruthenium Dichloride Complexes

3.1   Introduction

This chapter discusses the synthesis and characterisation of novel *bis*-picolinamide ruthenium (III) dichloride complexes. Ruthenium picolinamide complexes of the type ML_2X_2 have not been reported in the literature previously, nor have been attempted within the McGowan group before. The aim is to add a new series of complexes within the McGowan group and to study the reaction involving coordination chemistry of ruthenium together with the biological properties of the complexes.

3.2   Synthesis of *bis*-Picolinamide Ruthenium (III) Dichloride ($RuCl_2L_2$) Complexes

The design of *bis*-picolinamide ruthenium (III) dichloride ($RuCl_2L_2$) complexes involves planar aromatic groups, a carbonyl group and an acidic amide proton on the ligands, which may contribute to their interaction with the DNA chain. Also, the halide ligands bound to the metal centre and the various substituents on the aromatic phenyl rings could contribute to modify the complexes' hydrolysis, hydrophobicity and anti-cancer properties. **Scheme 3.1** outlines the general synthesis for these complexes, where the reaction proceeds via direct addition of two equivalents of ligand to the ruthenium precursor in the presence of triethylamine, and induces the binding between the ligands and ruthenium. Triethylamine in the reaction acts as a base in order to deprotonate the hydrogen atom of NH from one of the picolinamide ligands, forming triethylamine hydrochloride salt, to give an *(N,N)*-coordination of the ligand to the ruthenium metal centre. A number of structural isomers are possible for complexes of the type RuX_2L_2 in solution, shown in **Figure 3.1**.[1-4]

$$RuCl_3.3H_2O \ + \ 2 \quad \text{[picolinamide ligand]} \xrightarrow[\substack{30ml \ Ethanol \\ 1 \ eq. \ Et_3N}]{Reflux \ 2 \ h} \quad \text{[Ru complex]} \quad + \quad Et_3NH^+Cl^-$$
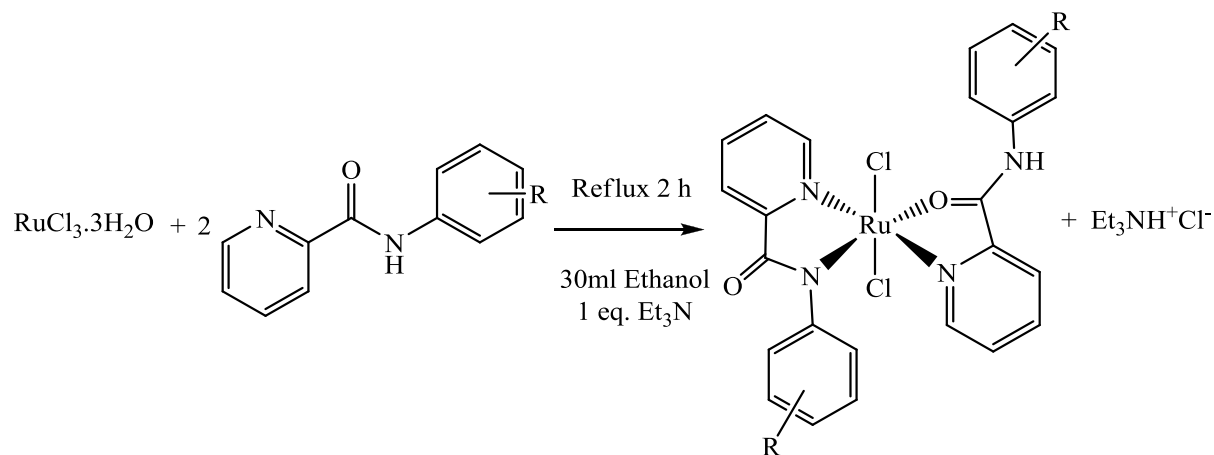
R	Complex	Yield
H	**3.1**	74%
2'-F	**3.2**	50%
4'-F	**3.3**	52%
2',4'-F	**3.4**	72%
2',5'-F	**3.5**	28%
2'-Cl	**3.6**	58%
3'-Cl	**3.7**	55%
4'-Cl	**3.8**	28%
2',4'-Cl	**3.9**	44%
2',5'-Cl	**3.10**	40%
2'-Br	**3.11**	46%
3'-Br	**3.12**	62%
4'-Br	**3.13**	44%
2',4'-Br	**3.14**	51%
2',5'-Br	**3.15**	54%
2'-I	**3.16**	33%

Scheme 3.1 *Synthesis of bis-picolinamide ruthenium (III) dichloride complexes*
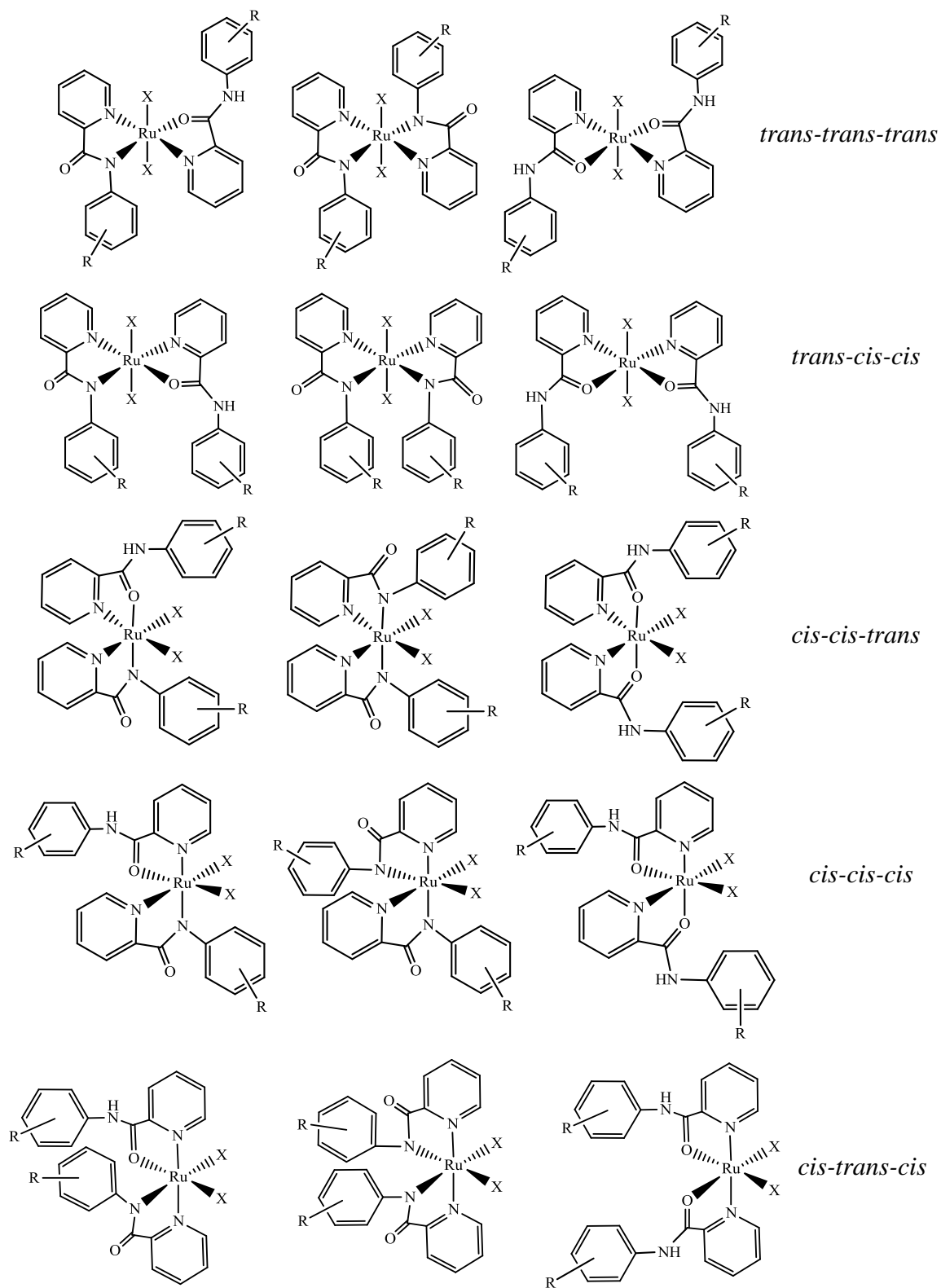
Figure 3.1 *Possible isomers of bis-picolinamide ruthenium dihalide complexes*

3.3   Characterisation of *bis*-Picolinamide Ruthenium (III) Dichloride Complexes

Bis-picolinamide ruthenium (III) dichloride complexes were prepared *via* **Scheme 3.1**, where two equivalents of the substituted picolinamide ligands were added to one equivalent of $RuCl_3.3H_2O$ in ethanol and heated under reflux for 2 hours. Complexes **3.1** - **3.16** were obtained as pure products in yields ranging from 28-74% and characterised using IR, ES-MS, elemental analysis and single crystal X-Ray diffraction. These complexes were found to be soluble in polar solvents, including acetonitrile, methanol, dichloromethane, chloroform and acetone, producing intense red-orange solutions.

The IR spectra of complexes **3.1** to **3.16** are very similar, with several bands of different intensities in the 1600-400 cm^{-1} area. A comparison was made between the spectra of the uncoordinated ligands and of the complexes. It can be seen that the CO and NH stretches were both shifted to lower wavenumber when the ligands were bonded to the metal centre. In the IR spectrum of these ruthenium complexes, there are two stretches for the NH group within the region 3000-3500 cm^{-1}, and one strong stretch for the CO group with a weak split in the 1548-1618 cm^{-1} region. The IR spectrum for ligand **2.11** and complex **3.11** are shown as an example of the comparison in **Figure 3.2**. Magnetic susceptibility measurements have shown that all of the complexes are low-spin d^5 with unpaired one-electron ($\mu_{eff} = 1.83$ - 2.53), which corresponds to the +3 state of ruthenium ($\mu_{eff} = 1.73$).

Three different types of structural isomers have been shown to exist for these complexes, which are the *cis-cis-cis, cis-trans-cis* and *trans-trans-trans* structural isomers confirmed by their single crystal structures. X-ray crystallography has been used to show the geometry of the different structural isomers, as well as to verify the coordination mode of the ligands in the complexes. The ligands are bonded in *N,N-* and *N,O-* coordination modes to the ruthenium metal centre. Single crystal structures and data are shown for complexes **3.1**, **3.3**, **3.5**, **3.6**, **3.7**, **3.9**, **3.11**, **3.12**, **3.13**, **3.14** and **3.16**, which were recrystallised by vapour diffusion, either from methanol/hexane or methanol/pentane.

3.4   IR Data for Ligand 2.11 and Complex 3.11

The IR spectra, with wavenumbers between 4000-450 cm^{-1}, of ligand **2.11** and complex **3.11** are shown in **Figure 3.2**. In the spectrum of the uncoordinated ligand, a strong CO stretch is observed at 1691 cm^{-1}, and is shifted to 1590 cm^{-1} showing a weak split of the stretch into two bands. The aromatic CH stretching is seen at 3105 cm^{-1} for the ligand, which is shifted to 3065 cm^{-1}, and an NH stretching is at 3281 cm^{-1} seen shifted to 3202 cm^{-1} for the complex. This pattern is consistent for all of the *bis*-picolinamide ruthenium dichloride complexes reported in this chapter.
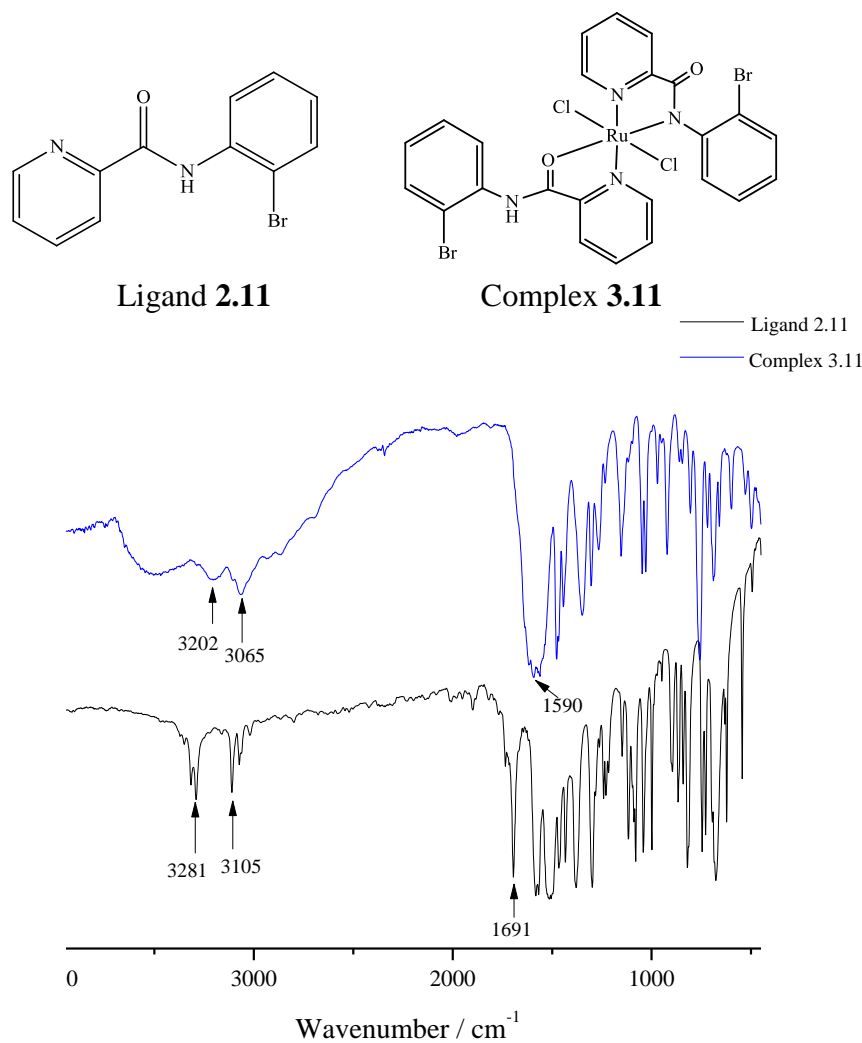
Figure 3.2 IR spectra of ligand 2.11 and complex 3.11

3.5   X-ray Crystallography Data for *bis*-Picolinamide Ruthenium (III) Dichloride Complexes

Single crystals suitable for x-ray crystallography were obtained by vapour diffusion of hexane/pentane into a methanolic solution of the crude product of the complexes. The *bis*-picolinamide ruthenium dichloride complexes have a distorted octahedral centre, with bond angles in the range 84.8°-107.7° between the ligands that are *cis* to each other, and bond angles of 170.5°-178.4° between the *trans* ligands about the ruthenium metal centre.

Both picolinamide ligands coordinated to the ruthenium metal centre adopt a non-planar configuration, in which the phenyl ring is almost perpendicular to the pyridine ring when it is coordinated in *N,N*-fashion, with a torsion angle for C(6)-N(2)-C(7)-C(12) of 73.2(4)°, and C(18)-N(4)-C(19)-C(20) of 45.3(5)° when it is *N,O*-coordinated (for complexes **3.5** and **3.11**). Complex **3.1a** has a torsion angle of 92.8(6)° between the planes of the phenyl ring and the pyridine ring for its *N,N*-coordinated ligand and of 47.8(9)° for its *N,O*-coordinated ligand. Complex **3.15** has an angle of 68.6(4)° and 51.5(5)° between the two planes for *N,N*- and *N,O*-coordinated ligands respectively.

The Ru-Cl bond distances for all the *bis*-picolinamide ruthenium dichloride complexes are similar, where one of the Ru-Cl bonds is longer than the other, with an average bond distance of 2.34 Å for Ru-Cl(1) and 2.37 Å for Ru-Cl(2). The average bond lengths of Ru(1)-N(1), Ru(1)-N(2), Ru(1)-N(3) and Ru(1)-O(2) for all complexes are 2.04 Å, 2.02 Å, 2.08 Å and 2.09 Å respectively, consistent and comparable with previously reported η^6-ruthenium arene picolinamide complexes.[5, 6]

3.5.1 X-ray Crystal Structure of Complex 3.1

Complex **3.1** crystallises as two different shapes of red crystals - red needles (complex **3.1a**) and red blocks (complex **3.1b**), both of which were suitable for x-ray crystallography. These crystals were obtained by vapour diffusion of pentane into a methanolic solution of the complex. Both sets of crystals **3.1a** and **3.1b** were crystallised in a monoclinic cell with the structural arrangement *trans-trans-trans* and *cis-cis-cis* respectively. Their structural solutions were performed in the space groups $P2_1/c$, and $P2_1/n$ respectively with the asymmetric unit containing one complex molecule and one methanol molecule for complex **3.1a** and two molecules of methanol for complex **3.1b**. The molecular structure for both complexes **3.1a** and **3.1b** are shown in **Figure 3.3** and selected bond lengths and angles are given in **Table 3.1**.

| (a) | (b) |

Figure 3.3 *Molecular structure of complex **3.1** showing (**a**) trans-trans-trans and (**b**) cis-cis-cis structural arrangements. Displacement ellipsoids are at the 50% probability level. Hydrogen atoms are omitted for clarity.*

Table 3.1 *Selected bond lengths and angles for complex **3.1a** and **3.1b** with s.u.s*

shown in parenthesis

Bond length (Å) / angle (°)	3.1a	3.1b
Ru(1)-Cl(1)	2.3408(14)	2.3540(9)
Ru(1)-Cl(2)	2.3498(13)	2.3769(9)
Ru(1)-N(1)	2.037(4)	2.018(3)
Ru(1)-N(2)	2.008(4)	1.997(3)
Ru(1)-N(3)	2.102(4)	2.045(3)
Ru(1)-O(2)	2.067(3)	2.087(3)
Cl(1) - Ru(1) - Cl(2)	175.93(5)	96.16(3)
N(1) - Ru(1) - O(2)	96.51(16)	175.63(10)
N(2) - Ru(1) - O(2)	175.18(16)	96.34(11)
N(2) - Ru(1) - N(3)	106.92(16)	86.23(11)
N(1) - Ru(1) - N(3)	174.22(16)	98.72(11)

Complex **3.1a** arranged itself into a diagonal linear distribution when packed along the *b*-axis as shown in **Figure 3.4**, held by intermolecular hydrogen bond between one methanol molecule with three complex molecules involving the amide group of one molecule (bond distance N(4)-O(3) of 2.756(6) Å), the carbonyl group of the second molecule (bond distance O(3)-O(1) of 2.699(5) Å) and the hydrogen of the phenyl ring of the third molecule (bond distance C(11)-O(3) of 3.329(7) Å). There is also an intramolecular hydrogen bonding between the carbonyl group and the hydrogen of the phenyl ring within a molecule (bond distance C(20)-O(2) of 2.920(9) Å).

*Figure 3.4 Packing diagram of complex **3.1a** viewed along the b-axis showing intermolecular hydrogen bond interactions between molecules. Hydrogen atoms are omitted for clarity.*

Complex **3.1b** packed in rows alternately along the *b*-axis, with the molecules pointing in alternate directions, as shown in **Figure 3.5a**. The molecules are held together by intermolecular hydrogen bonding (**Figure 3.5b**), between the amide group of a complex molecule with the oxygen of one methanol molecule (bond distance (N(4)-O(3) of 2.766(4) Å), between the two methanol molecules (bond distance O(3)-O(4) of 2.675(4) Å), between the second methanol molecule with the carbonyl of the second complex molecule (bond distance O(4)-O(1) of 2.673(4) Å), and between the carbonyl of the second complex molecule with the hydrogen of a pyridyl ring of the third complex molecule (bond distance O(1)-C(13) of 3.251(5) Å).

| (a) | (b) |
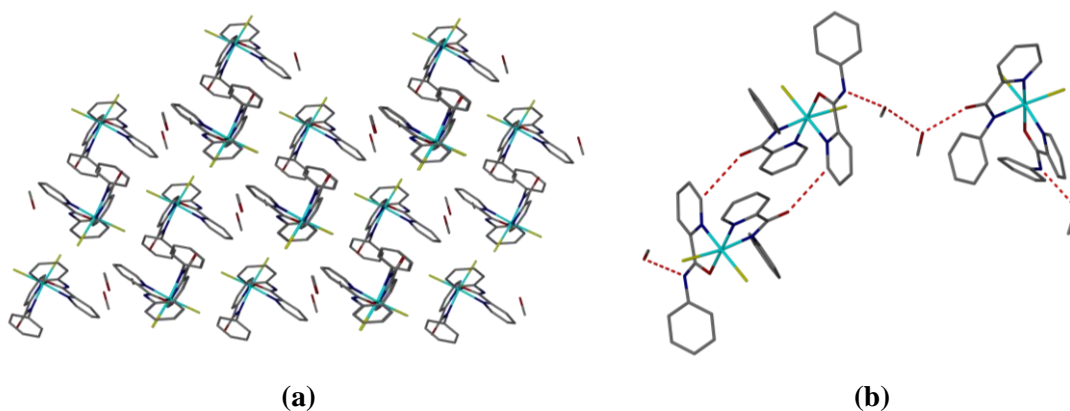
*Figure 3.5 (a) Packing diagram of complex **3.1b** viewed along the b-axis; (b) Intermolecular hydrogen bond interactions between three complex molecules and two methanol molecules. Hydrogen atoms are omitted for clarity.*

3.5.2   X-ray Crystal Structure of Complex 3.3

Red prisms of complex **3.3** suitable for X-ray crystallography were obtained *via* vapour diffusion of hexane into a methanolic solution of the complex. Complex **3.3** crystallised in a monoclinic cell with the arrangement of *trans-trans-trans* and structural solution was performed in the space group $P2_1/n$. The asymmetric unit contains one complex molecule. The molecular structure is shown in **Figure 3.6** and selected bond lengths and angles are given in **Table 3.2**.

Figure 3.6 *Molecular structure of complex **3.3**. Displacement ellipsoids are at the 50% probability level. Hydrogen atoms are omitted for clarity.*

Table 3.2 *Selected bond lengths and angles for complex **3.3** with s.u.s shown in parenthesis*

Bond length (Å)		Bond angle (°)	
Ru(1)-Cl(1)	2.3318(10)	Cl(1) - Ru(1) - Cl(2)	176.60(5)
Ru(1)-Cl(2)	2.3533(10)	N(1) - Ru(1) - O(2)	97.82(16)
Ru(1)-N(1)	1.999(3)	N(2) - Ru(1) - O(2)	176.38(16)
Ru(1)-N(2)	2.036(3)	N(2) - Ru(1) - N(3)	105.90(18)
Ru(1)-N(3)	2.113(3)	N(1) - Ru(1) - N(3)	175.45(18)
Ru(1)-O(2)	2.087(3)		

Complex **3.3** packed in a linear arrangement along the *a*-axis as shown in **Figure 3.7a**. **Figure 3.7b** shows the intermolecular hydrogen bonding interactions, in which one complex molecule interacts with three other complex molecules. The chloride ligand of the first molecule forms a hydrogen bond with the hydrogen on the pyridyl ring of the second molecule (bond distance Cl(1)-C(2) of 3.558(4) Å). The second chloride ligand of the first molecule interacts with two other complex molecules, one with the amide group of the second molecule (bond distance Cl(2)-N(4) of 3.283(3) Å), and the other with the hydrogen on the phenyl ring of the third molecule (bond distance Cl(2)-C(8) of 3.596(4) Å).

(a)   **(b)**
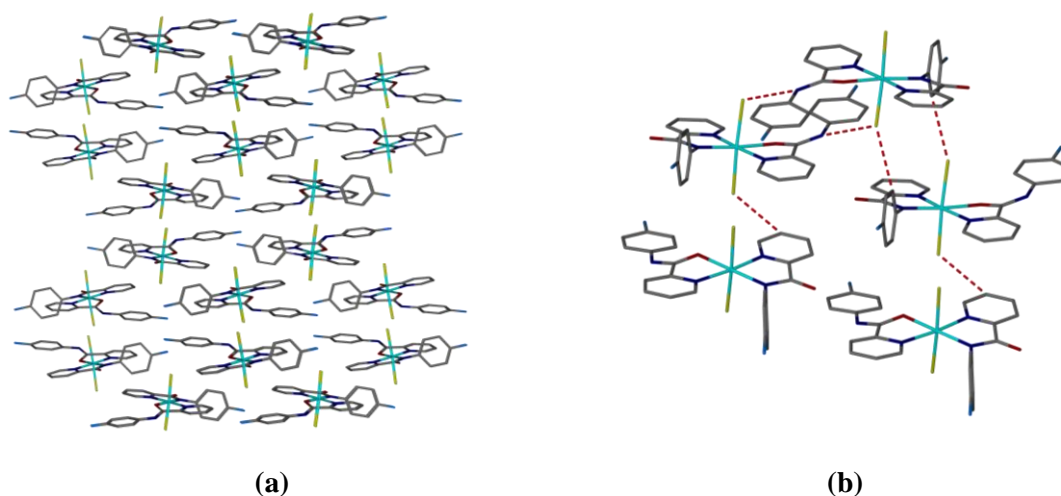
*Figure 3.7 (a) Packing diagram of complex **3.3** viewed along the a-axis; (b)*
Intermolecular hydrogen bond interactions between the complex molecules. Hydrogen
atoms are omitted for clarity.

3.5.3   X-ray Crystal Structure of Complex 3.5

Thin red rectangular crystals of complex **3.5** suitable for X-ray crystallography were obtained *via* vapour diffusion of hexane into a methanol solution of the complex. Complex **3.5** crystallised in a triclinic cell with the arrangement of *trans-trans-trans* and structural solution was performed in the space group $P\bar{1}$. The asymmetric unit contains one complex molecule and one methanol molecule. The molecular structure is shown in **Figure 3.8** and selected bond lengths and angles are given in **Table 3.3**.
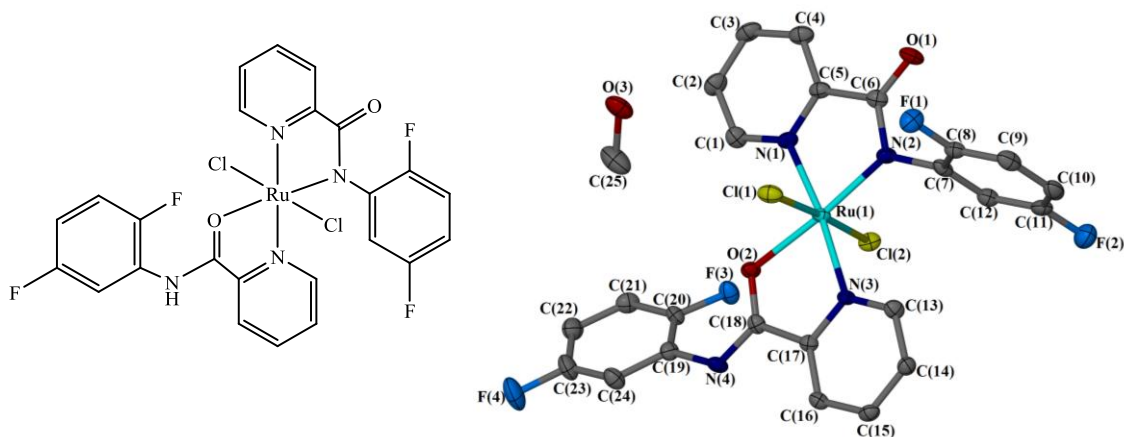
Figure 3.8 *Molecular structure of complex **3.5**. Displacement ellipsoids are at the 50% probability level. Hydrogen atoms are omitted for clarity*

Table 3.3 *Selected bond lengths and angles for complex **3.5** with s.u.s shown in parenthesis*

Bond length (Å)		Bond angle (°)	
Ru(1)-Cl(1)	2.3328(9)	Cl(1) - Ru(1) - Cl(2)	176.80(3)
Ru(1)-Cl(2)	2.3664(9)	N(1) - Ru(1) - O(2)	95.46(11)
Ru(1)-N(1)	2.036(3)	N(2) - Ru(1) - O(2)	174.21(10)
Ru(1)-N(2)	2.027(3)	N(2) - Ru(1) - N(3)	107.74(11)
Ru(1)-N(3)	2.102(3)	N(1) - Ru(1) - N(3)	173.36(11)
Ru(1)-O(2)	2.077(2)		

Complex **3.5 is** arranged in a diagonal linear distribution when viewed along the *a*-axis as shown in **Figure 3.9a**. Several intermolecular interactions are seen within the packing arrangement. Each molecule interacts with two adjacent molecules, where two molecules are held in pairs by hydrogen bonds with a methanol molecule, between the amide group of one molecule (bond distance N(4)-O(3) of 2.760(5) Å) and the carbonyl group of the second molecule (bond distance O(3)-O(1) of 2.689(4) Å) (**Figure 3.9b**). A second interaction is held by intermolecular hydrogen bonding between the fluorine of the phenyl ring and the hydrogen of the pyridyl ring (bond distance C(3)-F(3) of 3.241(5) Å), as shown in **Figure 3.9c**.

(b)

(a)   **(c)**
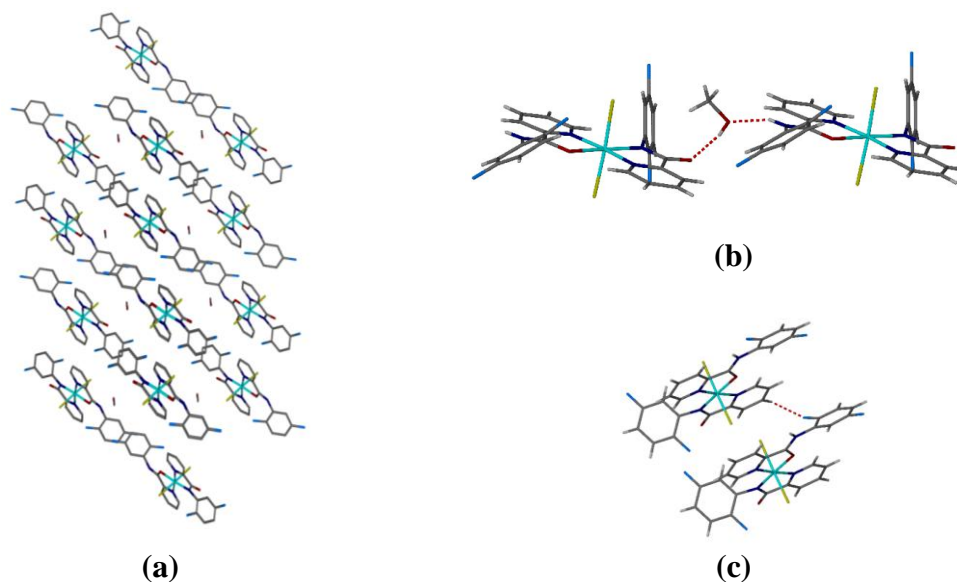
Figure 3.9 (a) Packing diagram of complex 3.5 viewed along the a-axis. Hydrogen atoms are omitted for clarity; (b) Intermolecular hydrogen bond interactions with a methanol molecule; (c) Intermolecular hydrogen bond interactions with fluorine substituent

3.5.4   X-ray Crystal Structure of Complex 3.6

Red fragments of complex **3.6** suitable for X-ray crystallography were obtained *via* vapour diffusion of hexane into a methanol solution of the complex. Complex **3.6** crystallised in a monoclinic cell with the arrangement of *cis-cis-cis* and structural solution was performed in the space group $P2_1/c$. The asymmetric unit contains two molecules of the complex and two molecules of methanol, with one of the complex molecule shown to have a positional disorder with an extra phenyl ring attached on the N atom of the *(N,O)*-coordinated ligand. The molecular structure of complex **3.6** is shown in **Figure 3.10** and selected bond lengths and angles are given in **Table 3.4**.

Figure 3.10 *Molecular structure of complex* ***3.6***. *Displacement ellipsoids are at the*
50% probability level. Hydrogen atoms are omitted for clarity

Table 3.4 *Selected bond lengths and angles for complex* ***3.6*** *with s.u.s shown in*
parenthesis

Bond length (Å)		Bond angle (°)	
Ru(1)-Cl(1)	2.345 (2)	Cl(1) - Ru(1) - Cl(2)	95.39(9)
Ru(1)-Cl(2)	2.381(3)	N(1) - Ru(1) - O(2)	176.8(3)
Ru(1)-N(1)	2.030(8)	N(2) - Ru(1) - O(2)	97.1(3)
Ru(1)-N(2)	2.013(8)	N(2) - Ru(1) - N(3)	87.7(3)
Ru(1)-N(3)	2.071(8)	N(1) - Ru(1) - N(3)	100.8(3)
Ru(1)-O(2)	2.091(7)		

3.5.5 X-ray Crystal Structure of Complex 3.7

Complex **3.7** crystallises as two different shapes of red crystals - red needles (complex **3.7a**) and red prisms (complex **3.7b**), both of which are suitable for x-ray crystallography. These crystals are obtained by vapour diffusion of pentane into a methanolic solution of the complex. The red needles crystallised in a triclinic cell with the structural arrangement *trans-trans-trans*, while the red prisms crystallised in a monoclinic cell with the structural arrangement *cis-cis-cis*. Their structural solutions were performed in the space group $P\bar{1}$ and $P2_1/n$ respectively, with the asymmetric unit containing one complex molecule for both complexes **3.7a** and **3.7b**, along with one methanol molecule for complex **3.7a**. The molecular structure for both complexes **3.7a** and **3.7b** are shown in **Figure 3.11** and selected bond lengths and angles are given in **Table 3.5**.

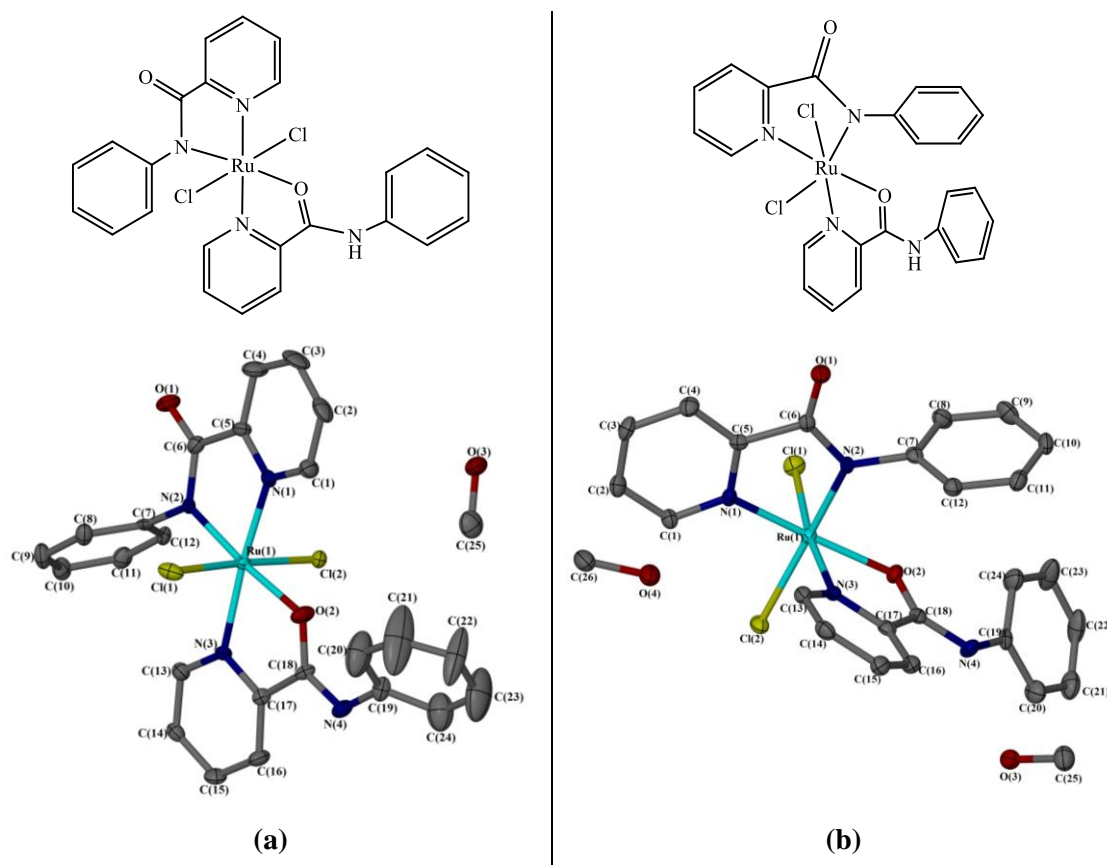| (a) | (b) |
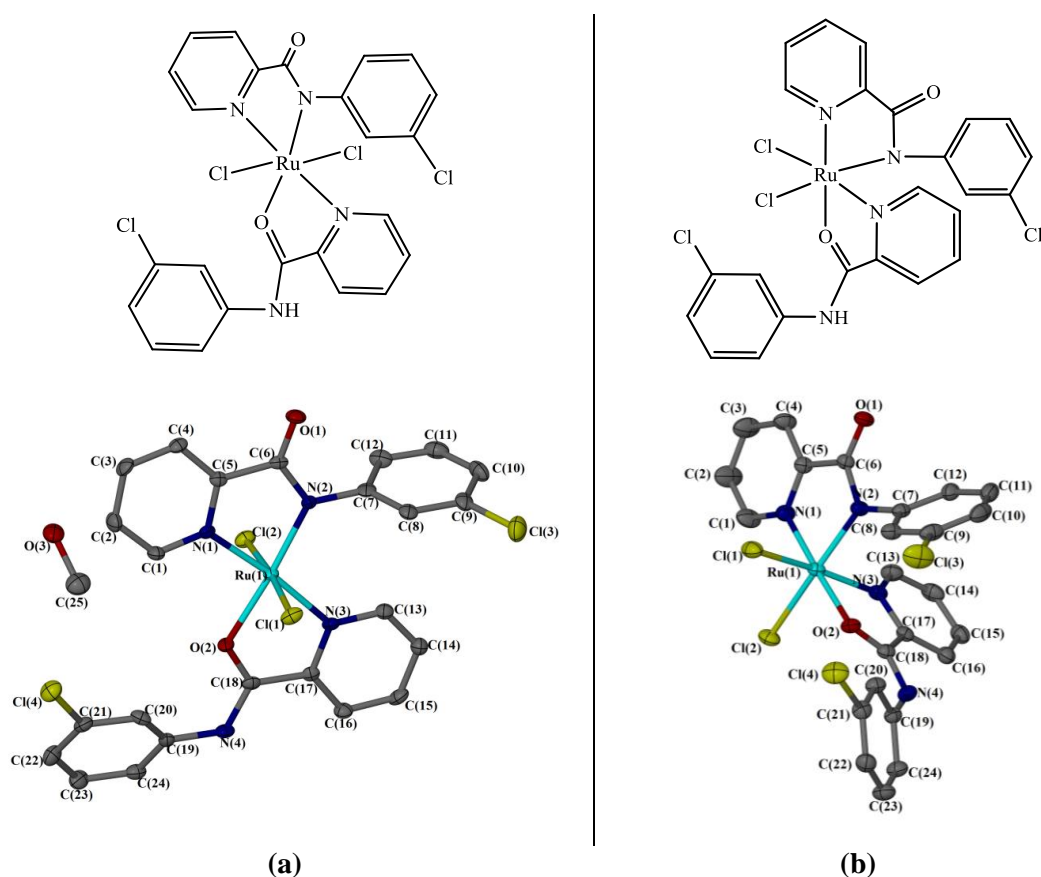
Figure 3.11 Molecular structure of complex *3.7* showing (*a*) trans-trans-trans and (*b*) cis-cis-cis structural arrangements. Displacement ellipsoids are at the 50% probability level. Hydrogen atoms are omitted for clarity

Table 3.5 *Selected bond lengths and angles for complexes **3.7a** and **3.7b** with s.u.s*

shown in parenthesis

Bond length (Å) / angle (°)	3.7a	3.7b
Ru(1)-Cl(1)	2.3355(9)	2.3594(6)
Ru(1)-Cl(2)	2.3362(9)	2.3848(5)
Ru(1)-N(1)	2.033(3)	2.0510(15)
Ru(1)-N(2)	2.006(3)	2.0270(14)
Ru(1)-N(3)	2.106(3)	2.0741(16)
Ru(1)-O(2)	2.061(2)	2.1089(12)
Cl(1) - Ru(1) - Cl(2)	174.66(3)	95.033(19)
N(1) - Ru(1) - O(2)	96.70(10)	177.80(6)
N(2) - Ru(1) - O(2)	175.10(10)	98.13(5)
N(2) - Ru(1) - N(3)	107.74(11)	88.07(6)
N(1) - Ru(1) - N(3)	173.84(10)	100.49(6)

Complex **3.7a** packed in a diagonal linear arrangement along the *a*-axis, as shown in **Figure 3.12a**, held together by intermolecular hydrogen bonding between two complex molecules and a methanol molecule with bond distance N(4)-O(3) of 2.831(4) Å and O(3)-O(1) of 2.782(3) Å to form a plane of complex molecules. Intermolecular hydrogen bonding interactions exists between three complex molecules with bond distance C(15)-Cl(1) of 3.409(4) Å, and Cl(2)-C(23) of 3.324(4) Å forming a second plane of complex molecules. These interactions are shown in **Figure 3.12b**.

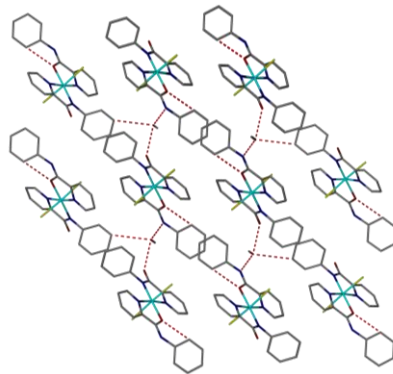**(a)**   **(b)**
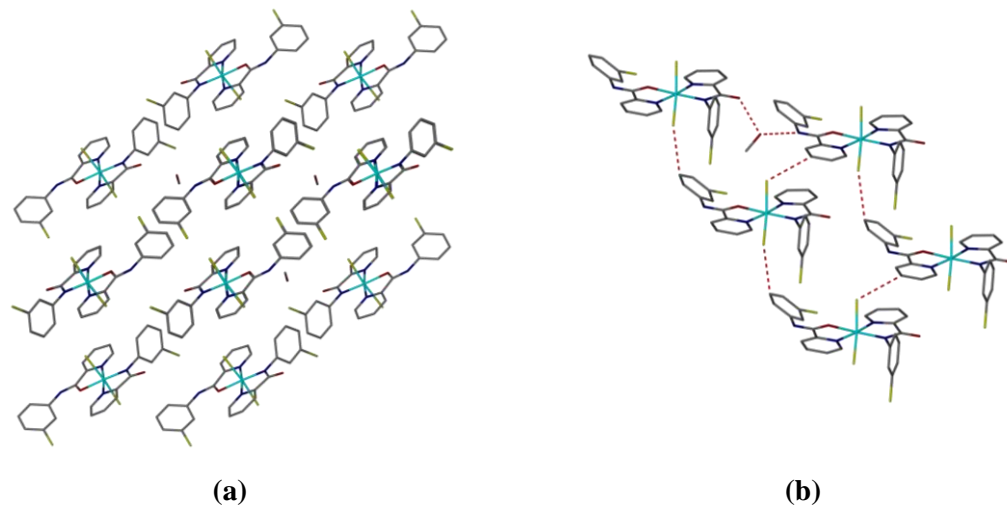
Figure 3.12 (a) Packing diagram of complex 3.7a along the a-axis; (b) Intermolecular hydrogen bonding interactions between molecules. Hydrogen atoms are omitted for clarity.

Complex **3.7b** packed in rows with a zig-zag pattern along the *a*-axis, as shown in **Figure 3.13**. Each molecule interacts with neighbouring molecules of the same row, *via* hydrogen bonds between the amide group of one molecule and the carbonyl group of the other molecule (bond distance N(4)-O(1) of 2.855(2) Å), as shown in **Figure 3.14a**. The row of complexes is held by intermolecular hydrogen bonding between C(2)-Cl(1) with a bond distance of 3.680(2) which can be seen in **Figure 3.14b**. The ligands also exhibit intramolecular hydrogen bonding with bond distances C(1)-Cl(2) of 3.347(4) and C(20)-O(2) of 2.866(2).
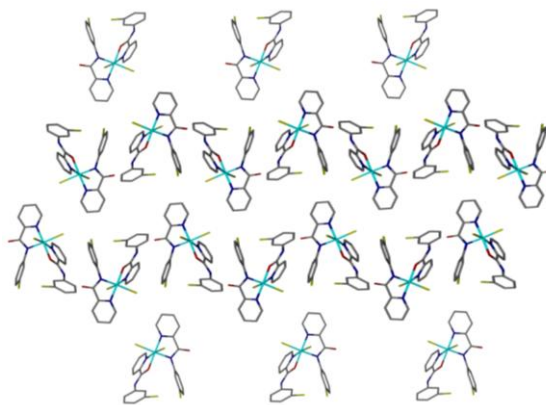
Figure 3.13 Packing diagram of complex 3.7b viewed along the a-axis. Hydrogen atoms are omitted for clarity.

(a)
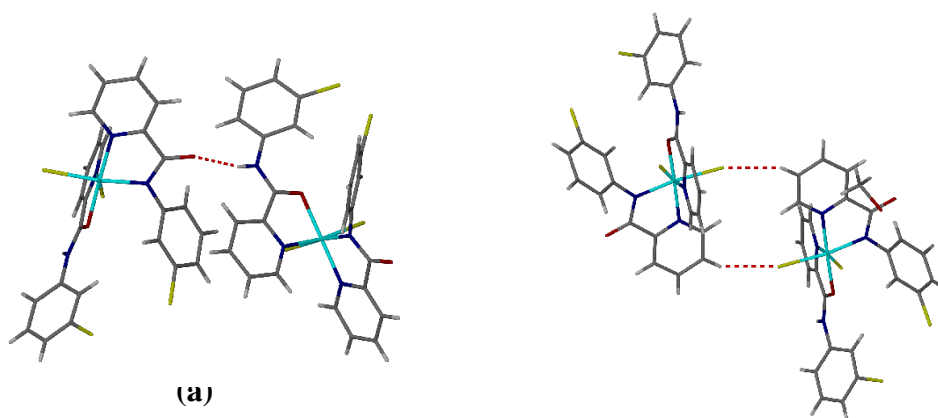
Figure 3.14 *Intermolecular hydrogen bond interactions of complex **3.7b** (**a**) along the rows and (**b**) between the rows*

3.5.6   X-ray Crystal Structure of Complex 3.9

Red cubic crystals of complex **3.9** suitable for X-ray crystallography were obtained *via* vapour diffusion of hexane into a methanol solution of the complex. Complex **3.9** crystallised in a triclinic cell with the arrangement of *trans-trans-trans* and structural solution was performed in the space group $P\,\overline{1}$. The asymmetric unit contains one complex molecule and one methanol molecule. The molecular structure is shown in **Figure 3.15** and selected bond lengths and angles are given in **Table 3.6**.
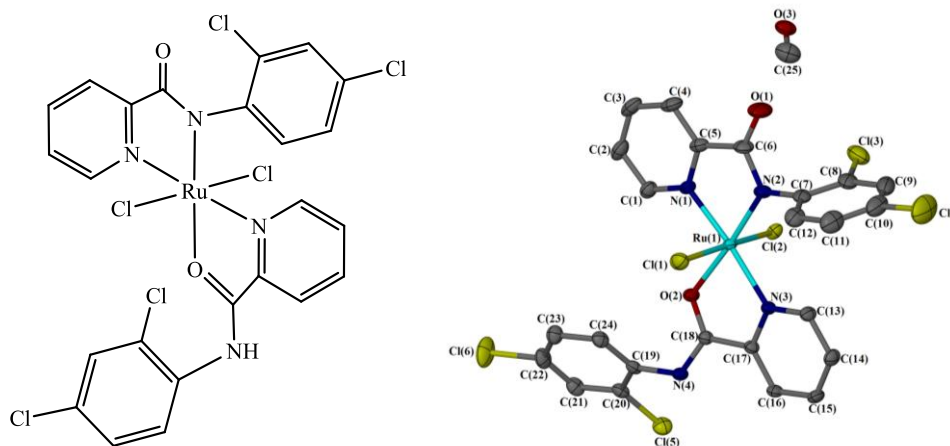
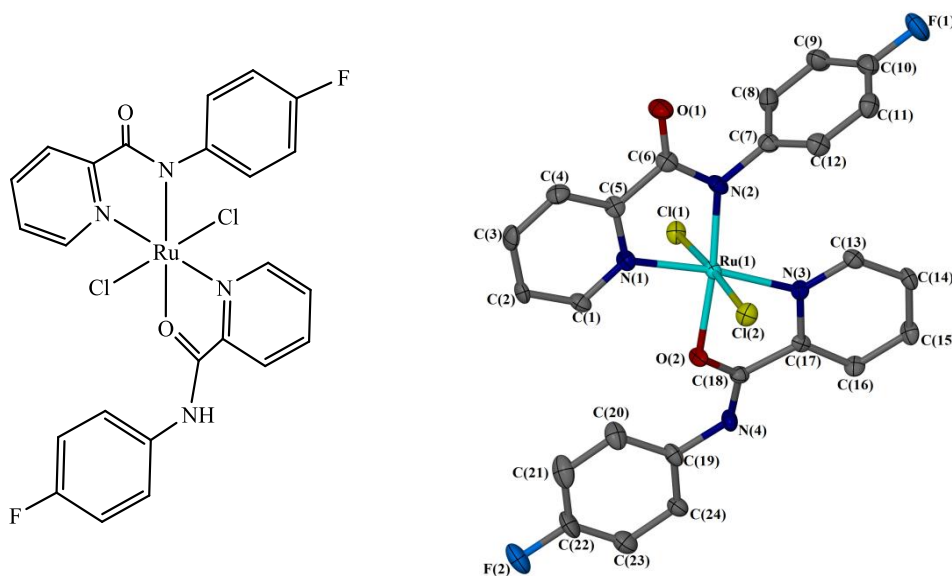***Figure 3.15*** *Molecular structure of complex **3.9**. Displacement ellipsoids are at the 50% probability level. Hydrogen atoms are omitted for clarity*

Table 3.6 Selected bond lengths and angles for complex 3.9 with s.u.s shown in parenthesis

Bond length (Å)		Bond angle (°)	
Ru(1)-Cl(1)	2.3543(6)	Cl(1) - Ru(1) - Cl(2)	173.54(18)
Ru(1)-Cl(2)	2.3767(5)	N(1) - Ru(1) - O(2)	96.08(6)
Ru(1)-N(1)	2.0514(15)	N(2) - Ru(1) - O(2)	175.25(6)
Ru(1)-N(2)	2.0273(15)	N(2) - Ru(1) - N(3)	106.95(6)
Ru(1)-N(3)	2.1219(15)	N(1) - Ru(1) - N(3)	173.80(6)
Ru(1)-O(2)	2.1056(13)		

Complex **3.9** packed in a diagonal linear distribution with a zig-zag pattern along the *a*-axis as shown in **Figure 3.16a**. Several intermolecular interactions are seen within the packing arrangement, as shown in **Figure 3.16b**. Two complex molecules are held in pairs by hydrogen bonds with a methanol molecule, between the amide group of one molecule (bond distance N(4)-O(3) of 2.899(3) Å) and the carbonyl group of the second complex molecule (bond distance O(3)-O(1) of 2.733(3) Å). A second interaction is held by intermolecular hydrogen bonding between the chlorine ligand and the hydrogen of the pyridyl ring of the third complex molecule (bond distance C(3)-Cl(2) of 3.593(4) Å). Another interaction is between one of the chloride substituent on the phenyl ring of the picolinamide ligand with the hydrogen of the pyridyl ring on another complex molecule forming a hydrogen bond (bond distance C(14)-Cl(6) of 3.652(3) Å).

(a)   (b)

Figure 3.16 (a) Packing diagram viewed along the a-axis of complex 3.9 (b) Intermolecular hydrogen bonding between molecules. Hydrogen atoms are omitted for clarity.

3.5.7   X-ray Crystal Structure of Complex 3.11

Red plates of complex **3.11** suitable for X-ray crystallography were obtained *via* vapour diffusion of pentane into a methanol solution of the complex. Complex **3.11** crystallised in a monoclinic cell with the arrangement of *trans-trans-trans* and structural solution was performed in the space group $P2_1/c$. The asymmetric unit contains one complex molecule and one methanol molecule. The molecular structure is shown in **Figure 3.17** and selected bond lengths and angles are given in **Table 3.7**.
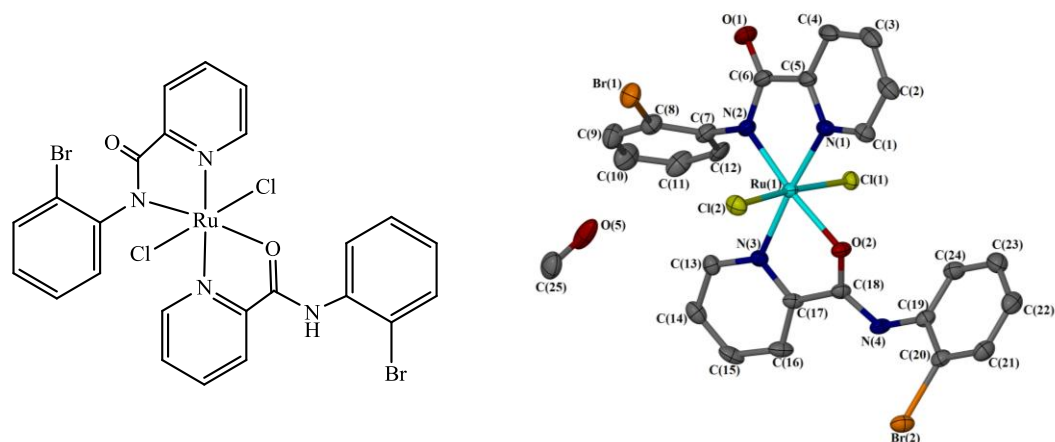
Figure 3.17 *Molecular structure of complex* **3.11**. *Displacement ellipsoids are at the 50% probability level. Hydrogen atoms are omitted for clarity.*

Table 3.7 *Selected bond lengths and angles for complex* **3.11** *with s.u.s shown in parenthesis*

Bond length (Å)		Bond angle (°)	
Ru(1)-Cl(1)	2.3452(9)	Cl(1) - Ru(1) - Cl(2)	174.27(3)
Ru(1)-Cl(2)	2.3914(8)	N(1) - Ru(1) - O(2)	96.76(10)
Ru(1)-N(1)	2.056(3)	N(2) - Ru(1) - O(2)	174.07(10)
Ru(1)-N(2)	2.036(3)	N(2) - Ru(1) - N(3)	106.13(11)
Ru(1)-N(3)	2.106(3)	N(1) - Ru(1) - N(3)	174.43(11)
Ru(1)-O(2)	2.095(2)		

Complex **3.11** packed in a herringbone motif along the *a*-axis as shown in **Figure 3.18**. Each molecule interacts with two adjacent complex molecules, held in pairs by hydrogen bonds with a methanol molecule, between the amide group of one complex molecule (bond distance N(4)-O(5) of 2.797(5) Å) and the carbonyl group of the second complex molecule (bond distance O(5)-O(1) of 2.672(5) Å).

Figure 3.18 *Packing diagram viewed along the a-axis of complex **3.11**, showing the intermolecular hydrogen bonding between molecules. Hydrogen atoms are omitted for clarity.*

3.5.8 X-ray Crystal Structure of Complex 3.12

Red cubic crystals of complex **3.12** suitable for X-ray crystallography were obtained *via* vapour diffusion of pentane into a methanol solution of the complex. Complex **3.12** crystallised in a monoclinic cell with the arrangement of *cis-cis-cis* and structural solution was performed in the space group $P2_1/n$. The asymmetric unit contains one complex molecule. The molecular structure is shown in **Figure 3.19** and selected bond lengths and angles are given in **Table 3.8**.
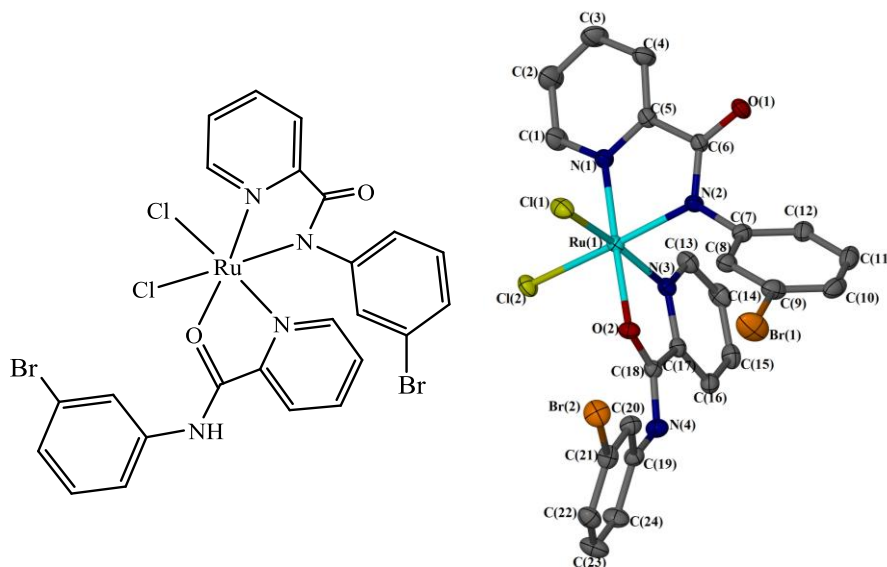
Figure 3.19 *Molecular structure of complex **3.12**. Displacement ellipsoids are at the 50% probability level. Hydrogen atoms are omitted for clarity*

Table 3.8 *Selected bond lengths and angles for complex **3.12** with s.u.s shown in parenthesis*

Bond length (Å)		Bond angle (°)	
Ru(1)-Cl(1)	2.3505(7)	Cl(1) - Ru(1) - Cl(2)	95.57(2)
Ru(1)-Cl(2)	2.3833(7)	N(1) - Ru(1) - O(2)	178.36(8)
Ru(1)-N(1)	2.053(2)	N(2) - Ru(1) - O(2)	98.69(8)
Ru(1)-N(2)	2.029(2)	N(2) - Ru(1) - N(3)	87.81(8)
Ru(1)-N(3)	2.080(2)	N(1) - Ru(1) - N(3)	102.07(8)
Ru(1)-O(2)	2.1043(17)		

Complex **3.12** packed in rows with a zig-zag pattern along the *a*-axis, as shown in **Figure 3.20a**. A pair of molecules interacts *via* hydrogen bonds between the amide group of one molecule and the carbonyl group of the other molecule (bond distance N(4)-O(1) of 2.857(3) Å), which again interacts with another molecule between a chloride ligand and the hydrogen of a pyridyl ring (bond distance C(14)-Cl(2) of 3.670(3) Å) (**Figure 3.20b**).

(a)   (b)
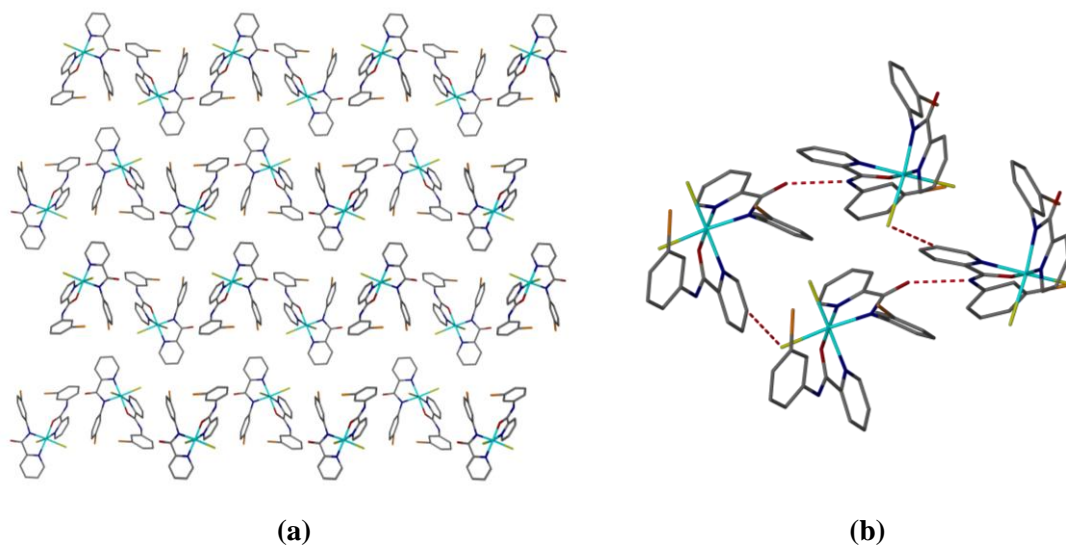
Figure 3.20 (a) Packing diagram viewed along the a-axis of complex 3.12 (b) Intermolecular hydrogen bonding between molecules. Hydrogen atoms are omitted for clarity.

3.5.9   X-ray Crystal Structure of Complex 3.13

Orange needles of complex **3.13** suitable for X-ray crystallography were obtained *via* vapour diffusion of pentane into a methanol solution of the complex. Complex **3.13** crystallised in a triclinic cell with the arrangement of *trans-trans-trans* and structural solution was performed in the space group $P\bar{1}$. The asymmetric unit contains one complex molecule and one methanol molecule. The molecular structure is shown in **Figure 3.21** and selected bond lengths and angles are given in **Table 3.9**.
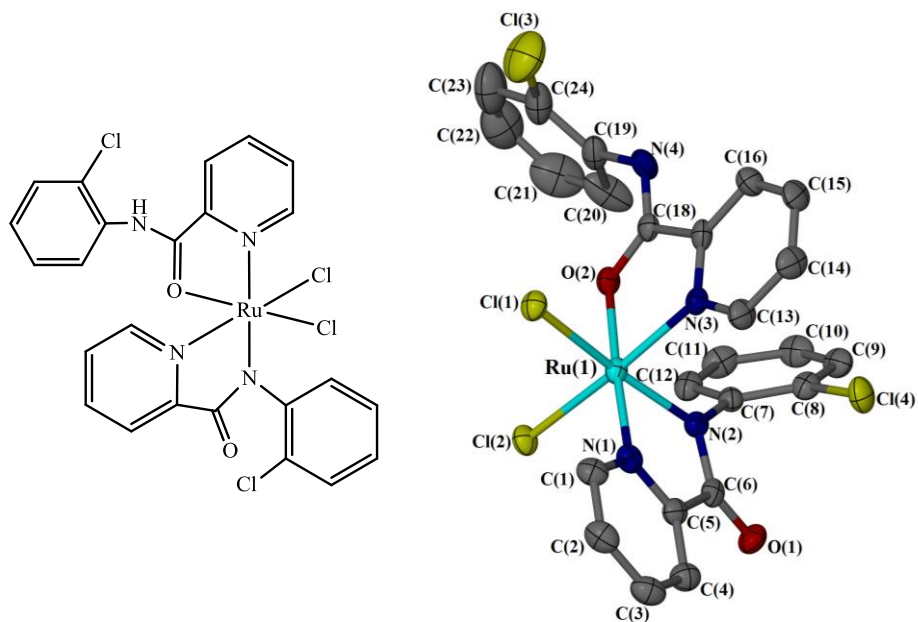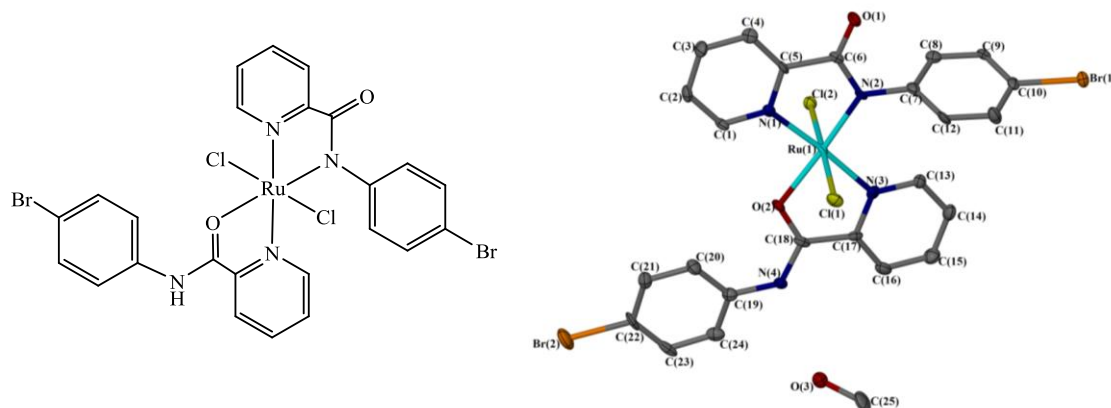
Figure 3.21 *Molecular structure of complex* **3.13**. *Displacement ellipsoids are at the 50% probability level. Hydrogen atoms are omitted for clarity.*

Table 3.9 *Selected bond lengths and angles for complex* **3.13** *with s.u.s shown in parenthesis*

Bond length (Å)		Bond angle (°)	
Ru(1)-Cl(1)	2.3397(13)	Cl(1) - Ru(1) - Cl(2)	176.59(5)
Ru(1)-Cl(2)	2.3425(14)	N(1) - Ru(1) - O(2)	97.83(16)
Ru(1)-N(1)	2.039(4)	N(2) - Ru(1) - O(2)	176.41(16)
Ru(1)-N(2)	1.996(4)	N(2) - Ru(1) - N(3)	105.86(18)
Ru(1)-N(3)	2.089(4)	N(1) - Ru(1) - N(3)	175.47(18)
Ru(1)-O(2)	2.100(4)		

Complex **3.13** packed in a linear arrangement along the *b*-axis, as shown in **Figure 3.22**. The complex molecules are held by intermolecular hydrogen bond between one methanol molecule with two complex molecules involving the amide group of one complex molecule (bond distance N(4)-O(3) of 2.850(6) Å) and the carbonyl group of the second molecule (bond distance O(3)-O(1) of 2.754(5) Å). Another intermolecular interaction is the hydrogen bonding between the bromine substituent of one molecule and the hydrogen of the pyridyl ring on another molecule (bond distance C(15)-Br(1) of 3.633(6) Å).
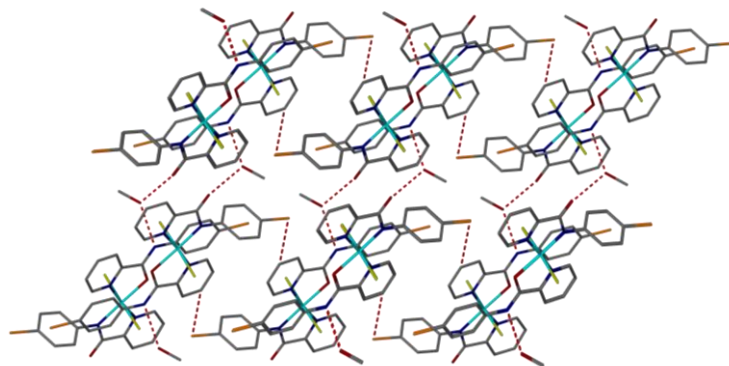
Figure 3.22 *Packing diagram viewed along the b-axis of complex **3.21**, showing the intermolecular hydrogen bonding between molecules. Hydrogen atoms are omitted for clarity.*

3.5.10 X-ray Crystal Structure of Complex 3.15

Red plates of complex **3.15** suitable for X-ray crystallography were obtained by vapour diffusion of pentane into a methanol solution of the complex. Complex **3.15** crystallised in a monoclinic cell with the arrangement *cis-trans-cis*, and structural solution was performed in the space group *P21/c*. The asymmetric unit contains one complex molecule and two methanol molecules. The molecular structure is shown in **Figure 3.23** and selected bond lengths and angles are given in **Table 3.10**.
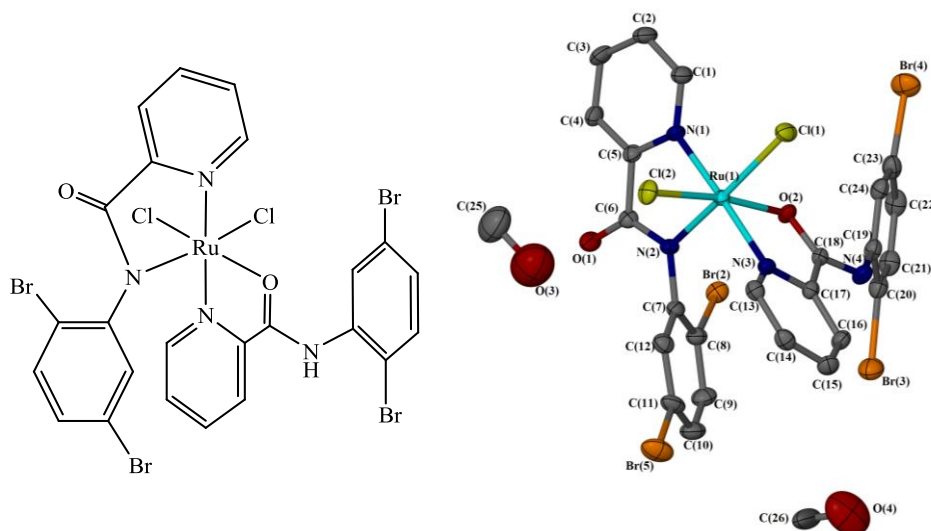
Figure 3.23 *Molecular structure of complex **3.15**. Displacement ellipsoids are at the 50% probability level. Hydrogen atoms are omitted for clarity.*

Table 3.10 *Selected bond lengths and angles for complex **3.15** with s.u.s shown in*

parenthesis

Bond Distance (Å)		Bond Angle (°)	
Ru(1)-Cl(1)	2.3462(10)	Cl(1)-Ru(1)-Cl(2)	94.71(4)
Ru(1)-Cl(2)	2.3943(10)	N(1) - Ru(1) - O(2)	98.88(10)
Ru(1)-N(1)	2.089(3)	N(2) - Ru(1) - O(2)	85.17(10)
Ru(1)-N(2)	2.052(3)	N(2) - Ru(1) - N(3)	97.05(11)
Ru(1)-N(3)	2.096(3)	N(1) - Ru(1) - N(3)	175.62(11)
Ru(1)-O(2)	2.113(2)		

Complex **3.15** packed in a herringbone motif along the *c*-axis (**Figure 3.24a**). A pair of molecules are held together by intermolecular hydrogen bonds between the amide group of one complex molecule and the oxygen of the carbonyl group of the second complex molecule (bond distance N(4)-O(1) of 2.776(4) Å). Another interaction between two complex molecules is *via* hydrogen bonding between one of the chloride ligands of one molecule with the hydrogen of the phenyl ring of another molecule (bond distance C(10)-Cl(2) of 3.574(4) Å). These interactions are as shown in **Figure 3.24b**. There is also a hydrogen bonding between two methanol molecules, however they do not interact within the packing of the complex molecules

(a)   (b)
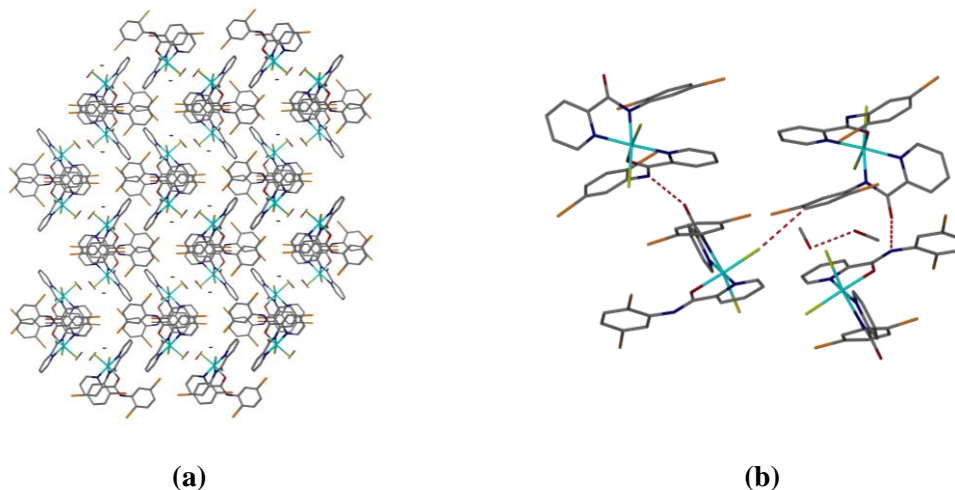
Figure 3.24 (a) *Herringbone packing of complex **3.15** viewed along the c-axis;*
(b) Intermolecular hydrogen bonding between a pair of complex molecules. Hydrogen
atoms are omitted for clarity.

3.5.11 X-ray Crystal Structure of Complex 3.16

Complex **3.16** crystallises as two different types of crystals - orange needles (complex **3.16a**) and red blocks (complex **3.16b**), which were suitable for x-ray crystallography. These crystals were obtained by vapour diffusion of pentane into a methanolic solution of the complex. The orange needles crystallised in an orthorhombic cell with the structural arrangement *trans-trans-trans*, while the red blocks crystallised in a monoclinic cell with the structural arrangement *cis-trans-cis*. Their structural solution was performed in the space group $P2_12_12_1$ and $P2_1/n$ respectively, with the asymmetric unit containing one complex molecule for both complexes **3.16a** and **3.16b**, along with one methanol molecule for complex **3.16a**. Complex **3.16b** has shown a positional disorder with an extra phenyl ring attached on the N2 atom of the *(N,N)*-coordinated ligand. The molecular structure for both complexes **3.16a** and **3.16b** are shown in **Figure 3.25** and selected bond lengths and angles are given in **Table 3.11**.

| (a) | (b) |
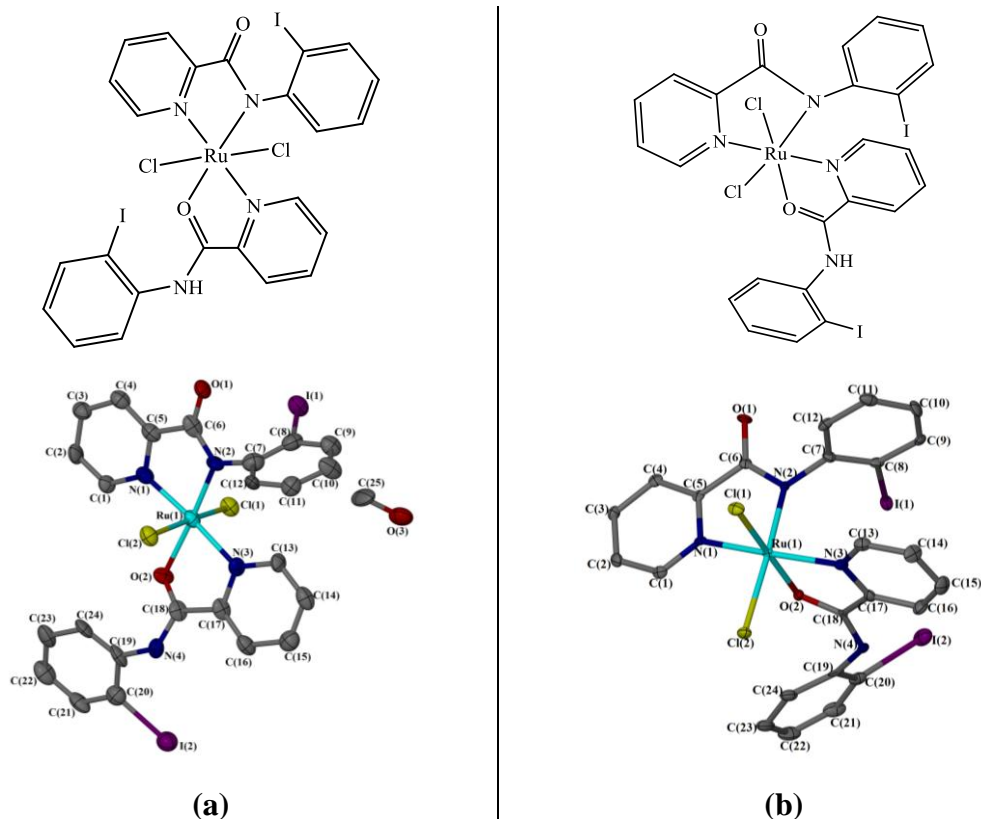
Figure 3.25 *Molecular structure of complex **3.16** showing **(a)** trans-trans-trans and **(b)** cis-trans-cis structural geometry. Displacement ellipsoids are at the 50% probability level. Hydrogen atoms are omitted for clarity.*

Table 3.11 *Selected bond lengths and angles for complex **3.16a** and **3.16b** with s.u.s*

shown in parenthesis

Bond length (Å) / angle (°)	3.16a	3.16b
Ru(1)-Cl(1)	2.330(4)	2.3241(13)
Ru(1)-Cl(2)	2.352(3)	2.3600(13)
Ru(1)-N(1)	2.023(13)	2.045(4)
Ru(1)-N(2)	2.016(10)	2.030(4)
Ru(1)-N(3)	2.067(12)	2.060(4)
Ru(1)-O(2)	2.116(9)	2.056(3)
Cl(1) - Ru(1) - Cl(2)	173.82(13)	92.54(5)
N(1) - Ru(1) - O(2)	98.3(4)	93.55(14)
N(2) - Ru(1) - O(2)	176.3(5)	91.98(14)
N(2) - Ru(1) - N(3)	104.6(5)	94.94(15)
N(1) - Ru(1) - N(3)	175.8(5)	171.69(15)

Complex **3.16a** packed in a vertical linear arrangement along the *b*-axis as shown in **Figure 3.26a**. Intermolecular hydrogen bonds are held between one methanol molecule with three complex molecules involving the amide group of one molecule (bond distance N(4)-O(3) of 2.757(17) Å), the carbonyl group of the second molecule (bond distance O(3)-O(1) of 2.757(16) Å) and the iodide substituent on the phenyl ring of the third molecule (bond distance C(25)-I(1) of 3.561(16) Å). A pair of complex molecules are also held together *via* hydrogen bond between the carbonyl group of one molecule and the hydrogen of the phenyl ring on another molecule (bond distance C(10)-O(1) of 3.268(17) Å) (**Figure 3.26b**).
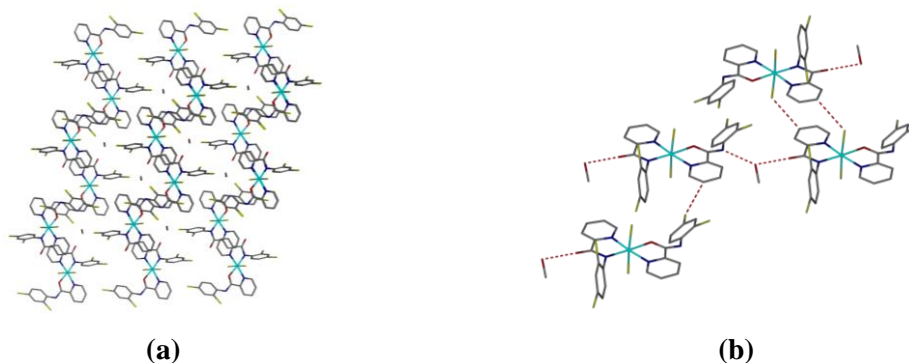
(a)   (b)
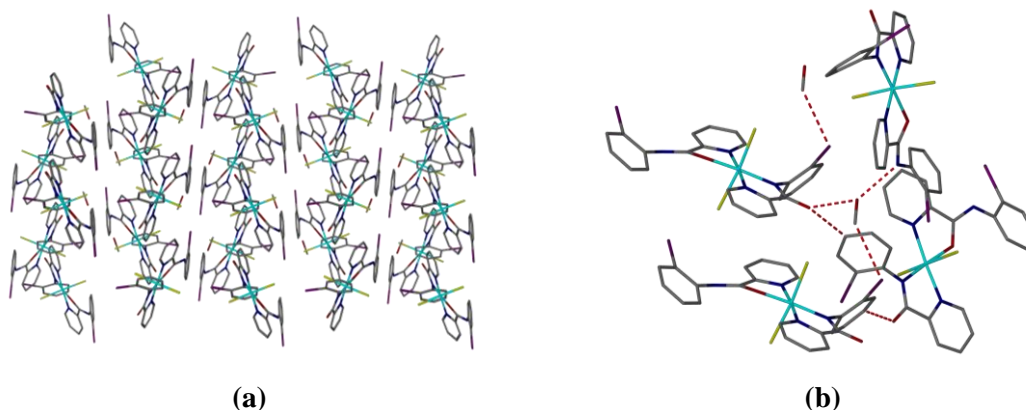
*Figure 3.26 (a) Packing diagram viewed along the b-axis of complex **3.16a** (b) Intermolecular hydrogen bonding between molecules. Hydrogen atoms are omitted for clarity.*

Complex **3.16b** packed in a zig-zag pattern when packed along the *c*-axis as shown in **Figure 3.27a**. The complex molecules are packed together by intermolecular hydrogen bonding between the amide group of one molecule and the carbonyl group of the second molecule (bond distance N(4)-O(1) of 2.751(5) Å), and between oxygen atom of the *(N,O)*-coordinated ligand and the hydrogen of the pyridyl ring of the third molecule (bond distance C(3)-O(2) of 3.161(6) Å) (**Figure 3.27b**).

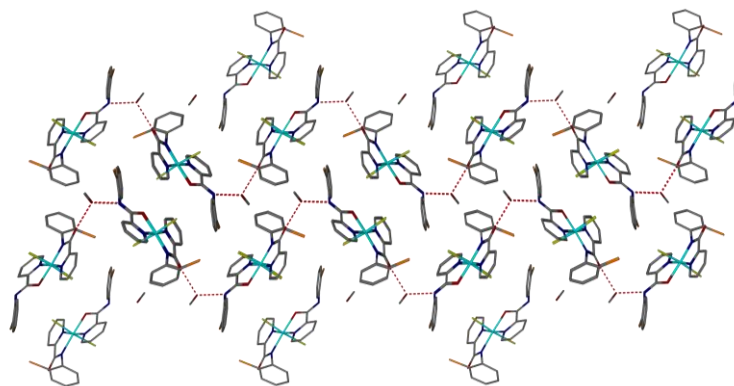(a)   (b)
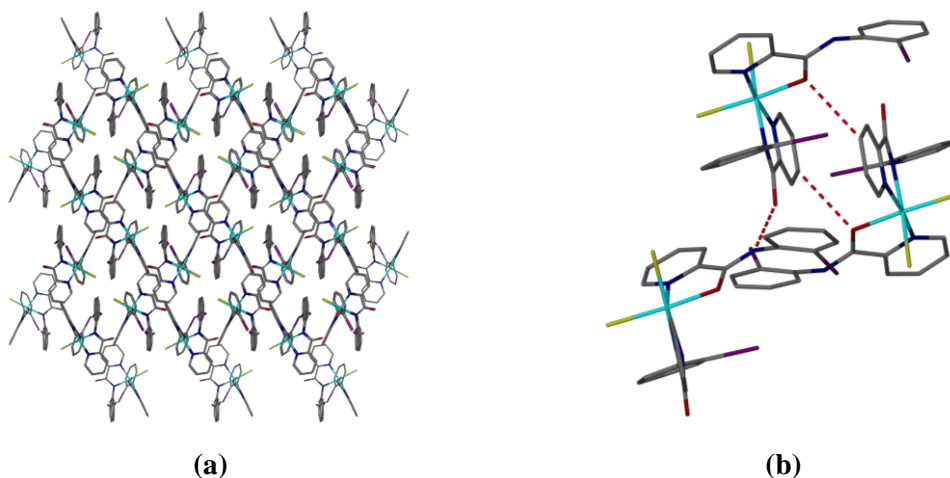
*Figure 3.27 (a) Packing diagram viewed along the c-axis of complex **3.16b** (b) Intermolecular hydrogen bonding between molecules. Hydrogen atoms are omitted for clarity.*

3.6 Isomerisation studies on bis-Picolinamide Ruthenium (III) Dichloride (RuCl$_2$L$_2$) Complexes

There have been many attempts to separate the isomers of *bis*-picolinamide ruthenium dichloride complexes from their main product, including fractional sublimation, column chromatography using a mixture of different good and poor solvents, washing off with a wide range of different solvents (assuming the different isomers have different solubility), and using different procedures to synthesise the respective isomers following the previously reported synthesis of complexes with different structural isomers. [1, 4, 7] However, no successful results have been obtained. Fractional recrystallisation has separated the isomers of the ruthenium dichloride complexes into different shapes and colours of crystals as described previously, but the different crystals were close to each other in the solution that collecting them separately for further studies was not possible. Comparison of IR spectra between each complex was used to observe the differences in their NH and CO group stretches as to whether the main product of the complex contains one single isomer or a mixture of isomers. However, all IR spectra have been shown to be similar, where the differences of shift or intensity of the bands between the spectra of each complex was insignificant.

Complex **3.7** has been shown to have two different structural isomers and was therefore analysed by uv-vis spectrophotometry as a function of time and temperature. Complex **3.7** was dissolved in dry methanol and was analysed to observe the effective changes in spectra that could result from an isomerisation process. **Figure 3.28(a)** shows a time-dependant spectra of complex **3.7** in dry methanol taken at 0 h, 24 h and 48 h. A slight change is seen for peak centred at about 298 nm, which has decreased in intensity after 48 h. A temperature-dependent spectra of complex **3.7** in dry methanol observed every decrease of 5°C from 58°C to 10°C, is as shown in **Figure 3.28(b)**. An increase in intensity of peak with maxima at 298 nm can be seen as the temperature decreases. These changes observed are very insignificant and no new peaks appeared over time and temperature to indicate that there are changes in their structural isomers in solution.

(a)   **(b)**
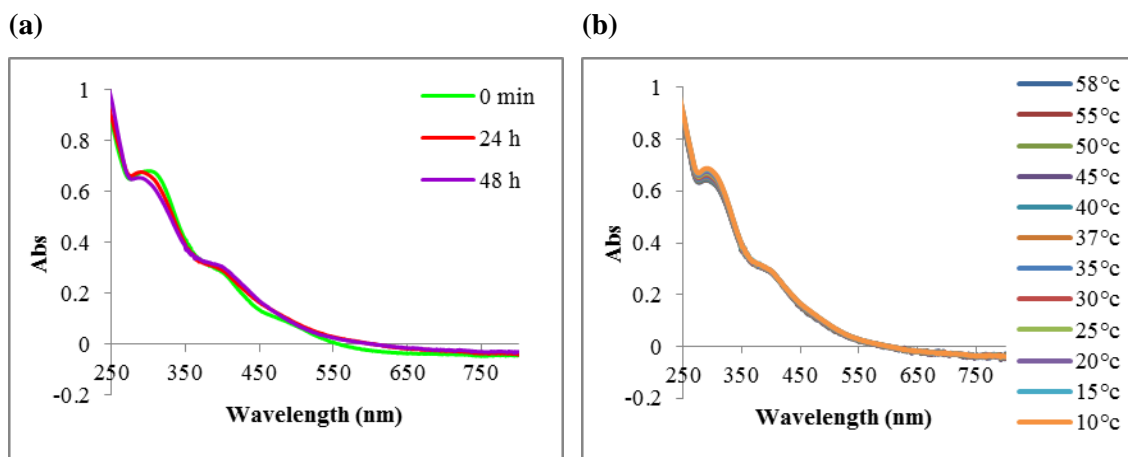
***Figure 3.28 (a)** Time-dependant, and **(b)** Temperature-dependant uv-vis solution studies in dry MeOH for complex **3.7** (30 µM)*

The powder diffraction (PXRD) pattern of complex **3.7** was also recorded. The diffraction patterns were compared between the bulk powder sample and its single *trans* and *cis* crystal structures for complexes **3.7a** and **3.7b** respectively, as shown in **Figure 3.29**. The patterns are very different between the diffractograms. The positions of the peaks in the simulated patterns do not match those of the recorded pattern of complex **3.7** hence it was not possible to obtain a ratio of *trans:cis* ratio. Furthermore, since the dried powder sample was used for the study, the presence of solvent in the *trans* crystal structure may also affect the pattern. Thus, separation of the mixtures to obtain pure isomers is useful for further characterisation studies.
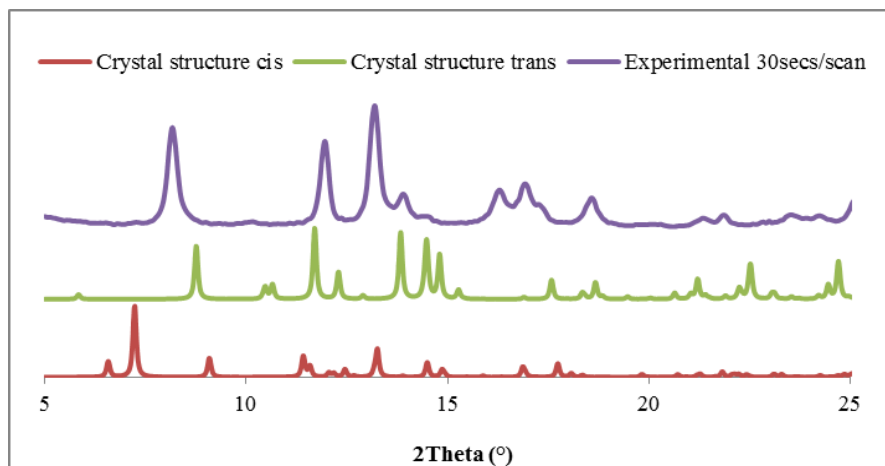
***Figure 3.29** PXRD diffractogram of complex **3.7** for simulated trans and cis, and experimental with scan rate at 30 secs/scan*

3.7   References

1.   R. A. Krause and K. Krause, *Inorg. Chem.*, 1980, **19**, 2600-2603.

2.   A. Seal and S. Ray, *Acta Crystallogr., Sect. C: Cryst. Struct. Commun.*, 1984, **40**, 929-932.

3.   S. Choudhury, M. Kakoti, A. K. Deb and S. Goswami, *Polyhedron*, 1992, **11**, 3183-3190.

4.   A. H. Velders, K. van der Schilden, A. C. Hotze, J. Reedijk, H. Kooijman and A. L. Spek, *Dalton Trans.*, 2004, 448-455.

5.   K. Rafferty, Ph.D Thesis, University of Leeds, 2008.

6.   Z. Almodares, S. J. Lucas, B. D. Crossley, A. M. Basri, C. M. Pask, A. J. Hebden, R. M. Phillips and P. C. McGowan, *Inorg. Chem.*, 2014, **53**, 727-736.

7.   A. C. G. Hotze, H. Kooijman, A. L. Spek, J. G. Haasnoot and J. Reedijk, *New J. Chem.*, 2004, **28**, 565-569.

CHAPTER 4

Synthesis and Characterisation of Functionalised *Bis*-Picolinamide Ruthenium Diiodide Complexes

4 Synthesis of Ruthenium Diiodide Complexes

4.1 Introduction

This chapter discusses previously reported *trans*-platinum diiodide anti-cancer complexes, followed by the synthesis of a series of novel *bis*-picolinamide ruthenium (III) diiodide complexes, and their characterisation. The aim for this synthesis is to extend the library of *bis*-picolinamide ruthenium (III) dihalide complexes, by coordinating monodentate iodide ligands to the ruthenium metal centre, as well as, the interest in investigating the effect of changing the ancillary halide ligands towards their biological activity.

4.2 Trans-platinum diiodide anti-cancer complexes

Monodentate iodide ligands have been used in the design of anti-cancer drugs for many years,[1] after numerous chemical studies on cisplatin clearly demonstrated that the chlorides are the reactive ligands.[2, 3] This led to the interest in observing the effects towards biological activity when varying the leaving groups on cisplatin.

The structural-activity rules for metal complexes as anti-cancer drugs were developed in the initial studies by Rosenberg,[4] and Cleare and Hoeschele.[1, 5] Their studies specifically focused on platinum (II) complexes based on the structure of cisplatin, observing the effects of varying the complexes' structural geometries, monodentate ligands and charge, on their anti-cancer activities *in vivo*. The platinum complex with *trans* dichloride ligands was shown to be inactive, revealing that *cis* geometry is important in anti-cancer activity. [1, 5] This could be due to two main factors. *Trans* geometry complexes are highly reactive due to kinetic instability, leading to an increase in toxicity. In addition, the complexes with *cis* geometry have the potential for biological interaction within the cells through chelate formation, which is stereochemically inaccessible for *trans* complexes. When the ancillary chloride ligands of cisplatin were changed to iodide, the complex has showed a decrease in potency. A very high dose was required for the platinum diiodide complex to create a maximum effect for its anti-cancer activity.

Despite these studies, several *trans*-platinum complexes have shown, in recent years, to be potent anti-cancer complexes when compared to their *cis* analogues, breaking the structural-activity rules for metal anti-cancer complexes.[6, 7] Based on the general structure of cisplatin, the cytotoxicity of *trans*-platinum complexes increase significantly both *in vitro* and *in vivo* when substituting the inert ammine ligands with more bulky ligands, as shown in **Figure 4.1**. Mechanistic studies suggest that these bulky ligands can hinder the substitution of the *trans* dichloride ligands, decreasing the kinetic instability of the *trans*-platinum complexes, hence leading to lower toxicity. Farrell *et al.* proposed TPA complexes, in which *trans* dichloride platinum complexes that contain at least one aromatic N-donor ligand (L = L' = Pyridine; Thiazole, or L = Quinoline, L' = RR'SO (R= Me, R' = Me, Bz, or Ph)), and have shown a 100-fold higher cytotoxicity than transplatin and comparable with cisplatin.[8] A recent platinum complex reported is the platinum (IV) diazido complex, *trans-trans-trans*-Pt(N$_3$)$_3$(OH)$_2$(Py)$_2$ that is photoactivated by visible light at 420 nm, and is more potent upon irradiation at 365 nm.[9]

L = L' = Pyridine; Thiazole, or L =
Quinoline, L' = RR'SO (R= Me, R' = Me, Bz,
or Ph

TPA complexes   *trans-trans-trans*-**Pt(N$_3$)$_3$(OH)$_2$(Py)$_2$**
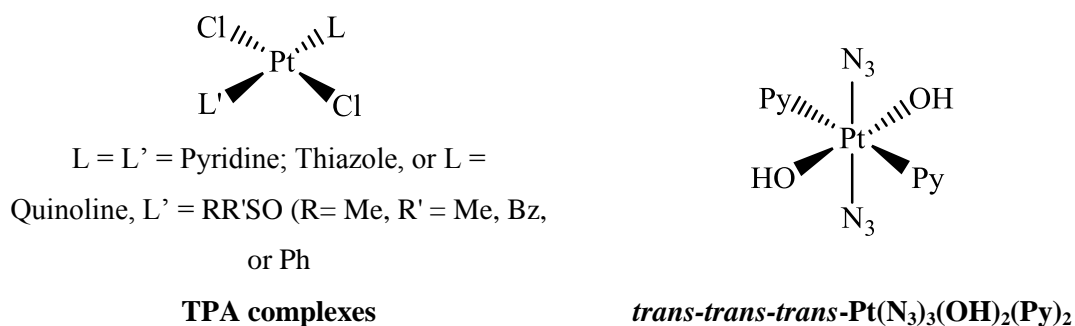
Figure 4.1 Recently reported active trans-platinum anti-cancer complexes

There is also a variety of platinum anti-cancer drugs with monodentate diiodide ligands as shown in **Figure 4.2**. Complex **1** has ethylenediamine as the neutral ligand, X = Cl or I as the anionic ligands, and various axial ligands, where Y is Cl, OH, OCOCH$_3$, OCOCF$_3$ or OSO$_2$CH$_3$. These complexes were studied to investigate the influence of anionic ligands on reduction rates and potentials, DNA binding ability, and cell growth inhibitory activity.[10] Carbohydrate 2,3-diamino-2,3-dideoxy-D-glucopyranose was chosen as a ligand for complex **2** to resemble the structure of the third generation platinum-based anticancer drug, oxalipatin, and diiodide ligands as the

leaving groups. These complexes were evaluated for their affinity toward dGMP by capillary electrophoresis (CE) and for their *in vitro* cytotoxicity by MTT assay.[11] In a more recent report, complexes **3** and **4** analogues of each other, having diiodide ligands either in *cis* or *trans* configuration, and diamine ligands, where Y is isopropylamine, dimethylamine or methylamine have been studied. They have shown a higher cytotoxicity is seen for complexes with *trans* diiodide ligands compared to their corresponding *cis* analogue, which brought them to further investigation on the possible molecular mechanisms of action, by analysing the reactivity of these complexes with a few representative biomolecules using various physicochemical techniques.[12]
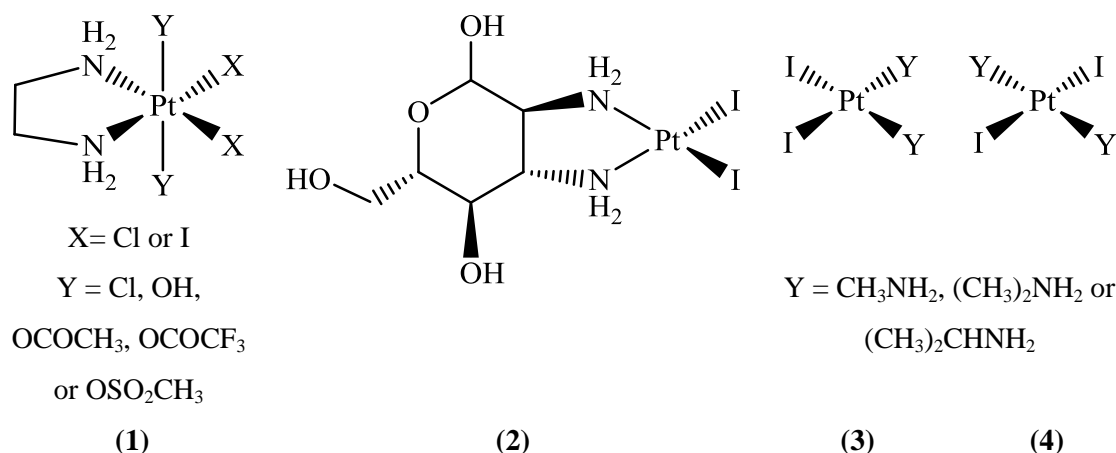
Figure 4.2 *Previously reported platinum-diiodide as potential anti-cancer complexes*

Sadler *et al.* have reported metal (Ru or Os) *p*-cymene complexes with a chloride or iodide as the monodentate ligand, and either azopyridine or iminopyridine as the chelating ligand. They have shown dramatic differences in biological activities, when substituting the coordinating chloride ligands to iodide, with remarkable advantages towards having the iodide ligand bonded to the metal centre.[13, 14] The IC_{50} values of $[Ru(\eta^6\text{-}p\text{-cym})(p\text{-Azpy-NMe}_2)Cl]PF_6$ and $[Ru(\eta^6\text{-}p\text{-cym})(p\text{-Azpy-NMe}_2)I]PF_6$ against A549 lung cancer cell lines were reported to be 15 ± 1 µM and 1.27 ± 0.01 µM respectively, which is about 15-fold difference. There are, however, only limited known ruthenium based anti-cancer complexes containing iodide monodentate ligands, furthermore, with two iodide ligands, encouraging the exploration of structural-activity relationships on *trans*-metal based anti-cancer complexes.

4.3   Synthesis of *bis*-Picolinamide Ruthenium (III) Diiodide (RuI$_2$L$_2$) Complexes

Bis-picolinamide ruthenium (III) diiodide (RuI$_2$L$_2$) complexes contain two bidentate ligands with planar aromatic rings, an amide group and a carbonyl group that are able to form interactions with biological molecules, and two monodentate iodide ligands coordinating to the metal centre, which may influence the biological properties of the whole complex. The general synthesis for these complexes is as shown in **Scheme 4.1**.
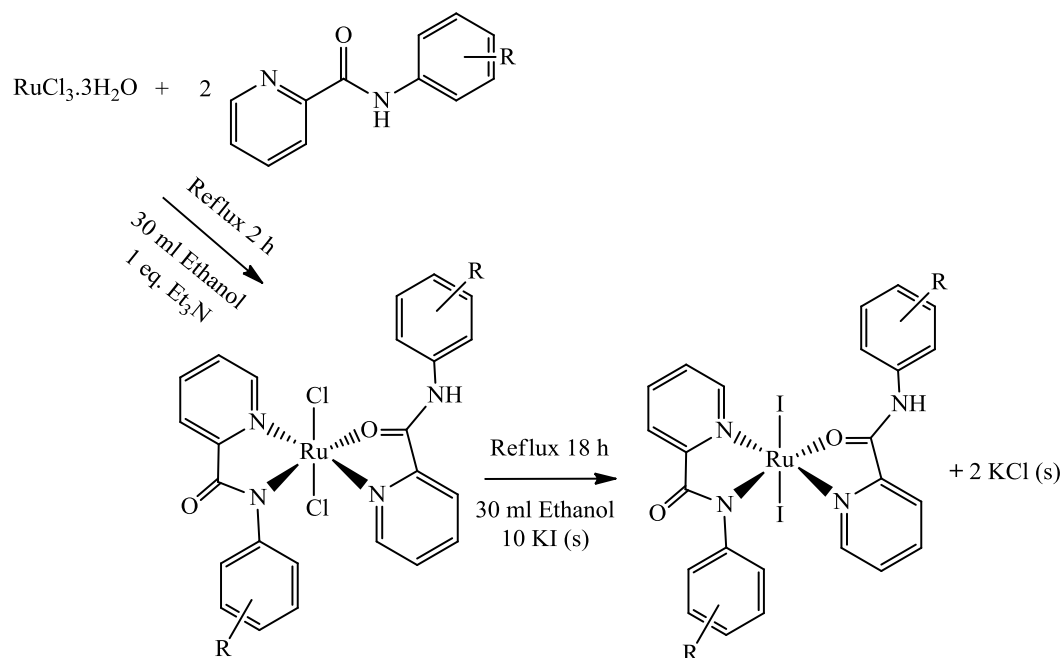
R =	H	(Complex **4.1**, Yield	2',4'-Cl	(Complex **4.9**, Yield
	2'-F	(Complex **4.2**, Yield	2',5'-Cl	(Complex **4.10**, Yield
	4'-F	(Complex **4.3**, Yield	2'-Br	(Complex **4.11**, Yield
	2',4'-F	(Complex **4.4**, Yield	3'-Br	(Complex **4.12**, Yield
	2',5'-F	(Complex **4.5**, Yield	4'-Br	(Complex **4.13**, Yield
	2'-Cl	(Complex **4.6**, Yield	2',4',-Br	(Complex **4.14**, Yield
	3'-Cl	(Complex **4.7**, Yield	2',5'-Br	(Complex **4.15** Yield
	4'-Cl	(Complex **4.8**, Yield		

Scheme 4.1 *Synthesis of bis-picolinamide ruthenium (III) diiodide complexes*

The reaction starts by synthesising the ruthenium dichloride analogue, and the addition of an excess of solid potassium iodide *in situ* during reflux favours halide-exchange reaction.[15, 16] The dichloride ligands of $RuCl_2L_2$ complex undergo substitution with iodide from solid KI, giving the ruthenium diiodide complex and forming a salt, potassium chloride, which was dissociated as white precipitate and filtered over celite after the 18 h reaction. Several filtration and washing were involved in order to fully discard the white precipitate of KCl, resulting in different percentage yield obtained in the series of *bis*-picolinamide ruthenium diiodide complexes.

4.4   Characterisation of *bis*-Picolinamide Ruthenium (III) Diiodide Complexes

Bis-picolinamide ruthenium (III) diiodide complexes were prepared by a halide-exchange reaction *via* **Scheme 4.1**, where an excess of potassium iodide was added directly to the functionalised *bis*-picolinamide ruthenium (III) dichloride complex and heated under reflux for 18 hours. Complexes **4.1** - **4.15** were obtained as pure products in yields ranging from 31-74% and characterised using IR, ES-MS, elemental analysis and single crystal X-Ray diffraction. These complexes are found to be soluble in dimethylformamide, tetrahydrofuran and nitromethane to give dark green-brown solutions.

Complexes **4.1** to **4.15** have similar IR spectra to their dichloride analogues, showing several bands with different intensities in the 1600-400 cm^{-1} area. There are two NH stretches with different intensities - medium and weak, within the region 3000-3500 cm^{-1}, and one strong stretch with a weak split for the CO group around the 1500-1600 cm^{-1} region. A shift of the stretches towards lower wavenumber is seen on the IR spectra of ruthenium diiodide when compared with the IR spectra of its dichloride analogue. **Figure 4.3** shows the IR spectra of ligand **2.11**, complex **3.11** and complex **4.11** as an example of the comparison. Magnetic susceptibility measurements have shown that all of the complexes are low-spin d^5 with unpaired one-electron ($\mu_{eff} = 1.60$ - 1.92 μ_B), which corresponds to the +3 state of ruthenium ($\mu_{eff} = 1.73$ μ_B).

Two different types of structural isomers have been shown to exist for these complexes, which are the *trans-trans-trans* and *trans-cis-cis* structural isomers confirmed by their single crystal structures. X-ray crystallography has been used to show the geometry of the different structural isomers, as well as to verify the coordination mode of the ligands in the complexes. The ligands are bonded in *N,N-* and *N,O-* coordination modes to the ruthenium metal centre. Single crystal structures and data are shown for complexes **4.2**, **4.3**, **4.12** and **4.13**, which were recrystallised by vapour diffusion of dimethylformamide/ether.

4.5   IR Data for Ligand 2.11, Complex 3.11 and Complex 4.11

The IR spectra of ligand **2.11**, complex **3.11** and complex **4.11** are shown in **Figure 4.3**. In the spectrum of the uncoordinated ligand, the strong CO stretch is observed at 1691 cm^{-1}, shifted to 1590 cm^{-1} in complex **3.11** and to 1563 cm^{-1} in complex **4.11** that splits into two bands. Two NH stretches seen in the region 3000-3300 cm^{-1} are shifted from 3290 cm^{-1} and 3108 cm^{-1} in ligand **2.11**, to 3209 cm^{-1} and 3062 cm^{-1} in complex **3.11** and to 3172 cm^{-1} and 3054 cm^{-1} in complex **4.11**.
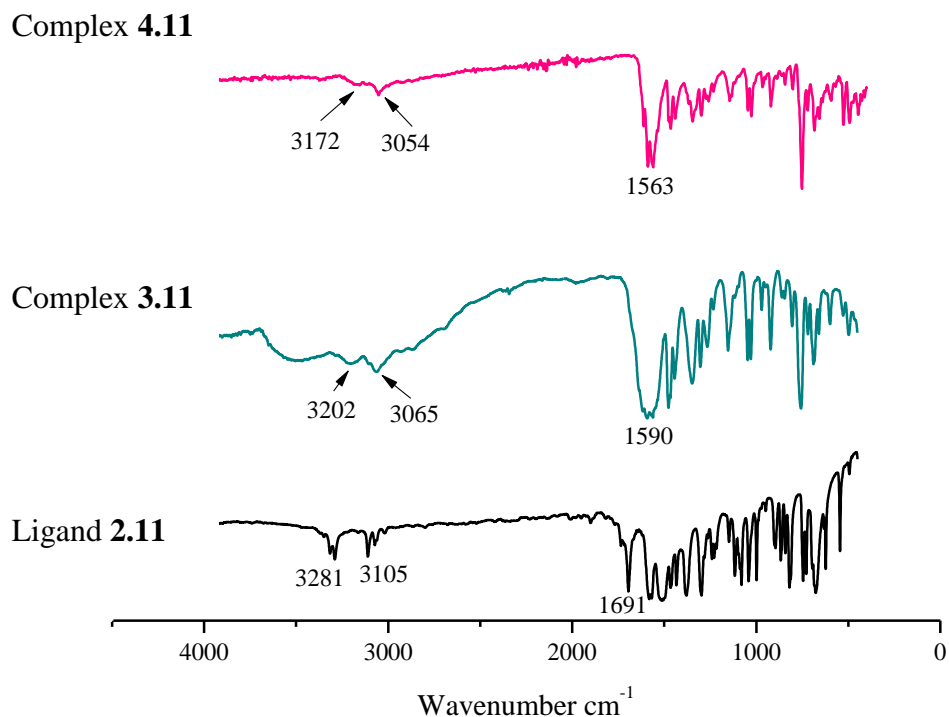
*Figure 4.3 IR Spectra of ligand **2.11**, complex **3.11** and complex **4.11***

4.6 X-ray Crystallography Data for *bis*-Picolinamide Ruthenium (III) Diiodide Complexes

Single crystals of complexes **4.2**, **4.3**, **4.12** and **4.13** which were suitable for X-ray crystallography were obtained by vapour diffusion of ether into a solution of the complex in dimethylformamide. The *bis*-picolinamide ruthenium diiodide complexes have a distorted octahedral centre, with bond angles in the range 96.2°-108.0° between the ligands that are *cis* to each other*,* and bond angles of 171.6°-177.9° between the *trans* ligands about the ruthenium metal centre.

The bond angle between the two N atoms of the *(N,N)*-coordinate ligand, and the N and O atom of the *(N,O)*-coordinated ligand, is less than 90° with the range between 76.9 - 78.8°, due to the rigidity of the picolinamide ligands. The angle between the two *trans* iodine atoms around the ruthenium centre is between 174.1 - 177.9°. The torsion angle for the *(N,N)-* and *(N,O)*-coordinated ligand is between 49.3 - 92.5°, and 17.6 - 39.5° respectively, adopting non-planar configurations between the picolinamide rings.

The Ru-I bond distances for all of the *bis*-picolinamide ruthenium diiodide complexes are similar, where one of the Ru-I bonds is longer than the other, with an average bond distance of 2.67 Å for Ru-I(1) and 2.69 Å for Ru-I(2). The average bond lengths of Ru(1)-N(1), Ru(1)-N(2), Ru(1)-N(3) and Ru(1)-O(2) for all the complexes are 2.05 Å, 2.02 Å, 2.12 Å and 2.09 Å respectively, consistent and comparable with *bis*-picolinamide ruthenium (III) dichloride complexes as discussed in Chapter 3.

4.6.1   X-ray Crystal Structure for Complex 4.2

Complex **4.2** crystallises to black block crystals that are suitable for X-ray crystallography. The complex crystallised in an orthorhombic cell with the arrangement of *trans-trans-trans* and structural solution was performed in the space group *Pna2₁*. The asymmetric unit contains one complex molecule. The molecular structure of complex **4.2** is shown in **Figure 4.4** and selected bond lengths and angles are given in **Table 4.1**.
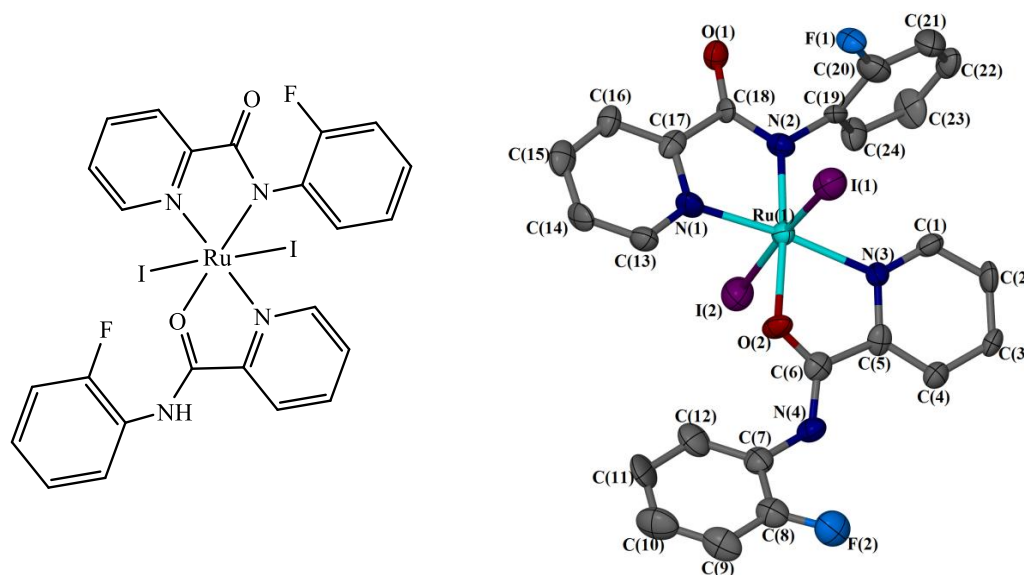
Figure 4.4 *Molecular structure of complex* ***4.2***. *Displacement ellipsoids are at the 50% probability level. Hydrogen atoms are omitted for clarity.*

Table 4.1 *Selected bond lengths and angles for complex* ***4.2*** *with s.u.s shown in parenthesis*

Bond length (Å)		Bond angle (°)	
Ru(1)-I(1)	2.6507(17)	I(1) - Ru(1) - I(2)	174.89(6)
Ru(1)-I(2)	2.6670(18)	N(1) - Ru(1) - O(2)	97.1(4)
Ru(1)-N(1)	2.031(13)	N(2) - Ru(1) - O(2)	175.4(5)
Ru(1)-N(2)	2.009(11)	N(2) - Ru(1) - N(3)	107.2(5)
Ru(1)-N(3)	2.123(12)	N(1) - Ru(1) - N(3)	173.7(5)
Ru(1)-O(2)	2.106(10)		

The crystal packing of complex **4.2** consists of wave-like layers when viewed along the *c*-axis, as shown in **Figure 4.5**. The molecules are held together by hydrogen bond interactions between the amide group of one molecule and the carbonyl group of the other molecule (bond distance N(4)-O(1) of 2.746(16) Å). Another interaction is between an oxygen atom of the *(N,O)*-coordinated ligand of one molecule and the hydrogen of a pyridyl ring of the second molecule (bond distance C(11)-O(2) of 3.383(14) Å).
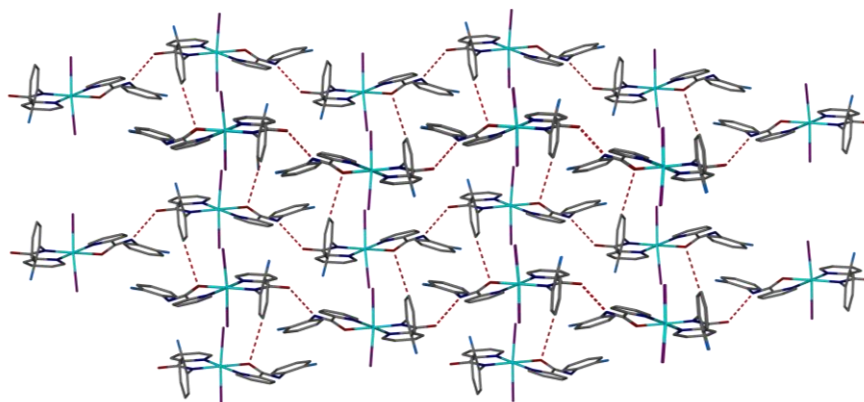
Figure 4.5 *Packing diagram of complex **4.2** viewed along the c-axis showing intermolecular hydrogen bond interactions between molecules. Hydrogen atoms are omitted for clarity.*

4.6.2 X-ray Crystal Structure for Complex 4.3

Green fragments of complex **4.3** suitable for X-ray crystallography crystallised in an orthorhombic cell with the arrangement of *trans-trans-trans*. The structural solution was performed in the space group *Pna2₁*, and the asymmetric unit contains one complex molecule. The molecular structure is shown in **Figure 4.6** and selected bond lengths and angles are given in **Table 4.2**. The molecules of complex **4.3** pack in layers when viewed along the *c*-axis, forming hydrogen bonds between molecules, similarly as complex **4.2**.
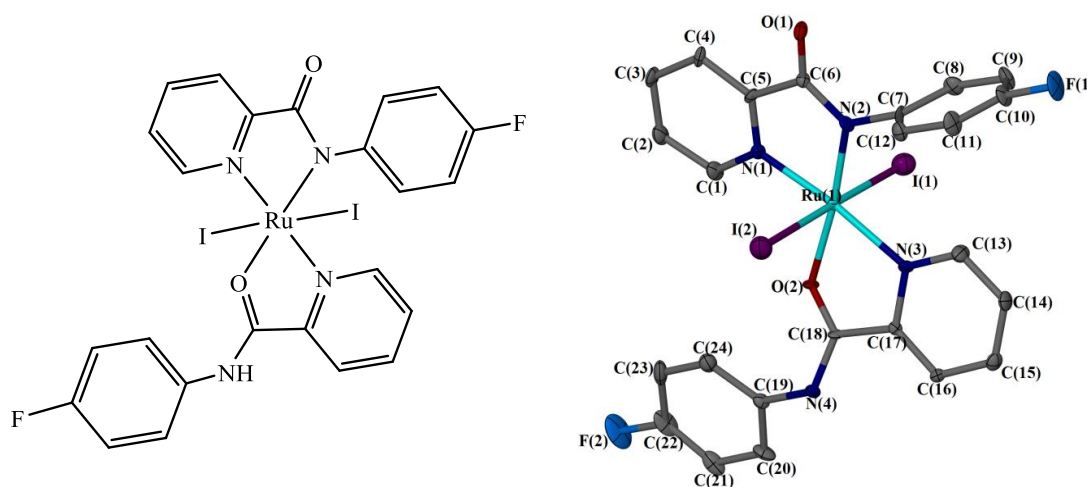
***Figure 4.6** Molecular structure of complex **4.3**. Displacement ellipsoids are at the 50% probability level. Hydrogen atoms are omitted for clarity.*

***Table 4.2** Selected bond lengths and angles for complex **4.3** with s.u.s shown in parenthesis*

Bond length (Å)		Bond angle (°)	
Ru(1)-I(1)	2.6589(8)	I(1) - Ru(1) - I(2)	177.93(3)
Ru(1)-I(2)	2.7149(8)	N(1) - Ru(1) - O(2)	96.6(2)
Ru(1)-N(1)	2.051(6)	N(2) - Ru(1) - O(2)	174.3(2)
Ru(1)-N(2)	2.021(6)	N(2) - Ru(1) - N(3)	107.4(2)
Ru(1)-N(3)	2.119(6)	N(1) - Ru(1) - N(3)	173.7(2)
Ru(1)-O(2)	2.089(5)		

4.6.3   X-ray Crystal Structure for Complex 4.12

Complex **4.12** crystallised as black prism crystals in a monoclinic unit cell with the arrangement of *trans-trans-trans*. Structural solution was performed in the space group *Cc*. The asymmetric unit contains one complex molecule and one dimethylformamide molecule. The molecular structure is shown in **Figure 4.7**, and the selected bond lengths and angles are given in **Table 4.3**.
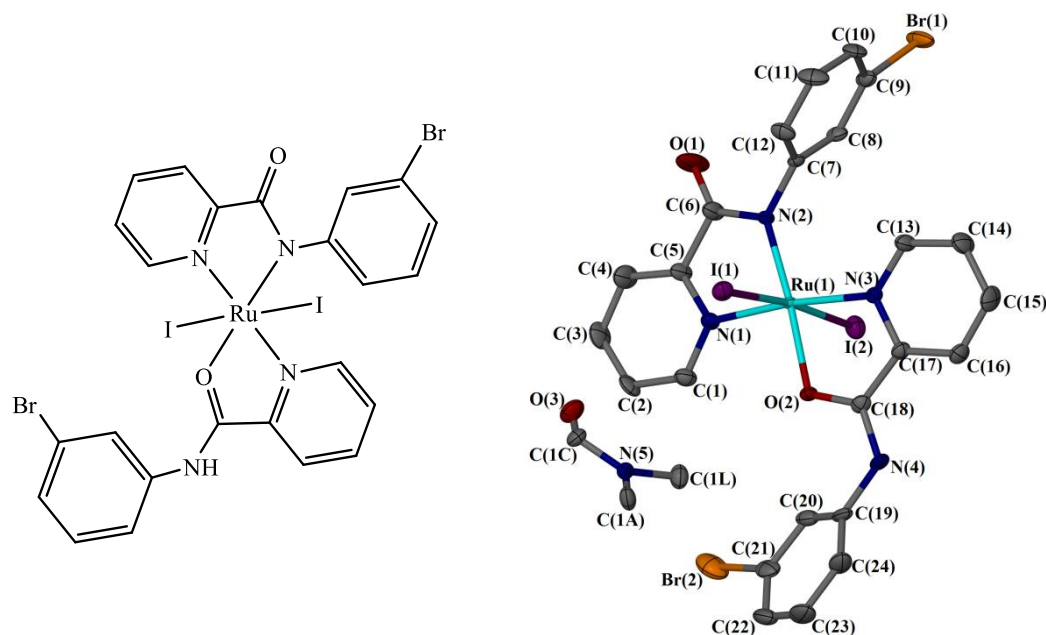
***Figure 4.7** Molecular structure of complex **4.12**. Displacement ellipsoids are at the 50% probability level. Hydrogen atoms are omitted for clarity.*

***Table 4.3** Selected bond lengths and angles for complex **4.12** with s.u.s shown in parenthesis*

Bond length (Å)		Bond angle (°)	
Ru(1)-I(1)	2.701(4)	I(1) - Ru(1) - I(2)	174.3 (14)
Ru(1)-I(2)	2.703(4)	N(1) - Ru(1) - O(2)	96.85(12)
Ru(1)-N(1)	2.065(3)	N(2) - Ru(1) - O(2)	175.56(13)
Ru(1)-N(2)	2.023(3)	N(2) - Ru(1) - N(3)	107.41(12)
Ru(1)-N(3)	2.122(3)	N(1) - Ru(1) - N(3)	173.65(13)
Ru(1)-O(2)	2.092(3)		

When viewed along the *b*-axis, complex **3.9** can be seen packed in a diagonal linear arrangement as shown in **Figure 4.8(a)**. Several intermolecular interactions are seen within the packing arrangement, as shown in **Figure 4.8(b)**. Three complex molecules are held together by hydrogen bond interactions with a dimethylformamide molecule. These interactions are between the amide group of one complex molecule and the oxygen atom of dimethylformamide molecule (bond distance N(4)-O(3) of 2.779(5) Å). Another interaction is between the carbonyl group of the second complex molecule and one of the carbon atoms of the dimethylformamide molecule (bond distance C(1A)-O(1) of 3.223(5) Å), and also, an interaction between the bromine substituent of another complex molecule and the carbon atom of the dimethylformamide molecule (bond distance C(1A)-Br(1) of 3.710(4) Å).

(a)   (b)
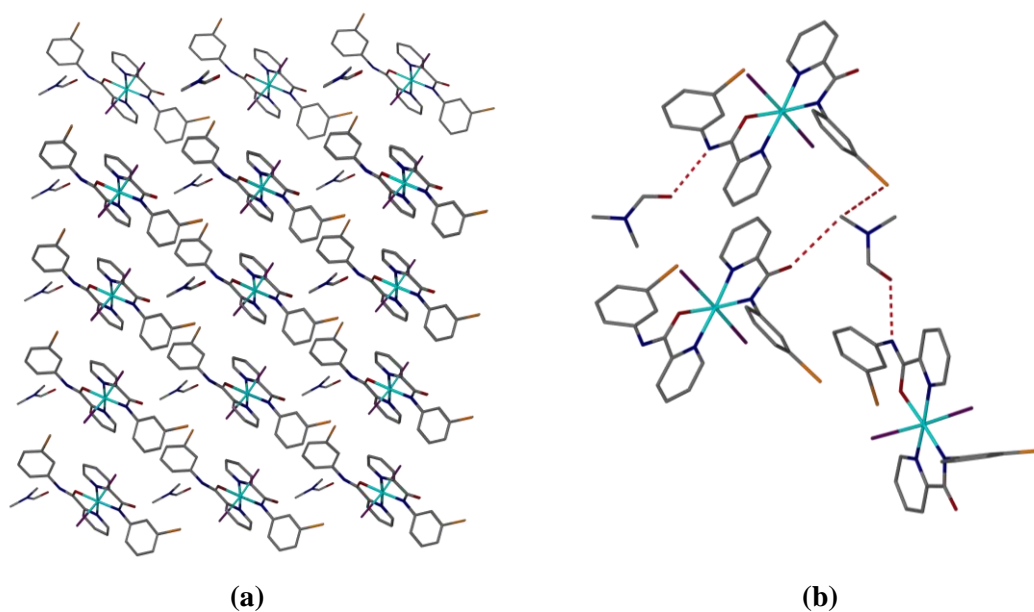
***Figure 4.8** (a) Packing diagram viewed along the b-axis of complex **4.12**; (b) Intermolecular hydrogen bonding between molecules. Hydrogen atoms are omitted for clarity.*

4.6.4   X-ray Crystal Structure for Complex 4.13

Black crystals of complex **4.13** suitable for X-ray crystallography crystallised in a monoclinic cell with the arrangement of *trans-cis-cis*. The structural solution was performed in the space group $P2_1/n$, and the asymmetric unit contains one complex molecule and one dimethylformamide molecule. The molecular structure of complex **4.13** is shown in **Figure 4.9** and the selected bond lengths and angles are given in **Table 4.4**.
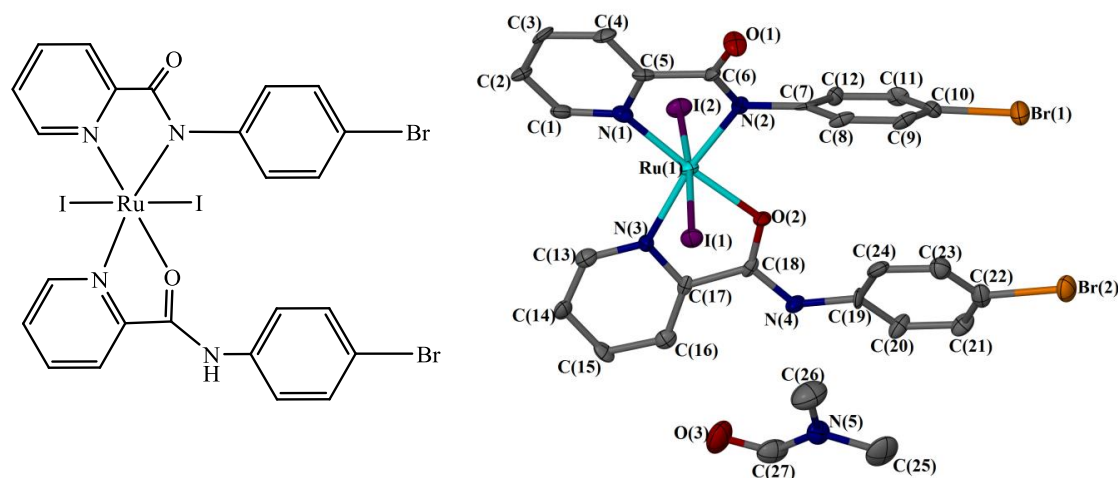
Figure 4.9 *Molecular structure of complex 4.13. Displacement ellipsoids are at the 50% probability level. Hydrogen atoms are omitted for clarity.*

Table 4.4 *Selected bond lengths and angles for complex 4.13 with s.u.s shown in parenthesis*

Bond length (Å)		Bond angle (°)	
Ru(1)-I(1)	2.664(11)	I(1) - Ru(1) - I(2)	174.1(4)
Ru(1)-I(2)	2.685(11)	N(1) - Ru(1) - O(2)	174.9(3)
Ru(1)-N(1)	2.039(7)	N(2) - Ru(1) - O(2)	96.2(3)
Ru(1)-N(2)	2.023(7)	N(2) - Ru(1) - N(3)	171.6(3)
Ru(1)-N(3)	2.118(7)	N(1) - Ru(1) - N(3)	108.0(3)
Ru(1)-O(2)	2.066(6)		

Complex **4.13** packs in a diagonal linear arrangement along the *b*-axis as shown in **Figure 4.10**. Each molecule interacts with the adjacent complex molecule *via* two hydrogen bond interactions from the carbonyl group of the *(N,N)*-coordinated ligand with the amide group of one molecule (bond distance N(4)-O(1) of 2.809(10) Å), and with the carbon atom of another molecule (bond distance C(16)-O(1) of 3.092(11) Å). Two intramolecular hydrogen bond interactions can also be found, where one is within the *(N,O)*-coordinated ligand of a complex molecule (bond distance C(24)-O(2) of 2.790(11) Å), and the other intramolecular interaction is within a dimethylformamide molecule (bond distance C(26)-O(3) of 2.803(15) Å).
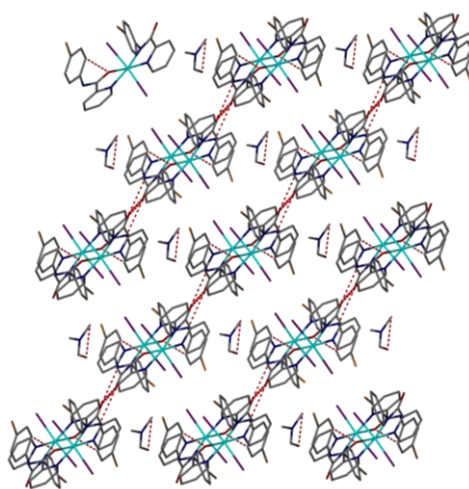
Figure 4.10 *Packing diagram of complex* *4.13* *viewed along the b-axis showing intermolecular hydrogen bond interactions between molecules. Hydrogen atoms are omitted for clarity.*

4.7 Isomerisation studies on *bis*-Picolinamide Ruthenium (III) Diiodide (RuI$_2$L$_2$) Complexes

The ruthenium diiodide complex **4.13** was studied for isomerisation in DMF solution by uv-vis spectrophotometry. **Figure 4.11(a)** and **(b)** show the uv-vis spectra of complex **4.13** at Day 0 and Day 5, and from 0°C - 100°C, in DMF solution respectively. Only one structural *trans* isomer is observed for ruthenium diiodide complexes from its crystal structure, and with no change observed in their uv-vis spectra it can be suggested that the *trans* structural geometry is also stable in solution over a period of time and also, over a wide temperature range. Following this, powder diffraction (PXRD) patterns were also recorded for complexes **4.2**, **4.3** and **4.13**. This was to further determine the stability of structural geometry in the bulk powder samples. The diffractogram simulated from the single crystal structure of complex **4.2** was compared with the diffractograms recorded from its powder sample at scan rate of 5secs/scan and 30secs/scan, and are shown in **Figure 4.12**. The PXRD patterns show similarities on the peaks between their diffractograms. Data analysis on the unit cell of the powder sample using DiffracEva[17] and ChekCell[18] software has shown that it is comparable and very well matches with the unit cell data obtained from the single crystal structure of the complex, suggesting the stability and purity of the ruthenium diiodide complex.

(a)   **(b)**
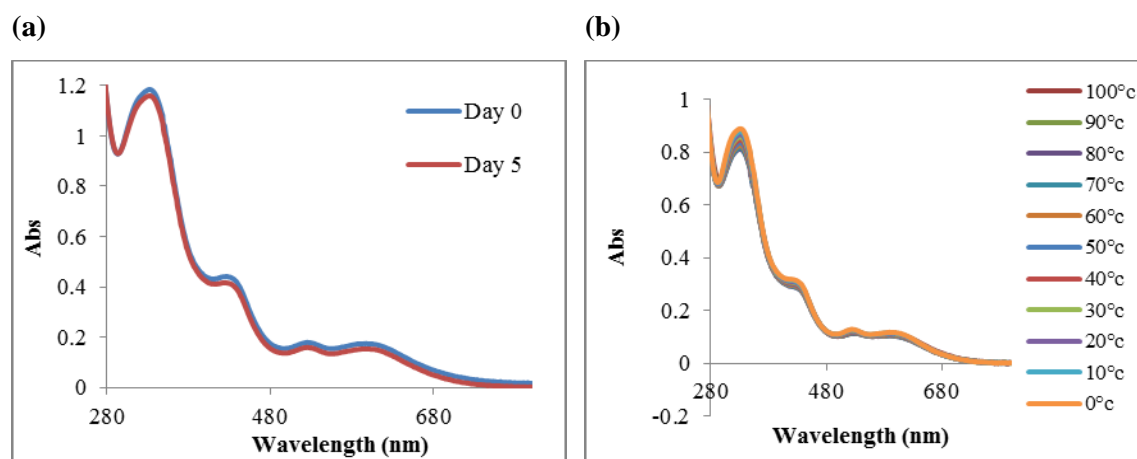
Figure 4.11(a) *Time-dependant and* ***(b)*** *Temperature-dependant uv-vis solution studies in DMF for complex* ***4.13*** *(30μM)*
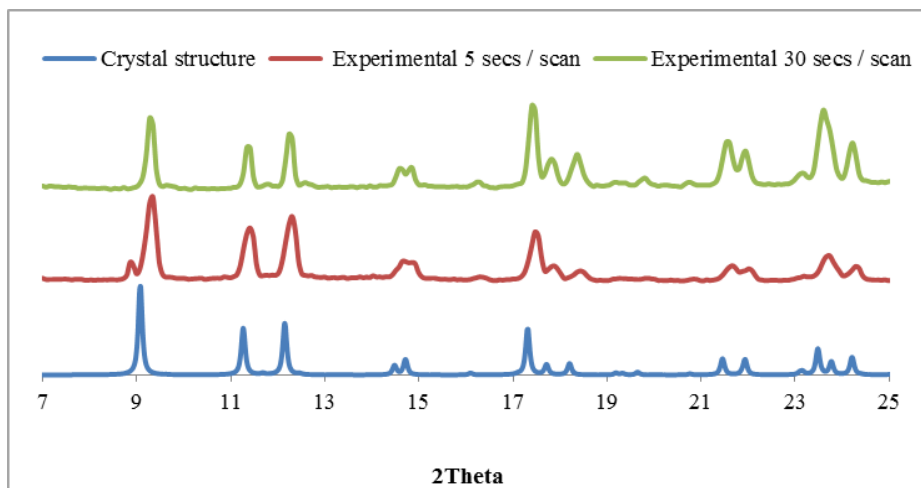
Figure 4.12 *PXRD data of complex* **4.2** *showing the simulated and experimental*

diffractograms recorded at scan rate of 5secs/scan and 30 secs/scan

4.8   References

1.   M. J. Cleare and J. D. Hoeschele, *Bioinorg. Chem.*, 1973, **2**, 187-210.

2.   D. Banerjea, F. Basolo and R. G. Pearson, *J. Am. Chem. Soc.*, 1957, **79**, 4055-4062.

3.   J. W. Reishus and D. S. Martin, *J. Am. Chem. Soc.*, 1961, **83**, 2457-2462.

4.   B. Rosenberg, L. Van Camp, E. B. Grimley and A. J. Thomson, *J. Biol. Chem.,* 1967, **242**, 1347-1352.

5.   M. J. Cleare and J. D. Hoeschele, *Plat. Metals Rev.*, 1973, **17**, 2-13.

6.   G. Natile and M. Coluccia, *Coor. Chem. Rev.*, 2001, **218-217**, 383-410.

7.   M. Coluccia and G. Natile, *Anti-Cancer Agents Med. Chem.*, 2007, **7**, 111-123.

8.   N. Farrell, L. R. Kelland, J. D. Roberts and M. Van Beusichem, *Cancer Res.*, 1992, **52**, 5065-5072.

9.   N. J. Farrer, J. A. Woods, L. Salassa, Y. Zhao, K. S. Robinson, G. Clarkson, F. S. Mackay and P. J. Sadler, *Angew. Chem. Intl. Ed.*, 2010, **49**, 8905-8908.

10.   N. A. Kratochwil and P. J. Bednarski, *Arch. Pharm.*, 1999, **332**, 279-285.

11.   I. Berger, A. A. Nazarov, C. G. Hartinger, M. Groessl, S.-M. Valiahdi, M. A. Jakupec and B. K. Keppler, *ChemMedChem*, 2007, **2**, 505-514.

12.   L. Messori, L. Cubo, C. Gabbiani, A. Alvarez-Valdes, E. Michelucci, G. Pieraccini, C. Rios-Luci, L. G. Leon, J. M. Padron, C. Navarro-Ranninger, A. Casini and A. G. Quiroga, *Inorg. Chem.*, 2012, **51**, 1717-1726.

13.   I. Romero-Canelon, A. M. Pizarro, A. Habtemariam and P. J. Sadler, *Metallomics*, 2012, **4**, 1271-1279.

14.   I. Romero-Canelon, L. Salassa and P. J. Sadler, *J. Med. Chem.*, 2013, **56**, 1291-1300.

15.   M. S. Sanford, J. A. Love and R. H. Grubbs, *J. Am. Chem. Soc.*, 2001, **123**, 6543-6554.

16.   T. J. Seiders, D. W. Ward and R. H. Grubbs, *Org. Lett.*, 2001, **3**, 3225-3228.

17.   Bruker AXS, *DiffracEva Suite*, 2009.

18.   J. Laugier and B. Bochu, *ChekCell*, 2004.

CHAPTER 5

Synthesis and Characterisation of Functionalised *Bis*-Picolinamide Rhodium Dihalide Complexes

5   Synthesis of Rhodium Dihalide Complexes

5.1   Introduction

Five *bis*-picolinamide rhodium (III) chloride complexes were recently reported. [1] The structural characterisation and spectroscopic analysis of Bhattacharya *et al* synthesised rhodium complexes of the type RhX_2L_2, to give *bis*-picolinamide rhodium dichloride complexes as shown in **Figure 5.1**.[1] The complexes consist of *trans* dichloride ligands and two picolinamide ligands coordinating *(N,N)* and *(N,O)* to the rhodium metal centre, with the two pyridine rings *trans* to each other. The picolinamide ligands are functionalised by a substituent specifically on the *para* position in this series of complexes.

$R = OCH_3, CH_3, H, Cl, NO_2$
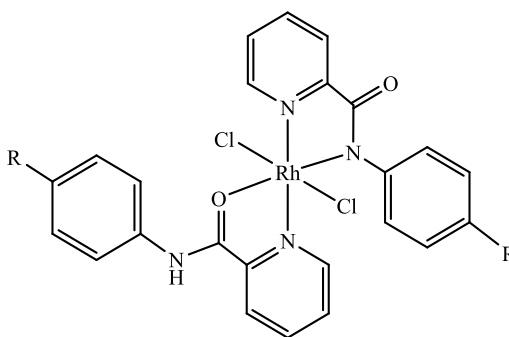
Figure 5.1 *General structure of bis-picolinamide rhodium (III) dichloride complexes developed by Bhattacharya et al[1]*

This chapter includes the synthesis and structural characterisation of a series of novel *bis*-picolinamide rhodium (III) dihalide complexes, functionalised with halide substituents on the *meta* position of the phenyl ring. The aim of this work was to create rhodium analogues of the *bis*-picolinamide ruthenium (III) dihalide complexes described in Chapters 3 and 4. The rhodium complexes were expected to have similar structural characteristics to their Ru analogues, in having five possible isomers (**Fig. 3.1**). The Ru(III) complexes were not suitable to study by NMR spectroscopy, Rh analogues were prepared to analyse their structural characterisation both in solid state using powder diffraction, and in solution by NMR techniques, as well as, their application as catalysts.[2]

5.2   Synthesis of *Bis*-picolinamide Rhodium (III) Dihalide Complexes

Bis-picolinamide rhodium (III) dihalide (RhX_2L_2) complexes were prepared following the general scheme shown in **Scheme 5.1**, where two equivalents of picolinamide ligands were heated under reflux for two hours with rhodium trichloride in ethanol in the presence of a base, triethylamine, to afford complexes **5.1** - **5.4**. A halide-exchange reaction of complexes **5.2** and **5.3** afforded the rhodium diiodide analogues, complexes **5.5** and **5.6** respectively after the addition of an excess of potassium iodide *in situ* and heating under reflux in ethanol for a further 18 h.
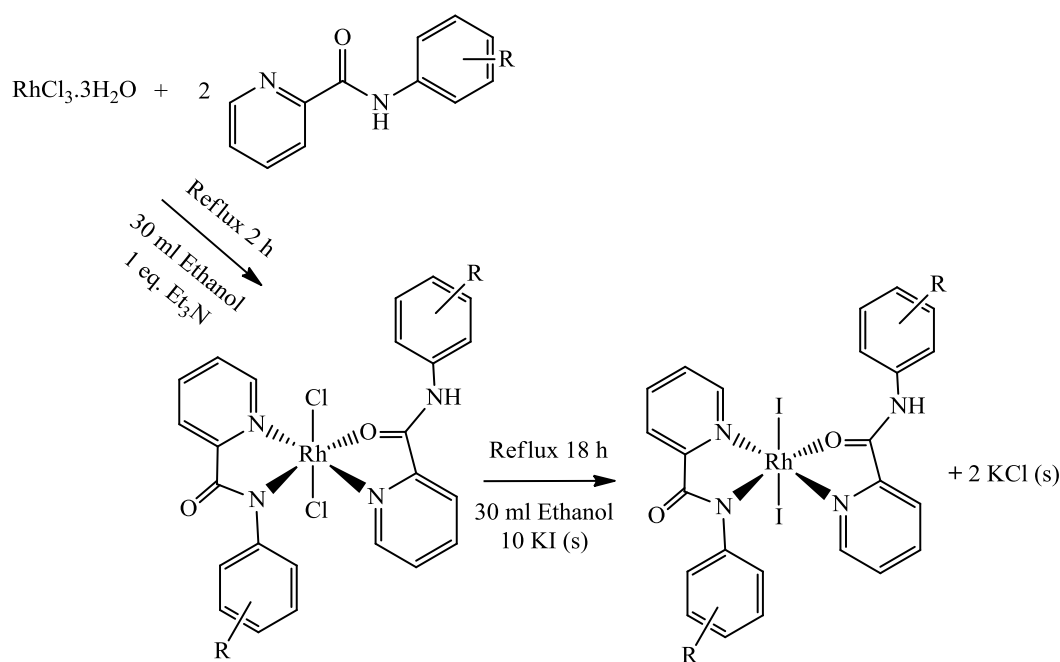
Complex	X	R	Yield
5.1	Cl	3'-F	49%
5.2	Cl	3'-Cl	62%
5.3	Cl	3'-Br	51%
5.4	Cl	3'-I	72%
5.5	I	3'-Cl	45%
5.6	I	3'-Br	36%

Scheme 5.1 *Synthesis of bis-picolinamide rhodium (III) dichloride complexes*

5.3   Characterisation of *bis*-picolinamide Rhodium Dihalide Complexes

Bis-picolinamide rhodium (III) dihalide complexes **5.1** - **5.6** were obtained with yields in a range from 36-72%. These complexes were characterised using IR, NMR, ES-MS, elemental analysis and single crystal X-Ray diffraction. Complexes **5.1** - **5.4** were soluble in polar solvents, including acetonitrile, methanol, dichloromethane, chloroform and acetone, giving orange/yellow solutions, whereas complexes **5.5** and **5.6** were soluble in more polar solvents such as dimethylformamide, tetrahydrofuran and nitromethane to give dark red-brown solutions. The IR spectra for complexes **5.1** - **5.6** show similar characteristics to their ruthenium analogues, with a shift to lower wavelength for both the CO and NH stretches between their respective uncoordinated ligands and the complexes. The IR spectrum for ligand **2.7**, complex **5.2** and complex **5.5** are shown in **Figure 5.2** to show the comparison.

The structural data of complexes **5.1**, **5.3**, **5.4** and **5.5** were collected by x-ray crystallography and show their structural geometry and the *N,N-* and *N,O-* coordination modes of the ligands to the rhodium metal. Interestingly, the rhodium dichloride complexes have shown a different structural geometry from the one reported by Bhattacharya *et al* of *trans-trans-trans* geometry. The single crystals of complexes **5.1**, **5.3** and **5.4**, were obtained from vapour diffusion of methanol/pentane and exhibit the *cis-trans-cis* structure, and *trans-trans-trans* geometry for complex **5.5** which were recrystallised from a dimethylformamide/ether solvent system, described in **Section 5.9**.

The NMR spectra of the complexes show signals between 6.0 - 10.0 ppm, which are thought to be due to the mixture of possible structural isomers, indicated by the two doublets at downfield region, between 8.91 - 9.85 ppm, which are assigned for the proton adjacent to the N atom of the pyridine ring from each picolinamide ligands (^{3}J (^{1}H-^{1}H) ~ 5 Hz).[3, 4] Upon fractional recrystallisation, these complexes crystallise in two or three different forms of shapes and colours, as seen with the ruthenium analogues. Complex **5.3** crystallises as red, orange and yellow crystals, and their characterisation data are described in **Sections 5.5** and **5.6**.

5.4   IR Data for Ligand 2.7, Complex 5.2 and Complex 5.5

The IR spectra of ligand **2.7**, complexes **5.2** and **5.5** are shown in **Figure 5.2**. In the spectrum of the uncoordinated ligand, a strong CO stretch observed at 1678 cm^{-1}, is shifted to 1558 cm^{-1} in both complexes **5.2** and **5.5**. Broad and weak NH stretches are also seen, in the region 3000-3500 cm^{-1}, shifted from 3328 cm^{-1} of ligand **2.7** to 3064 cm^{-1} and 3046 cm^{-1} for complexes **5.2** and **5.5** respectively. This pattern is consistent for all of the *bis*-picolinamide rhodium dichloride complexes reported in this chapter.

Ligand **2.7**   Complex **5.2**   Complex **5.5**
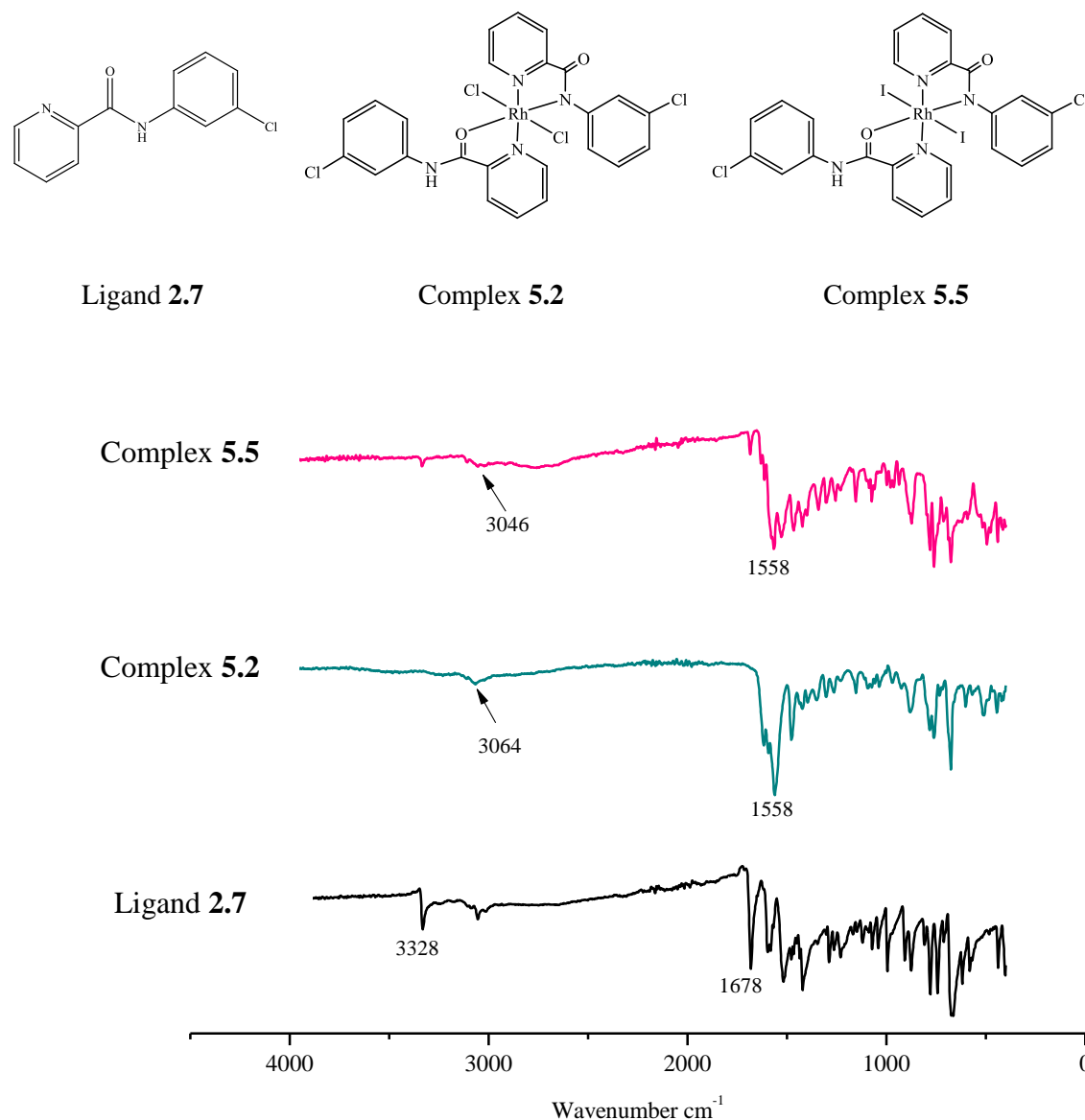
Figure 5.2 IR spectra of ligand 2.7, complex 5.2 and 5.5

5.5   IR Data of Complex 5.3

Complex **5.3** crystallised in three different fractions - red needles (complex **5.3a**), orange blocks (complex **5.3b**) and yellow microcrystals (complex **5.3c**). The different fractions were well-separated and collected for further characterisation. The IR spectra of complexes **5.3a**, **5.3b** and **5.3c** are shown in **Figure 5.3**. The weak NH stretch is observed at 3033, 3057 and 3065 cm^{-1} for complexes **5.3a**, **5.3b** and **5.3c** respectively. A strong CO stretch splits into two bands, within the 1543 - 1613 cm^{-1} region, which is clearly seen for complexes **5.3b** and **5.3c**. A difference in intensities can be seen between the C-Br stretches in the region 744 - 783 cm^{-1}. The two medium C-Br stretches for complex **5.3a** and **5.3b** appeared at 744 and 783 cm^{-1}, and 775 and 760 cm^{-1} respectively, whereas, the intensity of C-Br stretch for complex **5.3c** showed a strong intensity at 779 and 752 cm^{-1}.
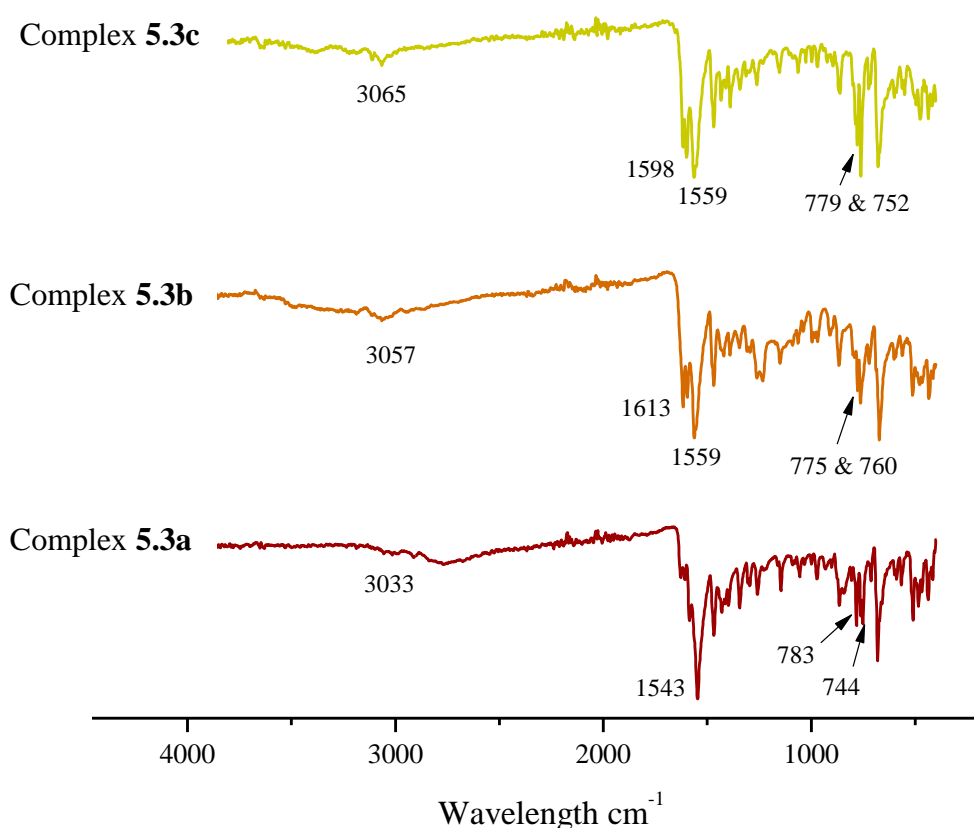
Figure 5.3 IR spectra of complexes 5.3a, 5.3b and 5.3c

5.6   NMR Data of Complex 5.3

The ^{1}H NMR spectra of complex **5.3a** and complex **5.3c** are shown in **Figure 5.5**. The ^{1}H NMR spectrum for complex **5.3b** showed very weak signals due to an insufficient amount obtained, therefore is not included in the figure. One molecule is expected to integrate to a total number of 17 protons. The spectra, however, did not show the presence of an NH peak and integrated to 16 protons. This was also the case with the rhodium complexes developed by Bhattacharya *et al*. [1] The reason for this it is as yet uncertain as it is known that the ligands are coordinated in *(N,N)* and *(N,O)* mode as determined from their crystal structures (shown in **Section 5.9**).

Both spectra showed similar peaks with strong and weak signals at certain chemical shifts. The weak signals are thought to be the presence of a different structural isomer as they integrate to a total number of 16 protons. Complex **5.3c** showed additional weak signals (highlighted), where some peaks can be seen overlapping with each other. These additional signals similarly gave a total of 16 protons, suggesting yet another isomer is present. The ratio of the possible isomers determined from the ^{1}H NMR peak integrals is 1:0.2 for complex **5.3a** and 1:0.2:0.1 for complex **5.3c**. The red crystals, complex **5.3a**, could be the pure and main structural isomer of complex **5.3**, but with a minor isomer molecule still present.

Based on the x-ray crystal structure obtained for complex **5.3a** (discussed in detailed in **Section 5.9.2**), it is known that this complex has a *cis-trans-cis* structure. In order to assign the NMR spectra, the x-ray structure was used as the general structure for complex **5.3** (**Figure 5.4**). The doublets at 8.91 - 9.85 ppm were assigned based on the account of the typical [3]J coupling ~ 5 Hz, for protons adjacent to the N atom of a pyridine ring.[3, 4] The peaks labelled (*) and (#) are assigned for the two unknown structural isomers, where peaks are not overlapping. These assignments are presented in **Table 5.1** based on the ^{1}H-^{1}H COSY spectra of complex **5.3c**, as shown in **Figure 5.6** and **Figure 5.7**.
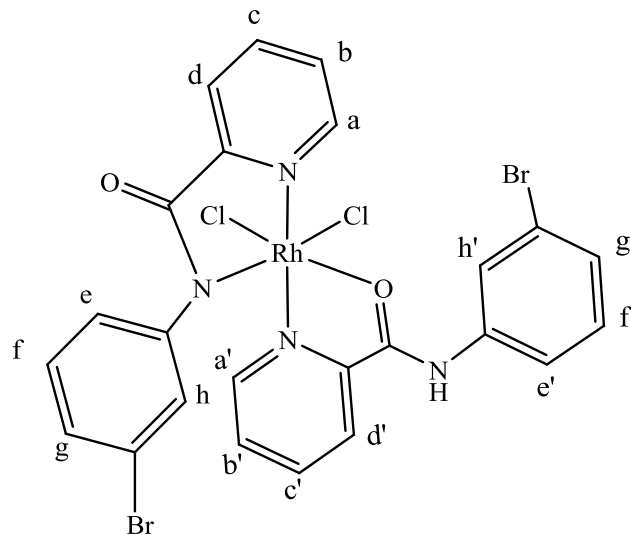
Figure 5.4 *General structure of complex 5.3a*
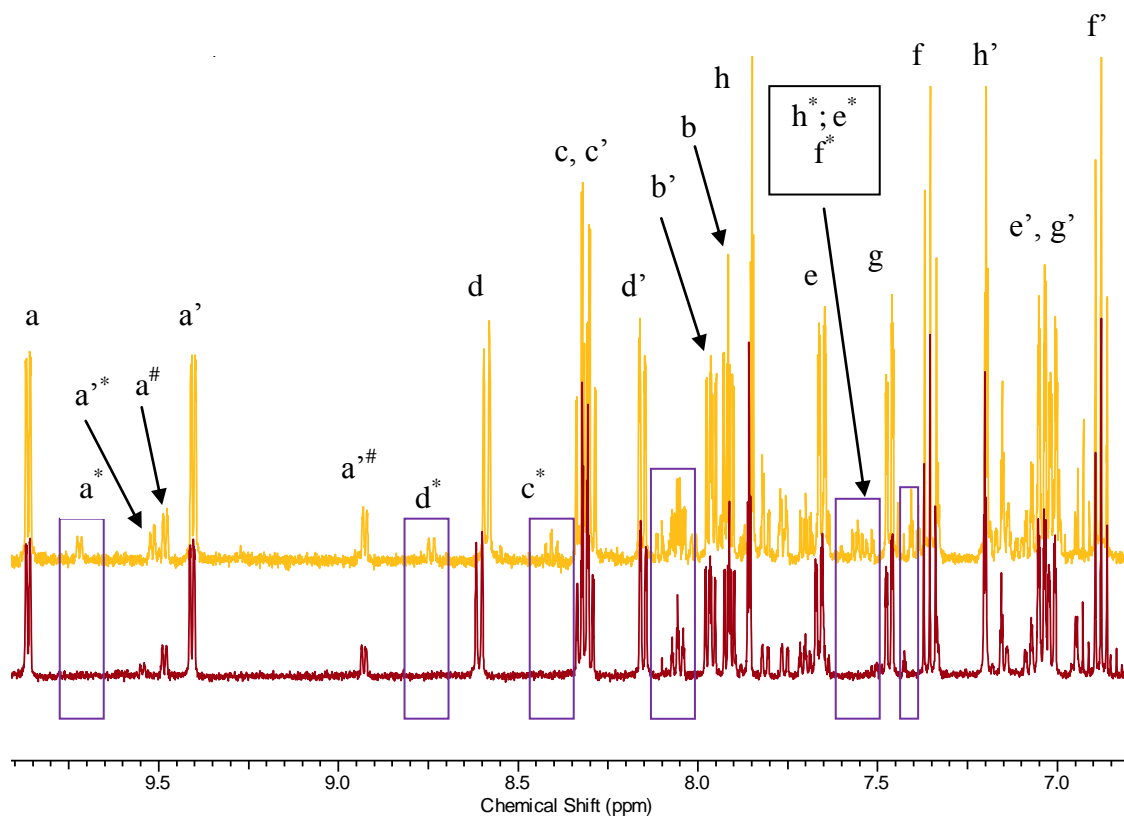
Figure 5.5 *^{1}H NMR spectra of complexes **5.3a** (shown in red), and **5.3c** (shown in yellow) (d$_6$-acetone, 300.13 MHz, 300 K)*

Table 5.1 ^{1}H chemical shift assignments for complex 5.3

Chemical Shift (δ ppm) ^{1}H	Splitting Pattern	Assignment
9.85, 9.7, 9.5, 9.46, 9.39, 8.91	d	a, a*, a'*, a$^\#$, a', a'#
7.95, 7.90	ddd	b, b'
8.29, 8.29, 8.39	dtd	c, c', c*
8.57, 8.14, 8.72	d	d, d', d*
7.64, 7.01, 7.55	ddd	e, e', e*
7.34, 6.86, 7.51	t	f, f', f*
7.45, 7.01	ddd	g, g'
7.83, 7.18, 7.62	t	h, h', h*
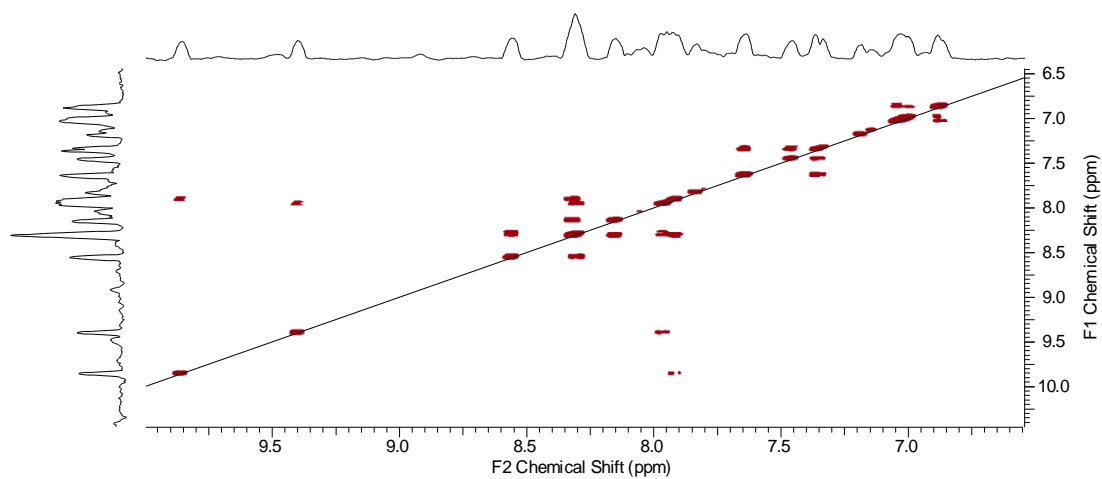
Figure 5.6 ^{1}H-^{1}H COSY NMR spectrum of complex 5.3c (d$_6$-acetone, 300.13 MHz, 300K)
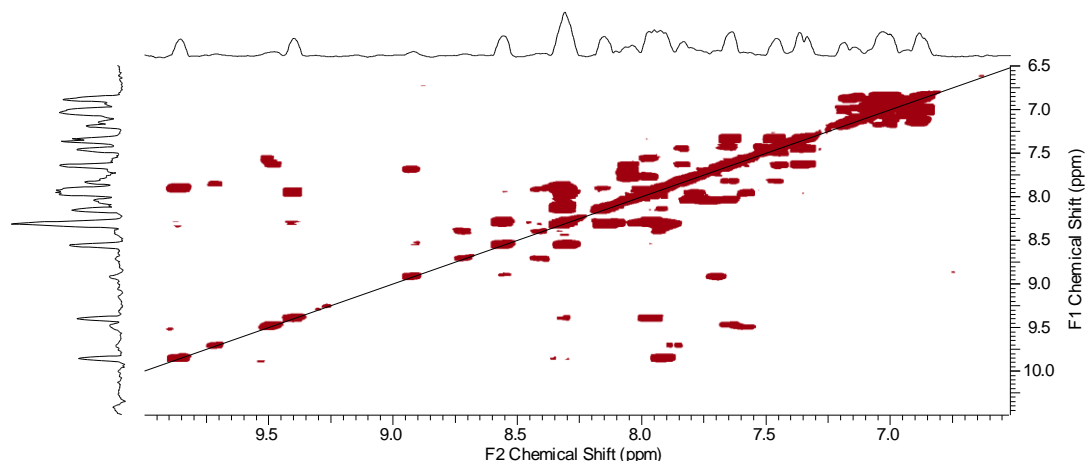
Figure 5.7 *^{1}H-^{1}H COSY NMR spectrum of complex **5.3c** with higher intensity showing the correlation of isomeric compounds (d_6-acetone, 300.13 MHz, 300K)*

5.7 ^{1}H- NMR Variable-Temperature Studies of Complex 5.3

Previously within the McGowan group, a titanium ethoxide complex was synthesised and studied to investigate fluxional processes between several isomers in solution.[5] A similar observation was also noted in the budotitane series of complexes developed by Keppler *et al.*[6] **Figure 5.8** shows the structure of the complex with the three isomers identified from the ^{1}H NMR spectra taken between 233 K and 333 K. As the temperature decreases, the timescale of the exchange process between the isomers also decreases that leads to the signal broadening and the appearance of more peaks. These signals are identified as the three *cis* isomers of the complex: *cis-cis-cis*, *cis-trans-cis* and *cis-cis-trans*. The two diketonate ligands in the *cis-cis-cis* isomer gives two signals each as they are not in identical environments, whereas the two other *cis* isomers show one signal each for the diketonate ligand and methyl protons.

cis-cis-cis   *cis-cis-trans*   *cis-trans-cis*
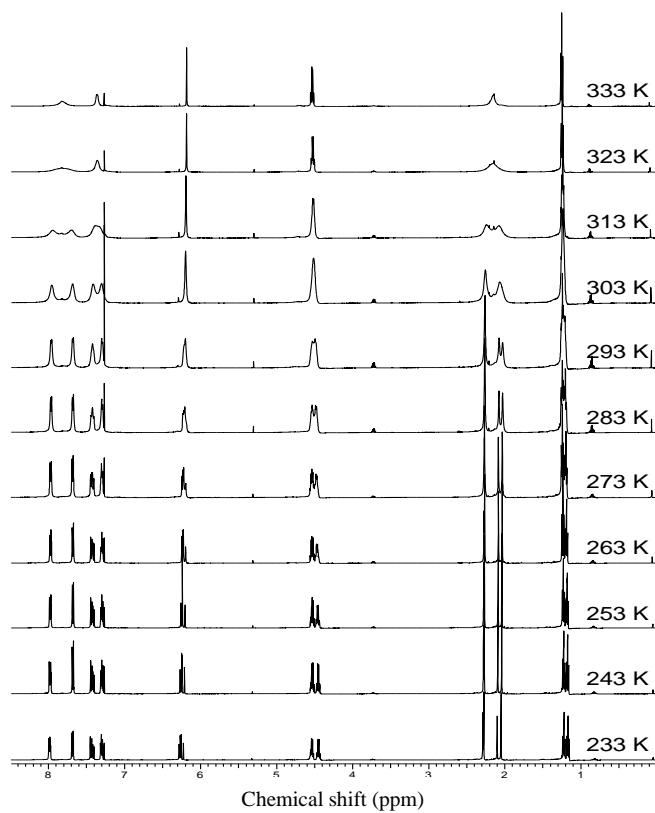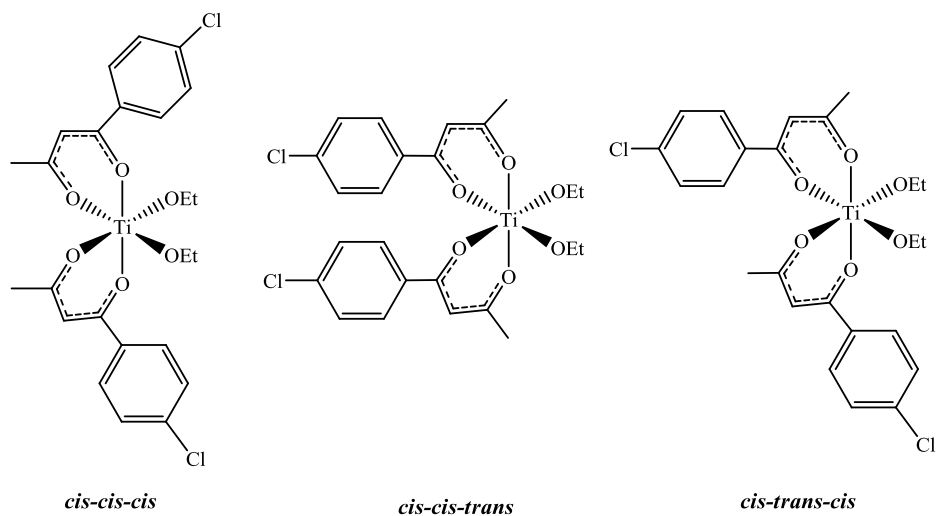
Figure 5.8 *The three cis isomers of titanium ethoxide complex observed at 233 K, and the variable temperature ^{1}H NMR study (CDCl$_{3}$, 300.13 MHz)*[5]

The *bis*-picolinamide rhodium dichloride complex **5.3** was studied for the possibility of fluxional processes between the structural isomers present in the solution. This study was carried out over a range of days and at variable temperature. The ^{1}H NMR spectra of complex **5.3a** and **5.3c** was taken at Day 1, Day 3 and Day 7 at room temperature. The spectra showed similar peak splitting and integration of 16 protons for each possible major and minor isomers present. This suggests that the complexes do not interchange between the different structural isomers present within the solution over time at room temperature.

The ^{1}H NMR spectra of complex **5.3** at lowest temperature, 213 K and at the highest temperature, 323 K, are as shown in **Figure 5.9**. These observations are different as previously seen with the budotitane series of complexes, whereby instead of having three different isomers with the same ratio at the lowest temperature, complex **5.3** showed a high ratio for one isomer, which is the *cis-trans-cis* structure. This is determined by the peak integrals that correspond to a total number of 16 protons for one complex, not including the NH peak. The presence of signals for isomeric compounds at 213 K is seen as very broad and weak signals.

Figure 5.10 shows the temperature-dependant ^{1}H NMR spectra of complex **5.3c** in increasing temperature at every 10 K from 213 K up to 323 K. Broadening of the peaks is observed at the lowest temperature, 213 K. In increasing the temperature, there is a slight shift for the protons on the pyridine rings, whereby the H(a) and H(a') protons are shifted downfield, and upfield shifts for the H(b), H(b'), H(c), H(c'), H(d) and H(d') protons. All the broad signals at 213 K sharpen as the temperature increases. These are particularly seen in the coupling of the pyridine H(b) and H(b') protons, and the phenyl H(e') – H(h') protons of the *(N,O)*-coordinated ligand. The signals become separated into doublets and triplets, including the weak signals of the isomeric compounds which become more resolved. The broad signals at low temperature are due to the molecules stacking together as they interact very close between each other.[7] The molecules are separated as the temperature increases, hence the appearance of the sharp resolved peaks.

When decreasing the temperature from 323 K, the signals show similar patterns as increasing the temperature. This indicates that the changes are reversible and that the molecules may not change in structure and are stable, even when at room temperature.
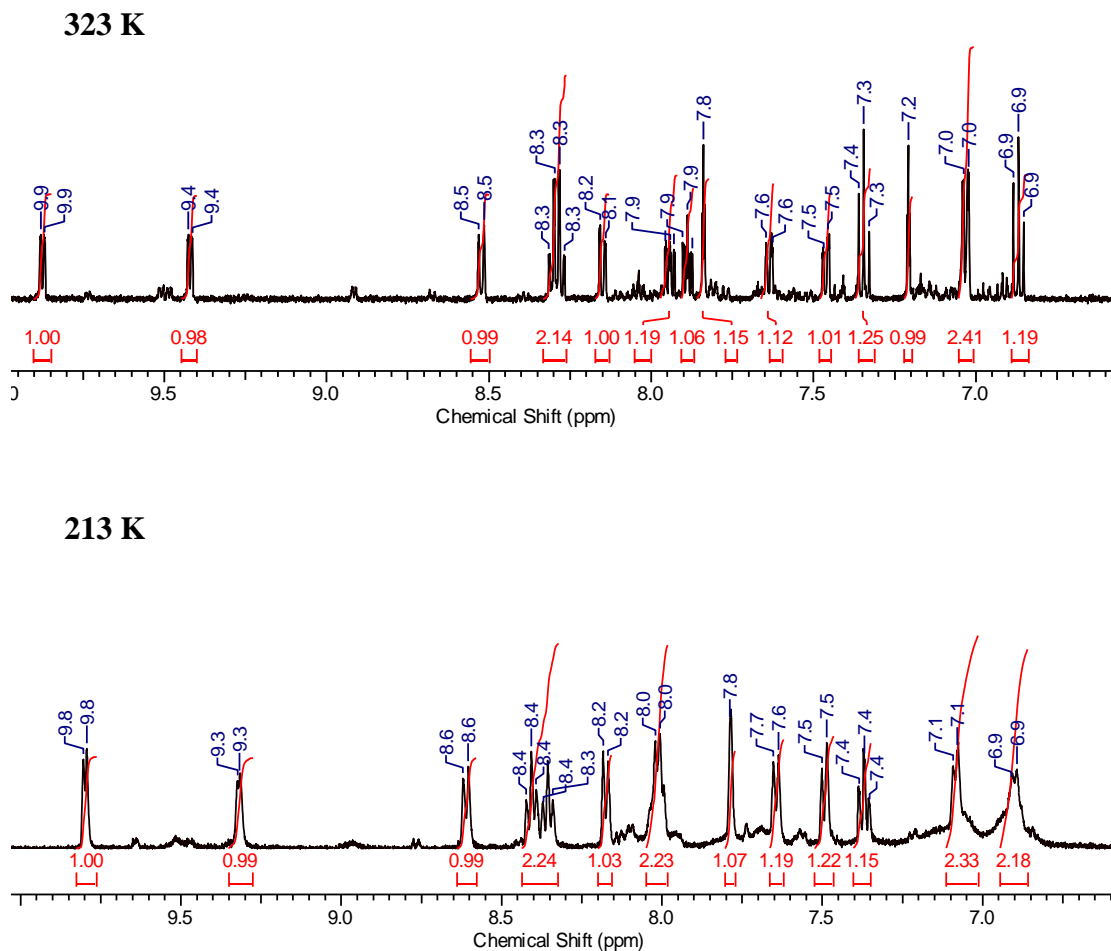
323 K

213 K

Figure 5.9 *^{1}H NMR spectra of complex **5.3** at 213 K and 323 K*
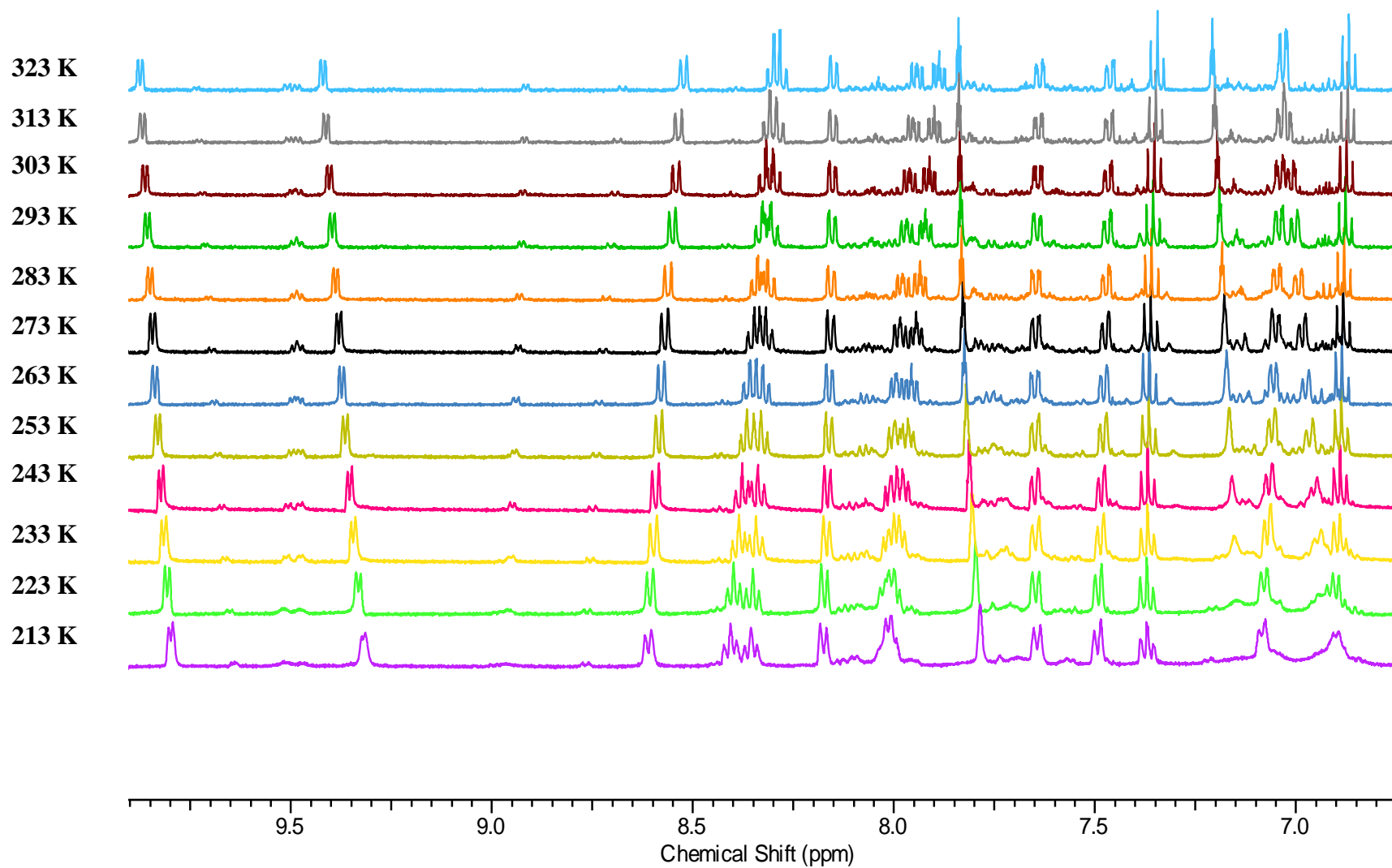
Figure 5.10 *Temperature-dependant ^{1}H NMR spectra of complex* ***5.3*** *(d_6-acetone, 300 MHz)*

5.8   NMR Data of Complex 5.5

The ^{1}H NMR characterisation of *bis*-picolinamide rhodium diiododide complex **5.5** has showed a different observation as compared to its dichloride analogue. The ^{1}H NMR spectrum and a general structure of complex **5.5** with the assigned protons are as shown in **Figure 5.11**. The signals integrate to a total number of 16 protons, and there is no presence of minor isomers seen, indicating that the complex only has one structural isomer present. This observation agrees well with the ruthenium diiodide analogue, whereby the complex has a stable *trans-trans-trans* structure both in solid state and in solution (**Section 4.7**). The proton adjacent to the N atom of the pyridine ring from each picolinamide ligands appear as two doublets at 8.45 and 9.62 ppm (^3J (^{1}H-^{1}H) ~ 5 Hz).
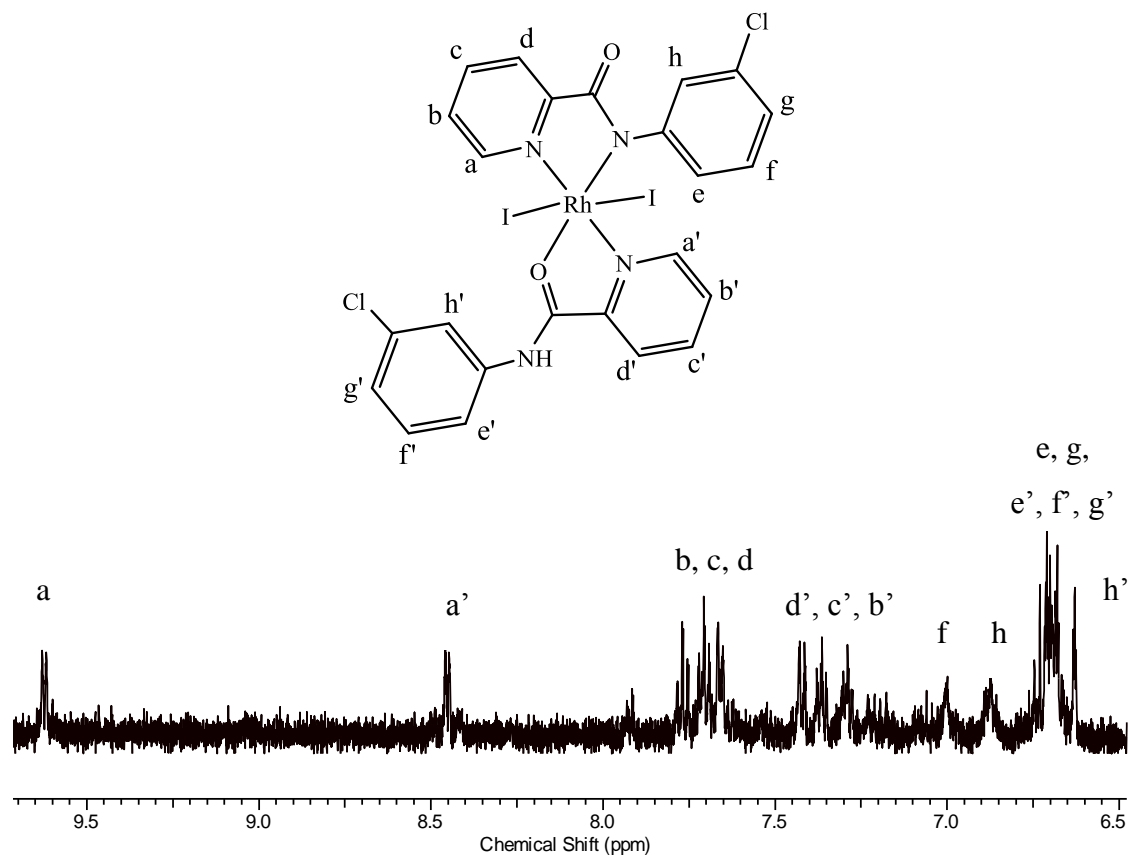
*Figure 5.11 ^{1}H NMR spectrum of complex **5.5** (d₄-MeOD, 500 MHz)*

5.9   X-ray Crystallography Data for *bis*-Picolinamide Rhodium (III) Dihalide Complexes

Single crystals of complexes **5.1**, **5.3** and **5.4** suitable for X-ray crystallography were obtained by vapour diffusion of pentane into a solution of the complex in methanol, while complex **5.5** which was crystallised by vapour diffusion of ether into a solution of dimethylformamide. The *bis*-picolinamide rhodium dihalide complexes have a distorted octahedral centre, with bond angles in the range 88.9°-97.1° between the ligands that are *cis* to each other, and bond angles of 171.5°-173.3° between the *trans* ligands about the rhodium metal centre.

Due to the rigidity of the picolinamide ligands, the bond angles between the two N atoms of the *(N,N)*-coordinate ligand, and the N and O atom of the *(N,O)*-coordinated ligand, are found to be less than 90°. The angle between the two *cis* chlorine atoms around the rhodium centre is between 90.9° - 93.0°, and between the two *trans* iodine atoms for complex **5.5** is 177.35(5)°. The *(N,N)*-coordinated picolinamide ligands adopt non-planar configurations, with the torsion angle between the picolinamide rings ranging from 83.4 to 111.7°. The *(N,O)*-coordinated ligands functionalised with a 3'-F and 3'-Br substituents on the phenyl ring for the *cis* complexes adopt an almost planar configurations with torsion angle of 171.6° and 177° respectively. The torsion angle for the 3'-I functionalised *(N,O)*-picolinamide ligand is 94.9°. This less planar configuration may be due to the extra steric bulk of the iodine atom pointing away from the chloride ligands.

The Rh-Cl bond distances for all the *bis*-picolinamide rhodium dichloride complexes are similar, where one of the Rh-Cl bonds is longer than the other, with an average bond distance of 2.31 Å for Rh-Cl(1) and 2.36 Å for Rh-Cl(2). The Rh-I bond distances for complex **5.5** are longer than its dichloride analogue with an average bond distance of 2.66 Å for Rh-I(1) and Rh-I(2). The average bond lengths of Rh(1)-N(1), Rh(1)-N(2), Rh(1)-N(3) and Rh(1)-O(2) for all complexes are 2.01 Å, 2.02 Å, 2.04 Å and 2.07 Å respectively, which are found to be quite normal.[8]

5.9.1 X-ray Crystal Structure of Complex 5.1

Complex **5.1** crystallised as orange blocks and yellow microcrystals, which were obtained by vapour diffusion of pentane into a methanolic solution of the complex. Only the orange blocks of complex **5.1** were found to be suitable for structure determination by X-ray crystallography. The complex crystallised in an orthorhombic cell and structural solution was performed in the space group $P2_12_12_1$. The asymmetric unit contains one molecule of the complex and one molecule of methanol. The molecular structure of complex **5.1** is shown in **Figure 5.12** with a *cis-trans-cis* arrangement, and selected bond lengths and angles are given in **Table 5.2**.
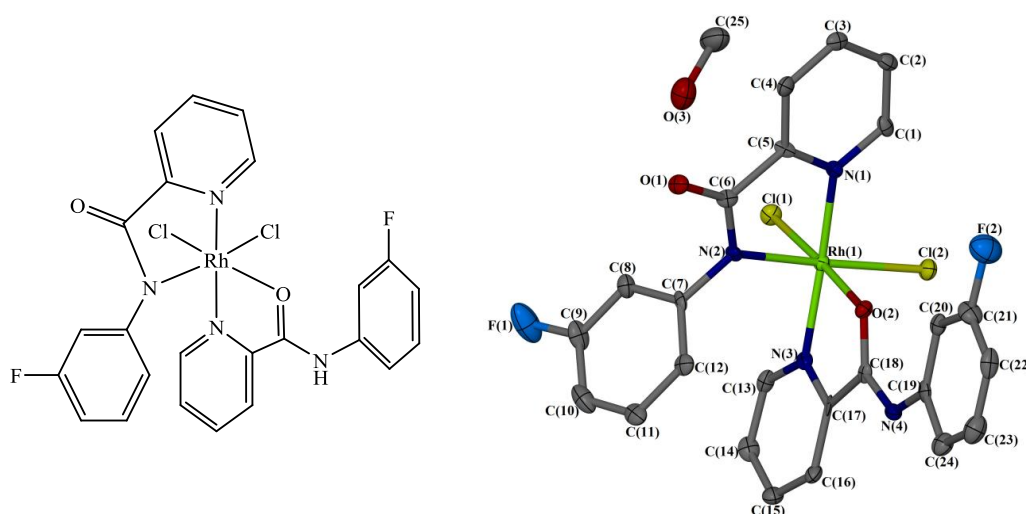
Figure 5.12 *Molecular structure of complex **5.1**. Displacement ellipsoids are at the 50% probability level. Hydrogen atoms are omitted for clarity.*

Table 5.2 *Selected bond lengths and angles for complex **5.1** with s.u.s shown in parenthesis*

Bond length (Å)		Bond angle (°)	
Rh(1)-Cl(1)	2.3166(15)	Cl(1) - Rh(1) - Cl(2)	92.34(5)
Rh(1)-Cl(2)	2.3569(13)	N(1) - Rh(1) - O(2)	93.29(16)
Rh(1)-N(1)	2.018(4)	N(2) - Rh(1) - O(2)	88.92(17)
Rh(1)-N(2)	2.023(4)	N(2) - Rh(1) - N(3)	94.17(19)
Rh(1)-N(3)	2.030(5)	N(1) - Rh(1) - N(3)	171.51(19)
Rh(1)-O(2)	2.043(4)		

Complex **5.1** is arranged in a herringbone motif along the *a*-axis, and in alternate layers along the *b*-axis, as shown in **Figure 5.13**. Two complex molecules are held together by a methanol molecule *via* hydrogen bond interactions between one of the chloride ligands (bond distance O(3)-Cl(1) 3.1877 Å) and the hydrogen on the pyridyl ring of the *(N,O)*-coordinated picolinamide ligand (bond distance C(14)-O(3) 3.470(8) Å) (**Figure 5.14a**). The other interactions are between an amide group of one molecule with a carbonyl group of another molecule (bond distance (N(4)-O(1) of 2.794(6) Å), and between a fluorine substituent on the phenyl ring with a hydrogen on the pyridyl ring (bond distance C(15)-F(1) of 3.221(8) Å). Intramolecular interactions can also be seen within a complex molecule, one with the chloride ligand (bond distance C(1)-Cl(2) of 3.348(6) Å), and the other interaction is within the *(N,O)*-coordinated ligand (C(20)-O(2) of 2.811(7) Å) (**Figure 5.14b**).

(a)   (b)
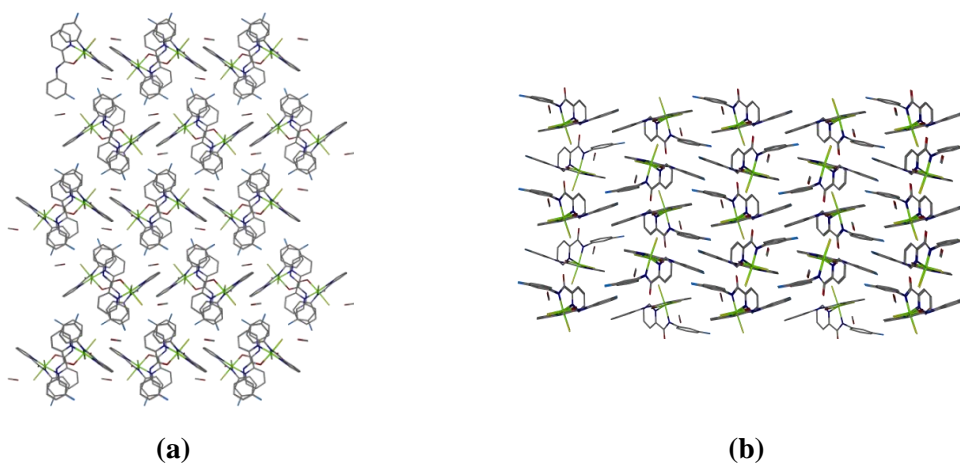
Figure 5.13 *Packing diagrams of complex **5.1** viewed along the (**a**) a-axis and (**b**) b-axis. Hydrogen atoms are omitted for clarity.*

(a)   (b)
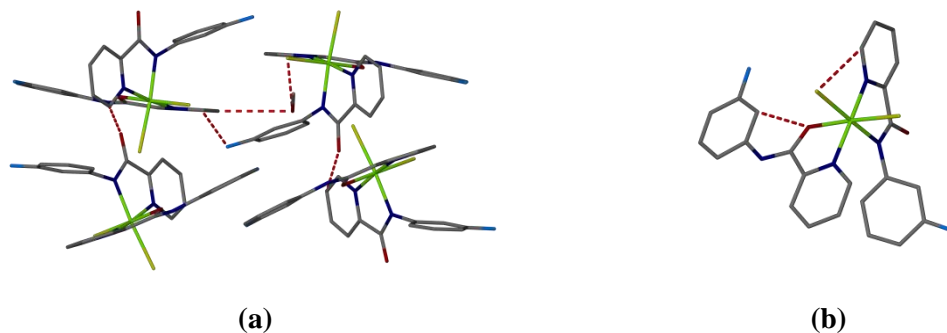
Figure 5.14 *(**a**) Intermolecular and (**b**) intramolecular hydrogen bond interactions of complex **5.1**. Hydrogen atoms are omitted for clarity.*

5.9.2 X-ray Crystal Structure of Complex 5.3

Complex **5.3** crystallised as red plates, orange blocks and yellow microcrystals, however only the red plates were found suitable for x-ray crystallography. These crystals were obtained by vapour diffusion of pentane into a methanolic solution of the complex. Red plates of complex **5.3** crystallised in a monoclinic cell and structural solution was performed in the space group *Cc*. The asymmetric unit contains one complex molecule. The molecular structure is shown in **Figure 5.15** with the structural arrangement of *cis-trans-cis* and selected bond lengths and angles are given in **Table 5.3**.
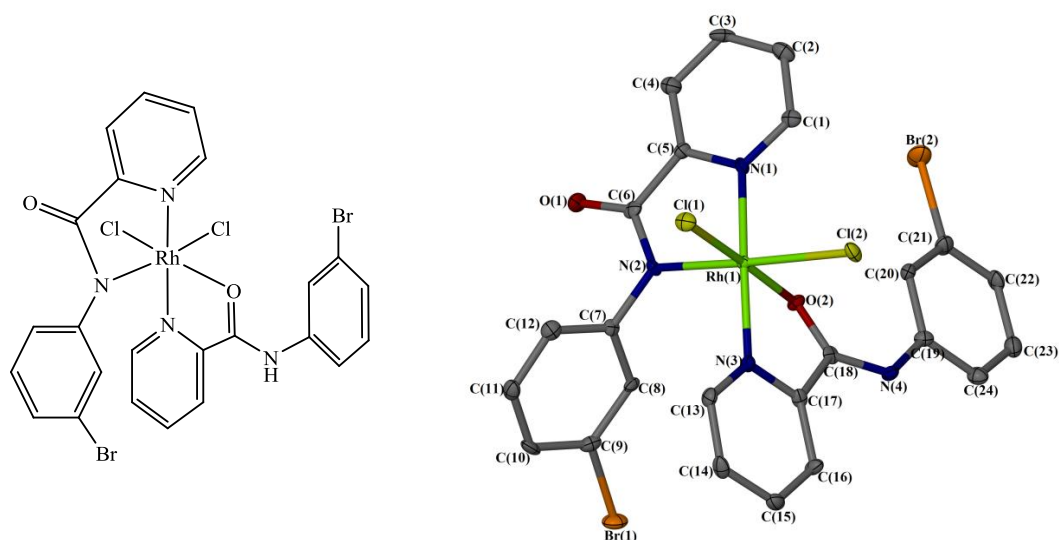
Figure 5.15 *Molecular structure of complex **5.3**. Displacement ellipsoids are at the 50% probability level. Hydrogen atoms are omitted for clarity.*

Table 5.3 *Selected bond lengths and angles for complex **5.3** with s.u.s shown in parenthesis*

Bond length (Å)		Bond angle (°)	
Rh(1)-Cl(1)	2.3130(15)	Cl(1) - Rh(1) - Cl(2)	92.92(6)
Rh(1)-Cl(2)	2.3643(14)	N(1) - Rh(1) - O(2)	92.92(18)
Rh(1)-N(1)	2.027(5)	N(2) - Rh(1) - O(2)	91.04(19)
Rh(1)-N(2)	2.018(5)	N(2) - Rh(1) - N(3)	97.1(2)
Rh(1)-N(3)	2.020(5)	N(1) - Rh(1) - N(3)	172.4(2)
Rh(1)-O(2)	2.044(4)		

Complex **5.3** packed in a zig-zag pattern along the *a*-axis, and alternate layers along the *c*-axis, as shown in **Figure 5.16**. The molecules are held together by several interactions of intermolecular hydrogen bonding, which are between the amide group of a complex molecule with the carbonyl group of the second complex molecule (bond distance (N(4)-O(1) of 2.680(6) Å), and between the oxygen atom of the second complex molecule with the bromine substituent of the third complex molecule (bond distance O(2)-Br(1) of 3.228 Å).

(a)   (b)
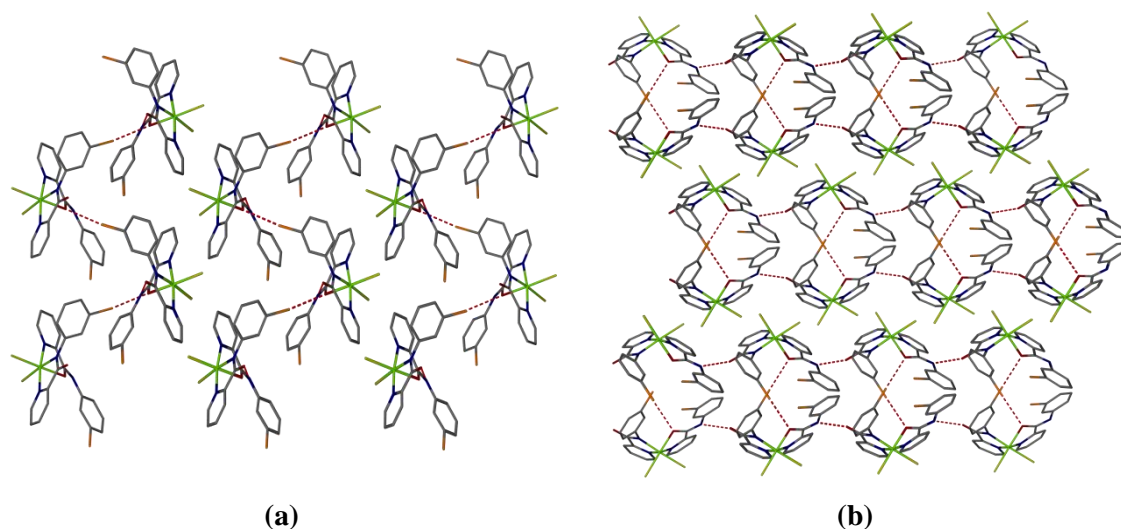
Figure 5.16 *Packing diagrams of complex **5.3** viewed along the (**a**) a-axis and (**b**) c-axis, showing intermolecular hydrogen bond interactions between the complex molecules. Hydrogen atoms are omitted for clarity.*

5.9.3 X-ray Crystal Structure for Complex 5.4

Red plates of complex **5.4** suitable for X-ray crystallography were obtained by vapour diffusion of pentane into a methanolic solution of the complex. Complex **5.4** crystallised in an orthorhombic cell and structural solution was performed in the space group *P2₁/c*. The asymmetric unit contains one molecule of the complex and two molecules of methanol solvent. The molecular structure is shown in **Figure 5.17** with the arrangement of *cis-trans-cis* and selected bond lengths and angles are given in **Table 5.4**.
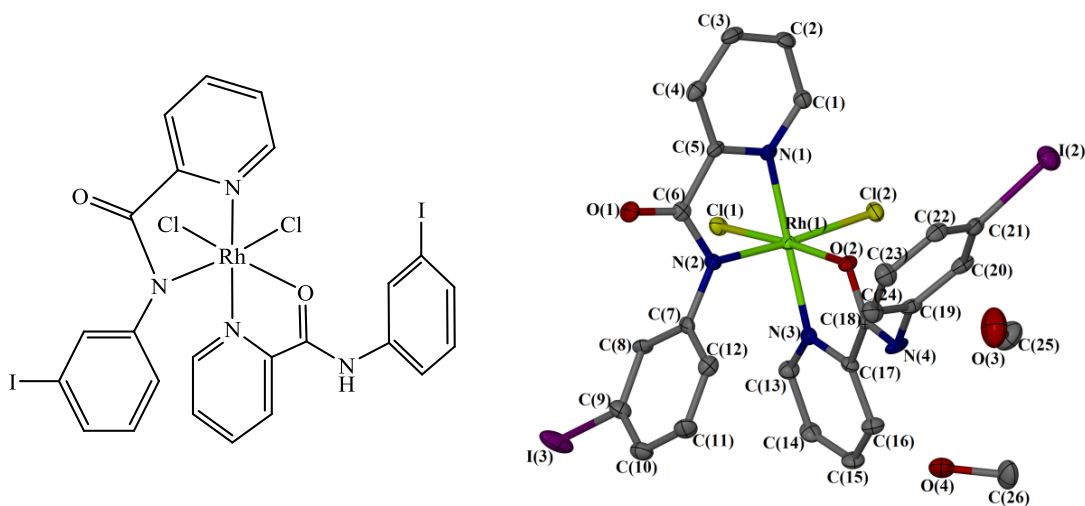
Figure 5.17 Molecular structure of complex 5.4. Displacement ellipsoids are at the 50% probability level. Hydrogen atoms are omitted for clarity.

Table 5.4 Selected bond lengths and angles for complex 5.4 with s.u.s shown in parenthesis

Bond length (Å)		Bond angle (°)	
Rh(1)-Cl(1)	2.3134(13)	Cl(1) - Rh(1) - Cl(2)	90.86(5)
Rh(1)-Cl(2)	2.3558(14)	N(1) - Rh(1) - O(2)	93.76(15)
Rh(1)-N(1)	2.030(4)	N(2) - Rh(1) - O(2)	88.77(16)
Rh(1)-N(2)	2.018(4)	N(2) - Rh(1) - N(3)	96.21(17)
Rh(1)-N(3)	2.031(4)	N(1) - Rh(1) - N(3)	173.27(17)
Rh(1)-O(2)	2.050(3)		

Complex **5.4** packed in a horizontal linear distribution along the *b*-axis, as shown in **Figure 5.18**. **Figure 5.19a** shows the intermolecular hydrogen bonding between the hydrogen on the pyridyl ring of the *(N,N)*-coordinated picolinamide ligand of one complex molecule and the oxygen atom of the *(N,O)*-coordinated picolinamide ligand of another complex molecule (bond distance of C(3)-O(2) of 3.419(7) Å). Another interaction involves the hydrogen bonding of two complexes with a methanol molecule, between a chloride ligand of one complex molecule (bond distance C(13)-Cl(1) of 3.336(5) Å) and a carbonyl group of another complex molecule (bond distance of O(3)-O(1) of 2.804(7) Å) (**Figure 5.19b**).
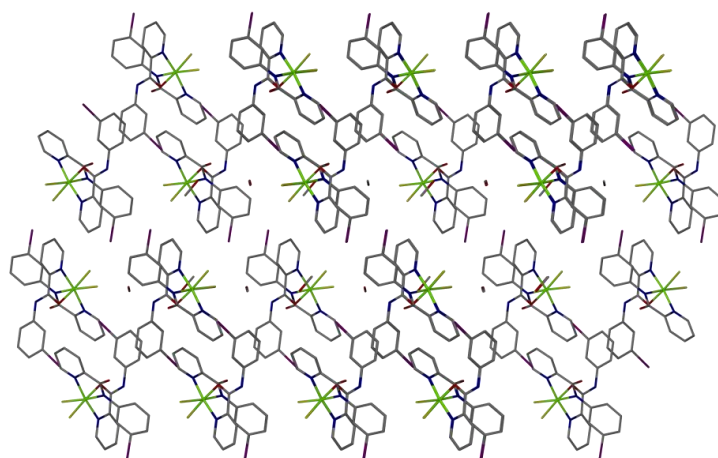
Figure 5.18 Packing diagram viewed along the b-axis of complex *5.4*. Hydrogen atoms are omitted for clarity.
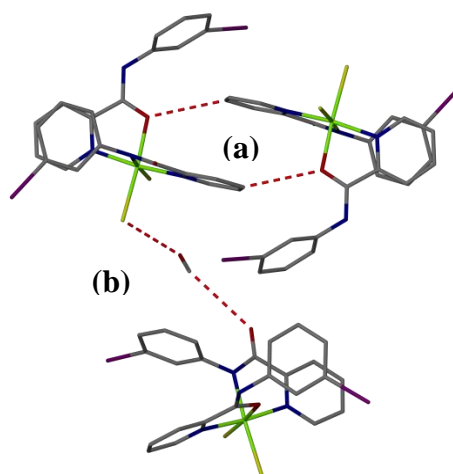
Figure 5.19 Intermolecular hydrogen bond interactions of (*a*) carbonyl group, and (*b*) chloride ligand with a methanol molecule

5.9.4   X-ray Crystal Structure for Complex 5.5

Complex **5.5** crystallised as red plates suitable for X-ray crystallography, which were obtained by vapour diffusion of diethyl ether into a dimethylformamide solution of the complex. The complex crystallised in a monoclinic cell and structural solution was performed in the space group *Cc*. The asymmetric unit contains one complex molecule and one dimethylformamide molecule. The molecular structure is shown in **Figure 5.20** with a *trans-trans-trans* structural geometry and selected bond lengths and angles are given in **Table 5.5**.
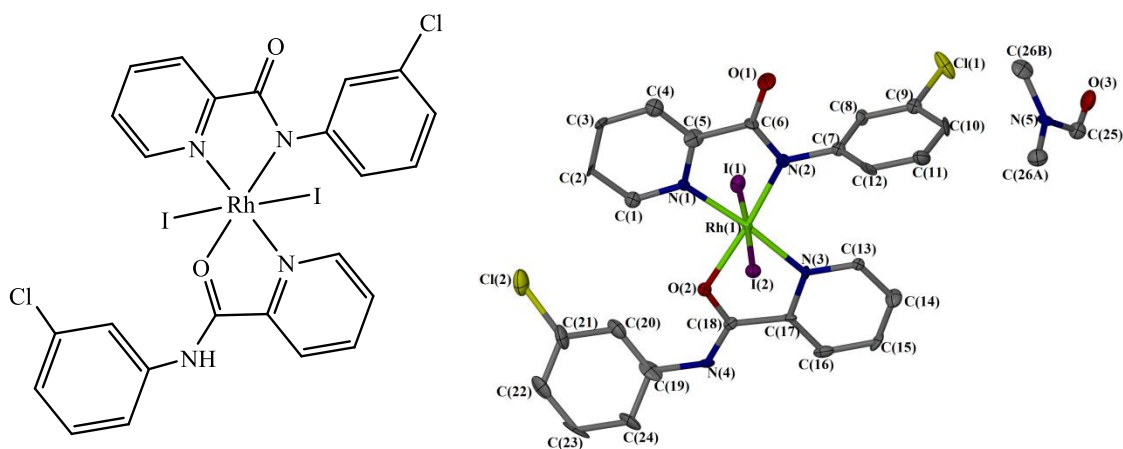
Figure 5.20 *Molecular structure of complex* **5.5**. *Displacement ellipsoids are at the 50% probability level. Hydrogen atoms are omitted for clarity.*

Table 5.5 *Selected bond lengths and angles for complex* **5.5** *with s.u.s shown in parenthesis*

Bond length (Å)		Bond angle (°)	
Rh(1)-I(1)	2.6620(13)	I(1) - Rh(1) - I(2)	177.35(5)
Rh(1)-I(2)	2.6640(13)	N(1) - Rh(1) - O(2)	95.0(4)
Rh(1)-N(1)	2.010(10)	N(2) - Rh(1) - O(2)	175.2(4)
Rh(1)-N(2)	2.015(10)	N(2) - Rh(1) - N(3)	106.7(4)
Rh(1)-N(3)	2.035(11)	N(1) - Rh(1) - N(3)	172.8(5)
Rh(1)-O(2)	2.067(8)		

Complex **5.5** packed in herringbone motif along the *a*-axis, and in diagonal linear arrangement along the *b*-axis, as shown in **Figure 5.21**. The molecules are held together by several interactions of intermolecular hydrogen bonding with the DMF molecule. **Figure 5.22** shows the intermolecular interactions of three complex molecules with one DMF molecule. The interactions involve the NH moiety of the first complex molecule with the oxygen atom of the DMF molecule (bond distance N(4)-O(3) of 2.756(15) Å), a chlorine substituent on the *(N,O)*-coordinated ligand of the second complex molecule with the DMF molecule (bond distance Cl(2)-C(25) of 3.348(6) Å), and the CO moiety of the third complex molecule with the methyl group of the DMF molecule (bond distance C(26A)-O(1) of 3.175(18) Å). Intramolecular interactions can also be seen within the molecule, which are between the oxygen atom of the *(N,O)*-coordinated ligand with the phenyl ring of the same ligand (bond distance C(20-O(2) of 2.751(17) Å), and pyridyl ring of the *(N,N)*-coordinated ligand (bond distance C(1)-O(2) of 3.146(7) Å).

| (a) | (b) |
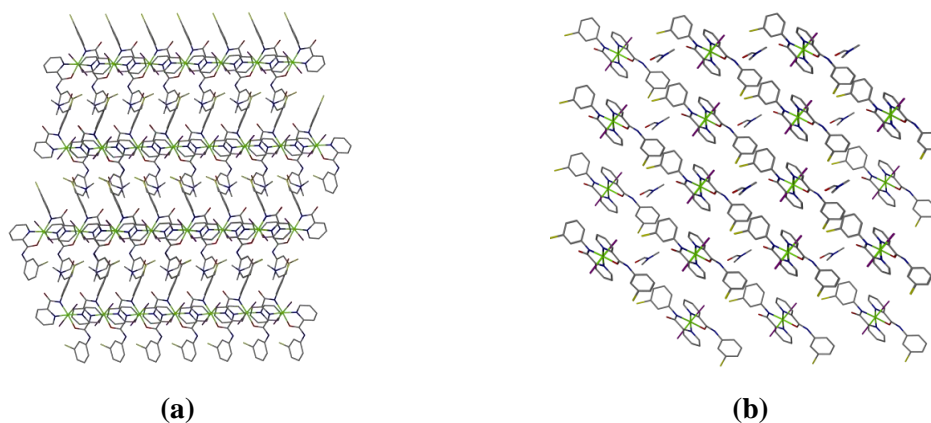
Figure 5.21 *Packing diagram viewed along the (**a**) a-axis (**b**) b-axis of complex **5.5**.*

Hydrogen atoms are omitted for clarity.

| (a) | (b) |
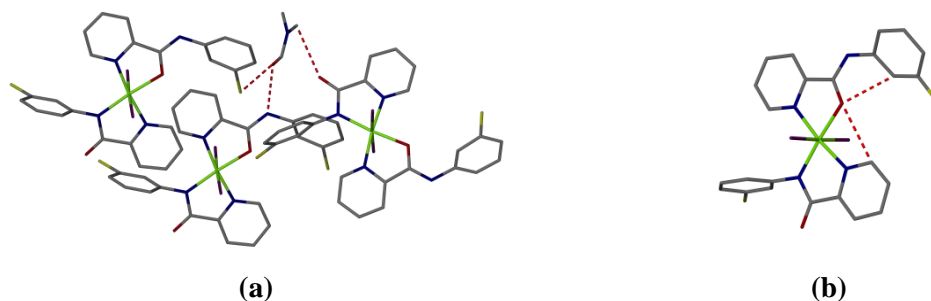
***Figure 5.22** (**a**) Intermolecular and (**b**) intramolecular hydrogen bond interactions of complex **5.5**. Hydrogen atoms are omitted for clarity.*

5.10 PXRD Powder Diffraction Studies

The powder diffraction (PXRD) pattern of complex **5.3** was recorded to compare between the bulk powder sample of the complex with its single crystal structure in order to determine the purity of its structural geometry in the bulk sample. The diffractogram simulated from a single *cis* crystal structure of complex **5.3** is compared with the diffractogram recorded from its powder sample, as shown in **Figure 5.23**.

The PXRD patterns show some similarities on the peaks between their diffractograms, with few additional peaks observed as well. There may be a possibility that most of the complex molecules from the bulk powder sample matches with the *cis-trans-cis* crystal data, and that the additional peaks are the presence of different isomeric compounds as seen from the NMR spectra. There are also peaks from the simulated diffractogram, which did not appear in the experimental powder data. However, the data collected are insufficient to conclude these observations, and an attempt to repeat the crystallisation of the complex would be useful. This is to obtain crystals suitable for x-ray crystallography that may have different unit cell and hence, a different structural geometry to the *cis-trans-cis* crystal structure, for comparison of their diffractograms.
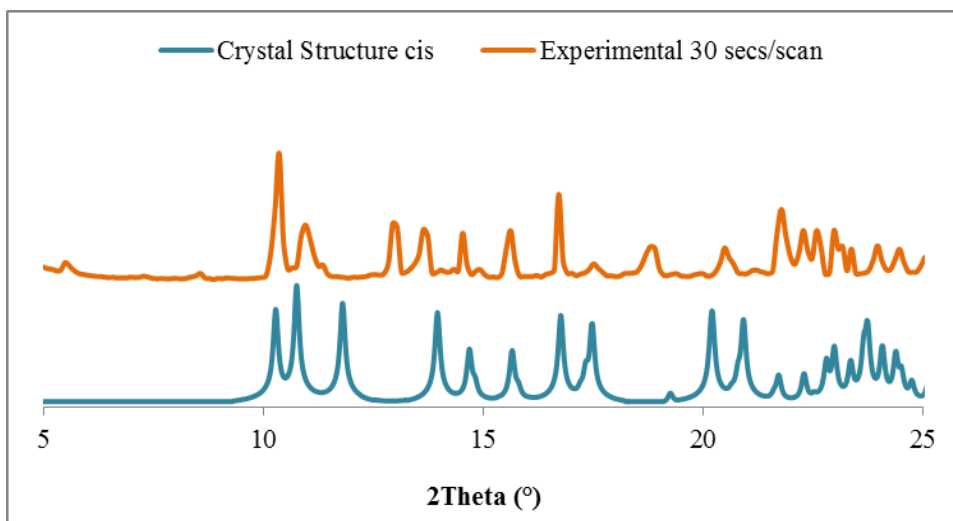
Figure 5.23 *PXRD data of complex **5.3** showing the simulated and experimental diffractograms*

Powder diffraction (PXRD) pattern for *bis*-picolinamide rhodium diiodide complex **5.5** was also recorded to determine the stability of its structural geometry in the bulk powder sample. The ruthenium diiodide analogues described in Chapter 4 have showed the unit cell data matches very well between the single crystal structure of the complex and from the data analysis of the powder sample. This indicates that the ruthenium diiodide complex has a stable structural geometry in the bulk powder sample. The diffractogram simulated from a single *trans* crystal structure of complex **5.5** is compared with the powder diffractogram recorded at scan rate of 30secs/scan, as shown in **Figure 5.24**.

The PXRD patterns have showed similarities on the peaks between their diffractograms. One aspect that may need to be considered is that the diffractogram was collected from a dry powder sample, whereas the crystal structure has a solvent molecule present within its crystal structure. Although, the attempt to record the diffractogram of the "wet" powder sample, containing the DMF molecule, did not show a clear pattern. However, apart from this, both diffractograms have showed similar pattern and may contain a stable structural geometry as observed with the ruthenium diiodide analogues.
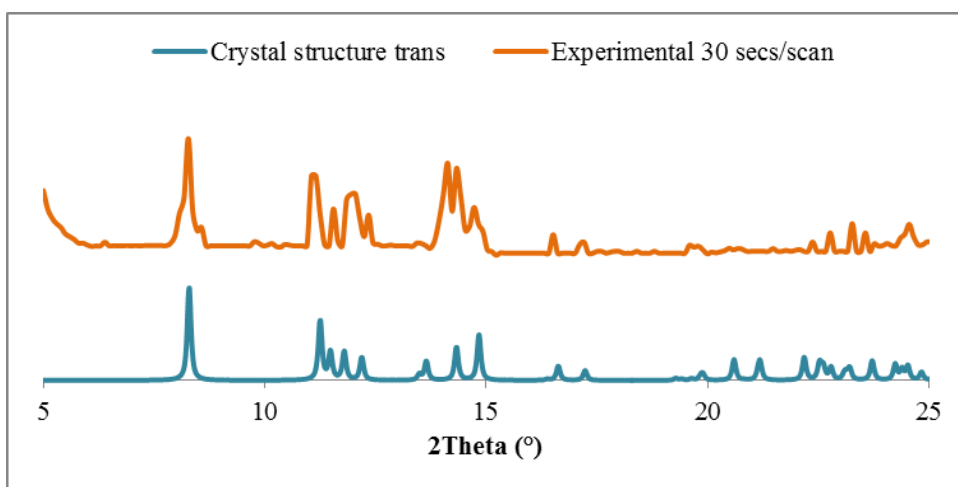
Figure 5.24 *PXRD data of complex* **5.5** *showing the simulated and experimental diffractograms recorded at scan rate 30 secs/scan*

5.11 References

1.   I. Bhattacharya, M. Dasgupta, M. G. B. Drew and S. Bhattacharya, *J. Indian Chem. Soc.*, 2012, **89**, 205-216.

2.   S. J. Lucas, Ph.D Thesis, University of Leeds, 2013.

3.   A. H. Velders, K. van der Schilden, A. C. Hotze, J. Reedijk, H. Kooijman and A. L. Spek, *Dalton Trans.*, 2004, 448-455.

4.   A. C. G. Hotze, H. Kooijman, A. L. Spek, J. G. Haasnoot and J. Reedijk, *New J. Chem.*, 2004, **28**, 565-569.

5.   R. M. Lord, J. J. Mannion, A. J. Hebden, A. E. Nako, B. D. Crossley, M. W. McMullon, F. D. Janeway, R. M. Phillips and P. C. McGowan, *ChemMedChem*, 2014, **9**, 1136-1139.

6.   P. Comba, H. Jakob, B. Nuber and B. K. Keppler, *Inorg. Chem.*, 1994, **33**, 3396-3400.

7.   S. M. Draper, D. J. Gregg, E. R. Schofield, W. R. Browne, M. Duati, J. G. Vos and P. Passaniti, *J Am Chem Soc*, 2004, **126**, 8694-8701.

8.   Z. Almodares, S. J. Lucas, B. D. Crossley, A. M. Basri, C. M. Pask, A. J. Hebden, R. M. Phillips and P. C. McGowan, *Inorg. Chem.*, 2014, **53**, 727-736.

CHAPTER 6

Cytotoxicity studies of *Bis*-functionalised Ruthenium Dihalide Complexes

6   Cytotoxicity Studies

6.1   Introduction

The first stage of the preclinical phase for anti-cancer drug discovery and development is *in vitro* cytotoxicity screening.[1] These assays are widely used to measure the effectiveness of drugs towards a variety of human cancer cell lines and to identify potential drugs for further analysis. Drug candidates can be classified as inactive, moderately active or highly active based on their IC_{50} values. IC_{50} is defined as the concentration of the drug that is required to inhibit 50% of cell proliferation. The screening for cytotoxicity of anti-cancer drugs can be monitored using the SRB[2] or MTT[3] assays. This chapter discusses these two different types of assays carried out in a 96-well plate setup, and the potency of ruthenium dihalide complexes under both normoxia and hypoxia conditions. Unfortunately, the rhodium dihalide complexes described in Chapter 5 were not evaluated for cytotoxicity. This is due to the limited access of the cell culture lab which was performed with the collaborators at the Institute of Cancer Therapeutics, Bradford. Therefore, cytotoxicity studies on *bis*-picolinamide rhodium dihalide complexes will be added to the future work for studies as comparison with its ruthenium analogue.

6.2   SRB Assay

The sulforhodamine B (SRB) assay is a colorimetric assay that was first developed by Skehan *et al*. in 1990.[2] This assay uses a bright pink anionic aminoxanthene dye containing two sulfonic acid groups that are able to bind electrostatically to basic protein components under mildly acidic conditions, and stain the cell cultures that are fixed by trichloroacetic acid (TCA). **Figure 6.1** shows the structure of SRB dye that is used in this assay. The dye can be extracted from the stained cells and dissolved by a weak base solution for optical density measurements.
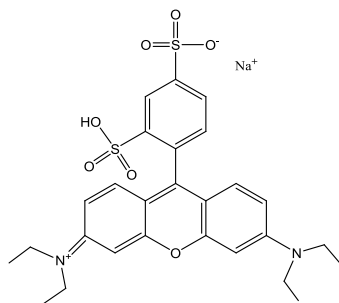
Figure 6.1 Structure of Sulforhodamine B (SRB) dye

6.3   MTT Assay

The MTT assay is a colorimetric assay used to measure cytotoxicity, cell proliferation and cell viability. This assay was first described by Mosmann[3] in 1983 and further optimised by Niks[4] and Sylvester.[5] It detects living cell cultures that generate signals in order to metabolically reduce the yellow water soluble salt, 3-(4,5-dimethylthiazol-2-yl)-2,5-diphenyltetrazoliumbromide (MTT) to dark blue or purple formazan crystals which are insoluble in water, as shown in **Figure 6.2**.

Yellow MTT salt   Dark blue/Purple Formazan
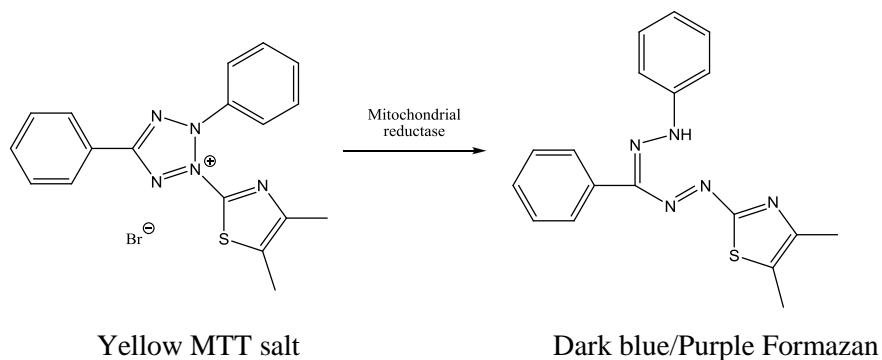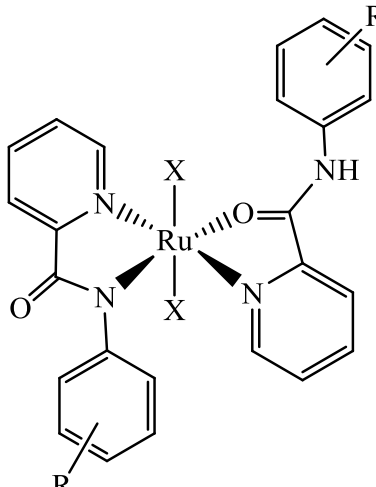
Figure 6.2 The reduction of yellow MTT salt to dark blue or purple formazan crystals

The reduction occurs outside the mitochondrial inner membrane *via* the NADP and NADPH-dependant mechanisms involving mitochondrial dehydrogenase enzymes that are metabolically active in living cells.[6] The dark blue or purple formazan crystals formed are solubilised and the colour produced can be read using a multiwell scanning spectrophotometer (ELISA reader). The amount of formazan formed is directly proportional to the number of living cells present during the MTT exposure. This assay is also applicable in detecting the number of cells that are not dividing but are still metabolically active. Therefore, besides measuring cytotoxicity, this method can also be used to differentiate between the measurement of cell proliferation and activation.[7]

6.4   Cytotoxicity of *Bis*-Picolinamide Ruthenium Dihalide Complexes

A series of *bis*-picolinamide ruthenium dihalide complexes described in Chapters 3 and 4, with the general structure shown in **Figure 6.3** were tested against A2780 human ovarian adenocarcinoma, A2780*cis* human ovarian cisplatin-resistant adenocarcinoma and HT-29 human colon adenocarcinoma.

Complex (X = Cl)	Complex (X = I)	R substituents
3.1	**4.1**	H
3.2	**4.2**	2'-F
3.3	**4.3**	4'-F
3.4	**4.4**	2',4'-F
3.5	**4.5**	2',5'-F
3.6	**4.6**	2'-Cl
3.7	**4.7**	3'-Cl
3.8	**4.8**	4'-Cl
3.9	**4.9**	2',4'-Cl
3.10	**4.10**	2',5'-Cl
3.11	**4.11**	2'-Br
3.12	**4.12**	3'-Br
3.13	**4.13**	4'-Br
3.14	**4.14**	2',4'-Br
3.15	**4.15**	2',5'-Br

*Figure 6.3 A general structure for complexes **3.1** - **3.15** and **4.1** - **4.15***

The 5-day cytotoxicity studies follow the general procedure performed at the Institute of Cancer Therapeutics, Bradford. The drugs were incubated for five days in the cell suspension, diluted with RPMI-1640 complete media. The drugs were first dissolved in DMSO at a concentration of 25 mM, and diluted further in the cell medium to 250 μM, which was found to be the approximate maximum concentration to obtain ten different concentrations, down to a minimum concentration of 0.49 μM. After five

days of incubation, the cells were exposed to yellow MTT solution and incubated at 37°C for four hours. The results to determine the cytotoxicity of the drugs were taken as IC_{50} values based on three independent experiments. The standard deviation is taken to be valid with a value of within 10%. If the value exceeded the limit of the standard deviation, the experiment was repeated again. The log of concentration is plotted against the percentage of cell survival, to obtain the drug concentration that gives 50% cell survival (IC_{50}).

The graph plotted is as shown in **Figure 6.4**, which show plots of one of the three independent experiments for an active (complex **3.12**), moderately active (complex **3.2**) and less active (complex **3.9**) anti-cancer drug against A2870 ovarian cancer cell line. The IC_{50} values for complexes **3.1** - **3.15** and **4.1** - **4.15**, along with cisplatin as a comparison, tested for cytotoxicity against A2780, A2780*cis* and HT-29 cancer cell lines are as shown in **Table 6.1**.
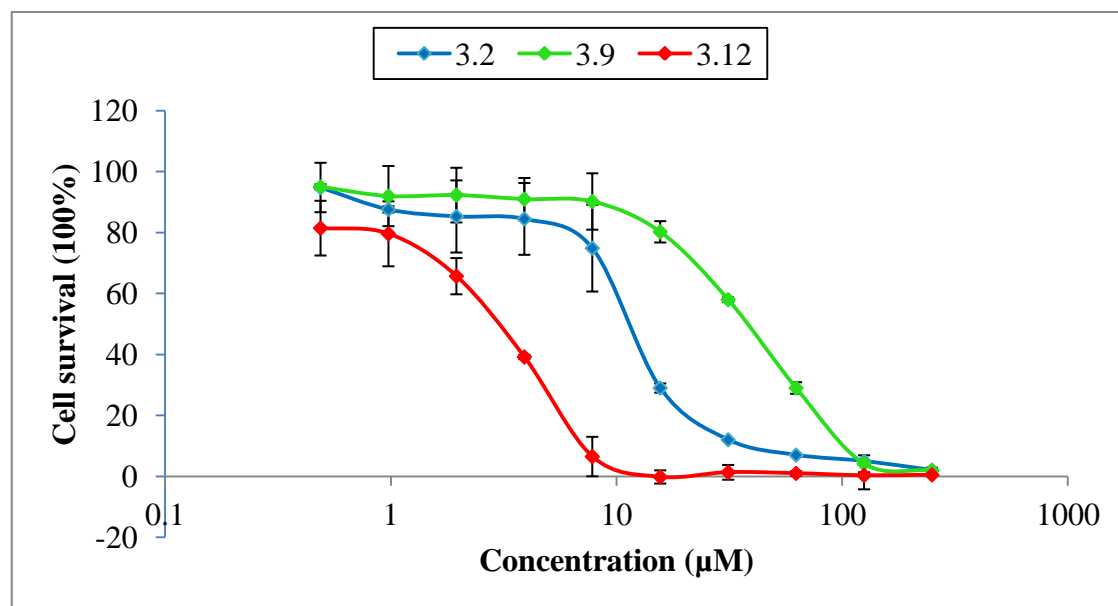
Figure 6.4 *Plot of percentage cell survival against drug concentration (in logarithmic scale) for complexes* *3.2, 3.9* *and* *3.12* *against A2780 ovarian cancer cell line after five days incubation*

Table 6.1 *The IC$_{50}$ values (µM) for ruthenium dihalide complexes **3.1** - **3.15**, **4.1** - **4.15***
and cisplatin, against A2780, A2780cis and HT-29. Results are expressed as the mean
IC$_{50}$ ± S.D for three independent experiments.

R	Complex		A2780		A2780cis		HT-29	
	X = Cl	X = I	X = Cl	X = I	X = Cl	X = I	X = Cl	X = I
H	**3.1**	**4.1**	24 ± 2	5.4 ± 0.5	47 ± 3	5.3 ± 0.2	23 ± 1	5.5 ± 0.4
2'-F	**3.2**	**4.2**	13 ± 1	13 ± 1	21 ± 2	31 ± 2	6.2 ± 0.4	13 ± 1
4'-F	**3.3**	**4.3**	6.9 ± 0.8	3.4 ± 0.1	35 ± 3	12 ± 1	17 ± 1	8.4 ± 0.3
2',4'-F	**3.4**	**4.4**	22 ± 1	14 ± 1	25 ± 1	13 ± 1	7.3 ± 0.4	8.5 ± 0.7
2',5'-F	**3.5**	**4.5**	45 ± 2	16 ± 1	93 ± 2	15 ± 1	20 ± 1	14 ± 2
2'-Cl	**3.6**	**4.6**	21 ± 1	7.2 ± 0.1	33 ± 1	22 ± 2	11 ± 1	10 ± 1
3'-Cl	**3.7**	**4.7**	3.6 ± 0.2	2.8 ± 0.3	6.7 ± 0.1	3.2 ± 0.1	3.0 ± 0.1	2.3 ± 0.1
4'-Cl	**3.8**	**4.8**	9.2 ± 0.4	2.5 ± 0.2	4.4 ± 0.4	2.4 ± 0.2	2.8 ± 0.3	0.9 ± 0.1
2',4'-Cl	**3.9**	**4.9**	41 ± 1	6.6 ± 0.6	55 ± 2	4.3 ± 0.3	9.7 ± 0.3	3.4 ± 0.3
2',5'-Cl	**3.10**	**4.10**	31 ± 1	10 ± 1	24 ± 2	12 ± 1	11 ± 1	6.5 ± 0.3
2'-Br	**3.11**	**4.11**	18 ± 2	11 ± 1	37 ± 1	40 ± 2	8.3 ± 0.3	24 ± 2
3'-Br	**3.12**	**4.12**	3.3 ± 0.2	2.0 ± 0.2	6.0 ± 0.4	3.3 ± 0.1	3.3 ± 0.2	1.5 ± 0.1
4'-Br	**3.13**	**4.13**	7.5 ± 0.3	2.3 ± 0.2	12 ± 1	2.9 ± 0.2	6.8 ± 0.3	0.8 ± 0.1
2',4'-Br	**3.14**	**4.14**	18 ± 1	6.7 ± 0.3	26 ± 1	6.6 ± 0.3	7.7 ± 0.3	4.3 ± 0.2
2',5'-Br	**3.15**	**4.15**	20 ± 2	11 ± 1	22 ± 2	7.6 ± 0.3	10 ± 1	4.9 ± 0.4
Cisplatin			1.4 ± 0.3		11 ± 1		2.8 ± 0.3	

6.4.1   Cytotoxicity of *bis*-picolinamide ruthenium dichloride complexes
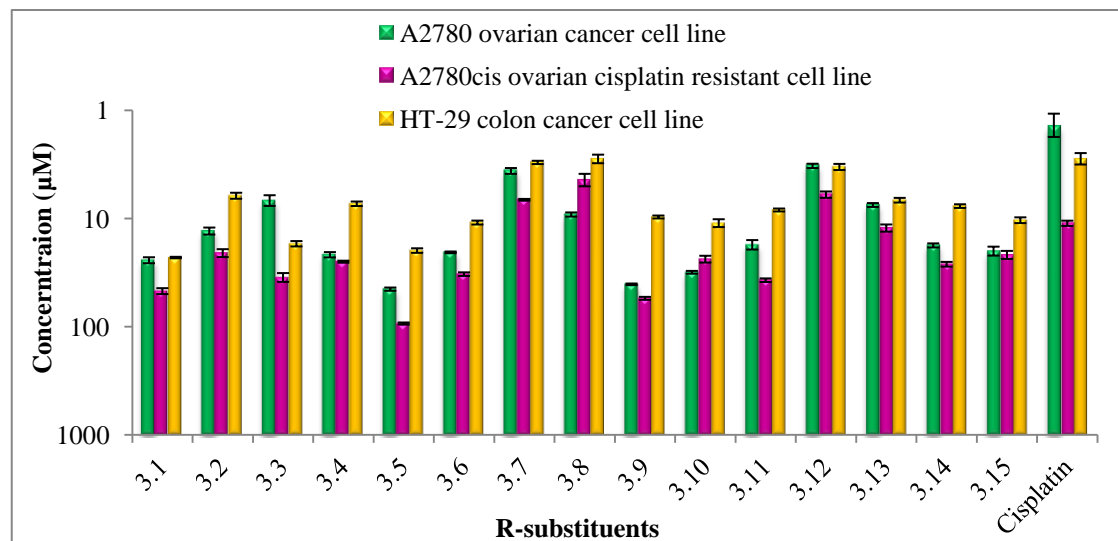
Figure 6.5 *A summary of IC$_{50}$ values (inverse log) for functionalised bis-picolinamide ruthenium dichloride complexes **3.1** - **3.15***

Bis-picolinamide ruthenium dichloride complexes vary in their cytotoxic acitivies when halide substituents are incorporated at different positions on the phenyl ring of the picolinamide ligands in the ruthenium complex. A chart of IC$_{50}$ values (inverse log) for *bis*-picolinamide ruthenium dichloride complexes **3.1** - **3.15** is shown in **Figure 6.5**. Complex **3.1** with an unsubstituted picolinamide ligand has an IC$_{50}$ value of 24 µM, found to be moderately active towards A2780 ovarian cancer cell line. When halide substituents are added to the phenyl ring of the picolinamide ligands, their potency increases especially when the substituents are on the *meta* or *para* position. This is shown by complexes **3.3**, **3.7**, **3.8**, **3.12** and **3.13** having IC$_{50}$ values of less than 10 µM, which is considered to be highly active as a drug ($p < 0.01$ relative to complex **3.1**). The most potent complex in the A2780 cell line is complex **3.12** having 3'-bromo substituent with an IC$_{50}$ value of 3.3 µM that is half as potent as cisplatin with IC$_{50}$ value of 1.4 µM ($p < 0.01$), and complex **3.5** having 2',5' difluoro substituent is the least potent complex with an IC$_{50}$ value of 45 µM ($p < 0.01$ between complex **3.12** and **3.5**).

In the A2780*cis* cell line, a similar trend of potency as in the A2780 cell line is observed for complexes **3.1** - **3.15**. An exception of the trend is for complexes with fluoride substituents, where the *ortho*-fluoro (complex **3.2**) is more potent than the *para*-fluoro (complex **3.3**) with IC_{50} values of 21 and 35 μM respectively ($p < 0.01$). Complexes **3.7** and **3.12** with IC_{50} values of 6.7 μM and 6.0 μM respectively, are two times more potent than cisplatin, with an IC_{50} value of 11 μM ($p < 0.01$ relative to cisplatin). The cytotoxic activity of complex **3.8** is increased by 2-fold, with an IC_{50} value of 9.2 μM in A2780 to 4.4 μM in A2780*cis* ($p < 0.01$), which is three times more potent than cisplatin and the most potent complex in A2780cis cell line. These complexes have shown that they may be able to overcome the mechanism that has become resistant towards cisplatin in the ovarian cancer cells.

Complexes **3.1** - **3.15** are found to be selective towards different cancer cells as their anti-cancer activity is seen to differ when comparing their IC_{50} values between A2780 and HT-29 cell line. Most of the complexes are more potent in the HT-29 cell line apart from complex **3.1** which performs similar cytotoxic activity towards both cell lines, and complex **3.3** that has higher anti-cancer activity towards A2780 cells. The highest relative increase in IC_{50} value can be seen from complex **3.9** that has higher potency of up to 4 times from 41 to 9.7 μM in A2780 and HT-29 cell line respectively ($p < 0.01$). Also following the trend as observed in A2780 cell line, complex **3.1** with unfunctionalised picolinamide ligands has an IC_{50} value of 23 μM, and is the least potent complex in HT-29 cell line. Their anti-cancer activity is seen to increase when there is an addition of a halide substituent, especially on the *meta* or *para* position. Complex **3.8** is the most potent having a *para*-chloro substituent with an IC_{50} value of 2.8 μM that is similar to the IC_{50} value obtained for cisplatin.

6.4.2 Cytotoxicity of *bis*-picolinamide ruthenium diiodide complexes
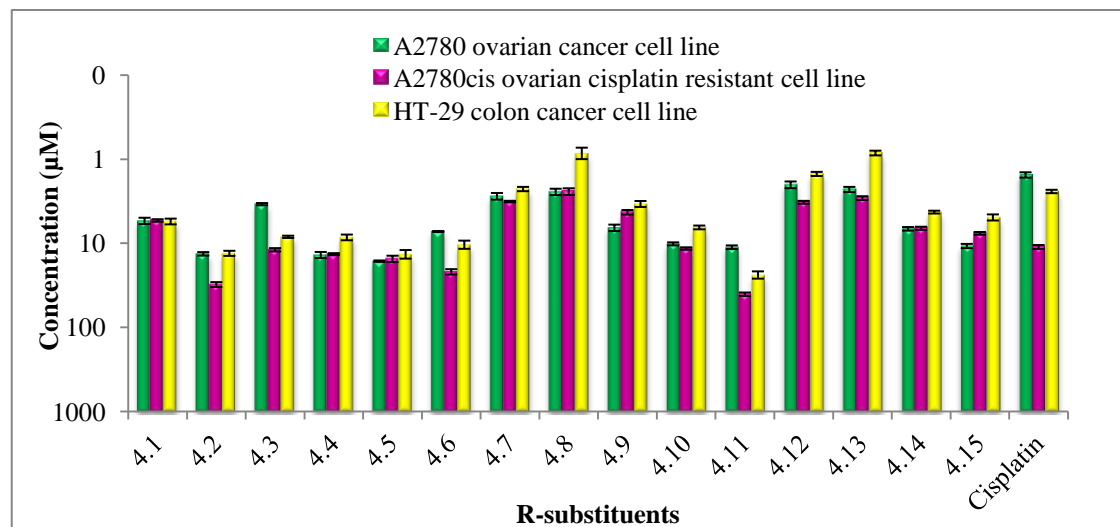
Figure 6.6 A summary of IC_{50} values (inverse log) for functionalised bis-picolinamide ruthenium diiodide complexes **4.1** - **4.15**

The IC_{50} values (inverse log) for *bis*-picolinamide ruthenium diiodide complexes **4.1** - **4.15**, along with cisplatin against A2780, A2780cis and HT-29 cancer cell lines are shown in **Figure 6.6**. Interestingly, complex **4.1** which contains the unsubstituted picolinamide ligands is found to be potent in all the three different cancer cell lines. IC_{50} values of complex **4.1** are 5.4 μM, 5.3 μM and 5.5 μM in A2780, A2780cis and HT-29 cancer cell line respectively. The addition of a halide substituent specifically on the *meta* or *para* position contributes to a higher increase in the anti-cancer activity of the complexes, with their IC_{50} values within the range of 0.8 - 3 μM against all the three different cancer cell lines ($p < 0.01$, for all respective complexes relative to complex **4.1**).

In the A2780 ovarian cancer cell line, most of the *bis*-picolinamide ruthenium diiodide complexes are found to be active with IC_{50} values of less than 10 μM. Complexes **4.3**, **4.7**, **4.8**, **4.12** and **4.13** are highly active having similar IC_{50} values of 2-3 μM which are comparable to cisplatin ($IC_{50} = 1.4$ μM), also suggesting that the different halide substituents on the phenyl ring of the picolinamide ligands do not affect the anti-cancer activity of the whole complex providing that the halide substituents are on the *meta* or

para position. Nevertheless, the addition of *ortho* halide substituents are also found to be active as anti-cancer complexes, as shown by complexes **4.6**, **4.9** and **4.14** with IC_{50} values of 7.2 µM, 6.6 µM and 6.7 µM respectively.

Investigating the cytotoxicity of complexes **4.1** - **4.15** against A2780*cis* gave a better insight of their potential as anti-cancer agents towards ovarian cancer cells. Most of the complexes are found to be more potent than cisplatin (IC_{50} = 11 µM) in the A2780*cis* cancer cell line. As mentioned previously, complex **4.1** that has the unsubstituted picolinamide ligands, is found to be active in all the three different cancer cell lines that includes the A2780*cis* cell line. It has an IC_{50} value of 5.3 µM being significantly more active than cisplatin ($p < 0.01$). Complexes that consist of chloride and bromide substituents on the phenyl ring of the ligands, with an exception of those on *ortho* position, have IC_{50} values which are comparable to cisplatin ranging from 2.4 to 7.6 µM ($p < 0.01$). It is also fascinating to see that complexes **4.1**, **4.7**, **4.8**, **4.12**, **4.13** and **4.14** maintained their cytotoxic activity between the A2780 and A2780*cis* cell lines with IC_{50} values that are comparable to cisplatin. Furthermore, complexes **4.9** and **4.15** showed a higher potency when in the A2780*cis* cell line which is an excellent contrast to cisplatin.

Most of the *bis*-picolinamide ruthenium diiodide complexes **4.1** - **4.15** are seen to be highly potent in the HT-29 colon cancer cell line. The different halide substituents do not seem to affect the anti-cancer activity of the complexes except for complexes **4.5**, **4.10** and **4.15** having 2',5' dihalide substituents, have shown an increase in activity with the halide substituents in the order of F < Cl < Br. Complexes **4.2**, **4.5**, **4.6** and **4.11** which have *ortho* halide substituents, in common, on their phenyl rings, are the only complexes that have shown to be moderately potent. Whereas, all of the other complexes have shown to have IC_{50} values of less than 10 µM. Complexes **4.7** and **4.9**, both functionalised by chloride substituents, are as active as cisplatin (IC_{50} = 2.8 µM) in the HT-29 cell line, with the IC_{50} value of 2.3 and 3.4 µM respectively. Complex **4.12** is almost twice more active than cisplatin with IC_{50} value of 1.5 µM ($p < 0.01$). The two most outstanding complexes in the HT-29 cancer cell line are found to be more active than cisplatin with up to 3-fold difference. These are complexes **4.8** and

4.13 having IC_{50} value of 0.86 µM and 0.84 µM respectively with both having a halide substituent on the *para* position of their phenyl rings ($p < 0.01$, for both complex **4.8** and **4.13** relative to cisplatin).

6.4.3   Cytotoxicity of *bis*-picolinamide ruthenium dichloride VS diidodide complexes

As mentioned previously in Chapter 4, several initial studies have showed platinum complexes with *cis* geometry have higher cytotoxicity *in vitro* and *in vivo* when compared to complexes having *trans* geometry.[8, 9] However, in recent studies, most *trans*-platinum complexes have been shown to be more active than their *cis* analogues when the ammine ligand is replaced with a more bulky ligand.[10, 11] Sadler *et al.* has reported their studies on [Ru(*p*-cym)(ImpyNMe$_2$)X]PF$_6$ complexes with contrasting activities when changing their X ligands from chloride to iodide, with the latter being more cytotoxic.[12, 13] These results have accumulated in breaking the initial rules of structural-activity relationship as anti-cancer drugs. **Figure 6.7** - **6.9** shows the comparison of IC_{50} values (inverse log) between *bis*-picolinamide ruthenium dichloride and diiodide complexes against A2780, A2780cis and HT-29 cancer cell line respectively. This is to investigate the differences of their cytotoxicity when changing the ancillary halide ligand between chloride and iodide, especially with the ruthenium dichloride complexes consisting of a mixture of structural isomers and ruthenium diiodide complexes having a stable *trans* geometry, as described in Chapter 3 and 4.
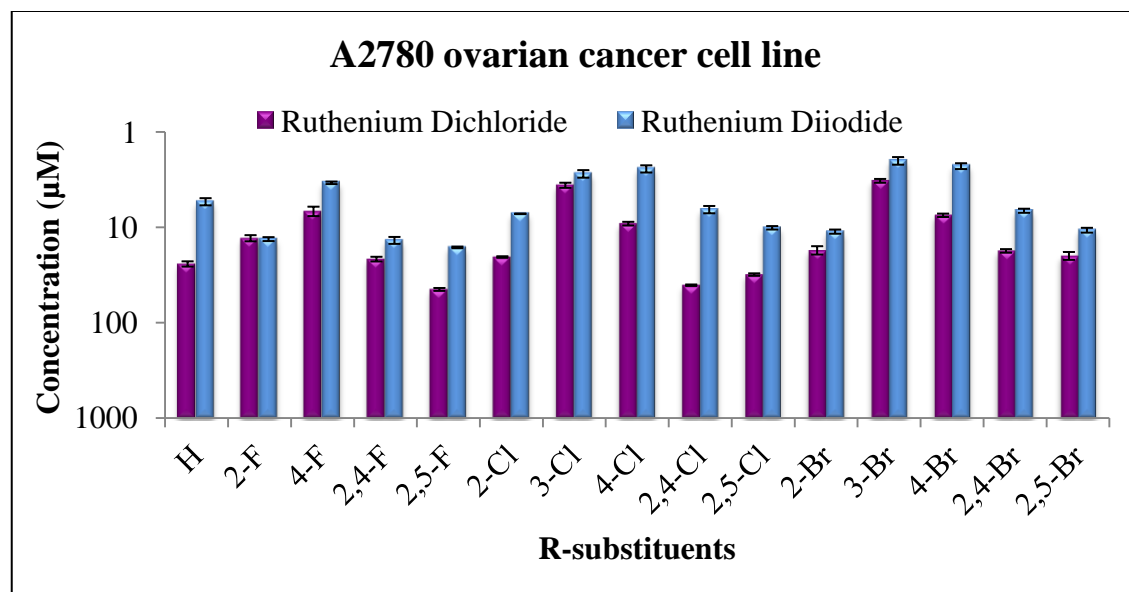
Figure 6.7 *The comparison of IC$_{50}$ values (inverse log) between bis-picolinamide ruthenium dichloride and diiodide complexes against A2780 ovarian cancer cell line*
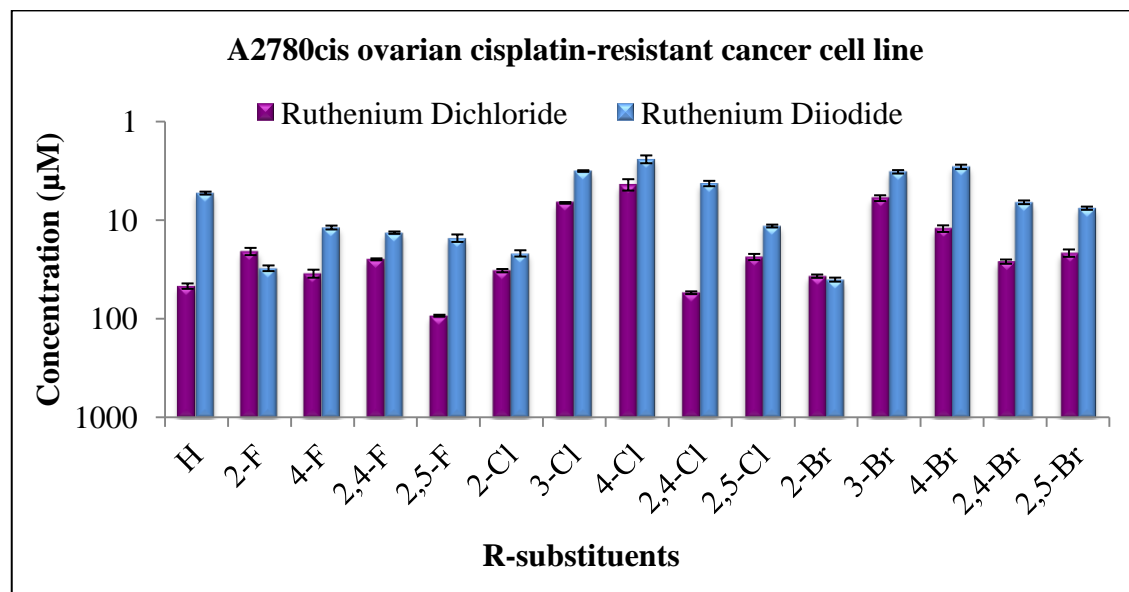
Figure 6.8 *The comparison of IC$_{50}$ values (inverse log) between bis-picolinamide ruthenium dichloride and diiodide complexes against A2780cis ovarian cisplatin-resistant cancer cell line*
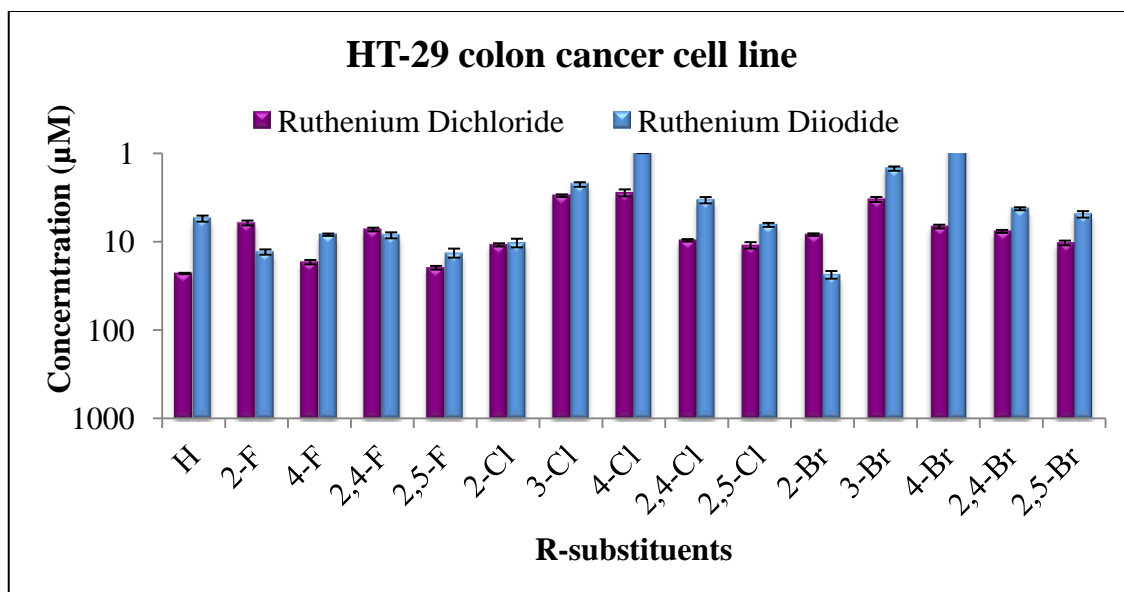
Figure 6.9 *The comparison of IC$_{50}$ values (inverse log) between bis-picolinamide ruthenium dichloride and diiodide complexes against HT-29 colon cancer cell line*

The highest relative increase of cytotoxicity up to 6-fold and 13-fold, is seen when the ancillary chloride ligand of complex **3.9** is changed to iodide, complex **4.9**, with IC$_{50}$ value from 41 and 55 µM to 6.6 and 4.3 µM in the A2780 and A2780cis cell line respectively ($p < 0.01$). In the HT-29 cell line, complex **3.13** with dichloride ligands gave the highest increase in cytotoxicity of up to 8-fold when changing the halide ligands to iodide, complex **4.13**, with IC$_{50}$ value of 6.8 to 0.84 µM ($p < 0.01$). These dramatic cytotoxicity changes have clearly shown that the halide ligands bonded to ruthenium metal centre play a crucial role in their anti-cancer activity.

Surprisingly, complex **3.2** and **4.2** having an *ortho*-fluoro substituent on the phenyl ring of the picolinamide ligands, and complex **3.11** and **4.11** functionalised with an *ortho*-bromo substituent, have shown different structural-activity relationship from the rest of the *bis*-picolinamide ruthenium dihalide complexes. Their anti-cancer activity either changes insignificantly or substantially decreases on switching the halide ligands from chloride to iodide. This is especially true between ruthenium dichloride complex **3.2** and ruthenium diiodide complex **4.2** that have shown a consistent cytotoxic activity with IC$_{50}$ value of 13 µM in the A2780 cell line, and a decrease in cytotoxicity by 3-fold in the HT-29 cell line of IC$_{50}$ value 8.3 to 24 µM.

Both ruthenium dichloride and diiodide complexes are the most active in the HT-29 cell line. Interestingly, complex **3.8** which is the most potent among the dichloride analogue in the HT-29 cell line, having a *para*-chloro substituent on the functionalised picolinamide ligands, has increased its potency by 3-fold when substituted to diiodide ligands, complex **4.8**, and is also the most potent among the diiodide analogue in the HT-29 cell line, with IC_{50} values of 2.8 and 0.86 μM respectively. This may suggest that both the leaving halide ligands and *para*-chloro substituent contribute together towards the anti-cancer activity of the whole complex, and mechanistic studies such as hydrolysis, hydrophobicity, cell uptake, cell fractionation, DNA binding studies, of both complexes may lead to a better understanding of their mechanism of action.

With a few exceptions of the ruthenium dihalide complexes, those with diiodide ligands have shown, in general, a remarkably higher potency compared to the ruthenium dichloride complexes in all the three different cancer cell lines. **Table 6.2** summarises the important ruthenium anti-cancer agents previously reported in the literature. KP1019 and KP1339 are the promising candidates which are currently in Phase II clinical trials, and have moderate cytotoxicity *in vitro* of IC_{50} values 36.6 and 34.7 μM against colon cancer cells respectively. Reedijk *et al*. synthesised α-Ru(Azpy)Cl$_2$ which has a *cis-trans-cis* geometry, with an IC_{50} value of 1.90 μM. Organometallic compounds developed by Sadler *et al*. and McGowan *et al*. showed that when an iodide ligand is attached to the ruthenium metal centre, it increases the anti-cancer activity of the whole complex. Despite the different cytotoxicity assays used by the different researchers, complexes **4.8** and **4.13** which consist of a stable *trans* geometry and diiodide as their halide ligands, are seen to be more potent than the previously reported anti-cancer agents, and also in the series of *bis*-picolinamide ruthenium dihalide complex. These results have extended further the rule-breaking of structural-activity relationship for anti-cancer drugs.

Table 6.2 *Previously reported ruthenium anti-cancer agents and their IC$_{50}$ values against colon cancer cells*

Anti-cancer agents		Cancer Cell line	Cytotoxicity Assay	IC$_{50}$ (µM)	Ref.
KP1019		HCT-116 colon cancer cell line	MTT assay 3-day incubation	36.6 ± 17.0	Keppler *et al.*[14]
KP1339				34.7 ± 3.6	
α-Ru(Azpy)Cl$_2$		WiDR colon cancer cell line	SRB assay 5-day incubation	1.90 ± 0.01	Reedijk *et al.*[15]
[Ru(η^6-*p*-cym)(*p*-AzpyNMe$_2$)I]PF$_6$		HCT-116 colon cancer cell line	SRB assay 24 hr incubation	1.37 ± 0.04	Sadler *et al.*[13]
RuCl(η^6-*p*-cym(2,5-Cl-picolinamide)		HT-29 colon cancer cell line	MTT assay 5-day incubation	5.9 ± 0.8	McGowan *et al.*[16]

6.5   Hypoxia

Cancer cells are characterised by a low concentration of oxygen level that leads to a more reducing environment when compared to normal tissues. This unique reducing microenvironment is a result of poor formation of new blood vessels to supply enough oxygen during its rapid cell growth.[17] These cells which are distant from the blood vessels only allow limited amount of oxygen to diffuse through, giving the cells progressively gradual regions of oxygen concentration from having sufficient oxygen on the thin outer layer of the cells to less oxygen towards the inside of the cells.[18] The distance between the blood vessels and the hypoxic regions depends on the rate of oxygen consumed by the cells, and typical cells tend to receive insufficient oxygen when the distance of the cells is more than 70 μm from the blood vessels.[19]

Hypoxic cells are well recognised in their resistance towards chemotherapy and radiotherapy treatments, offering a great challenge in cancer therapeutics. The unsuccessful treatments against the hypoxic cells are related to their distance from the blood vessels, for which the anti-cancer drugs are not able to reach.[20] For any treatments that destroy the cancer cells with sufficient oxygen may cause the hypoxic cells to reoxygenate and grow, hence repopulating the cancer cells in the body.[21] The cells can also create tolerance within the hypoxic atmosphere,[22] causing it to upregulate the genes in drug resistance, and promote cancer cell growth.[23] Since hypoxic cells differ from normal healthy cells, this brings excellent opportunities on selective therapeutics to target cancerous cells.

Recent evidence has suggested that protein complex HIF-1 plays a key factor in carcinogenesis. Hypoxia-inducible factor 1 (HIF-1) is a heterodimeric transcription factor that comprises of an O_2-regulated HIF-1α subunit and a constitutively expressed HIF-1β subunit.[24] **Figure 6.10** shows the signalling pathway of HIF-1 in the expression of its target genes.[25] The HIF-α subunit is normally synthesised in the cytosol and is continuously degraded under normoxic conditions.[26] However, under an environment of low oxygen concentration, this subunit starts to rapidly accumulate.[26] HIF-α is then transported into the nucleus and is reduced by thioredoxin reductase enzyme (Trx) that is regulated with an intermediate protein, Ref-1.[27] A transcriptional

co-activator, CBP/p300 is recruited by the redox reaction of Trx/Ref-1, and binds with the reduced state of HIF-1α,[28] where it dimerises with HIF-1β to form the HIF-1 complex.[29] Then, in order to activate the gene expression, HIF-1 complex binds to the hypoxia responsive element (HRE) in the promoters of the target genes.[29]
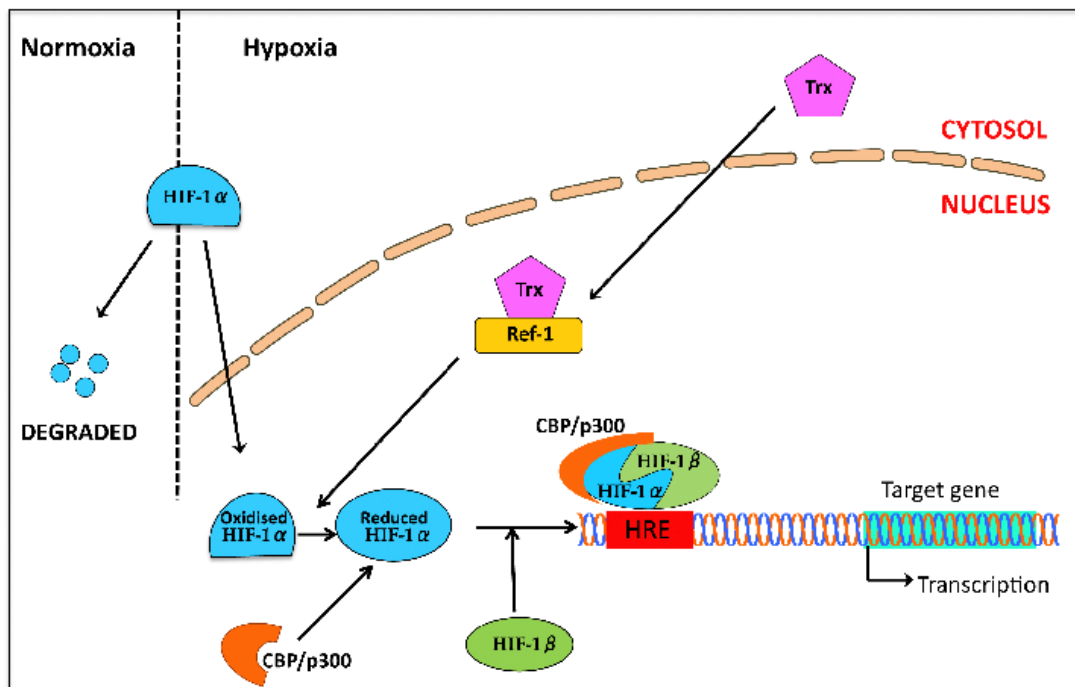
Figure 6.10 *HIF-1 signalling pathway and target genes expression, adapted from "The Interaction Between Redox and Hypoxic Signalling Pathways in the Dynamic Oxygen Environment of Cancer Cells, Carcinogenesis"* [25]

HIF-1 upregulates hundreds of genes to alter expression in the hypoxic cells and code for proteins which are involved in pathways close related to cancer, facilitating adaptation and cell survival in the low oxygen environment.[30-33] **Figure 6.11** shows the role of HIF-1 activation in carcinogenesis. The overexpression of HIF-1 has been associated with several cancer types that includes lung, breast, prostate and colon cancer cells,[34] producing the resistance of apoptosis, cell invasion and angiogenesis.[35] Furthermore, HIF-1 activates glycolysis that generates energy as ATP, maintaining the cell survival and so favours cell invasion, angiogenesis and proliferation.[36]
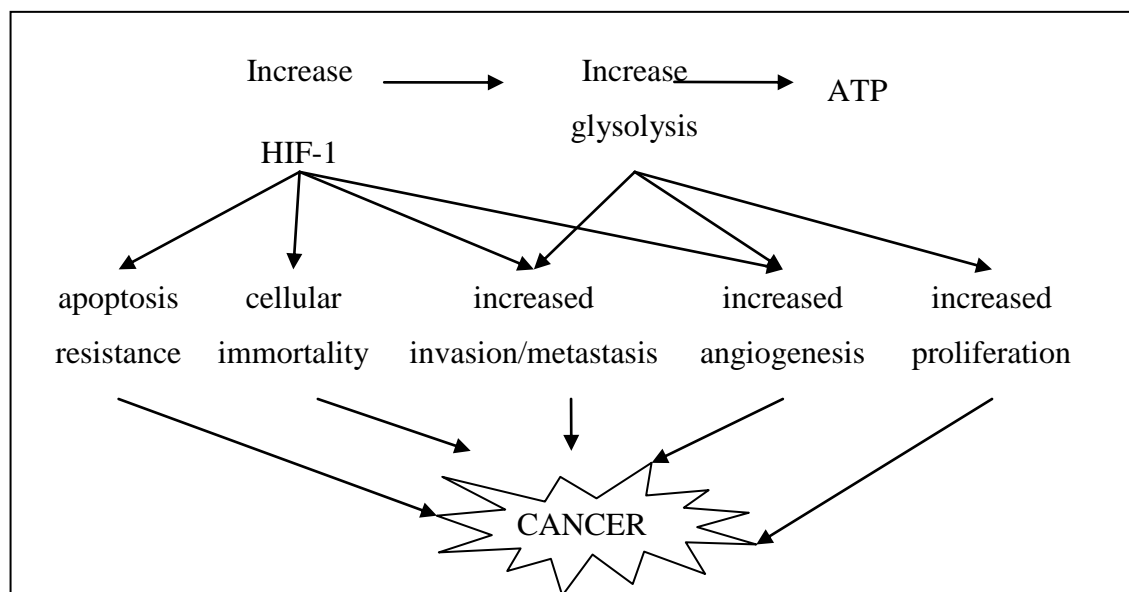
Figure 6.11 *The role of HIF-1 activation in carcinogenesis.*[37]

An excellent approach to overcome the resistance of hypoxic cells to chemotherapy and radiotherapy treatment is to develop selective bioreductive drugs that become activated when they reach the hypoxic cells with reducing environment. Metal complexes have the advantages to this approach as they have the ability to vary their coordination number, geometry and redox states making them accessible in the reducing biological surrounding. They can serve as inert prodrugs, being transported into the targeted environment, and become reduced metabolically into its active form. The use of transition metal complexes for hypoxia-selective metabolism has been focused on the possibility of a one-electron reduction when in the cell reducing environment.[38]

6.5.1   Hypoxia-activated metal-based anti-cancer drugs

Cobalt. The mechanism of action of hypoxia-selective cobalt (III) anti-cancer drugs is known to consist of a cytotoxic ligand that is released in the low oxygen environment.[39] Co(III) provides an inert framework that serves to protect the cytotoxic ligand prior to reaching the cancer cells. This complex is transported to its target and the cytotoxic ligand is then released into the hypoxic environment, after Co(III) is reduced to Co(II). **Figure 6.12a** shows a Co(III) complex that is associated with a tetradentate *tris*(2-methylpyridiyl)-amine (tpa) ligand acting as a carrier ligand, and a

matrix metalloproteinases (MMP) inhibitor, marimastat as the cytotoxic ligand.[40] Marimastat was in the Phase III clinical trials as an anti-cancer drug, but it was discontinued as it did not produce sufficient therapeutic benefits in patients.[41] When incorporating marimastat to the Co(III) metal centre, studies have shown that there is an increase in cytotoxicity when compared to the free cytotoxic ligand.[40, 42] Denny *et al.* studied several different series of Co(III) complexes containing bidentate nitrogen mustard ligands, as shown in **Figure 6.12b**, and for this complex, the bidentate nitrogen mustard ligand is the cytotoxic ligand released for its anti-cancer activity.[39, 43]

(a)   (b)
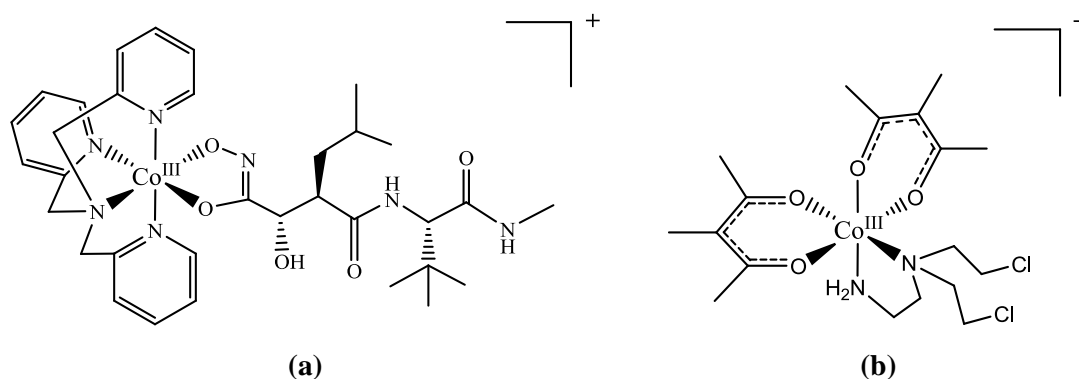
Figure 6.12 Hypoxia-selective Co(III) anti-cancer complex with (a) tetradentate tpa and bidentate marimastat ligands; (b) bidentate acac and bisalkylating nitrogen mustard ligands

Iron. Hypoxia-selective Fe complexes as anti-cancer drugs are able to interconvert between +3 and +2 oxidation states. They are known to be cytotoxic by generating radicals to form reactive oxygen species (ROS) that can induce DNA damage in the cells.[44] This is shown by the ferrocene analogue of tamoxifen, in which the third phenyl ring of tamoxifen is substituted by ferrocene (**Figure 6.13a**).[45] An Fe analogue of Co(III) marimastat complex is as shown in **Figure 6.13b** consisting of a tetradentate (*N*,*N*-*bis*(salicylidene)ethane-1,2-diimine (salen) ligand instead of a tpa ligand.[46] This complex was found to be more potent than its Co(III) analogue, and may undergo a similar mechanism of action.

(a)   **(b)**
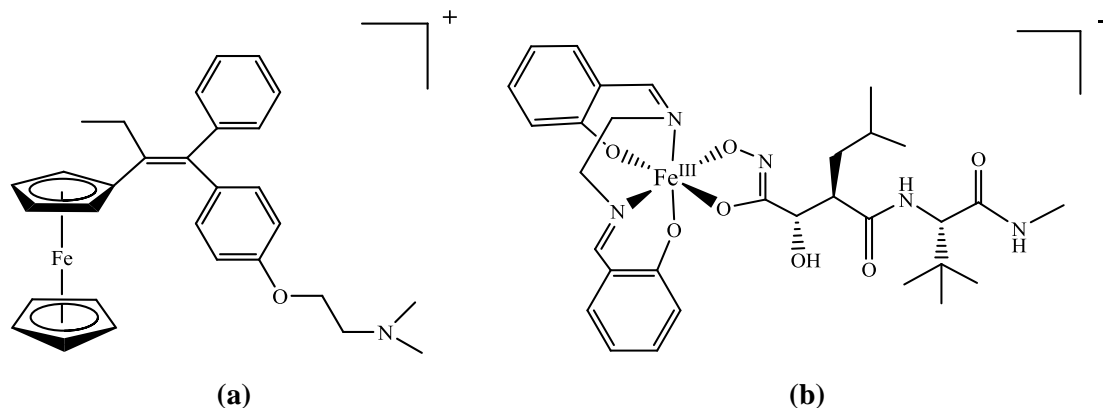
Figure 6.13 *Hypoxia-activated Fe(III/II) anti-cancer complexes containing* ***(a)***
ferrocene analogue of tamoxifen; ***(b)*** *tetradentate salen and bidentate marimastat*
ligands

Copper. Cu-based complexes offer an attractive chemistry in developing hypoxia-
selective drugs. It has two oxidation states with accessible reduction potential within
the physiological potential range in cells.[47] A Cu(II) complex containing a macrocylic
cyclen ligand has shown a high increase in cytotoxicity when under hypoxic
conditions compared to normoxic conditions, indicating it is hypoxia-selective.[48] The
complex acts as a prodrug, with Cu(II) undergoing a reduction to Cu(I) when in the
hypoxic environment, releasing the cytotoxic cyclen ligand to its target cell, as shown
in **Scheme 6.1**.
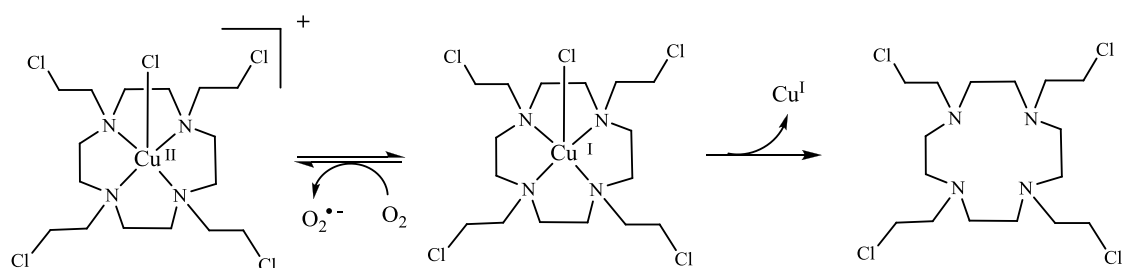
Scheme 6.1 *Mechanism of inert Cu(II) prodrug in releasing its cytotoxic cyclen ligand*

Platinum. Several platinum (IV) complexes have been shown to have advantages over
cisplatin.[49, 50] Pt(IV) may act as an inert prodrug that is reduced to its active Pt(II)
complex in the hypoxic cells, believed to interact with few biological reducing agents
including glutathione, L-methionine, L-cysteine, ascorbate, metallothionein and

albumin.[51] **Scheme 6.2** shows the reduction of Pt(IV) prodrug that yields a Pt(II) species when in the reducing environment. The Pt(IV) complex consists of two ammine ligands, two chloride ligands and two axial ligands that are lost upon reduction, to give the active cisplatin drug. The reduction rate of a Pt(IV) prodrug is highly dependant on the nature of the axial ligands, and the non-leaving ammine ligands, though the latter is less likely to affect the rate.[52] Pt(IV) prodrug is easily reduced when the axial ligands are the chloro ligands, followed by acetato ligands, then those with the hydroxyl groups.[53]

$$L = Cl, OCOCH_3, OH$$
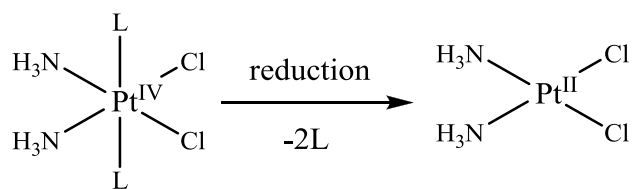
Scheme 6.2 Reduction of inert prodrug Pt(IV) to the active Pt(II) cisplatin

6.5.2   MTT Assay under Hypoxic conditions

Cytotoxicity studies under hypoxic conditions were determined using the MTT assay, which has been described previously in this chapter. HT-29 colon cancer cell line was selected for this assay as the ruthenium dihalide complexes were found to be more potent in this cell line compared to A2780 ovarian cancer cell line. Hypoxic studies were performed in a Whitley H35 Hypoxystation, with the oxygen level set at 0.1%, which is a physiologically relevant hypoxia level that leads to the drug resistance in radiotherapy and chemotherapy, and the activation of HIF-1 complex.[54] The media used for this study was conditioned for at least 24 hours under the hypoxic atmosphere before starting the experiment. HT-29 colon cancer cells were cultured in a 96-well plate and incubated overnight in hypoxic conditions of 0.1% oxygen level at 37°C with 5.0% CO_2 atmosphere. The cells were then exposed to different concentrations of the drugs to be tested, with a range from 250 µM to 0.49 µM, and incubated for five days under hypoxic conditions. Then which, the cell survival analysis is done to determine the IC_{50} values of the drugs against the HT-29 cancer cells.

Tirapazamine (TPZ) was used to act as a positive control and to validate the hypoxic condition in the study. TPZ is a known hypoxia-selective drug, found to be more cytotoxic of up to 200-fold when in low oxygen environment compared to when it is in normoxic condition.[55] TPZ undergoes a one-electron reduction metabolically in hypoxic atmosphere to give a free DNA-damaging TPZ radical that spontaneously gives oxidising hydroxyl and benzotriazinyl radicals (**Scheme 6.3**).[56, 57] TPZ has finished Phase III clinical trials, however the results of the outcome are still pending.[58]
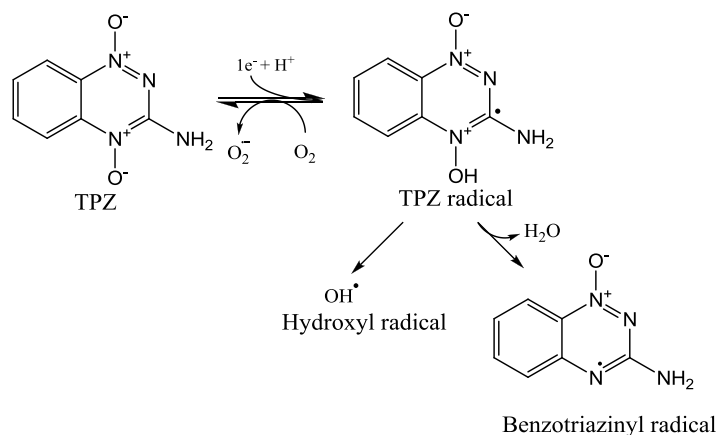
Scheme 6.3 *One-electron reduction of TPZ to generate a free radical*

Four *bis*-picolinamide ruthenium dihalide complexes, as shown in **Figure 6.14**, have been selected for cytotoxicity studies under hypoxic conditions of 0.1% oxygen level. These complexes have been selected due to being the most potent in their respective series of analogue. The cytotoxicity study under hypoxia condition is to determine the hypoxia-selevtive characteristic of the ruthenium dihalide complexes.

Complex	X	R
3.7	Cl	3'-Cl
3.12	Cl	3'-Br
4.8	I	4'-Cl
4.13	I	4'-Br
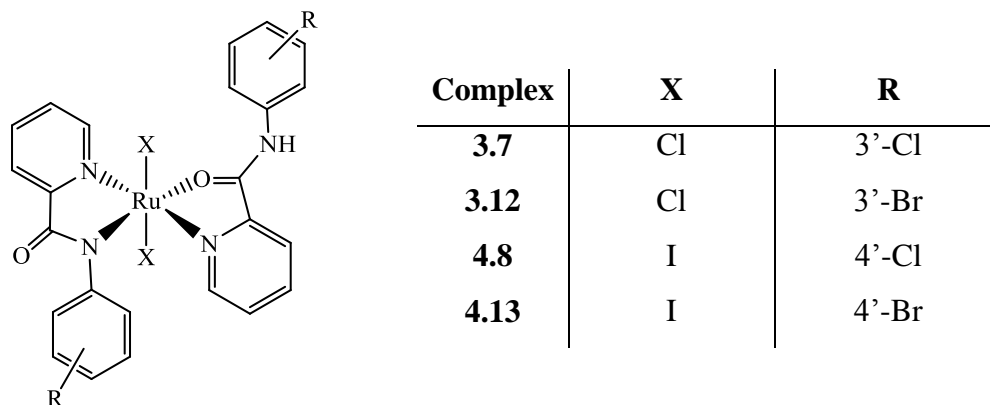
Figure 6.14 *Selected bis-picolinamide ruthenium dihalide complexes tested for cytotoxicity under hypoxic conditions*

Table 6.3 The IC_{50} values (μM) for TPZ, cisplatin and $RuX_2(L-R)_2$ complexes *3.7*,
3.12, *4.8* and *4.13* against HT-29 cell line under normoxic and hypoxic conditions.
Results are expressed as the mean IC_{50} ± S.D for three independent experiments.

Complex	Normoxia 21% oxygen	Hypoxia 0.1% oxygen
Tirapazamine (TPZ)	33 ± 2	2.8 ± 0.2
Cisplatin	2.8 ± 0.1	2.3 ± 0.2
3.7	3.0 ± 0.1	2.6 ± 0.3
3.12	3.3 ± 0.2	3.9 ± 0.2
4.8	0.86 ± 0.1	1.2 ± 0.2
4.13	0.84 ± 0.1	1.3 ± 0.1

Table 6.3 shows the IC_{50} values obtained for TPZ, cisplatin and complexes **3.7**, **3.12**, **4.8** and **4.13** both in normoxic and hypoxic conditions. In general, some of the ruthenium dihalide complexes have displayed a significant difference in their IC_{50} values when comparing between the two different conditions. The potency of complex **3.12** increased when under hypoxic conditions ($p < 0.05$). Complexes **3.7** and **4.8** have shown an insignificant decrease in potency from normoxic to hypoxic ($p > 0.05$). Complex **4.13** significantly lowered its cytotoxicity with differences of almost 2-fold between their IC_{50} values in the respective conditions ($p < 0.01$).

Nevertheless, the *bis*-picolinamide ruthenium dihalide complexes **3.7**, **3.12**, **4.8** and **4.13** are potent both under normoxic and hypoxic conditions. They have shown equal cytotoxicity in the HT-29 cell line suggesting that their anti-cancer mechanisms are independent of the oxygen concentration in the atmosphere. The IC_{50} values for all complexes are also seen to be comparable to the cytotoxic activity of cisplatin and TPZ when in the hypoxic condition, with the exception for complex **3.12** that has an IC_{50} value of 3.9 μM, about 2-fold less potent than cisplatin and TPZ ($p < 0.01$). Complex **3.7** has an IC_{50} value similar to cisplatin and TPZ of 2.6, 2.3 and 2.8 μM respectively. As for the *bis*-picolinamide ruthenium diiodide complexes **4.8** and **4.13**, both complexes have shown to be twice more potent than cisplatin and TPZ, making them the two most promising candidates for further studies *in vitro* and *in vivo* as anti-cancer agents.

6.6   References

1.   J. P. Hughes, S. Rees, S. B. Kalindjian and K. L. Philpott, *Br. J. Pharm.*, 2011, **162**, 1239-1249.

2.   P. Skehan, R. Storeng, D. Scudiero, A. Monks, J. McMahon, D. Vistica, J. T. Warren, H. Bokesch, S. Kenney and M. R. Boyd, *J. Natl. Cancer Inst.*, 1990, **82**, 1107-1112.

3.   T. Mosmann, *J. Immunol. Methods*, 1983, **65**, 55-63.

4.   M. Niks and M. Otto, *J. Immunol. Methods*, 1990, **130**, 149-151.

5.   P. W. Sylvester, *Drug Design and Discovery: Methods and Protocol*, Humana Press, New York, 2011.

6.   M. V. Berridge and A. S. Tan, *Arch. Biochem. Biophys.*, 1993, **303**, 474-482.

7.   D. Gerlier and N. Thomasset, *J. Immunol. Methods*, 1986, **94**, 57-63.

8.   M. J. Cleare and J. D. Hoeschele, *J. Bioinorg. Chem*, 1973, **2**, 187-210.

9.   M. J. Cleare and J. D. Hoeschele, *Plat. Metals Rev.*, 1973, **17**, 2.

10.   M. Coluccia and G. Natile, *Anticancer Agents Med. Chem.*, 2007, **7**, 111-123.

11.   G. Natile and M. Coluccia, *Coor. Chem. Rev.*, 2001, **218-217**, 383-410.

12.   I. Romero-Canelon, A. M. Pizarro, A. Habtemariam and P. J. Sadler, *Metallomics*, 2012, **4**, 1271-1279.

13.   I. Romero-Canelon, L. Salassa and P. J. Sadler, *J. Med. Chem.*, 2013, **56**, 1291-1300.

14.   P. Heffeter, K. Böck, B. Atil, M. Reza Hoda, W. Körner, C. Bartel, U. Jungwirth, B. Keppler, M. Micksche, W. Berger and G. Koellensperger, *J. Biol. Inorg. Chem.*, 2010, **15**, 737-748.

15.   A. H. Velders, H. Kooijman, A. L. Spek, J. G. Haasnoot, D. de Vos and J. Reedijk, *Inorg. Chem.*, 2000, **39**, 2966-2967.

16.   Z. Almodares, S. J. Lucas, B. D. Crossley, A. M. Basri, C. M. Pask, A. J. Hebden, R. M. Phillips and P. C. McGowan, *Inorg. Chem.*, 2014, **53**, 727-736.

17.   M. R. Alison and C. E. Sarraf, *Understanding Cancer: From Basic Science to Clinical Practice*, Cambridge University Press, Cambridge, 1997.

18.   C. N. Coleman, *J. Natl. Cancer Inst.*, 1988, **80**, 310-317.

19.   P. Vaupel and L. Harrison, *The Oncologist*, 2004, **9 Suppl 5**, 4-9.

20.   I. F. Tannock, *The Lancet*, 1998, **351**, SII9-SII16.

21. J. M. Brown and R. W. William, *Nat. Rev. Cancer*, 2004, **4**, 437-447.

22. T. G. Graeber, C. Osmanian, T. Jacks, D. E. Housman, C. J. Koch, S. W. Lowe and A. J. Giaccia, *Nature*, 1996, **379**, 88-91.

23. K. M. Comerford, T. J. Wallace, J. Karhausen, N. A. Louis, M. C. Montalto and S. P. Colgan, *Cancer Res.*, 2002, **62**, 3387-3394.

24. G. L. Wang, B. H. Jiang, E. A. Rue and G. L. Semenza, *Proc. Natl. Acad. Sci.*, 1995, **92**, 5510-5514.

25. M. Bhatia, T. C. Karlenius, G. D. Trapani and K. F. Tonissen, *Carcigonesis*, Intech, Croatia, 2013.

26. S. Salceda and J. Caro, *J. Biol. Chem.*, 1997, **272**, 22642-22647.

27. M. Ema, K. Hirota, J. Mimura, H. Abe, J. Yodoi, K. Sogawa, L. Poellinger and Y. Fujii-Kuriyama, *EMBO J.*, 1999, **18**, 1905-1914.

28. P. J. Kallio, K. Okamoto, S. O'Brien, P. Carrero, Y. Makino, H. Tanaka and L. Poellinger, *EMBO J.*, 1998, **17**, 6573-6586.

29. S. N. Greer, J. L. Metcalf, Y. Wang and M. Ohh, *EMBO J.*, 2012, **31**, 2448-2460.

30. D. J. Manalo, A. Rowan, T. Lavoie, L. Natarajan, B. D. Kelly, S. Q. Ye, J. G. Garcia and G. L. Semenza, *Blood*, 2005, **105**, 659-669.

31. J.-T. Chi, Z. Wang, D. S. A. Nuyten, E. H. Rodriguez, M. E. Schaner, A. Salim, Y. Wang, G. B. Kristensen, Å. Helland, A.-L. Børresen-Dale, A. Giaccia, M. T. Longaker, T. Hastie, G. P. Yang, M. J. van de Vijver and P. O. Brown, *PLoS Med*, 2006, **3**, e47.

32. A. L. Harris, *Nat. Rev. Cancer*, 2002, **2**, 38-47.

33. G. L. Semenza, *Nat. Rev. Cancer*, 2003, **3**, 721-732.

34. H. Zhong, A. M. De Marzo, E. Laughner, M. Lim, D. A. Hilton, D. Zagzag, P. Buechler, W. B. Isaacs, G. L. Semenza and J. W. Simons, *Cancer Res.*, 1999, **59**, 5830-5835.

35. D. Hanahan and R. A. Weinberg, *Cell*, 2000, **100**, 57-70.

36. R. A. Gatenby and R. J. Gillies, *Nat. Rev. Cancer*, 2004, **4**, 891-899.

37. M. López-Lázaro, *Cancer Epidem. Biomar.*, 2006, **15**, 2332-2335.

38. N. Graf and S. J. Lippard, *Adv. Drug Deliver. Rev*, 2012, **64**, 993-1004.

39.   D. C. Ware, B. D. Palmer, W. R. Wilson and W. A. Denny, *J. Med. Chem.*, 1993, **36**, 1839-1846.

40.   T. W. Failes, C. I. Diakos, C. K. Underwood, T. W. Hambley, C. M. Cullinane and J. Guy Lyons, *J. Inorg. Biochem*, 2003, **96**, 128.

41.   S. R. Bramhall, A. Rosemurgy, P. D. Brown, C. Bowry and J. A. Buckels, *J. Clin. Oncol.*, 2001, **19**, 3447-3455.

42.   T. W. Failes, C. Cullinane, C. I. Diakos, N. Yamamoto, J. G. Lyons and T. W. Hambley, *Chemistry*, 2007, **13**, 2974-2982.

43.   P. R. Craig, P. J. Brothers, G. R. Clark, W. R. Wilson, W. A. Denny and D. C. Ware, *Dalton Trans.*, 2004, 611-618.

44.   X. Peng and V. Gandhi, *Ther. Deliv.,* 2012, **3**, 823-833.

45.   C. Ornelas, *New J. Chem.*, 2011, **35**, 1973-1985.

46.   T. W. Failes and T. W. Hambley, *J. Inorg. Biochem.*, 2007, **101**, 396-403.

47.   P. J. Blower, J. R. Dilworth, R. I. Maurer, G. D. Mullen, C. A. Reynolds and Y. Zheng, *J. Inorg. Biochem.*, 2001, **85**, 15-22.

48.   L. L. Parker, S. M. Lacy, L. J. Farrugia, C. Evans, D. J. Robins, C. C. O'Hare, J. A. Hartley, M. Jaffar and I. J. Stratford, *J. Med. Chem.*, 2004, **47**, 5683-5689.

49.   H. R. Mellor, S. Snelling, M. D. Hall, S. Modok, M. Jaffar, T. W. Hambley and R. Callaghan, *Biochem. Pharm.*, 2005, **70**, 1137-1146.

50.   C. F. Chin, D. Y. Wong, R. Jothibasu and W. H. Ang, *Curr. Top. Med. Chem.*, 2011, **11**, 2602-2612.

51.   M. D. Hall and T. W. Hambley, *Coor. Chem. Rev.*, 2002, **232**, 49-67.

52.   L. Ellis, H. Er and T. Hambley, *Aust. J. Chem.*, 1995, **48**, 793-806.

53.   M. D. Hall, S. Amjadi, M. Zhang, P. J. Beale and T. W. Hambley, *J. Inorg. Biochem.*, 2004, **98**, 1614-1624.

54.   W. R. Wilson and M. P. Hay, *Nat. Rev. Cancer*, 2011, **11**, 393-410.

55.   J. M. Brown, *Br. J. Cancer*, 1993, **67**, 1163-1170.

56.   G. Chowdhury, V. Junnotula, J. S. Daniels, M. M. Greenberg and K. S. Gates, *J. Am. Chem. Soc.*, 2007, **129**, 12870-12877.

57.   S. S. Shinde, M. P. Hay, A. V. Patterson, W. A. Denny and R. F. Anderson, *J. Am. Chem. Soc.*, 2009, **131**, 14220-14221.

58.   P. A. DiSilvestro, S. Ali, P. S. Craighead, J. A. Lucci, Y. C. Lee, D. E. Cohn, N. M. Spirtos, K. S. Tewari, C. Muller, W. H. Gajewski, M. M. Steinhoff and B. J. Monk, *J. Clin. Oncol.*, 2014, **32**, 458-464.

CHAPTER 7

Structural-Activity Relationship Studies of *Bis*-Picolinamide Ruthenium Dihalide Complexes

7 Structural-Activity Relationship Studies

7.1 Introduction

By understanding the relationship between the molecular structure of a drug and its biological activity, modifications and improvements can be ensured to offer a pharmaceutical drug with high potency and very much less toxicity. Few of the many important structural-activity relationship (SAR) studies were conducted for *bis*-picolinamide ruthenium dihalide complexes. This chapter includes the results and discussion for hydrolysis and hydrophobicity tests on selected ruthenium dihalide complexes.

7.2 Hydrolysis

An important mechanism of action known for anti-cancer drugs is the activation by hydrolysis mechanism that has been shown by cisplatin,[1-4] NAMI-A[5] and KP-1019.[6] These complexes are initially inert when administered intravenously into the blood plasma, which is due to the high chloride concentration, hence suppressing the ligand substitution reaction. Once these complexes have entered cancer cells that have low chloride concentration, they then undergo hydrolysis and became activated. Generally, ruthenium complexes with dichloride ligands are hydrolysed to form cationic monoaqua or diaqua intermediates under physiological conditions.[7, 8]

Bis-picolinamide ruthenium dihalide complexes are assumed to undergo a hydrolysis reaction, following **Scheme 7.1**, which is a similar mechanism to that of cisplatin, NAMI-A and KP1019. In this reaction, the neutral ruthenium dihalide complexes undergo a halide substitution with an aqua ligand to form a charged monoaqua intermediate, which then undergoes its second substitution with an aqua ligand to give a 2+ charged diaqua complex. Following previous reported studies of known anti-cancer drugs, the aqua complex is the active analogue that is able to bind with DNA base molecules by cross-linking thus damaging the DNA structure.[1-8]
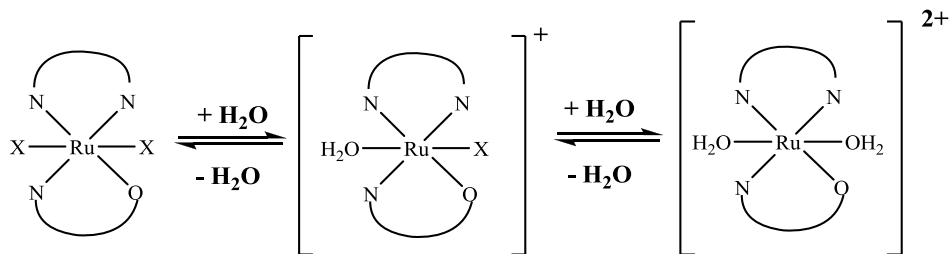
Scheme 7.1 *Hydrolysis mechanism for bis-picolinamide ruthenium dihalide complexes*

A range of complexes from the least to most cytotoxic was selected for hydrolysis study. The samples were prepared following the conditions used in hydrolysis studies previously reported in the literature.[9-12] The samples for ruthenium dichloride complexes **3.3**, **3.5**, **3.7**, **3.10**, **3.12** and **3.14** were prepared in 10% MeOH/90% H_2O, and ruthenium diiodide complexes **4.7**, **4.10**, **4.11** and **4.12** in 10% DMF/90% H_2O to give a final concentration of 50 μM. These solutions were scanned using uv-vis spectrophotometry every 24 hours at 293 K over a period of 5 days, to correlate with the 5-day drug incubation in cytotoxicity tests, and after 5 days, the uv-vis samples were analysed by ESI-MS. **Figure 7.1** shows the uv-vis spectra obtained from hydrolysis studies for ruthenium dichloride complexes **3.3**, **3.5**, **3.7**, **3.10**, **3.12** and **3.14** and four ruthenium diiodide complexes **4.7**, **4.10**, **4.11** and **4.12** taken every 24 hours for 5 days at 293 K. The arrows on the graphs indicate the intensities of the peaks that change from Day 0 to Day 5. At Day 0, each complex shows an intense absorption in the ultraviolet region (200 – 350 nm), except for complex **3.3** that shows two peaks with intense absorption. A few relatively weak peaks are seen in the visible light range (350 – 700 nm) for all complexes. The changes of the absorption bands indicate that there are ligand substitution reactions occurring when the complexes are in aqueous solution. [7] For most of the ruthenium dichloride complexes, the highest energy absorption band at Day 1 has increased in intensity at Day 5, whereas the intensity for the bands at lower energy wavelength decreases, followed by the disappearance of the absorption band at the lowest energy wavelength. As for the ruthenium diiodide complexes, they have shown a decrease in intensity on all the absorption bands, with an appearance of a band at the lower energy at Day 5 seen in complex **4.7** and **4.12**. **Table 7.1** lists the wavelength where the maxima of each absorption bands are seen in the respective complexes at Day 0 and Day 5.
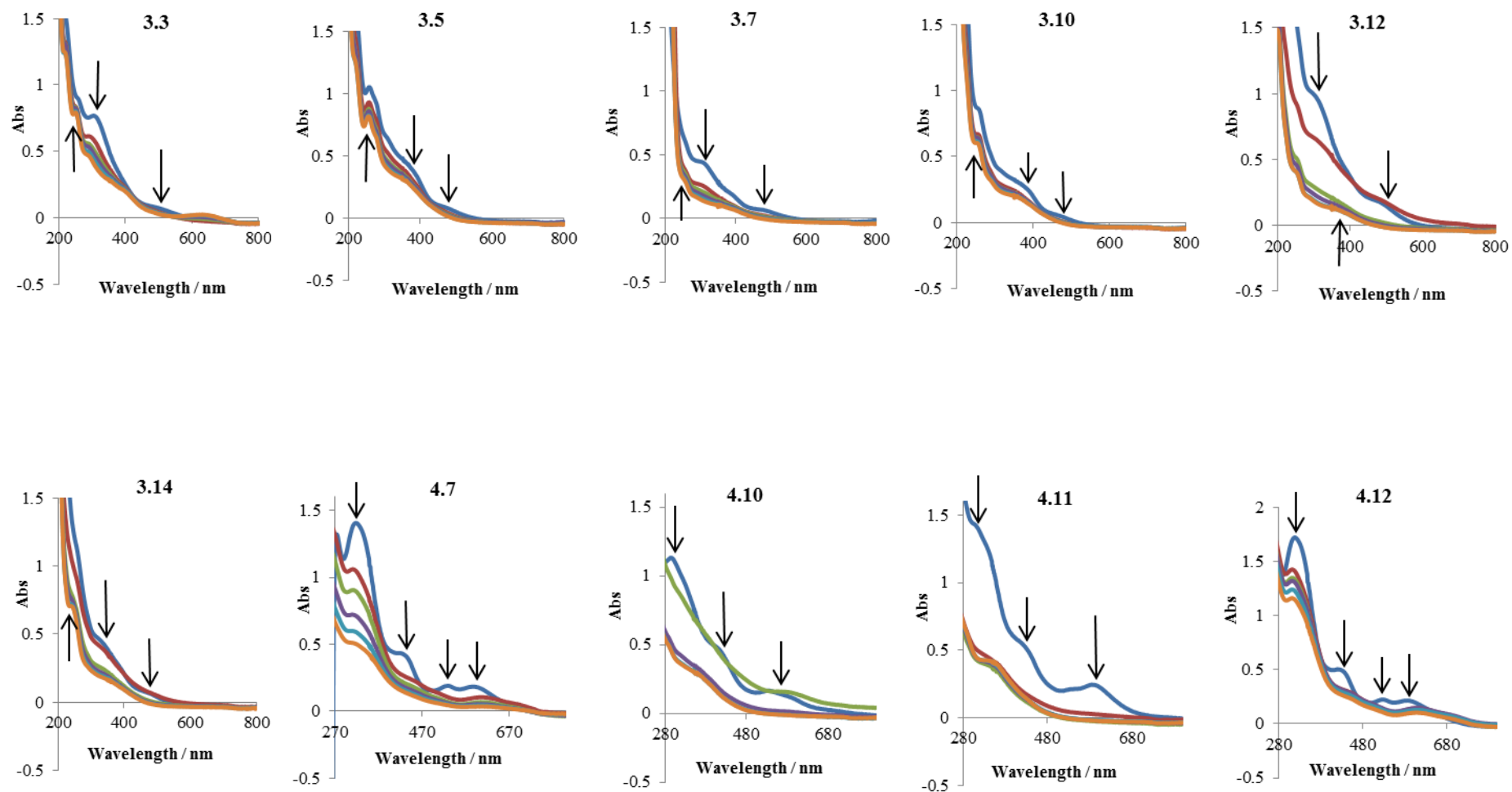
Figure 7.1 *Time-evolution UV-Vis spectra for hydrolysis of Ru complexes (50 μM) at 293 K*

Table 7.1 Wavelength of absorption bands (λ_{max}) for Ru complexes

RuX$_2$(L-R)$_2$	R	λ_{max} / nm	
		Day 0	**Day 5**
3.3	4-F	258, 310, 488	223, 258, 310, 403, 627
3.5	2,5-F	258, 393, 480	258, 364
3.7	3-Cl	258, 314, 488	258, 394
3.10	2,5-Cl	258, 393, 475	258, 368
3.12	3-Br	309, 393, 480	258, 368
3.14	2,5-Br	258, 335, 475	242, 347
4.7	3-Cl	315, 432, 525, 591	315, 613
4.10	2,5-Cl	292, 414, 547	370
4.11	2-Br	310, 432, 587	360
4.12	3-Br	315, 432, 525, 591	315, 613

All ruthenium dichloride complexes show the disappearance of peaks with maxima at 475 − 488 nm at Day 5. Complex **3.3**, unlike all the other RuCl$_2$ complexes, has the appearance of additional absorption bands at 223, 403 and 627 nm. Interestingly, an intense colour change was observed in the aqueous solution of complex **3.3** after Day 5, from a red-brown to a bluish-green solution, which was not shown by the other RuCl$_2$ complexes.

Mercer and Dumas reported the preparation and characterisation of blue ruthenium chloride dimer complexes involving the reduction of hydrated ruthenium trichloride by heating with strong reducing agents.[13] Quite recently, Pushkar *et al.* have revealed the catalytic process of blue ruthenium dimer in water oxidation cycle.[14] **Figure 7.2** shows the structure of the dimer, BD[3,3]$^{4+}$, *cis,cis*-[(bpy)$_2$(H$_2$O)Ru(III)ORu(III)(OH$_2$)(bpy)$_2$]$^{4+}$, having two ruthenium complexes with each consisting of two bipyridine ligands and a water molecule, bound together by an oxygen atom between the two ruthenium metal centres.
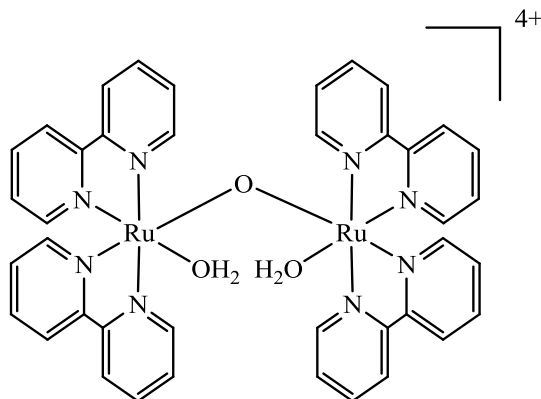
Figure 7.2 *Structure of blue ruthenium dimer*[14, 15]

There is a possibility that complex **3.3** may have formed a dimer with an oxygen atom bridging with the two ruthenium metal centres, which could explain the appearance of more absorption bands at Day 5. **Figure 7.3** shows the possible structure of a blue *bis*-picolinamide ruthenium aqua dimer complex. ES-MS analysis on this complex has shown an m/z ratio of 1221.9 [M Na$^+$] which satisfies with the mass of the complex **3.3** having their chloride ligands substituted with a water molecule, making a dimer by two ruthenium metal centres bridging with an oxygen atom. Attempts to isolate the product from the blue ruthenium aqua solution, however, was unsuccessful, and so this will be added to the list of future work, as it will be interesting to study the blue ruthenium *bis*-picolinamide dimer complex as an anti-cancer agent.
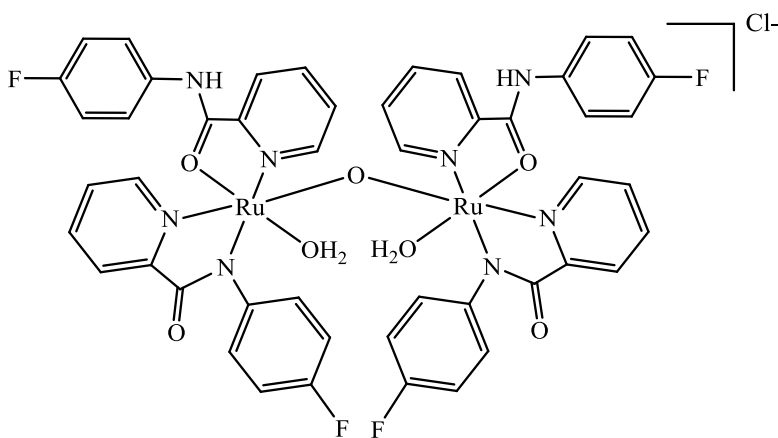
Figure 7.3 *Possible structure of blue bis-picolinamide ruthenium aqua dimer complex*

A calibration curve for each complex was used to determine the final concentration of the aqua complex formed in solution by taking the wavelength with maximum absorbance, and using the formula below to obtain the percentage of the hydrolysed complex after Day 5.

$$\% \; hydrolysed \; complex = \left(\frac{[C]_{initial} - [C]_{final}}{[C]_{initial}} \right) \times 100\%$$

The IC_{50} values against A2780 and HT-29 cell line, and percentage of hydrolysed complexes **3.3**, **3.5**, **3.7**, **3.10**, **3.12** and **3.14** are shown in **Table 7.2**, and their plot against time, fitted to a kinetic curve are as shown in **Figure 7.4**. Ruthenium chloride complexes **3.7** and **3.12** have been shown to undergone the fastest hydrolysis rate forming the highest percentage of hydrolysed complex from Day 1 to Day 5, in comparison to complex **3.3**, **3.5**, **3.10** and **3.14**. Complexes **3.7** and **3.12**, being the two most cytotoxic among the ruthenium dichloride complexes, hydrolyses up to 90% after five days, with complex **3.7** showing a faster hydrolysis rate. Complex **3.3** is more cytotoxic than complex **3.14** against A2780 ovarian cancer cell line, but is less cytotoxic than complex **3.14** towards HT-29 colon cancer cell line, their hydrolysis reaction undergoes a similar rate nevertheless, whereas for complexes **3.10** and **3.5**, being the two least cytotoxic in the selected hydrolysis series of complexes, form 48% and 25% of hydrolysed complex after 5 days. The uv-vis hydrolysis samples were analysed by ESI-MS after five days to investigate the ruthenium complexes that are formed in the aqueous solution. Ruthenium dichloride complexes **3.3**, **3.7** and **3.12**, which are the active anti-cancer complexes, have formed the di-aqua complexes, in which their two chloride ligands have been replaced by water molecules when in solution. Complex **3.5**, **3.10** and **3.15** are moderately active towards A2780 and HT-29 cancer cell lines contained the mono-aqua complex, where only one chloride ligand is substituted with a water molecule, supporting their rate of reaction of fast and slow hydrolysis respectively. The rate of hydrolysis for ruthenium dichloride complexes increases in the order from **3.5** < **3.10** < **3.14** ~ **3.3** < **3.7** < **3.12**, correlating very well with their cytotoxicity against the A2780 and HT-29 cancer cell line indicating that hydrolysis may be one of their mechanisms for anti-cancer activities.

Table 7.2 IC$_{50}$ values against A2780 and HT-29 cell line, and percentage of hydrolysed bis-picolinamide ruthenium diiodide complexes

Complexes	IC$_{50}$ / μM		% hydrolysed
	A2780	HT-29	
Ruthenium dichloride complexes (10% MeOH/90% H$_2$O)			
3.3	6.9 ± 0.8	17 ± 1	69.7
3.5	45 ± 2	20 ± 1	24.7
3.7	3.6 ± 0.2	3.0 ± 0.1	91.6
3.10	31 ± 1	11 ± 1	47.9
3.12	3.3 ± 0.2	3.3 ± 0.2	90.2
3.14	18 ± 1	7.7 ± 0.3	64.8
Ruthenium diiodide complexes (10% DMF/90% H$_2$O)			
4.7	2.8 ± 0.3	2.3 ± 0.1	64.6
4.10	10.0 ± 0.4	6.5 ±0.3	61.0
4.11	11 ± 1	24 ± 2	72.5
4.12	2.0 ± 0.2	1.5 ± 0.1	34.6
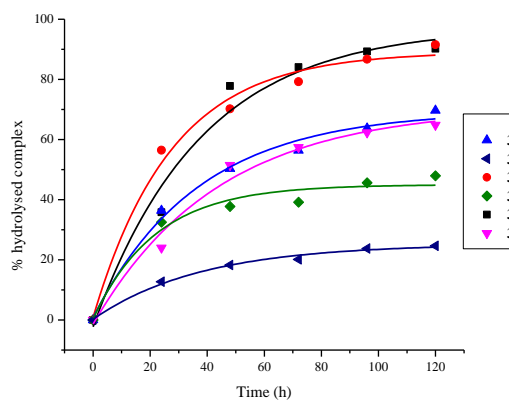
(a)   **(b)**
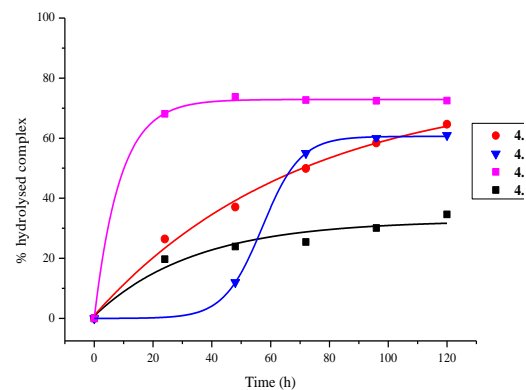
Figure 7.4 Time-dependence formation of (a) hydrolysed ruthenium dichloride complexes in 10% MeOH/90% H$_2$O and, (b) hydrolysed ruthenium diiodide complexes in 10% DMF/90% H$_2$O

The percentage of hydrolysed complexes **4.7**, **4.10**, **4.11** and **4.12** over five days fitted to a kinetic curve are shown in **Figure 7.4b**. Ruthenium diiodide complex **4.12** is the most cytotoxic in the selected series of complexes, forming 26% of hydrolysed complex after five days. Complex **4.10** undergoes the slowest hydrolysis within 72 hours, reaching its maximum from 55% to 61% from Day 3 to Day 5. Complex **4.7** has hydrolysed slightly more than complex **4.10** reaching 65% after five days in aqueous solution. The least cytotoxic complex in the series is complex **4.11**, which has gone the fastest hydrolysis, with almost reaching its maximum of 72% hydrolysed after 24 hours. Their ES-MS analysis has shown that the ruthenium diiodide complexes have formed mono-aqua complexes in the aqueous solution after 5 days, which does not correlate with their rate of hydrolysis. Complex **4.11** has reached its maximum hydrolysis of 72% but has only substituted one chloride ligand with a water molecule.

The increasing rate of hydrolysis for ruthenium diiodide complexes is in the order from complex **4.12** > **4.7** ~ **4.10** > **4.11**, opposing their order of cytotoxic activity against A2780 ovarian cancer cell line and HT-29 colon cancer cell line. These observations are in contrast to their dichloride analogues, similarly shown by Sadler *et. al.* on contrasting activity between chlorido and iodo ruthenium arene complexes.[16, 17] This could suggest that the ruthenium diiodide complexes do undergo hydrolysis, however, it may not be their major anti-cancer mechanism. In addition to complex **4.12** being the most cytotoxic in the series and is the least hydrolysed, indicates that it is more stable than their chloride analogues that could give the benefit in lowering the toxic side effects with respect to its high cytotoxic anti-cancer activities. This, again, breaks the rule proposed by Rosenberg,[18] and Cleare and Hoeschele,[19, 20] specifying that the *trans* geometry complexes could lead to an increase in toxicity as they were found to be highly reactive due to kinetic instability.

There have been many unsuccessful attempts to isolate the aqua products from the aqueous solution, and also to synthesise the aqua analogue of the ruthenium dihalide complexes. **Figure 7.5** shows the structure of complex **8.1**, an aqua analogue of complex **3.12**, which has been synthesised with the presence of a silver salt, $AgSbF_6$, and characterised by IR, ESI-MS and microanalysis. The IR spectra for complex **8.1**,

along with the spectra of its dichloride (complex **3.12**) and diiodide (complex **4.12**) analogue, is as shown in **Figure 7.6**, where most differences are observed in the fingerprint region particularly between 950-400 cm^{-1} region. Attempted crystallisation was also carried out on complex **8.1** to obtain crystals suitable for x-ray crystallography, although has been unsuccessful up to this point.
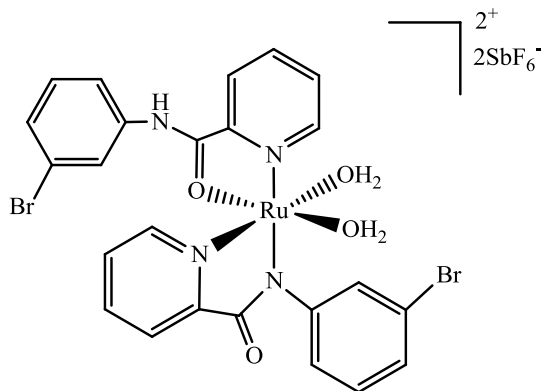
Figure 7.5 Structure of complex 8.1
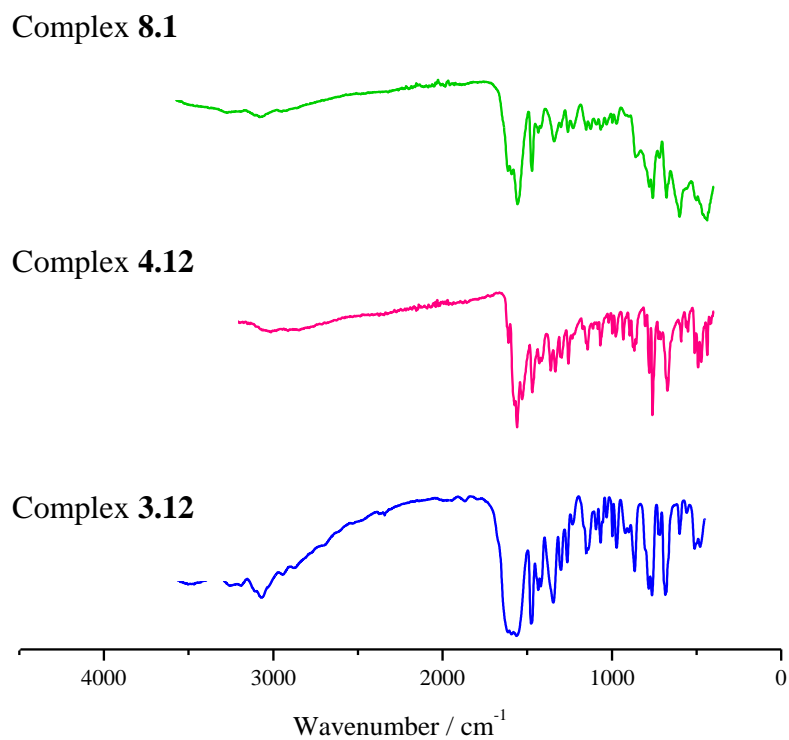
Figure 7.6 IR Spectra of complex 3.12, 4.12 and 8.1

7.3   Hydrophobicity

The decrease in cellular uptake of drugs has become one of the main factors that could lead to acquired drug resistance.[21] Drugs are required to be hydrophobic to enter the cells easily by passive diffusion through the cell membrane of hydrophobic layers.[22] Increasing the hydrophobicity of the drug will aid the increase of their uptake into cells, hence increasing their cytotoxicity. However, hydrophobicity has to fall within the optimum range, as the drug may become very insoluble in aqueous media or is embedded within the cell membrane leading to decrease in their activities and increase in toxicities.

The hydrophobicity of a drug can be determined by shake-flask method of octanol-water partition coefficient to obtain log P values.[23] Deionised water containing 300mM of NaCl was used to prevent the complexes from undergoing hydrolysis during the study. Several *bis*-picolinamide ruthenium dichloride complexes were selected, and dissolved in water-saturated octanol to be shaken with octanol-saturated water for 4 hours to ensure equilibrium is reached. The organic layer of the samples before and after the partition were analysed by uv-vis spectrophotometry to determine the concentration of the complex, obtained from a calibration curve of the respective complex. The log P values of the complexes are obtained by using the following formula,

$$Log\ P = Log\left(\frac{[C]_{org}}{[C]_{aq}}\right)$$

In a shake-flask method, the organic phase serves as a model for the hydrophobic layers on the cell membrane. A complex is measured as hydrophobic where its concentration is higher in the organic phase than in the aqueous phase, giving a positive log P value. Hence, a negative log P value defines the drug being hydrophilic with higher concentration in the aqueous phase of the partition coefficient. The log P values for the selected *bis*-picolinamide ruthenium dichloride complexes **3.2**, **3.3**, **3.5**, **3.7** and **3.10 - 3.14** are as shown in **Figure 7.7**. All of the complexes are found to be hydrophobic as they partition preferentially in the organic layer. Their log P values are

within the range 0.67 - 1.39, that applies well within Lipinski's 'rule of five'. The rule states that poor absorption and distribution of drugs is expected when it has molecular weight over 500 Da, Log P value is greater than 5, number of H-bond donors is more than 5, and number of H-bond acceptors is more than 10.[24] Although, transition metal anti-cancer drugs have proved exceptions of the Lipinski rule, as many tend to have a higher molecular weight than as stated.[25] Hansch's principle of minimum hydrophobicity in drug design assert that for drugs to avoid related side effects with the central nervous system (CNS), such as depressions and hallucinations, their log P value must be less than 2.0.[26] The two most cytotoxic ruthenium dichloride complex **3.7** and **3.13** have a log P value of 1.37 and 1.39 respectively, which are also the two most hydrophobic in the series. Complex **3.5**, the least cytotoxic complex of the series is also the least hydrophobic.
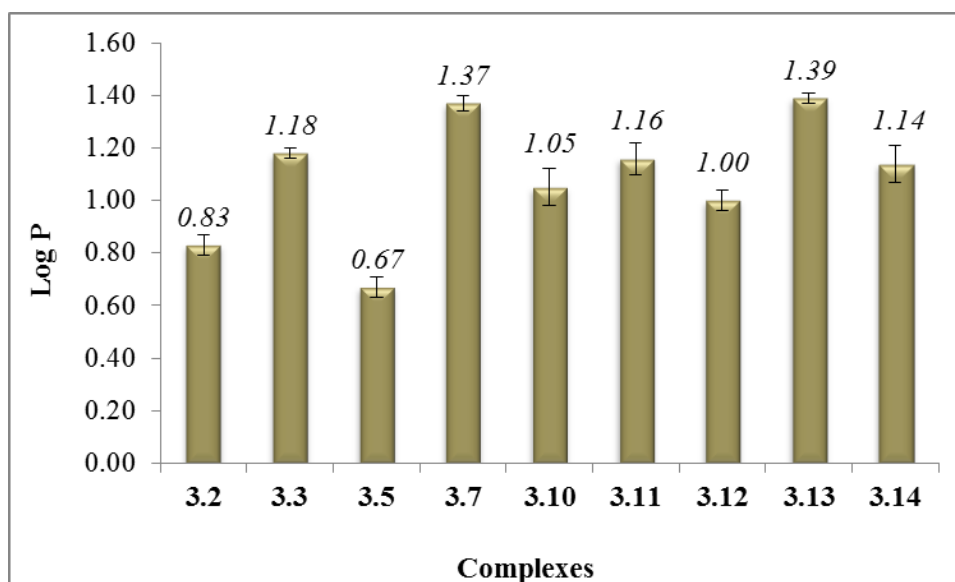
Figure 7.7 *Log P values of bis-picolinamide ruthenium dichloride complexes from the average of six independent experiments*

Platinum complexes have intermediate hydrophobicity and have been shown that their increase in hydrophobicity correlates well with the increase in their anti-cancer activity.[27] **Figure 7.8** shows the correlation between log P values and cytotoxicity of *bis*-picolinamide ruthenium dichloride complexes against A2780 and HT-29 cancer cell lines. Only very few correlations are seen with respect to the complexes that have

fallen within the linear relationship. However, most complexes are outliers from the correlation and have showed an irregularity of log P values in the order of their cytotoxic activity.
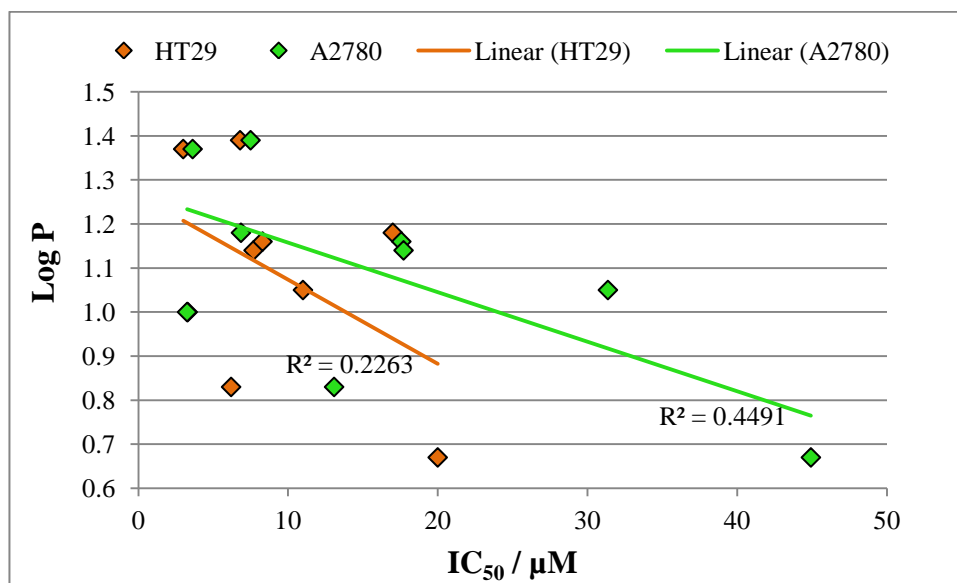
Figure 7.8 *Correlation between log P values and cytotoxicity of bis-picolinamide ruthenium dichloride complexes against A2780 and HT-29 cancer cell lines*

From the observations, these may suggest that with the complexes being hydrophobic, they may easily enter the cells by passive diffusion. However, with only very few correlations seen between their cytotoxicity and log P values, their cell uptake mechanism may not be related to their anti-cancer activity within the cells. Studies have also shown that cisplatin have the ability to enter the cells via copper transporters,[28, 29] and cell uptake of KP-1019 via overexpressed protein transferrin receptor within the cancer cell membrane.[30, 31] *Bis*-picolinamide ruthenium dichloride complexes may also have this binding potential to a specific transporter as their cell uptake mechanism with relation to their anti-cancer activity. Cell uptake studies on ruthenium dichloride complexes may provide further evidence to understand their anti-cancer mechanism.

7.4   References

1.   Z. Guo and P. J. Sadler, *Angew. Chem. Int. Ed.*, 1999, **38**, 1512-1531.

2.   M. A. Jakupec, M. Galanski and B. K. Keppler, *Rev. Physiol. Biochem. Pharmacol.*, Springer Berlin Heidelberg, 2003, pp. 1-53.

3.   V. Brabec and J. Kasparkova, *Drug Resist. Updates*, 2005, **8**, 131-146.

4.   H. Zorbas and B. K. Keppler, *Chembiochem*, 2005, **6**, 1157-1166.

5.   M. Bouma, B. Nuijen, M. T. Jansen, G. Sava, A. Flaibani, A. Bult and J. H. Beijnen, *Int. J. Pharm.*, 2002, **248**, 239-246.

6.   G. Mestroni, E. Alessio, G. Sava, S. Pacor, M. Coluccia and A. Boccarelli, *Met. Based Drugs*, 1994, **1**, 41-63.

7.   S. Betanzos-Lara, A. Habtemariam, G. J. Clarkson and P. J. Sadler, *Eur. J. Inorg. Chem.*, 2011, **2011**, 3257-3264.

8.   S. Roy, P. U. Maheswari, A. Golobič, B. Kozlevčar and J. Reedijk, *Inorg. Chim. Acta*, 2012, **393**, 239-245.

9.   A. F. A. Peacock, A. Habtemariam, S. A. Moggach, A. Prescimone, S. Parsons and P. J. Sadler, *Inorg. Chem.*, 2007, **46**, 4049-4059.

10.   S. H. van Rijt, A. Mukherjee, A. M. Pizarro and P. J. Sadler, *J. Med. Chem.*, 2009, **53**, 840-849.

11.   S. H. van Rijt, A. J. Hebden, T. Amaresekera, R. J. Deeth, G. J. Clarkson, S. Parsons, P. C. McGowan and P. J. Sadler, *J. Med. Chem.*, 2009, **52**, 7753-7764.

12.   Z. Liu, I. Romero-Canelón, B. Qamar, J. M. Hearn, A. Habtemariam, N. P. E. Barry, A. M. Pizarro, G. J. Clarkson and P. J. Sadler, *Angew. Chem. Int. Ed.*, 2014, **53**, 3941-3946.

13.   E. E. Mercer and P. E. Dumas, *Inorg. Chem.*, 1971, **10**, 2755-2759.

14.   D. Moonshiram, J. W. Jurss, J. J. Concepcion, T. Zakharova, I. Alperovich, T. J. Meyer and Y. Pushkar, *J. Am. Chem. Soc.*, 2012, **134**, 4625-4636.

15.   J. J. Concepcion, J. W. Jurss, J. L. Templeton and T. J. Meyer, *Proc. Natl. Acad. Sci.*, 2008, **105**, 17632-17635.

16.   S. J. Dougan, A. Habtemariam, S. E. McHale, S. Parsons and P. J. Sadler, *Proc. Natl. Acad. Sci. U. S. A.*, 2008, **105**, 11628-11633.

17.   I. Romero-Canelon, A. M. Pizarro, A. Habtemariam and P. J. Sadler, *Metallomics,* 2012, **4**, 1271-1279.

18.   B. Rosenberg, L. Van Camp, E. B. Grimley and A. J. Thomson, *J. Biol. Chem.*, 1967, **242**, 1347-1352.

19.   M. J. Cleare and J. D. Hoeschele, *J. Bioinorg. Chem*, 1973, **2**, 187-210.

20.   M. J. Cleare and J. D. Hoeschele, *Plat. Metals Rev.*, 1973, **17**, 2.

21.   S. Y. Loh, P. Mistry, L. R. Kelland, G. Abel and K. R. Harrap, *Br. J. Cancer*, 1992, **66**, 1109-1115.

22.   P. W. J. Ratain MJ, in *Holland-Frei Cancer Medicine*, ed. R. E. P. Donald W Kufe, Ralph R Weichselbaum, Robert C Bast, Jr, Ted S Gansler, James F Holland, and Emil Frei, III, BC Decker, Hamilton, 2003.

23.   K. Takacs-Novak and A. Avdeef, *J. Pharm. Biomed. Anal.*, 1996, **14**, 1405-1413.

24.   C. A. Lipinski, F. Lombardo, B. W. Dominy and P. J. Feeney, *Adv. Drug Delivery Rev.*, 1997, **23**, 3-25.

25.   S. Neidle and D. E. Thurston, *Nat. Rev. Cancer*, 2005, **5**, 285 - 296.

26.   C. Hansch, J. P. Bjorkroth and A. Leo, *J. Pharm. Sci.*, 1987, **76**, 663-687.

27.   J. A. Platts, D. E. Hibbs, T. W. Hambley and M. D. Hall, *J. Med. Chem.*, 2000, **44**, 472-474.

28.   S. Ishida, J. Lee, D. J. Thiele and I. Herskowitz, *Proc. Natl. Acad. Sci. U. S. A.*, 2002, **99**, 14298-14302.

29.   B. G. Blair, C. A. Larson, P. L. Adams, P. B. Abada, R. Safaei and S. B. Howell, *Mol. Pharm.*, 2010, **77**, 912-921.

30.   M. Pongratz, P. Schluga, M. A. Jakupec, V. B. Arion, C. G. Hartinger, G. Allmaier and B. K. Keppler, *J. Anal. At. Spectrom.*, 2004, **19**, 46-51.

31.   P. Heffeter, M. Pongratz, E. Steiner, P. Chiba, M. A. Jakupec, L. Elbling, B. Marian, W. Korner, F. Sevelda, M. Micksche, B. K. Keppler and W. Berger, *J. Pharmacol. Exp. Ther.*, 2005, **312**, 281-289.

CHAPTER 8

Catalytic Transfer Hydrogenation Studies of *Bis*-Picolinamide Ruthenium and Rhodium Dihalide Complexes

8   Catalytic Transfer Hydrogenation

8.1   Introduction

Transfer hydrogenation is a catalytic process for either the oxidation of a substrate through the removal of hydrogen from using a hydrogen acceptor, or the reduction of a substrate through the addition of hydrogen using a hydrogen donor. The substrate for oxidation is generally an alcohol or amine, and for reduction is an unsaturated compound such as aldehyde/ketone, imine or alkene. A metal catalyst is required to mediate the transfer of hydrogen in the reaction, by removing the hydrogen from a hydrogen donor with itself forming a metal hydride species, and then adding this hydrogen to a hydrogen acceptor. **Scheme 8.1** shows the general scheme for a transfer hydrogenation reaction.
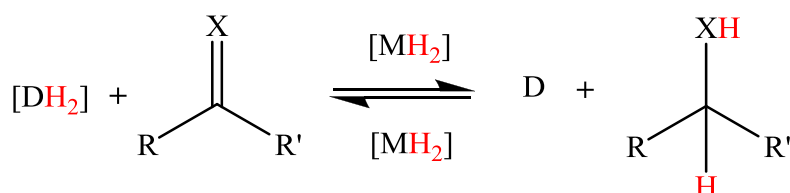
Scheme 8.1 *General reaction scheme for transfer hydrogenation processes, where [DH₂] = hydrogen donor*

This reaction offers a mild and safer method for practical use on both laboratory and industrial scales compared to conventional hydrogenation reactions that involve hazardous hydrogen gas at high pressure. A number of cheap and readily available alcohols can be used as a reagent for hydrogen donor in transfer hydrogenation reactions, which generally proceed through an intermediate metal hydride species. The research on this catalytic reaction is targeted towards metal catalysts that favour high activity under mild operating conditions, preferably while also being selective and recyclable.[1] In addition, metal catalysts that can provide extra stability is also of importance to prevent it from degrading easily during the reaction, hence possible for it to catalyse reactions as many as possible.[2, 3] Recyclable systems serve the purpose of the catalyst being able to be separated from the product after the reaction. In order to develop newly improved procedures for efficient transfer hydrogenation reactions, the catalytic reactivity and selectivity can be finely tuned by modifying the chirality and, steric and electronic properties of the different ligands that are coordinated to the metal centre.

The first part of this chapter will focus on a number of reported ruthenium catalysts that have been used in the reduction of ketones and aldehydes in *iso*-propanol. This reaction is important to provide a wide range of alcohols, which are used as building blocks for the synthesis of pharmaceuticals, agrochemicals, materials, flavours, fragrances and fine chemicals.[4-8] The second part of this chapter will review the possible catalytic mechanisms that have been proposed using different metal catalysts in transfer hydrogenation reactions. Finally, this chapter will describe the catalytic activities of a selection of *bis*-picolinamide metal dihalide complexes.

8.2   The IPA system

The most common hydrogen donor system is the use of *iso*-propanol, which is cheap, relatively safe and easily available. It is used as the reaction solvent in reduction reactions, as shown in **Scheme 8.2**, whereby it is oxidised to produce acetone.[9] In the IPA system, the reaction is reversible between the substrate and the product, and is initially controlled by kinetics. As the product concentration increases, the reaction becomes thermodynamically controlled, as the reverse rate of reaction also increases.[9] This causes limited conversions in the reaction, affecting the yield and the enantiomeric purity of the product over time. In order to prevent this drawback, a large excess of *iso*-propanol is used in the reaction, hence as the solvent, to shift the equilibirium to the favoured product.
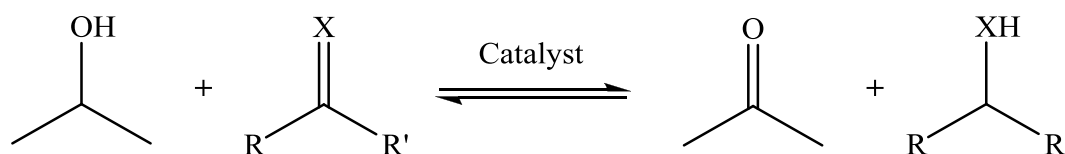
Scheme 8.2 Reductive IPA system of catalytic transfer hydrogenation reaction

Iso-butanol may also be used as a hydrogen donor, however, is generally less active when compared to *iso*-propanol.[9] Primary alcohols tend to form aldehyde as by-product, which may interfere within the catalytic reactions.[9] Alcohols containing glucose or ascorbic acid may be used at a lower concentration as the reaction solvent in transfer hydrogenation.[9] Acetone is used as a hydrogen acceptor in dehydrogenations, where it is reduced to *iso*-propanol.[10] In most cases, a base is also required in order to activate the pre-catalyst within the system. The base

generates the intermediate metal hydride species which is the active species for the transfer of hydrogen.[11-13]

8.3   Ruthenium-Catalysed Transfer Hydrogenation of Aldehydes/Ketones

Noyori *et al.* have developed a series of highly efficient Ru-arene complexes as catalysts for the asymmetric transfer hydrogenation (ATH) of ketones and imines in the presence of a base.[14] The first generation of Ru complexes consisted of an arene ring, a chloride ligand and chiral *N*-substituted-1,2-diphenylethylamine (DPEN) ligand, as shown in **Figure 8.1**.

R = 2,4,6-CH$_3$

C$_6$H$_6$

X = SO$_2$C$_6$H$_4$-*p*-CH$_3$ (Ts)

COC$_6$H$_5$

SO$_2$C$_6$H$_5$

SO$_2$CF$_3$
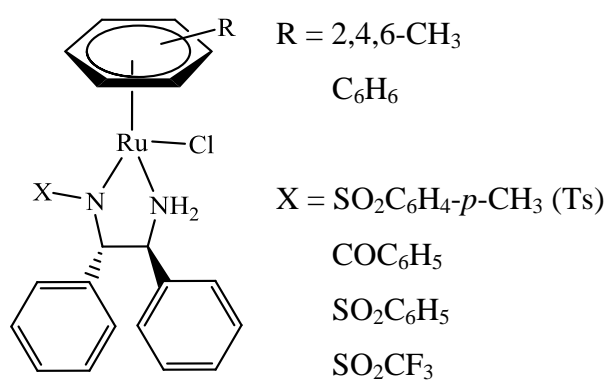
Figure 8.1 First generation of Noyori Ru-arene ATH catalysts

The best catalytic reaction from the initial series of Noyori Ru-arene chiral complexes was for the transfer hydrogenation of acetophenone, as shown in **Scheme 8.3**. The Ru catalyst was prepared *in situ* from the reaction of [RuCl$_2$(mesitylene)]$_2$ and (*S*,*S*)-TsDPEN, in IPA with KOH at room temperature. The reaction gave a 95% conversion of acetophenone to (*S*)-1-phenylethanol with 97% ee in 15 hours.

[RuCl$_2$(mesitylene)]$_2$
(S,S)-TsDPEN
Ru:TsDPEN = 1:2

KOH (5 equiv. to Ru)
IPA, rt, Ar
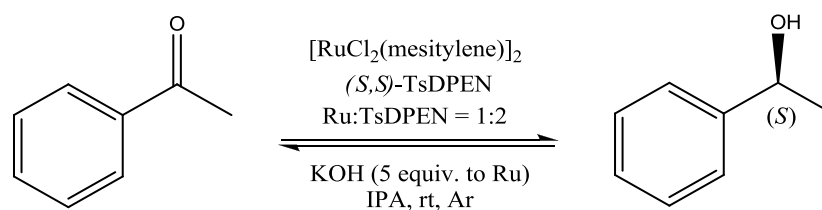
Scheme 8.3 ATH of acetophenone using [RuCl$_2$(mesitylene)]$_2$ and (S,S)-TsDPEN

The catalytic screening of the Ru-arene complexes revealed that the rate and enantioselectivity of the reaction depends on the *N*-substituted based ligand of the complex.[14] The reactivity decreases with increasing electron-withdrawing *N*-

substituents for Ru(η^6-benzene) complexes, in the order of $COC_6H_5 > SO_2C_6H_4$-*p*-$CH_3 > SO_2C_6H_5 > SO_2CF_3$, where the complexes with the sulfonyl substituents gave higher enantioselectivity. The same reaction as in **Scheme 8.3** was also performed without the presence of (*S*,*S*)-TsDPEN ligand, which gave a conversion of <8% from acetophenone to (*S*)-1-phenylethanol in 15 hours.

The second generation of Noyori catalysts for ATH of acetophenones consist of an arene ring, a chloride ligand and an amino-alcohol ligand, as shown in **Figure 8.2**.[15] The Ru catalyst was generated *in situ* from the reaction of Ru-arene dimer and *N*-substituted amino-alcohol in IPA with KOH.
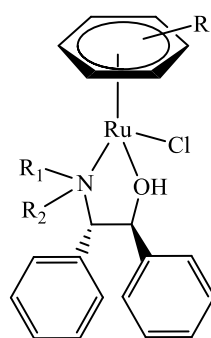
Figure 8.2 Second generation of Noyori Ru-arene ATH catalysts

Replacing the *(N,N)* DPEN ligands with *(N,O)* amino-alcohol ligands significantly increased the catalytic activity when the appropriate arene and amino-alcohol were combined. **Scheme 8.4** shows the combination of [(RuCl$_2$(hexamethylbenzene)$_2$] and (*S*,*S*)-2-methylamino-1,2-diphenylethanol which gave a 94% yield and 92% e.e after 1 h.[15] The catalytic screening of the Ru-arene amino-alcohol complexes have shown that the presence of NH proximity in the ligand increases the catalytic activity, whereas an increase in steric bulk of the arene ring tends to decrease the reactivity of the whole catalyst.
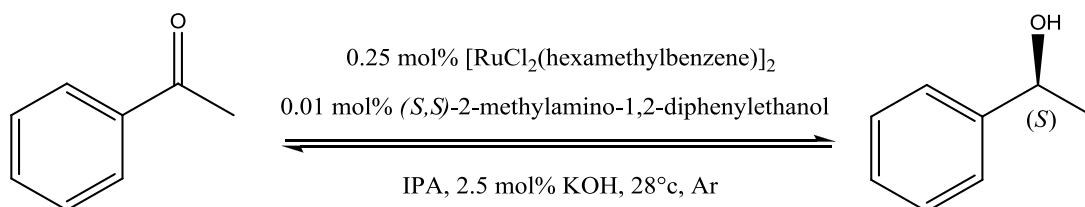
Scheme 8.4 ATH of acetophenone using [(RuCl$_2$(hexamethylbenzene)$_2$] and (S,S)-2-methylamino-1,2-diphenylethanol

Noyori catalysts have also been studied for ATH on deuteurated benzylaldehyde following the reaction schemes as shown in **Scheme 8.5**.[16] The most active catalyst in the series was RuCl(*p*-cymene)(*R,R*)-TsDPEN which gave 100% yield of deuteurated benzylalcohol with 98% ee in 30 mins. When increasing the reaction time to 48 mins, the catalytic activity still maintained with 100% product yield, however the enantiomeric purity of the product decreases to 96%. This suggests that unnecessary prolonged standing of the reaction after reaching 100% conversion should be avoided as to maintain a high degree of kinetic enantioselectivity.
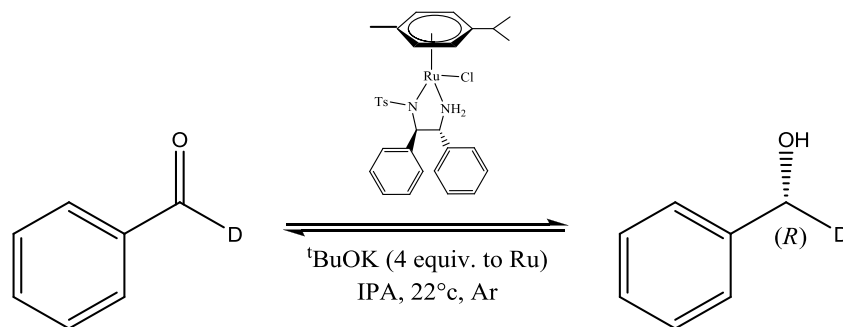
Scheme 8.5 *ATH of benzaldehyde using RuCl(p-cymene)(R,R)-TsDPEN catalyst in IPA*

Following Noyori's work, many researchers have explored and extended the work in order to optimise the catalytic system for transfer hydrogenation reactions, as well as to design and create novel ligands and catalysts. **Table 8.1** illustrates three of the active ruthenium catalysts that were studied for transfer hydrogenation of acetophenone in the IPA/base system (**Scheme 8.6**) under different reaction conditions. Catalyst **1** has shown that their catalytic activity using the optimised conditions, is strongly influenced by the substituents on the pyrimidine ring, whereby their activity increases as the electron donation from the substituent increases.[17] The high conversion rate when using catalyst **2** for the reaction of acetophenone is thought due to the presence of the bulky substituent adjacent to the O or N donor atom of the ligand, in which in this case is the *ortho*-methoxy phenyl group attached to the N donor atom.[18] Baratta *et al.* have developed an arene-free Ru catalyst **3**, consisting of the combination of 2-amido-6-methylpyridine (ampy) and an N-heterocyclic carbene (NHC) as the ligands.[19] Its high catalytic performance in reducing acetophenone to 1-phenyl-ethanol within 5 mins is believed to be due to the presence of the RuH/NH$_2$ motif,[20, 21] and with the addition

of a carbene that adds stability to the Ru centre, preventing degradation; favouring long-lived catalytic species.
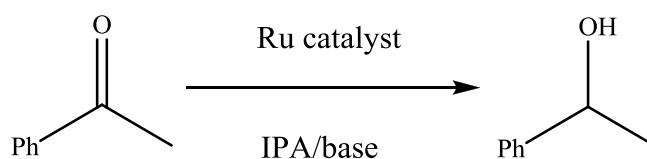
Scheme 8.6 *Reduction of acetophenone in IPA/base system*

Ru Catalyst	Reaction Conditions	% conversion	Ref
1	0.0125 mmol Ru catalyst 0.125 mmol KOH 82°C	98% in 6h	Taghizadeh Goochany *et al.*[17]
2	0.05 mmol Ru catalyst 0.125 mmol KOH Reflux, N$_2$ atm.	98% in 6h	Rath *et al.*[18]
3	0.05 mol% Ru catalyst 2 mol% NaOH Reflux, Ar atm.	99% in 5 mins	Baratta *et al.*[19]

Table 8.1 *Highly active Ru catalysts for ATH of acetophenone in IPA/base system*

There has been much work using Ru catalyst for the reduction of benzaldehyde to benzylalcohol in the IPA/base system. A series of Ru-*p*-cymene complexes containing diphosphine ligands,[22] and Ir-Cp* picolinamide complexes[23] were synthesised within the McGowan group, for a study on ATH of benzaldehyde. The work involved preparing the Ru catalysts with a series of diphosphine ligands *in situ*, and monitoring their catalytic reactions, as well as the comparison of

reactivities when the ligands are coordinating either *(N,N)* or *(N,O)* to the metal centre for Ir-Cp* picolinamide complexes.

A series of control experiments were performed by Dr. Andrea Rodríguez-Bárzano in order to optimise the catalytic reactions of benzaldehyde reduction using [RuCl2(*p*-cymene)]2 and dppf ligand (**Figure 8.3**).[22] The catalysts were prepared *in situ* with the presence of dppf ligand and/or base, Et3N, in IPA at 85°C. The results showed a 100% conversion after 24 hours when both dppf and Et3N is present in the reaction (**Table 8.2**). Dr. Stephanie Lucas focused on Ir-Cp* picolinamide catalysts (**Figure 8.3**) for benzaldehyde reductions with 0.08 mmol KO^{t}Bu in IPA at 60°C.[23] Her work has shown that a higher catalytic activity was seen when the picolinamide ligand coordinates *(N,O)* to the Ir metal centre with 97% conversion compared to the *(N,N)*-coordinated ligand with 26% after 24 hours.

[RuCl2(*p*-cymene)]2   dppf ligand

IrCp*(*N,N*)-picolinamide   IrCp*(*N,O*)-picolinamide
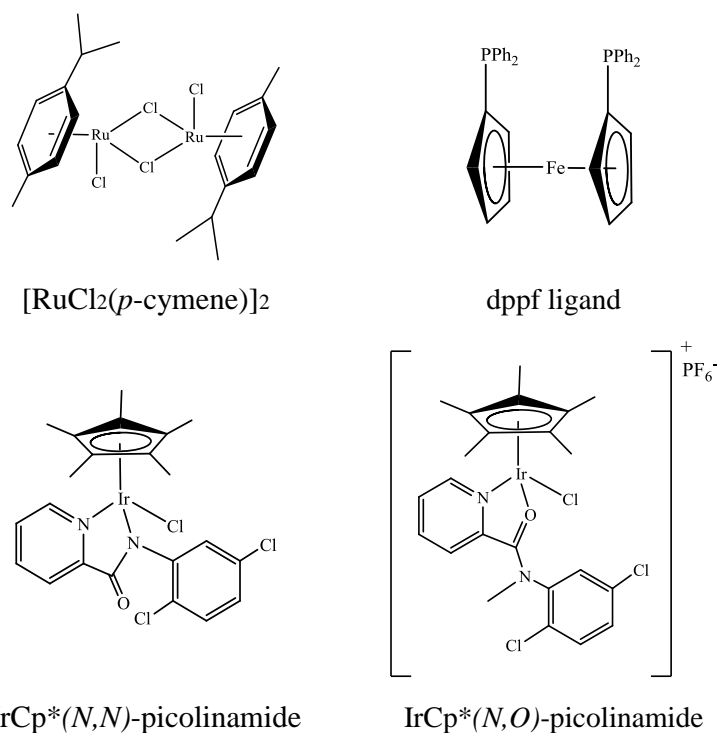
Figure 8.3 *Structure of Ru and Ir catalysts studied for benzaldehyde reductions*

Table 8.2 *Summary of conversions in IPA at 85°C for benzaldehyde reduction*

Entry	Ru species	Ligand (5 mol%)	Base (8 mol%)	% conversion		
				3h	9h	24h
1	[RuCl2(*p*-cymene)]2	dppf	Et3N	100	100	100
2	[RuCl2(*p*-cymene)]2	dppf	-	14.3	60.9	88.8
3	[RuCl2(*p*-cymene)]2	-	Et3N	38.5	50.6	56.3
4	[RuCl2(*p*-cymene)]2	-	-	4.2	11.8	22.2

8.4   Catalytic Mechanisms

Brandt *et al*. have reviewed recent catalytic mechanistic studies in transfer hydrogenation reactions of ketones/aldehydes.[24] Two different mechanistic pathways have been proposed, which are the "direct hydrogen transfer", [25-27] and the "hydridic route", with the latter can be further classified into "monohydride route" or "dihydride route".

8.4.1 Hydridic Route

Transfer hydrogenation reactions using transition metal complexes as catalysts generally involve the formation of metal hydride intermediates. This mechanism is known as the "hydridic route". It has been reported that the presence of base activates the pre-catalyst in the reaction, promoting the formation of highly active metal hydride intermediates, hence increasing the rate of reaction.[13, 28] **Scheme 8.7** shows the general monohydride and dihydride route for catalytic transfer hydrogenation reactions.

(a) Monohydride Route   (b) Dihydride Route
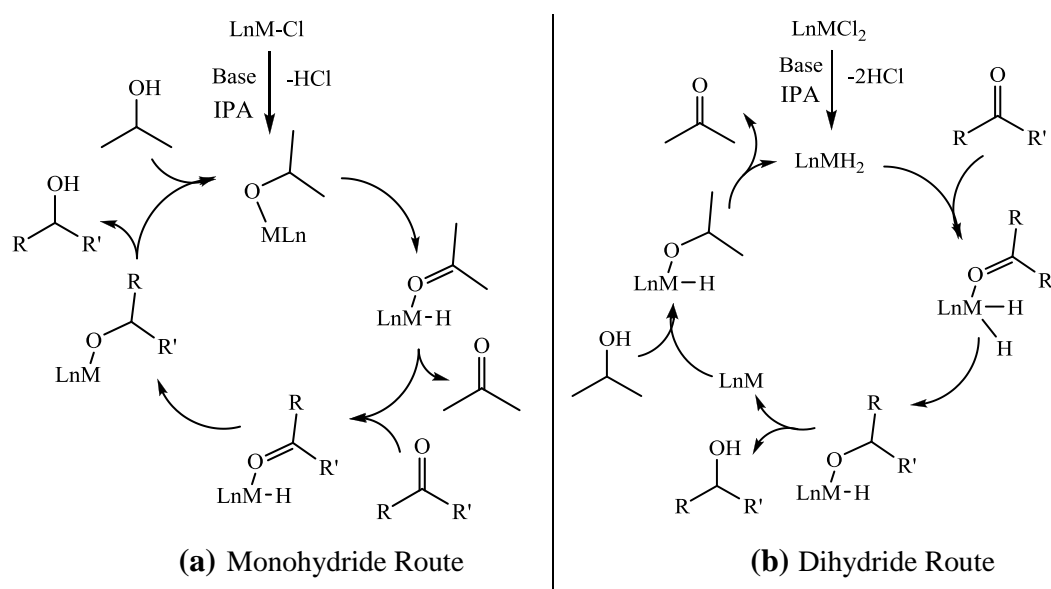
Scheme 8.7 Catalytic transfer hydrogenation via (a) Monohydride route (b) Dihydride route[13, 28]

In the monohydride mechanism, the chloride from the catalyst precursor is substituted by the hydrogen donor to generate an alkoxide, and then forming a metal hydride complex *via* β-elimination. The CO from ketonic substrate inserts into the metal-hydride bond to give the alcohol product. In the dihydride mechanism, metal dihydride intermediates are formed through alkoxide formation and β-elimination. Insertion of the ketonic substrate, followed by reductive elimination produces the product. The metal dihydride complex is regenerated *via* oxidative addition on the hydrogen donor followed by β-elimination. These two mechanisms can be differentiated experimentally by using optically active deuteurated alcohol for racemisation.[29, 30]

The monohydride route occurs in the inner sphere mechanism, whereby the substrate coordinates to the metal centre of the catalyst precursor during the reaction. Another pathway that has been suggested for metal catalysts that operate through the monohydride route is the outer sphere mechanism, in which the substrate does not coordinate to the metal centre. The outer sphere mechanism can either proceed in a concerted manner, or in stepwise mechanism.

Noyori *et al*. have proposed the concerted outer sphere mechanism for the ruthenium complex, Ru[II]-TsDPEN, as catalyst for asymmetric transfer hydrogenation of ketones (**Scheme 8.8**).[14, 31] The base present in the reaction eliminates HCl from the Ru catalyst precursor, generating the 16-electron active species. The hydride and a proton from the hydrogen donor are transferred in a concerted manner to the ligand and metal of Ru intermediate respectively, giving an 18-electron Ru hydride species. The Ru hydride species then transfer the proton and hydride to the substrate forming a cyclic six-membered transition state to give the alcohol product.
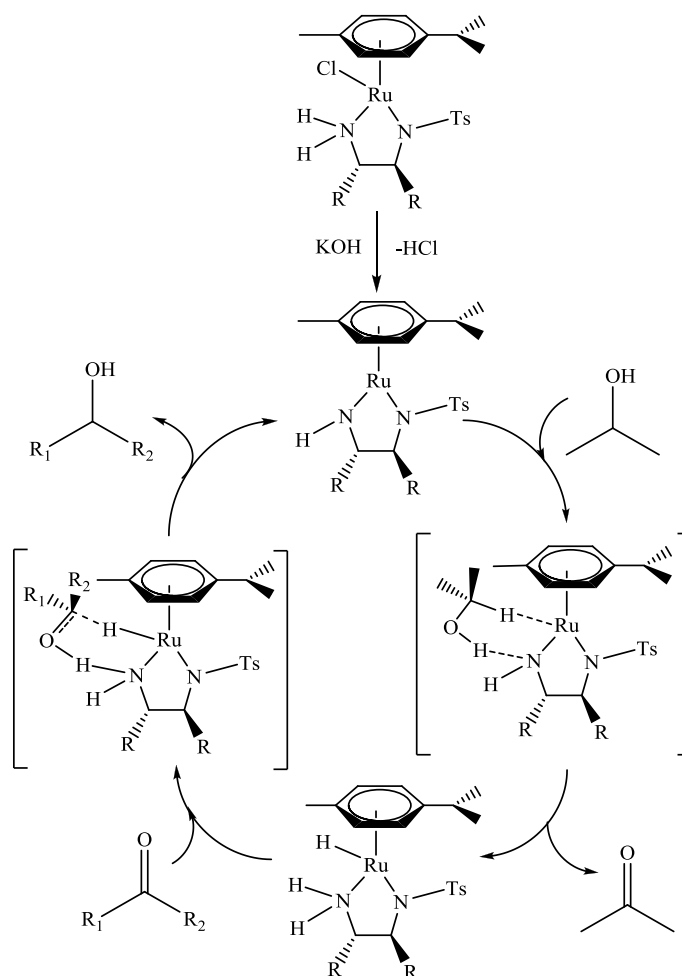
Scheme 8.8 *The concerted outer sphere mechanism for Noyori's Ru catalyst*[14, 31]
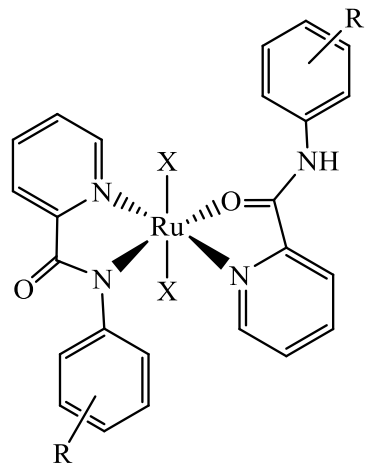
The function of the amine group in the ligand of the Ru catalyst plays a very important role to deliver the hydroxyl proton from the hydrogen donor to the substrate. This type of catalyst is termed "metal-ligand bifunctional catalysts", in which one of the sites of the ligands acts as a basic centre and forms a hydrogen bond interaction with the substrate to facilitate the transfer of hydrogen in the reaction.[32]

8.5   Catalytic Studies of *bis*-Picolinamide Metal Dihalide Complexes

Several *bis*-picolinamide metal dihalide complexes ($MX_2(L-R_2)$) with the general structure as shown in **Figure 8.4** were selected to study for their application as catalysts for the reduction of benzaldehyde. These complexes are interesting as the ligands can be easily functionalised giving advantages towards investigating structural-activity relationships. Their catalytic activities were studied based on the complexes having different metal centres (M = Ru or Rh), different halides (X = Cl

or I), and different R substituents attached at different positions on the phenyl ring of the picolinamide ligands. Previous studies have shown that the presence of leaving groups, hydrogen donor atoms, and having NH functionality in the ligand close to the metal centre can improve the catalytic activity of the whole complex.[16-19]

Complex	M	X	R
3.4	Ru	Cl	2',4'-F
3.9	Ru	Cl	2',4'-Cl
4.1	Ru	I	H
4.4	Ru	I	2',4'-F
4.7	Ru	I	3'-Cl
4.9	Ru	I	2',4'-Cl
4.12	Ru	I	3'-Br
5.2	Rh	Cl	3'-Cl
5.3	Rh	Cl	3'-Br
5.5	Rh	I	3'-Cl
5.6	Rh	I	3'-Br

Figure 8.4 Bis-picolinamide metal dihalide complexes as catalysts

The reaction procedure for the reduction of benzaldehyde is as shown in **Scheme 8.9**. This catalytic experiment is used as the first step towards exploring the relationship between structure and catalytic activities of *bis*-picolinamide metal dihalide complexes. Isopropanol acts as the hydrogen donor, and was used in excess as to avoid the reverse reaction. The conditions used were based on previous studies on Ru and Ir catalysts carried out within the McGowan group.[22, 23]
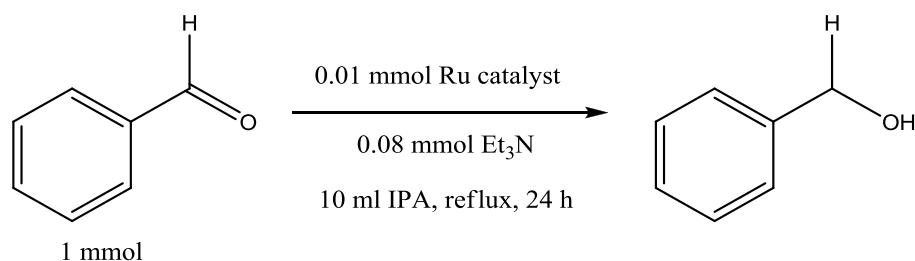
Scheme 8.9 Catalytic benzaldehyde reduction

8.5.1   Catalytic Activities of RuX$_2$(L-R)$_2$ Complexes

Ru complexes **3.4**, **3.9**, **4.4** and **4.9** were tested for their catalytic activity in the reduction of benzaldehyde using the conditions as shown in **Scheme 8.9**. The results are as shown in **Figure 8.5**, with RuCl$_3$.3H$_2$O as a comparison.
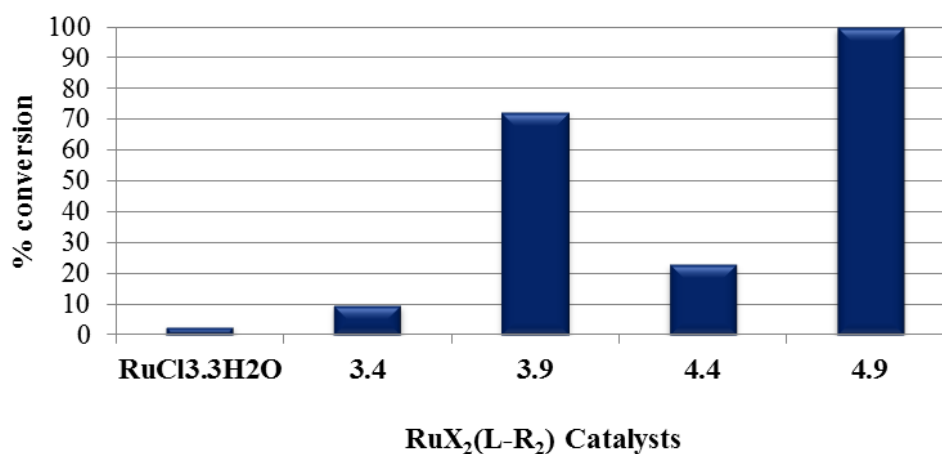
Figure 8.5 *Catalytic activities of RuX$_2$(L-R$_2$) complexes in benzaldehyde reduction*

RuCl$_3$.3H$_2$O is the starting material used in synthesising the catalysts, as described previously in Chapters 3 and 4. When comparing between the RuCl$_3$.3H$_2$O and RuX$_2$(L-R$_2$) complexes, the starting material showed the least activity within the series, with only 3% conversion after 24 h, suggesting that the picolinamide ligands play very important role in catalytic activity when coordinated to the Ru metal centre. The activity increases especially when the picolinamide ligands are functionalised with a chloride substituent on the *ortho* and *para* position on the phenyl ring of the picolinamide ligands, as shown by catalysts **3.9** and **4.9**, with conversions of 72% and 100% respectively. The high catalytic performance of catalyst **4.9** with 100% conversion, showing zero presence of the substrate from GC and NMR analysis after 24 h, also resulted from having an iodide substituent attached to the Ru metal centre. This shows that the choice of X ligand is essential in the reduction of benzaldehyde.

Moreover, with respect to a contrast in structural isomers, for which Ru diiodide complexes have shown a *trans* geometry, whereas Ru dichloride complexes showed a *cis* geometry with a mixture of few other structural isomers in solution.

These could indicate that a Ru complex with diiodide ligands, in addition of it being *trans* and that there is no mixture of isomers, is of importance in increasing the catalytic activities of the complex.

Figure 8.6 shows a different view to illustrate the catalytic effects of the Ru complexes with different combinations of X ligand and R substituent. It can be seen that there is a significant increase when the substituents are changed from 2',4'-difluoro to 2',4'-dichloro, as in comparison to the difference of reactivities based on their X ligands. This could specify that the functionalised picolinamide ligands play a large effect in the catalytic activity of the complex. Furthermore, when in combination with an iodide as the X ligand, the catalytic reactivity can be improved.
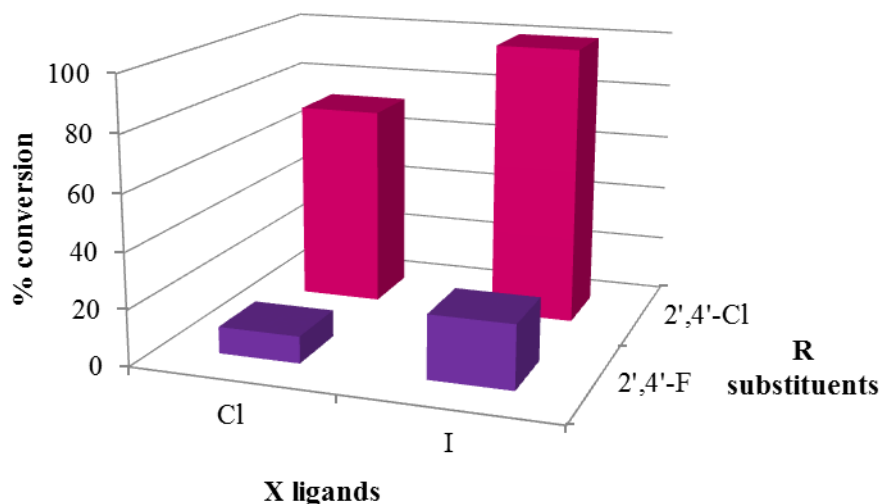
Figure 8.6 The catalytic effects of Ru complex with different combinations of X ligand and R substituent in benzaldehyde reduction

8.5.2 Catalytic Activity of $RuI_2(L\text{-}R)_2$ Complexes

The structural-catalytic activities of RuI_2L_2 complexes **4.1**, **4.4**, **4.7**, **4.9** and **4.12** were studied for catalytic transfer hydrogenation of benzaldehyde reduction in IPA following **Scheme 8.9**. The Ru complexes only differ through the functionalisations on the picolinamide ligands, specifically on the phenyl ring. **Figure 8.7** shows the catalytic activities of the selected RuI_2L_2 complexes. The results for catalysts **4.4** and **4.9** have been discussed in the previous section, but are also included in the figure for additional comparison within the series.
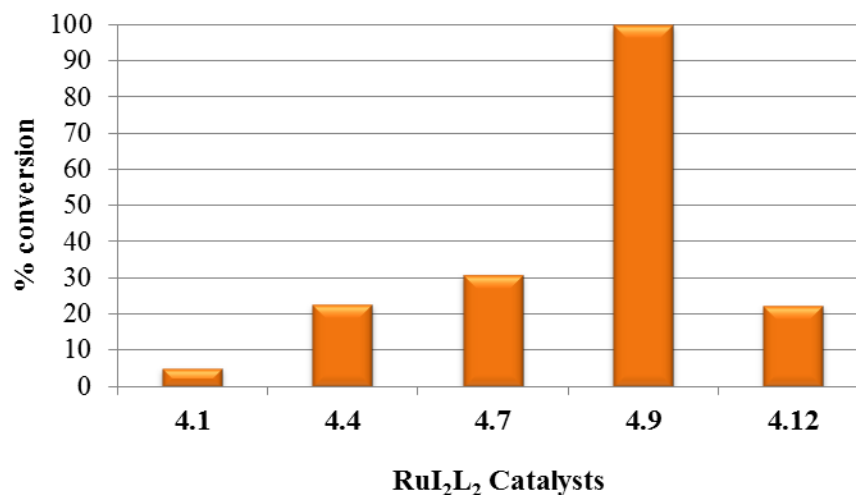
Figure 8.7 *Catalytic activities of RuI$_2$L$_2$ complexes in benzaldehyde reduction*

With the exception of catalyst **4.9**, all of the other complexes showed poor catalytic activity in reducing benzaldehyde within 24 hours. Catalyst **4.1**, with unfunctionalised picolinamide ligand, is the least active in the series with only 2% conversion. When an electron-withdrawing substituent is attached on the phenyl ring of the picolinamide ligands, their catalytic activities slightly increase. Catalyst **4.7** functionalised by *meta*-chloride, and catalyst **4.12** with *meta*-bromide gave a 31% and 22% benzaldehyde reduction, respectively. Catalyst **4.9** is the most active within the series with 100% conversion, giving the same result in repeated reactions. This could agree that the functionalised picolinamide ligands specifically on the *ortho* and *para* position may highly affect the catalytic activities for transfer hydrogenation in the reduction of benzaldehyde.

Catalysts **4.1**, **4.7** and **4.12** were also monitored for their catalytic reactions in benzaldehyde reduction, with their samples taken at 1h, 3h, 5h, 7h, 9h and 24h. Their results are as shown in**Figure 8.8**. Catalyst **4.7** starts up its catalytic activity after 3 hours in the reaction, from 7% conversion and slowly increases after every 2 hours until it reaches a 31% conversion at 24 h. The reactivity of catalyst **4.12** is slower and only starts to reduce benzaldehyde after 5 hours with 6% conversion and giving 22% conversion at 24 h, whereas catalyst **4.1**, with unsubstituted picolinamide ligands is the most inactive, with only 0 - 2 % conversion after 9 hours. These results have also been previously observed from within the McGowan group, of using Ir/Rh catalysts consisting of a picolinamide ligand with halide

substituents on the *meta* position of the phenyl ring.[23] The catalysts showed low activity, but have slightly improved with the *meta*-halide substituents on the picolinamide ligands, when compared to the unsubstituted catalyst.
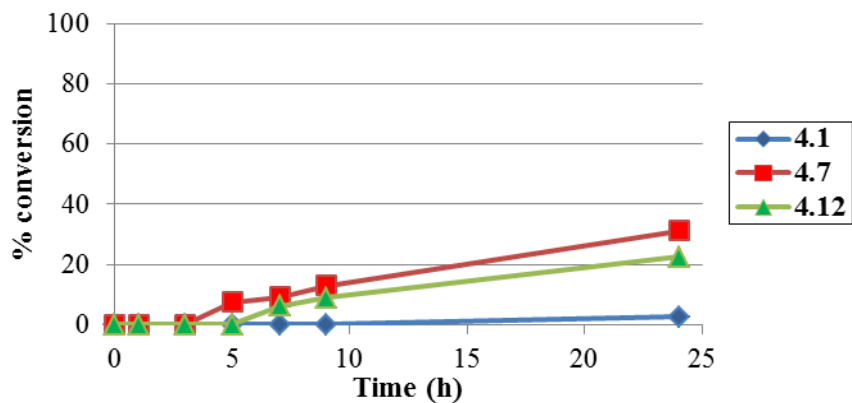
Figure 8.8 *Catalytic activities of RuI$_2$L$_2$ complexes in benzaldehyde reduction*

8.5.3 Catalytic Activities of RhX$_2$(L-R)$_2$ Complexes

A series of RhX$_2$(L-R)$_2$ complexes with different X ligand and functionalisation of the picolinamide ligands were investigated as catalysts in the reduction of benzaldehyde *via* transfer hydrogenation reactions using the reaction procedure as in **Scheme 8.9**. The catalytic activities of the few selected RhX$_2$(L-R)$_2$ complexes are as shown in **Figure 8.9**, along with RhCl$_3$.3H$_2$O as comparison, which was used as the starting material to prepare a series of the Rh complexes, described previously in Chapter 5.
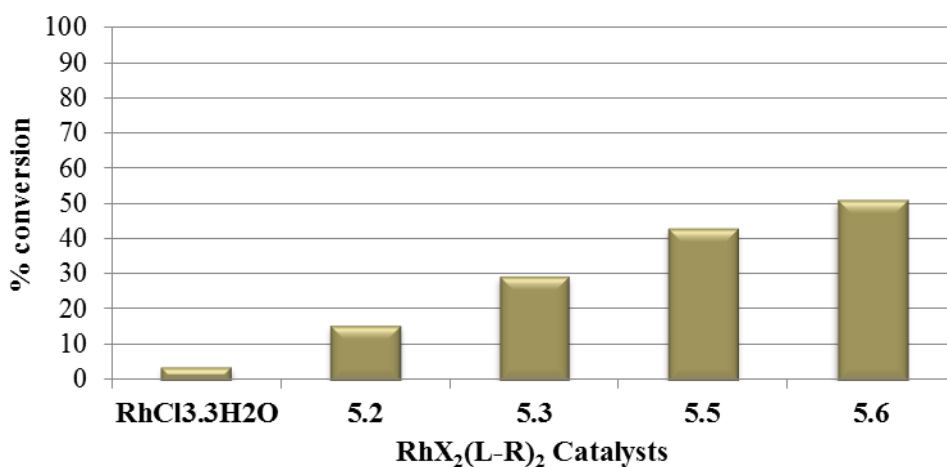
Figure 8.9 *Catalytic activities of RhX$_2$(L-R)$_2$ complexes in benzaldehyde reduction*

RhCl$_3$.3H$_2$O has the lowest catalytic activity giving only 3% benzaldehyde conversion according to the GC and NMR analysis of the samples after 24 hours. Their activities are slightly improved when picolinamide ligands are coordinated to the Rh metal centre. In general, the *bis*-picolinamide rhodium dihalide complexes have shown moderate catalytic activities with the overall range between 15-50%. Interestingly, a trend can be seen as both the X ligand and the R substituents on the functionalised picolinamide ligands increase in electron withdrawing. Their catalytic activity increases following the X/R substituents in the order of **5.2** (Cl/3'-Cl) < **5.3** (Cl/3'Br) < **5.5** (I/3'-Cl) < **5.6** (I/3'-Br). **Figure 8.10** shows the effects of the Rh complexes as catalysts in reduction of benzaldehyde, when combining the different X ligands and R substituents. When the X ligands are changed from chloride to iodide, their catalytic performance increases from 15% to 42% for RhX$_2$(L-3'Cl)$_2$ catalysts, and 28% to 50% for RhX$_2$(L-3'Br)$_2$ catalysts. These results could indicate that the X ligands may be the most important factor in their catalytic reactivities. Also, in addition to Rh diiodide complexes having only one geometry showing a *trans*, increases the catalytic activity, with contrast to Rh dichloride complexes consisting of *cis* structure as the major isomer and a mixture of few structural isomers in solution.
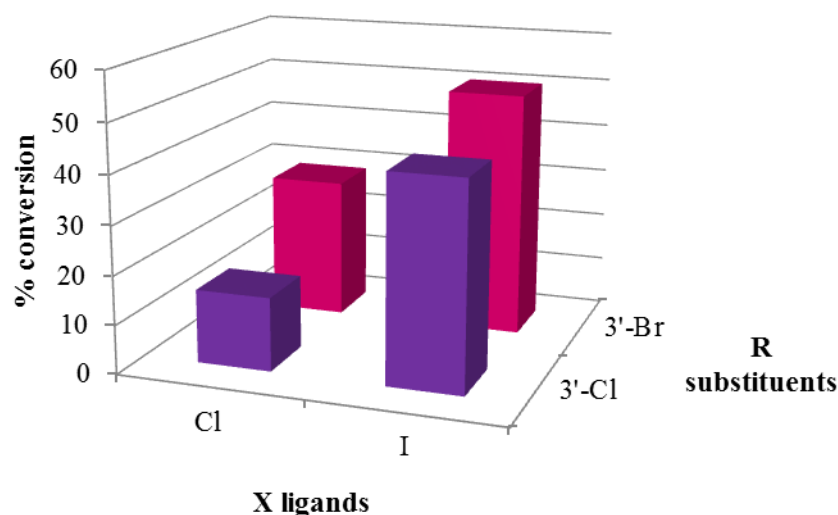
Figure 8.10 *The catalytic effects of Rh complex with different combinations of X ligand and R substituent in benzaldehyde reduction*

8.5.4   Catalytic Activities of MI$_2$(L-R)$_2$ Complexes

In order to gain structural-activity relationship for catalytic activities of *bis*-picolinamide metal dihalide complexes, four selected complexes were used to test for catalytic transfer hydrogenation in the reduction of benzaldehyde. These complexes vary in their metal centre (M = Ru or Rh) and the R substituents of the picolinamide ligands (R = 3'-Cl or 3'-Br) for comparison on their reactivities. **Figure 8.11** shows the results of complexes **4.7**, **4.12**, **5.5** and **5.6** from the catalytic reactions of benzaldehyde reduction.
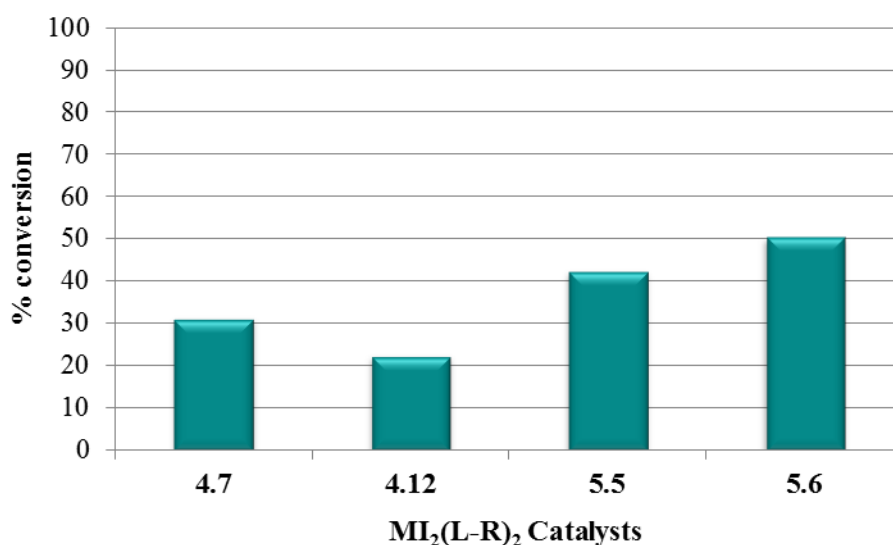
Figure 8.11 *Catalytic activities of MI$_2$(L-R)$_2$ complexes in benzaldehyde reduction*

Rh catalysts **5.5** and **5.6** can be seen to have a higher catalytic activity than the Ru catalysts **4.7** and **4.12**. The percentage conversion for Rh catalysts **5.5** and **5.6** is 42% and 50% respectively, and for Ru catalysts **4.7** and **4.12** is 31% and 22% respectively. Interestingly, there is a contrasting catalytic activity between the two groups of metal catalyst, when comparing it along with the different functionalised picolinamide ligands. For Ru catalysts, there is a decrease in catalytic activity when changing the R substituent from 3'-Cl (catalyst **4.7**) to 3'-Br (catalyst **4.12**), whereas for Rh catalysts, the activity increases from 3'Cl (catalyst **5.5**) to 3'-Br (catalyst **5.6**). These observations have showed that the choices of metals and functionalised picolinamide ligands can be used to finely tune the reactivity of *bis*-picolinamide metal dihalide catalysts in benzaldehyde reduction.

8.6 References

1. R. A. Sheldon, I. Arends and U. Hanefeld, *Green Chemistry and Catalysis*, Wiley-VCH, Weinheim, Germany, 2007.

2. H. Matsunaga, T. Ishizuka and T. Kunieda, *Tetrahedron Lett.*, 2005, **46**, 3645-3648.

3. F. K. Cheung, C. Lin, F. Minissi, A. L. Crivillé, M. A. Graham, D. J. Fox and M. Wills, *Org. Lett.*, 2007, **9**, 4659-4662.

4. W. Bonrath, J. Medlock, J. Schütz, B. Wüstenberg and T. Netscher, *Hydrogenation in the Vitamins and Fine Chemicals Industry – An Overview*, InTech, 2012.

5. T. Ohkuma, H. Ooka, T. Ikariya and R. Noyori, *J. Am. Chem. Soc.*, 1995, **117**, 10417-10418.

6. F. D. Klingler, *Acc. Chem. Res.*, 2007, **40**, 1367-1376.

7. T. Ohkuma, *Proc. Jpn. Acad. B, Phys. Biol. Sci.*, 2010, **86**, 202-219.

8. R. Noyori and T. Ohkuma, *Angew. Chem. Int. Ed.*, 2001, **40**, 40-73.

9. A. J. Blacker and P. Thompson, in *Asymmetric Catalysis on Industrial Scale*, Wiley-VCH Verlag GmbH & Co. KGaA, 2010, pp. 265-290.

10. R. V. Oppenauer, *Recl. Trav. Chim. Pays-Bas*, 1937, **56**, 137-144.

11. R. Uson, L. A. Oro, R. Sariego and M. A. Esteruelas, *J. Organomet. Chem.*, 1981, **214**, 399-404.

12. D. Morton and D. J. Cole-Hamilton, *J. Chem. Soc., Chem. Commun.*, 1988, 1154-1156.

13. R. L. Chowdhury and J.-E. Backvall, *J. Chem. Soc., Chem. Commun.,* 1991, 1063-1064.

14. S. Hashiguchi, A. Fujii, J. Takehara, T. Ikariya and R. Noyori, *J. Am. Chem. Soc.*, 1995, **117**, 7562-7563.

15. J. Takehara, S. Hashiguchi, A. Fujii, S.-i. Inoue, T. Ikariya and R. Noyori, *Chem. Commun.*, 1996, 233-234.

16. I. Yamada and R. Noyori, *Org.Lett.*, 2000, **2**, 3425-3427.

17. L. Taghizadeh Ghoochany, C. Kerner, S. Farsadpour, F. Menges, Y. Sun, G. Niedner-Schatteburg and W. R. Thiel, *Eur. J. Inorg. Chem.,* 2013, **2013**, 4305-4317.

18. R. K. Rath, M. Nethaji and A. R. Chakravarty, *Polyhedron*, 2001, **20**, 2735-2739.

19.   W. Baratta, J. Schütz, E. Herdtweck, W. A. Herrmann and P. Rigo, *J. Organomet. Chem.*, 2005, **690**, 5570-5575.

20.   M. Yamakawa, H. Ito and R. Noyori, *J. Am. Chem. Soc.,* 2000, **122**, 1466-1478.

21.   K. Abdur-Rashid, S. E. Clapham, A. Hadzovic, J. N. Harvey, A. J. Lough and R. H. Morris, *J. Am. Chem. Soc.*, 2002, **124**, 15104-15118.

22.   A. Rodríguez-Bárzano, Ph.D Thesis, University of Leeds, 2013.

23.   S. J. Lucas, Ph.D Thesis, University of Leeds, 2013.

24.   J. S. M. Samec, J.-E. Backvall, P. G. Andersson and P. Brandt, *Chem. Soc. Rev.*, 2006, **35**, 237-248.

25.   H. Meerwein and R. Schmidt, *Justus Liebigs Ann. Chem.*, 1925, **444**, 221-238.

26.   W. Ponndorf, *Angew. Chem. Int. Ed.*, 1926, **39**, 138-143.

27.   A. Verley, *Bull. Soc. Chim. Fr.*, 1925, **37**, 537-871.

28.   A. Aranyos, G. Csjernyik, K. J. Szabo and J.-E. Backvall, *Chem. Commun.*, 1999, 351-352.

29.   O. Pàmies and J.-E. Bäckvall, *Chem. Eur. J.*, 2001, **7**, 5052-5058.

30.   Y. R. S. Laxmi and J.-E. Backvall, *Chem. Commun.*, 2000, 611-612.

31.   K.-J. Haack, S. Hashiguchi, A. Fujii, T. Ikariya and R. Noyori, *Angew. Chem. Int. Ed.*, 1997, **36**, 285-288.

32.   R. Noyori, M. Yamakawa and S. Hashiguchi, *J. Org. Chem.*, 2001, **66**, 7931-7944.

CHAPTER 9

Experimental Details

9   Experimental Details

9.1   General Experimental Procedures

All ligands and complexes are air stable, and all reactions were carried out in air. All chemicals were obtained from Sigma-Aldrich Chemical Co, Acros Organics, Alfa Aesar and Strem Chemical Co. and were all used as supplied. Deuterated NMR solvents were purchased from Sigma-Aldrich Chemical Co. or Acros Organics.

9.2   Instrumentation

All NMR spectra were recorded either by the author on a Bruker DPX 300 or DRX 500 spectrometer, or by Mr. Simon Barrett on a Bruker DRX 500 spectrometer. Elemental analyses were acquired by Mr. Ian Blakeley or Ms. Tanya Marinko-Covell at the University of Leeds Microanalytical Service. Mass Spectra were recorded either by the author on a Bruker maXis impact mass spectrometer or by Ms. Tanya Marinko-Covell on a Micromass ZMD spectrometer with electrospray ionisation and photoiodide array analyser at the University of Leeds Mass Spectrometry Service. Infrared spectra were obtained using a Platinum ATR Spectrometer on a crystal plate with samples analysed using OPUS software.[1] Magnetic susceptibilities were measured using a Sherwood Scientific Susceptibility at room temperature. UV-Vis absorption spectra were recorded on a Cary Series UV-Vis Spectrophotometer using 1 cm path length quartz cuvettes and a Cary temperature controller. The spectra were processed using Cary WinUV software[2] for Windows 7. Gas chromatography analyses were obtained by the author on a Bruker 430-GC System using a Bruker GC capillary column with a length of 30 m, a diameter of 0.25 mm and a film thickness of 0.25 μm.

9.3   X-Ray Crystallography

Single crystal X-ray diffraction data were collected either by the author, Mr. Felix Janeway, Dr. Andrea Rodríguez-Bárzano, Dr. Stephanie Lucas or Dr. Helena Shepherd. A suitable single crystal was selected and immersed in an inert oil. The crystal was then mounted on a glass capillary and attached to a goniometer head on a Bruker X8 Apex diffractometer or Agilent SuperNova X-ray diffractometer fitted with an Atlas area detector and a kappa-geometry 4-circle goniometer, using graphite

monochromated Mo-Kα radiation (λ = 0.71073 Å) using 1.0° φ-rotation frames. The crystal was cooled to 100-120 K by an Oxford cryostream low temperature device.[3] The full data set was recorded and the images processed using DENZO and SCALEPACK programs on the Bruker diffractometer, and CrysAlis on the SuperNova.[4] The structures were solved either by the author, Mr. Felix Janeway, Dr. Marc Little, Dr. Christopher Pask, or Dr. Helena Shepherd.

Structure solution by direct method was achieved through the use of SHELXS86,[5] SIR92[6] or SIR97[7] programs and the structural model defined by full matrix least squares on F^2 using SHELX97.[8] Molecular graphics were plotted using POV-Ray[9] *via* the XSeed[9] program. Editing of CIFs and construction of tables and bond lengths and angles was achieved using WC[10] and PLATON,[11] or Olex2 program.[12] Unless otherwise stated, hydrogen atoms were placed using idealised geometric positions (with free rotation for methyl groups), allowed to move in a "riding model" along with the atoms to which they are attached, and refined isotropically. SQUEEZE[13] routine was used to remove disordered solvent molecules present in complex **3.7** and **3.12**.

9.4   X-Ray Powder Diffraction

X-Ray powder diffraction data were collected and processed by the author and Dr. Christopher Pask, on a Bruker AXS D2Phaser Diffractometer. Powdered samples were mounted on a silicon wafer by evenly distributing the powder over the wafer. All samples were rotated during data collection to ensure more homogeneous (i.e. isotropic) diffraction patterns. Data collection was carried out at room temperature, using Cu Kα radiation (λ = 1.54184 Å). Diffraction patterns were recorded in step-scan mode with a step size of (2θ) 0.7°, from (2θ) 5° to 50° (5 or 30 secs per step) using a 0.1 or 0.6mm divergent slit. Samples showed no significant evidence of degradation within the X-ray beam. The software packages Diffrac.Suite Eva[14] and Chekcell[15] were used to process the experimental powder X-ray diffraction data collected, and Mercury[16] was used to simulate the powder diffraction pattern of the single crystal structures.

9.5   Preparation of Arene Functionalised Picolinamide Ligands

The ligands used for complexes **3.1** - **3.10**, **3.16** and **4.1** - **4.10** have been previously reported,[17, 18] and were prepared using the same synthetic route, being a modification of the published procedure by Bhattacharya *et al*.[17] The yields varied in the range 37 - 69%, and characterisation data of new ligands used for complexes **3.11** - **3.15** and **4.11** - **4.15** are given in detail.

9.5.1   Pyridine-2-carboxylic acid (2-bromo-phenyl)-amide, $C_{12}H_9N_2OBr$ (2.11)

2-Bromoaniline (2.74 ml, 25 mmol) was added to a solution of pyridine-2-carboxylic acid (3.08 g, 25 mmol) in pyridine (15 ml) and warmed to 50°C for 15 minutes. To this mixture, triphenylphosphite (6.60 ml, 25 mmol) was added and heated to 110°C for 18 hours yielding an orange solution. Addition of water (100 ml) yielded a white paste. Dichloromethane (40 ml) was added to the solution and the organic layer separated from the aqueous layer. The product in the organic layer was extracted with 1:1 (v/v) aqueous HCl (3 x 100 ml). To neutralise the extract, sodium bicarbonate was added until pH 7 was reached. A brown solid was isolated by filtration then washed with distilled water. After recrystallisation of the product from methanol, washing with water and drying *in vacuo*, pale brown needle-like crystals were obtained.
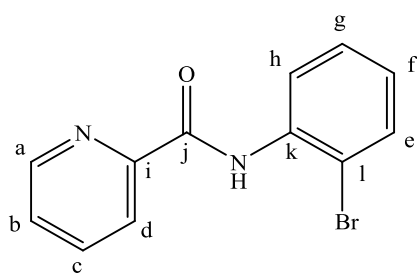
Yield: 3.48 g, 12.6 mmol, 50%. **ES+MS** (CHCl$_3$, m/z): 298.98 [M+Na$^+$]. **Analysis Calculated**: C 52.0%, H 3.3%, N 10.1%, Br 28.8%. **Analysis Found**: C 52.0%, H 3.2%, N 10.3%, Br 28.9%. **IR (cm^{-1})**: 3288 (m), 3105 (m), 1691 (s), 1577 (m), 1503 (m), 1462 (w), 1429 (w), 1375 (s), 1294 (s), 1227 (w), 1146 (w), 1119 (m), 1072 (s), 1038 (s), 997 (s), 890 (m), 857 (m), 822 (s), 748 (s), 682 (s), 621 (m), 540 (s). **^{1}H NMR** (CDCl$_3$, 300.13 MHz, 300K) δ 10.72 (br. s, 1H, NH), 8.70 (d, 1H, ^{3}J$_{(H-H)}$ = 4.7 Hz, H$_a$), 8.66 (dd, 1H, ^{3}J$_{(H-H)}$ = 8.3 Hz, ^{4}J$_{(H-H)}$ = 1.4 Hz CH of H$_d$), 8.32 (d, 1H, ^{3}J$_{(H-H)}$ = 7.8 Hz, CH of H$_h$), 7.94 (td, 1H, ^{3}J$_{(H-H)}$ = 7.7 Hz, ^{4}J$_{(H-H)}$ = 1.7, H$_c$), 7.62 (dd, 1H, ^{3}J$_{(H-H)}$ = 8 Hz, ^{4}J$_{(H-H)}$ = 1.3 Hz, H$_e$), 7.53 (ddd, 1H, ^{3}J$_{(H-H)}$ = 7.5 Hz, ^{4}J$_{(H-H)}$ = 4.8 Hz, ^{5}J$_{(H-H)}$ = 1.6 Hz, H$_b$), 7.40 (m, 1H, CH of H$_{g/f}$), 7.04 (td, 1H, ^{3}J$_{(H-H)}$ = 7.7 Hz, ^{4}J$_{(H-H)}$ = 1.5 Hz, H$_{g/f}$). **^{13}C{^{1}H} NMR** (CDCl$_3$, 75.47 MHz,

300 K) δ 162.28 (C=O), 149.78 (C_i), 148.33 (C_a), 137.64 (C_c), 135.94 (C_k), 132.49 (C_e), 128.37 (C_g), 126.62 (C_b), 125.13 (C_f), 122.43 (C_h), 121.41 (C_d), 113.90 (C-Br).

9.5.2 Pyridine-2-carboxylic acid (3-bromo-phenyl)-amide, $C_{12}H_9N_2OBr$ (2.12)

3-Bromoaniline (2.72 ml, 25 mmol) was added to a solution of pyridine-2-carboxylic acid (3.08 g, 25 mmol) in pyridine (15 ml) and warmed to 50°C for 15 minutes. To this mixture, triphenylphosphite (6.60 ml, 25 mmol) was added and heated to 110°C for 18 hours yielding an orange solution. Addition of water (100 ml) yielded a white paste. Dichloromethane (40 ml) was added to the solution and the organic layer separated from the aqueous layer. The product in the organic layer was extracted with 1:1 (v/v) aqueous HCl (3 x 100 ml). To neutralise the extract, sodium bicarbonate was added until pH 7 was reached. A brown solid was isolated by filtration then washed with distilled water. After recrystallisation of the product from methanol, washing with water and drying *in vacuo*, white needle-like crystals were obtained.

Yield: 3.90 g, 14.1 mmol, 56%. **ES+MS** (CHCl$_3$, m/z): 298.98 [M+Na$^+$]. **Analysis Calculated**: C 52.0%, H 3.3%, N 10.1%, Br 28.8%. **Analysis Found**: C 52.1%, H 3.2%, N 10.3%, Br 28.5%. **IR (cm^{-1})**: 3335 (s), 3058 (m), 1698 (s), 1590 (m), 1537 (m), 1483 (m), 1402 (m), 1314 (s), 1234 (s), 1160 (w), 1125 (m), 1092 (m), 1038 (m), 997 (s), 897 (m), 850 (s), 810 (m), 769 (s), 661 (s), 587 (s). **^{1}H NMR** (CDCl$_3$, 300.13 MHz, 300K) δ 10.06 (br. s, 1H, NH), 8.61 (d, 1H, $^3J_{(H-H)}$ = 3.6 Hz, H$_a$), 8.29 (d, 1H, $^3J_{(H-H)}$ = 7.8 Hz, H$_d$), 8.05 (s, 1H, H$_e$), 7.92 (t, 1H, $^3J_{(H-H)}$ = 7.6 Hz, H$_c$), 7.69 (d, 1H, $^3J_{(H-H)}$ = 7.7 Hz, H$_f$), 7.5 (dd, 1H, $^3J_{(H-H)}$ = 7.0 Hz, $^4J_{(H-H)}$ = 4.8 Hz, H$_b$), 7.25 (m, 2H, H$_{g/h}$). **^{13}C{^{1}H} NMR** (CDCl$_3$, 75.47 MHz, 300 K) δ 161.96 (C=O), 149.37 (C$_i$), 147.93 (C$_a$), 139.04 (C$_k$), 137.88 (C$_c$), 130.36 (C$_g$), 127.30 (C$_h$), 126.70 (C$_b$), 122.76 (C-Br), 122.61 (C$_{d/e}$), 118.15 (C$_f$).

9.5.3   Pyridine-2-carboxylic acid (4-bromo-phenyl)-amide, $C_{12}H_9N_2OBr$ (2.13)

4-Bromoaniline (4.30 g, 25 mmol) was added to a solution of pyridine-2-carboxylic acid (3.08 g, 25 mmol) in pyridine (15 ml) and warmed to 50°C for 15 minutes. To this mixture, triphenylphosphite (6.60 ml, 25 mmol) was added and heated to 110°C for 18 hours yielding an orange solution. Addition of water (100 ml) yielded a white paste. Dichloromethane (40 ml) was added to the solution and the organic layer separated from the aqueous layer. The product in the organic layer was extracted with 1:1 (v/v) aqueous HCl (3 x 100 ml). To neutralise the extract, sodium bicarbonate was added until pH 7 was reached. A brown solid was isolated by filtration then washed with distilled water. After recrystallisation of the product from methanol, washing with water and drying *in vacuo*, white crystals were obtained.
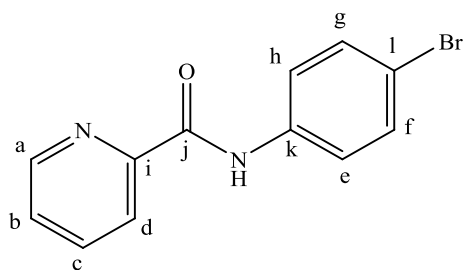
Yield: 4.78 g, 17.2 mmol, 69%. **ES+MS** (CHCl$_3$, m/z): 298.98 [M+Na$^+$]. **Analysis Calculated**: C 52.0%, H 3.3%, N 10.1%, Br 28.8%. **Analysis Found**: C 51.8%, H 3.2%, N 10.4%, Br 28.9%. **IR (cm^{-1})**: 3335 (s), 3058 (m), 1691 (w), 1590 (w), 1490 (w), 1227 (m), 1186 (w), 1099 (w), 1038 (w), 997 (m), 816 (m), 688 (m), 614 (s), 506 (s), 486 (m) **^{1}H NMR** (CDCl$_3$, 300.13 MHz, 300K) δ 10.06 (br. s, 1H, NH), 8.63 (d, 1H, $^3J_{(H\text{-}H)}$ = 4.7 Hz, H$_a$), 8.31 (d, 1H, $^3J_{(H\text{-}H)}$ = 7.8 Hz, H$_d$), 7.94 (td, 1H, $^3J_{(H\text{-}H)}$ = 7.7 Hz, $^4J_{(H\text{-}H)}$ = 1.7 Hz, H$_c$), 7.71 (d, 2H, $^3J_{(H\text{-}H)}$ = 8.8 Hz, H$_{e,h}$), 7.52 (m, 3H, H$_{b,g,f}$). **^{13}C{^{1}H} NMR** (CDCl$_3$, 75.47 MHz, 300 K) δ 161.99 (C=O), 149.51 (C$_i$), 147.98 (C$_a$), 137.79 (C$_c$), 136.85 (C$_k$), 132.06 (C$_{b/g/f}$), 126.63 (C$_{b/g/f}$), 122.47 (C$_d$), 121.21 (C$_{e,h}$) 116.87 (C-Br)

9.5.4   Pyridine-2-carboxylic acid (2,4-dibromo-phenyl)-amide, $C_{12}H_9N_2OBr_2$ (2.14)

2,4-dibromoaniline (6.27 g, 25 mmol) was added to a solution of pyridine-2-carboxylic acid (3.08 g, 25 mmol) in pyridine (15 ml) and warmed to 50°C for 15 minutes. To this mixture, triphenylphosphite (6.60 ml, 25 mmol) was added and heated to 110°C for 18 hours yielding an orange solution. Addition of water (100 ml) yielded a white paste. Dichloromethane (40 ml) was added to the solution and the organic layer separated

from the aqueous layer. The product in the organic layer was extracted with 1:1 (v/v) aqueous HCl (3 x 100 ml). To neutralise the extract, sodium bicarbonate was added until pH 7 was reached. A brown solid was isolated by filtration then washed with distilled water. After recrystallisation of the product from methanol, washing with water and drying *in vacuo*, white needle-like crystals were obtained.

Yield: 3.83 g, 10.8 mmol, 43%. **ES+MS** (CHCl$_3$, m/z): 378.9 [M+Na$^+$]. **Analysis Calculated**: C 40.5%, H 2.3%, N 7.9%, Br 44.9%. **Analysis Found**: C 40.6%, H 2.2%, N 7.7%, Br 44.7%. **IR (cm^{-1})**: 3288 (m), 3112 (m), 1691 (s), 1563 (m), 1509 (m), 1456 (w), 1381 (m), 1301 (s), 1234 (w), 1113 (m), 1078 (m), 1038 (s), 997 (m), 890 (m), 863 (m), 810 (s), 742 (m), 669 (s), 621 (m), 540 (m). **^{1}H NMR** (CDCl$_3$, 300.13 MHz, 300K) δ 10.63 (br. s, 1H, NH), 8.60 (d, 1H, $^3J_{(H-H)}$ = 4.7 Hz, H$_a$), 8.50 (d, 1H, $^3J_{(H-H)}$ = 8.9 Hz, H$_d$), 8.22 (d, 1H, $^3J_{(H-H)}$ = 7.8 Hz, H$_g$), 7.86 (td, 1H, $^3J_{(H-H)}$ = 7.7 Hz, $^4J_{(H-H)}$ = 1.7, H$_c$), 7.68 (d, 1H, $^3J_{(H-H)}$ = 2.3 Hz, H$_e$), 7.44 (m, CH of H$_{b,f}$). **^{13}C{^{1}H} NMR** (CDCl$_3$, 75.47 MHz, 300 K) δ 162.31 (C=O), 149.50 (C$_h$), 148.39 (C$_a$), 137.76 (C$_c$), 135.24 (C$_j$), 134.68 (C$_e$), 131.43 (C$_f$), 126.83 (C$_b$), 122.56 (C$_g$), 122.27 (C$_d$), 116.65 (C-Br), 114.28 (C-Br)

9.5.5   Pyridine-2-carboxylic acid (2,5-dibromo-phenyl)-amide, C$_{12}$H$_9$N$_2$OBr$_2$ (2.15)

2,5-dibromoaniline (6.27 g, 25 mmol) was added to a solution of pyridine-2-carboxylic acid (3.08 g, 25 mmol) in pyridine (15 ml) and warmed to 50°C for 15 minutes. To this mixture, triphenylphosphite (6.60 ml, 25 mmol) was added and heated to 110°C for 18 hours yielding an orange solution. Addition of water (100 ml) yielded a white paste. Dichloromethane (40 ml) was added to the solution and the organic layer separated from the aqueous layer. The product in the organic layer was extracted with 1:1 (v/v) aqueous HCl (3 x 100 ml). To neutralise the extract, sodium bicarbonate was added until pH 7 was reached. A brown solid was isolated by filtration then washed with distilled water. After recrystallisation of the product from methanol, washing with water and drying *in vacuo*, white needle-like crystals were obtained.

Yield: 3.26 g, 9.17 mmol, 37%. **ES+MS** (CHCl$_3$, m/z): 356.90 [M+H$^+$]. **Analysis Calculated**: C 40.5%, H 2.3%, N 7.9%, Br 44.9%. **Analysis Found**: C 40.6%, H 2.3%, N 7.7%, Br 44.8%. **IR (cm^{-1})**: 3301 (s), 3112 (s), 1698 (m), 1570 (m), 1516 (m), 1288 (m), 1227 (m), 1112 (m), 1018 (s), 870 (s), 803 (s), 742 (s), 675 (s), 580 (m), 500 (m). **^{1}H NMR** (CDCl$_3$, 300.13 MHz, 300K) δ 10.65 (br. s, 1H, NH), 8.82 (d, 1H, $^3J_{(H-H)}$ = 2.4 Hz, H$_g$), 8.61 (d, 1H, $^3J_{(H-H)}$ = 4.7 Hz, Ha), 8.22 (d, 1H, $^3J_{(H-H)}$ = 7.8 Hz, H$_d$), 7.86 (td, 1H, $^3J_{(H-H)}$ = 7.7 Hz, $^4J_{(H-H)}$ = 1.7, H$_c$), 7.45 (ddd, 1H, $^3J_{(H-H)}$ = 7.6 Hz, $^4J_{(H-H)}$ = 4.7 Hz, $^5J_{(H-H)}$ = 1.2 Hz, H$_b$), 7.38 (d, 1H, $^3J_{(H-H)}$ = 8.6 Hz, H$_e$), 7.08 (dd, $^3J_{(H-H)}$ = 8.5 Hz, $^4J_{(H-H)}$ = 2.4 Hz, 1H, H$_f$). **^{13}C{^{1}H} NMR** (CDCl$_3$, 75.47 MHz, 300 K) δ 162.31 (C=O), 149.38 (C$_h$), 148.38 (C$_a$), 137.76 (C$_c$), 137.05 (C$_j$), 133.36 (C$_e$), 128.00 (C$_f$), 126.87 (C$_b$), 124.01 (C$_g$), 122.58 (C$_d$), 121.25 (C-Br), 112.21 (C-Br).

9.6 Preparation of *Bis*-Picolinamide Ruthenium Dichloride Complexes

9.6.1 *Bis*(*N*-Ph-picolinamide) ruthenium dichloride, RuC$_{24}$H$_{19}$Cl$_2$N$_4$O$_2$ (3.1)

Ligand **2.1** (0.336 g, 1.70 mmol) was added to a solution of RuCl$_3$.3H$_2$O (0.215 g, 0.82 mmol) in ethanol (30 mL), followed by triethylamine (0.086 g, 0.85 mmol). The solution was heated under reflux for 2 hours giving a dark red-brown solution. On adding pentane, the complex precipitated as brick red-orange solid which was then filtered, washed with pentane and dried *in vacuo* and recrystallised *via* vapour diffusion in methanol-hexane giving red crystals.

Yield: 0.347 g, 0.60 mmol, 73%. **μ_{eff}** = 1.97 ± 0.12 μ_β. **ES+MS** (CH$_3$OH, m/z): 568.0 [M+H$^+$]. **Analysis Calculated**: C 46.4; H 4.1; N 9.0%. **Analysis found** (with 0.75 molecules of H$_2$O): C 46.9; H 3.60; N 8.9 %. **IR (cm^{-1})**: 3482 (b), 3260 (w), 3200 (m), 3058 (s), 1617 (b), 1570 (s), 1490 (b), 1449 (b), 1355 (s), 1294 (s), 1146 (s), 1025 (s), 997 (w), 971 (s), 897 (s), 836 (w), 803 (s), 748 (s), 688 (s), 587 (s), 506 (s)

9.6.2 *Bis*(*N*-2'-fluoro-Ph-picolinamide) ruthenium dichloride, $RuC_{24}H_{17}Cl_2N_4O_2F_2$ (3.2)

Ligand **2.2** (0.184 g, 0.85 mmol) was added to a solution of $RuCl_3.3H_2O$ (0.106 g, 0.40 mmol) in ethanol (30 mL), followed by triethylamine (0.046 g, 0.45 mmol). The solution was heated under reflux for 2 hours giving a red-brown solution. On adding pentane, the complex precipitated as orange solid which was then filtered, washed with pentane, dried *in vacuo* and recrystallised *via* vapour diffusion in methanol-pentane giving red-orange microcrystals.

Yield: 0.121 g, 0.20 mmol, 50%. $\mu_{eff} = 1.97 \pm 0.12 \ \mu_\beta$. **ES+MS** ($CH_3OH$, m/z): 604.0 [M+H⁺]. **Analysis Calculated**: C 45.1; H 3.3; N 8.8%. **Analysis found** (with 0.67 molecules of H_2O): C 45.1; H 3.3; N 8.6%. **IR (cm⁻¹)**: 3489 (b), 3200 (w), 3065 (m), 1617 (b), 1577 (s), 1496 (s), 1449 (w), 1355 (s), 1301 (s), 1267 (s), 1206 (s), 1153 (s), 1099 (s), 1031 (s), 964 (s), 917 (s), 863 (s), 755 (s), 682 (s), 601 (s), 547 (w), 519 (w), 473 (s)

9.6.3 *Bis*(*N*-4'-fluoro-Ph-picolinamide) ruthenium dichloride, $RuC_{24}H_{17}Cl_2N_4O_2F_2$ (3.3)

Ligand **2.3** (0.178 g, 0.82 mmol) was added to a solution of $RuCl_3.3H_2O$ (0.106 g, 0.41 mmol) in ethanol (30 mL), followed by triethylamine (0.038 g, 0.38 mmol). The solution was heated under reflux for 2 hours giving a dark red-brown solution. On adding pentane, the complex precipitated as brick orange solid which was then filtered, washed with pentane, dried *in vacuo* and recrystallised *via* vapour diffusion in methanol-pentane giving red crystals.

Yield: 0.126 g, 0.21 mmol, 51%. $\mu_{eff} = 1.83 \pm 0.03 \ \mu_\beta$. **ES+MS** ($CH_3OH$, m/z): 604.0 [M+H⁺]. **Analysis Calculated**: C 43.9; H 3.3; N 8.8%. **Analysis found** (with 0.75 molecules of H_2O): C 44.4; H 3.1; N 8.4%. **IR (cm⁻¹)**: 3510 (b), 3254 (w), 3220 (w), 3058 (m), 1624 (b), 1469 (w), 1409 (s), 1348 (s), 1294 (w), 1234 (s), 1153 (s), 1092 (w), 1058 (w), 1018 (w), 971 (w), 904 (s), 829 (s), 762 (w), 688 (s), 547 (w), 507 (w), 493 (w)

9.6.4 *Bis*(*N*-2',4'-difluoro-Ph-picolinamide) ruthenium dichloride, RuC$_{24}$H$_{15}$Cl$_2$N$_4$O$_2$F$_4$ (3.4)

Ligand **2.4** (0.187 g, 0.80 mmol) was added to a solution of RuCl$_3$.3H$_2$O (0.102 g, 0.39 mmol) in ethanol (30 mL), followed by triethylamine (0.040 g, 0.40 mmol). The solution was heated under reflux for 2 hours giving a red solution. On adding pentane, the complex precipitated as orange solid which was then filtered, washed with pentane, dried *in vacuo* and recrystallised *via* vapour diffusion in methanol-pentane giving red microcrystals.

Yield: 0.181 g, 0.28 mmol, 72%. $\boldsymbol{\mu}_{\text{eff}}$ = 1.87 ± 0.07 μ_β. **ES+MS** (CH$_3$OH, m/z): 640.0 [M+H$^+$]. **Analysis Calculated**: C 42.7; H 2.6; N 8.5%. **Analysis found** (with 0.67 molecules of H$_2$O): C 43.1; H 2.8; N 8.0%. **IR (cm^{-1})**: 3470 (b), 3220 (w), 3058 (m), 1611 (b), 1503 (w), 1469 (w), 1429 (w), 1355 (s), 1301 (w), 1260 (w), 1220 (m), 1139 (s), 1092 (s), 1052 (m), 1031 (m), 964 (s), 924 (m), 850 (m), 803 (m), 755 (m), 735 (w), 694 (s), 607 (m), 540 (m), 459 (m)

9.6.5 *Bis*(*N*-2',5'-difluoro-Ph-picolinamide) ruthenium dichloride, RuC$_{24}$H$_{15}$Cl$_2$N$_4$O$_2$F$_4$ (3.5)

Ligand **2.5** (0.184 g, 0.79 mmol) was added to a solution of RuCl$_3$.3H$_2$O (0.102 g, 0.39 mmol) in ethanol (30 mL), followed by triethylamine (0.038 g, 0.38 mmol). The solution was heated under reflux for 2 hours giving a red-orange solution. On adding pentane, the complex precipitated as orange solid which was then filtered, washed with pentane, dried *in vacuo* and recrystallised *via* vapour diffusion in methanol-pentane giving red crystals.

Yield: 0.070 g, 0.11 mmol, 28%. $\boldsymbol{\mu}_{\text{eff}}$ = 1.96 ± 0.16 μ_β. **ES+MS** (CH$_3$OH, m/z): 641.96 [M$^+$]. **Analysis Calculated**: C 42.7; H 2.8; N 8.3%. **Analysis found** (with 0.67 molecules of H$_2$O): C 43.1; H 3.1; N 8.2%. **IR (cm^{-1})**: 3482 (b), 3207 (w), 3065 (m), 1584 (b), 1496 (w), 1341 (m), 1241 (m), 1206 (w), 1173 (s), 1099 (s), 1058 (w), 978 (s), 924 (w), 870 (m), 762 (s), 688 (s), 587 (w), 506 (w), 473 (s).

9.6.6 *Bis*(*N*-2'-chloro-Ph-picolinamide) ruthenium dichloride, $RuC_{24}H_{17}Cl_4N_4O_2$ (3.6)

Ligand **2.6** (0.179 g, 0.77 mmol) was added to a solution of $RuCl_3.3H_2O$ (0.103 g, 0.39 mmol) in ethanol (30 mL), followed by triethylamine (0.040 g, 0.39 mmol). The solution was heated under reflux for 2 hours giving a dark red solution. On adding pentane, the complex precipitated as red-orange solid which was then filtered, washed with pentane, dried *in vacuo* and recrystallised *via* vapour diffusion in methanol-pentane giving red crystals.

Yield: 0.146 g, 0.23 mmol, 59%. μ_{eff} = 2.21 ± 0.07 μ_β. **ES+MS** (CH_3OH, m/z): 637.9 [M+H⁺]. **Analysis Calculated**: C 42.9; H 2.9; N 8.6; Cl 21.7%. **Analysis found** (with 0.67 molecules of H_2O): C 43.4; H 3.1; N 8.1; Cl 22.1%. **IR (cm⁻¹)**: 3476 (b), 3220 (w), 3065 (w), 2856 (w), 1590 (b), 1469 (w), 1442 (w), 1341 (m), 1301 (w), 1260 (w), 1146 (s), 1052 (s), 1031 (m), 964 (m), 924 (s), 850 (w), 803 (m), 755 (s), 688 (s), 601 (m), 500 (m), 452 (w)

9.6.7 *Bis*(*N*-3'-chloro-Ph-picolinamide) ruthenium dichloride, $RuC_{24}H_{17}Cl_4N_4O_2$ (3.7)

Ligand **2.7** (0.200 g, 0.86 mmol) was added to a solution of $RuCl_3.3H_2O$ (0.111 g, 0.42 mmol) in ethanol (30 mL), followed by triethylamine (0.043 g, 0.42 mmol). The solution was heated under reflux for 2 hours giving a dark red-brown solution. On adding pentane, the complex precipitated as orange solid which was then filtered, washed with pentane, dried *in vacuo* and recrystallised *via* vapour diffusion in methanol-hexane giving red crystals.

Yield: 0.149 g, 0.23 mmol, 55%. μ_{eff} = 2.40 ± 0.04 μ_β. **ES+MS** (CH_3OH, m/z): 637.9 [M+H⁺]. **Analysis Calculated**: C 44.1; H 2.9; N 8.6; Cl 21.7%. **Analysis found** (with 0.5 molecules of H_2O): C 44.0; H 3.2; N 8.3; Cl 21.5%. **IR (cm⁻¹)**: 3442 (b), 3254 (w), 3193 (w), 3065 (m), 1597 (b), 1476 (m), 1435 (w), 1391 (s), 1307 (m), 1260 (m), 1146 (m), 1065 (w), 965 (m), 883 (m), 762 (s), 675 (s), 594 (w), 513 (w)

9.6.8 *Bis*(*N*-4'-chloro-Ph-picolinamide) ruthenium dichloride,

$RuC_{24}H_{17}Cl_4N_4O_2$ (3.8)

Ligand **2.8** (0.191 g, 0.82 mmol) was added to a solution of $RuCl_3.3H_2O$ (0.103 g, 0.39 mmol) in ethanol (30 mL), followed by triethylamine (0.041 g, 0.41 mmol). The solution was heated under reflux for 2 hours giving a red-brown solution. On adding pentane, the complex precipitated as brick-orange solid which was then filtered, washed with pentane, dried *in vacuo* and recrystallised *via* vapour diffusion in methanol-pentane giving red microcrystals.

Yield: 0.070 g, 0.11 mmol, 28%. $\boldsymbol{\mu_{eff}}$ = 2.08 ± 0.03 μ_β. **ES+MS** (CH_3OH, m/z): 637.9 [M+H$^+$]. **Analysis Calculated**: C 42.9; H 2.9; N 8.6; Cl 21.7%. **Analysis found** (with 0.67 molecules of H_2O): C 43.2; H 3.0; N 8.1, Cl 21.8%. **IR (cm^{-1})**: 3496 (b), 3247 (w), 3058 (m), 1584 (b), 1490 (m), 1409 (m), 1355 (m), 1294 (m), 1260 (w), 1241 (w), 1146 (m), 1085 (s), 1052 (w), 1018 (s), 971 (m), 910 (m), 822 (s), 755 (s), 722 (m), 688 (s), 506 (s), 466 (w)

9.6.9 *Bis*(*N*-2',4'-dichloro-Ph-picolinamide) ruthenium dichloride,

$RuC_{24}H_{15}Cl_6N_4O_2$ (3.9)

Ligand **2.9** (0.217 g, 0.81 mmol) was added to a solution of $RuCl_3.3H_2O$ (0.104 g, 0.40 mmol) in ethanol (30 mL), followed by triethylamine (0.044 g, 0.43 mmol). The solution was heated under reflux for 2 hours giving a red-orange solution. On adding pentane, the complex precipitated as orange solid which was then filtered, washed with pentane, dried *in vacuo* and recrystallised *via* vapour diffusion in methanol-pentane giving red crystals.

Yield: 0.120 g, 0.17 mmol, 43%. $\boldsymbol{\mu_{eff}}$ = 1.99 ± 0.06 μ_β. **ES+MS** (CH_3OH, m/z): 705.8 [M+H$^+$]. **Analysis Calculated**: C 39.9; H 2.4; N 7.8; Cl 29.4%. **Analysis found** (with 0.5 molecules of H_2O): C 39.7; H 2.5; N 7.6, Cl 29.5%. **IR (cm^{-1})**: 3510 (b), 3207 (w), 3058 (m), 1590 (b), 1469 (m), 1341 (m), 1301 (w), 1260 (w), 1146 (m), 1099 (s), 1052 (s), 1025 (w), 964 (w), 917 (m), 857 (m), 803 (m), 762 (s), 688 (m), 560 (w), 526 (m)

9.6.10 *Bis*(*N*-2',5'-dichloro-Ph-picolinamide) ruthenium dichloride,

$RuC_{24}H_{15}Cl_6N_4O_2$ (3.10)

Ligand **2.10** (0.218 g, 0.82 mmol) was added to a solution of $RuCl_3.3H_2O$ (0.104 g, 0.40 mmol) in ethanol (30 mL), followed by triethylamine (0.044 g, 0.43 mmol). The solution was heated under reflux for 2 hours giving an orange solution. On adding pentane, the complex precipitated as red-orange solid which was then filtered, washed with pentane, dried *in vacuo* and recrystallised *via* vapour diffusion in methanol-pentane giving red microcrystals.

Yield: 0.113 g, 0.16 mmol, 40%. **μ$_{eff}$** = 2.53 ± 0.02 μ_β. **ES+MS** (CH$_3$OH, m/z): 705.8 [M+H$^+$]. **Analysis Calculated**: C 39.9; H 2.4; N 7.9; Cl 30.2%. **Analysis found** (with 0.5 molecules of H$_2$O): C 40.6; H 2.9; N 7.5, Cl 30.0%. **IR (cm^{-1})**: 3496 (b), 3200 (w), 3065 (w), 1577 (b), 1469 (m), 1388 (m), 1334 (m), 1301 (w), 1260 (w), 1139 (m), 1092 (m), 1052 (m), 964 (m), 931 (m), 890 (w), 863 (w), 803 (s), 762 (s), 688 (s), 594 (m), 566 (m), 519 (w), 459 (w)

9.6.11 *Bis*(*N*-2'-bromo-Ph-picolinamide) ruthenium dichloride,

$RuC_{24}H_{17}Cl_2Br_2N_4O_2$ (3.11)

Ligand **2.11** (0.217 g, 0.78 mmol) was added to a solution of $RuCl_3.3H_2O$ (0.102 g, 0.39 mmol) in ethanol (30 mL), followed by triethylamine (0.040 g, 0.39 mmol). The solution was heated under reflux for 2 hours giving a red-orange solution. On adding pentane, the complex precipitated as orange solid which was then filtered, washed with pentane, dried *in vacuo* and recrystallised *via* vapour diffusion in methanol-pentane giving red crystals.

Yield: 0.131 g, 0.18 mmol, 46%. **μ$_{eff}$** = 2.02 ± 0.06 μ_β. **ES+MS** (CH$_3$OH, m/z): 725.8 [M+H$^+$]. **Analysis Calculated**: C 37.9; H 2.8; N 7.4%. **Analysis found** (with 0.67 molecules of H$_2$O): C 37.6; H 2.6; N 7.1%. **IR (cm^{-1})**: 3496 (b), 3214 (m), 3065 (m), 1584 (s), 1476 (s), 1442 (w), 1348 (s), 1307 (s), 1260 (m), 1146 (m), 1052 (s), 971 (w), 924 (s), 843 (w), 810 (m), 748 (s), 688 (m), 594 (w), 533 (w), 493 (w)

9.6.12 *Bis*(*N*-3'-bromo-Ph-picolinamide) ruthenium dichloride,

$RuC_{24}H_{17}Cl_2Br_2N_4O_2$ (3.12)

Ligand **2.12** (0.229 g, 0.83 mmol) was added to a solution of $RuCl_3.3H_2O$ (0.106 g, 0.41 mmol) in ethanol (30 mL), followed by triethylamine (0.042 g, 0.41 mmol). The solution was heated under reflux for 2 hours giving a dark red-brown solution. On adding pentane, the complex precipitated as brick-orange solid which was then filtered, washed with pentane, dried *in vacuo* and recrystallised *via* vapour diffusion in methanol-pentane giving red crystals.

Yield: 0.186 g, 0.25 mmol, 61%. $\mathbf{\mu_{eff}} = 2.05 \pm 0.10 \; \mu_\beta$. **ES+MS** ($CH_3OH$, m/z): 725.8 [M+H$^+$]. **Analysis Calculated**: C 38.8; H 2.6; N 7.5%. **Analysis found** (with 0.5 molecules of H_2O): C 38.9; H 2.8; N 7.4%. **IR (cm^{-1})**: 3489 (b), 3254 (w), 3072 (m), 1570 (b), 1476 (s), 1429 (w), 1348 (s), 1294 (m), 1260 (m), 1146 (m), 1065 (w), 997 (w), 971 (m), 857 (m), 762 (s), 722 (w), 675 (s), 601 (w), 560 (w), 500 (w)

9.6.13 *Bis*(*N*-4'-bromo-Ph-picolinamide) ruthenium dichloride,

$RuC_{24}H_{17}Cl_2Br_2N_4O_2$ (3.13)

Ligand **2.13** (0.228 g, 0.82 mmol) was added to a solution of $RuCl_3.3H_2O$ (0.106 g, 0.40 mmol) in ethanol (30 mL), followed by triethylamine (0.042 g, 0.41 mmol). The solution was heated under reflux for 2 hours giving a dark red solution. On adding pentane, the complex precipitated as brick-orange solid which was then filtered, washed with pentane, dried *in vacuo* and recrystallised *via* vapour diffusion in methanol-pentane giving red crystals.

Yield: 0.126 g, 0.17 mmol, 43%. $\mathbf{\mu_{eff}} = 2.04 \pm 0.16 \; \mu_\beta$. **ES+MS** ($CH_3OH$, m/z): 725.8 [M+H$^+$]. **Analysis Calculated**: C 38.8; H 2.6; N 7.5%. **Analysis found** (with 0.5 molecules of H_2O): C 38.9; H 2.8; N 7.4%. **IR (cm^{-1})**: 3482 (b), 3247 (w), 3072 (m), 1570 (b), 1490 (m), 1402 (w), 1348 (m), 1288 (m), 1260 (w), 1146 (m), 1065 (m), 1025 (w), 1004 (s), 964 (w), 910 (w), 822 (s) 755 (s), 688 (s), 513 (s)

9.6.14 *Bis*(*N*-2',4'-dibromo-Ph-picolinamide) ruthenium dichloride,

$RuC_{24}H_{15}Cl_2Br_4N_4O_2$ (3.14)

Ligand **2.14** (0.291 g, 0.82 mmol) was added to a solution of $RuCl_3.3H_2O$ (0.106 g, 0.41 mmol) in ethanol (30 mL), followed by triethylamine (0.041 g, 0.41 mmol). The solution was heated under reflux for 2 hours giving a dark red-brown solution. On adding pentane, the complex precipitated as bright orange solid which was then filtered, washed with pentane, dried *in vacuo* and recrystallised *via* vapour diffusion in methanol-pentane giving red crystals.

Yield: 0.186 g, 0.21 mmol, 51%. **μ$_{eff}$** = 2.10 ± 0.14 μ_β. **ES+MS** (CH_3OH, m/z): 882.6 [M$^+$]. **Analysis Calculated**: C 32.0; H 1.9; N 6.2%. **Analysis found** (with 0.5 molecules of H_2O): C 31.8; H 2.1; N 5.9%. **IR (cm^{-1})**: 3496 (b), 3200 (w), 3065 (m), 1584 (b), 1462 (m), 1341 (m), 1301 (m), 1260 (m), 1146 (s), 1072 (s), 1045 (s), 964 (w), 917 (s), 850 (w), 816 (w), 748 (m), 682 (m), 547 (w), 506 (m)

9.6.15 *Bis*(*N*-2',5'-dibromo-Ph-picolinamide) ruthenium dichloride,

$RuC_{24}H_{15}Cl_2Br_4N_4O_2$ (3.15)

Ligand **2.15** (0.281 g, 0.79 mmol) was added to a solution of $RuCl_3.3H_2O$ (0.103 g, 0.39 mmol) in ethanol (30 mL), followed by triethylamine (0.040 g, 0.39 mmol). The solution was heated under reflux for 2 hours giving a red solution. On adding pentane, the complex precipitated as orange solid which was then filtered, washed with pentane, dried *in vacuo* and recrystallised *via* vapour diffusion in methanol-pentane giving red microcrystals.

Yield: 0.192 g, 0.21 mmol, 54%. **μ$_{eff}$** = 2.03 ± 0.02 μ_β. **ES+MS** (CH_3OH, m/z): 882.6 [M$^+$]. **Analysis Calculated**: C 32.0; H 1.9; N 6.2%. **Analysis found** (with 0.5 molecules of H_2O): C 31.8; H 2.2; N 5.9%. **IR (cm^{-1})**: 3510 (b), 3186 (w), 3065 (m), 1584 (b), 1469 (m), 1388 (m), 1334 (m), 1301 (w), 1267 (w), 1146 (s), 1085 (s), 1031 (s), 971 (m), 931 (m), 870 (m), 810 (m), 755 (s), 694 (s), 601 (w), 566 (w), 506 (m)

9.6.16 *Bis*(*N*-2'-iodo-Ph-picolinamide) ruthenium dichloride,

$RuC_{24}H_{17}Cl_2I_2N_4O_2$ (3.16)

Ligand **2.16** (0.224 g, 0.81 mmol) was added to a solution of $RuCl_3.3H_2O$ (0.101 g, 0.38 mmol) in ethanol (30 mL), followed by triethylamine (0.040 g, 0.40 mmol). The solution was heated under reflux for 2 hours giving a dark red solution. On adding pentane, the complex precipitated as brick yellow solid which was then filtered, washed with pentane, dried *in vacuo* and recrystallised *via* vapour diffusion in methanol-pentane giving a mixture of red and orange crystals.

Yield: 0.091 g, 0.13 mmol, 34%. **μ_{eff}** $_=$ 2.01 ± 0.01 μ_β. **ES+MS** (CH_3OH, m/z): 819.79 [M^+]. **Analysis Calculated**: C 33.7; H 2.5; N 6.6%. **Analysis found** (with 0.67 molecules of H_2O): C 33.3; H 2.2; N 6.2%. **IR (cm^{-1})**: 3476 (b), 3200 (w), 3051 (m), 1590 (s), 1556 (s), 1469 (s), 1435 (w), 1341 (m), 1301 (m), 1146 (m), 1018 (m), 917 (m), 803 (w), 748 (s), 722 (w), 682 (m), 647 (m), 594 (m), 526 (w), 500(m)

9.7   Preparation of *Bis*-picolinamide Ruthenium Diiodide Complexes

9.7.1   *Bis*(*N*-Ph-picolinamide) ruthenium diiodide, $RuC_{24}H_{19}I_2N_4O_2$ (4.1)

Ligand **2.1** (0.241 g, 1.21 mmol) was added to a solution of $RuCl_3.3H_2O$ (0.156 g, 0.60 mmol) in ethanol (30 mL), followed by triethylamine (0.061 g, 0.60 mmol). The solution was heated under reflux for 2 hours giving a dark red-brown solution. An excess of potassium iodide (1.014 g, 6.11 mmol) was then added and heated under reflux for another 18 hours. The precipitate was filtered, washed with ethanol and water, dried *in vacuo* and recrystallised *via* vapour diffusion in dimethylformamide-diethyl ether giving dark coloured microcrystals.

Yield: 0.260 g, 0.35 mmol, 58%. **μ_{eff}** = 1.68 ± 0.07 μ_β. **ES+MS** (DMF, m/z): 751.9 [$M+H^+$]. **Analysis Calculated**: C 39.2; H 3.2; N 7.0%. **Analysis found** (with 0.5 molecules of C_2H_6O): C 39.8; H 2.7; N 7.3%. **IR (cm^{-1})**: 3032 (b), 2937 (w), 2836 (b), 1556 (s), 1544 (s), 1490 (m), 1381 (m), 1355 (m), 1301 (m), 1260 (m), 1173 (w), 1146 (m), 1018 (w), 964 (w), 931 (m), 903 (m), 843 (w), 803 (w), 755 (s), 688 (s), 594 (m), 513 (m), 486 (s), 459 (m)

9.7.2 *Bis*(*N*-2'-fluoro-Ph-picolinamide) ruthenium diiodide, $RuC_{24}H_{17}I_2F_2N_4O_2$ (4.2)

Ligand **2.2** (0.275 g, 1.27 mmol) was added to a solution of $RuCl_3.3H_2O$ (0.164 g, 0.63 mmol) in ethanol (30 mL), followed by triethylamine (0.061 g, 0.60 mmol). The solution was heated under reflux for 2 hours giving a red-brown solution. An excess of potassium iodide (1.058 g, 6.37 mmol) was added to the solution and heated again under reflux for 18 hours. The solid was filtered, washed with ethanol and water, dried *in vacuo* and recrystallised *via* vapour diffusion in dimethylformamide-diethyl ether giving dark coloured crystals.

Yield: 0.289 g, 0.37 mmol, 58%. μ_{eff} = 1.71 ± 0.07 μ_β. **ES+MS** (DMF, m/z): 787.9 [M+H$^+$]. **Analysis Calculated**: C 36.7; H 2.2; N 7.1%. **Analysis found**: C 36.7; H 2.2; N 7.1%. **IR (cm^{-1})**: 3025 (b), 2943 (w), 2854 (b), 1604 (m), 1557 (s), 1488 (s), 1454 (m), 1358 (m), 1304 (w), 1256 (m), 1215 (w), 1146 (w), 1099 (m), 1023 (w), 969 (w), 914 (s), 853 (m), 792 (m), 751 (s), 689 (m), 669 (m), 593 (w), 553 (w), 512 (m), 464 (m), 430 (w)

9.7.3 *Bis*(*N*-4'-fluoro-Ph-picolinamide) ruthenium diiodide, $RuC_{24}H_{17}I_2F_2N_4O_2$ (4.3)

Ligand **2.3** (0.261 g, 1.21 mmol) was added to a solution of $RuCl_3.3H_2O$ (0.158 g, 0.60 mmol) in ethanol (30 mL), followed by triethylamine (0.061 g, 0.60 mmol). The solution was heated under reflux for 2 hours giving a dark red-brown solution. An excess of potassium iodide (1.014 g, 6.11 mmol)) was added to the solution and heated again under reflux for 18 hours. The solid was filtered, washed with ethanol and water, dried *in vacuo* and recrystallised *via* vapour diffusion in dimethylformamide-diethyl ether giving dark coloured crystals.

Yield: 0.276 g, 0.35 mmol, 58%. μ_{eff} = 1.70 ± 0.09 μ_β. **ES+MS** (DMF, m/z): 787.8 [M+H$^+$]. **Analysis Calculated**: C 36.7; H 2.2; N 7.1%. **Analysis found**: C 37.0; H 2.2; N 7.0%. **IR (cm^{-1})**: 3038 (b), 2854 (b), 1563 (s), 1502 (s), 1413 (w), 1372 (w), 1345 (w), 1208 (s), 1146 (m), 1079 (w), 1004 (w), 969 (w), 914 (m), 832 (m), 792 (w), 765 (s), 689 (m), 609 (m), 539 (m), 491 (m), 402 (w)

9.7.4 *Bis*(*N*-2',4'-difluoro-Ph-picolinamide) ruthenium diiodide, $RuC_{24}H_{15}I_2F_4N_4O_2$ (4.4)

Ligand **2.4** (0.276 g, 1.18 mmol) was added to a solution of $RuCl_3.3H_2O$ (0.151 g, 0.58 mmol) in ethanol (30 mL), followed by triethylamine (0.061 g, 0.60 mmol). The solution was heated under reflux for 2 hours giving a red solution. An excess of potassium iodide (0.959 g, 5.78 mmol) was added to the solution and heated again under reflux for 18 hours. The solid was filtered, washed with ethanol and water, dried *in vacuo* and recrystallised *via* vapour diffusion in dimethylformamide-diethyl ether giving dark coloured microcrystals.

Yield: 0.174 g, 0.21 mmol, 36%. **μ_{eff}** = 1.83 $\pm$ 0.05 μ_β. **ES+MS** (DMF, m/z): 823.8 [M+H$^+$]. **Analysis Calculated**: C 35.1; H 1.8; N 6.8%. **Analysis found**: C 35.1; H 1.8; N 6.6%. **IR (cm^{-1})**: 3196 (w), 3052 (w), 2868 (w), 1557 (s), 1495 (s), 1427 (m), 1365 (m), 1297 (w), 1256 (m), 1140 (s), 1099 (s), 955 (s), 907 (m), 853 (m), 805 (m), 765 (s), 689 (m), 669 (m), 600 (m), 573 (w), 539 (s), 498 (m), 464 (m), 437 (w)

9.7.5 *Bis*(*N*-2',5'-difluoro-Ph-picolinamide) ruthenium diiodide, $RuC_{24}H_{15}I_2F_4N_4O_2$ (4.5)

Ligand **2.5** (0.38 g, 1.62 mmol) was added to a solution of $RuCl_3.3H_2O$ (0.20 g, 0.76 mmol) in ethanol (30 mL), followed by triethylamine (0.076 g, 0.75 mmol). The solution was heated under reflux for 2 hours giving a red-orange solution. An excess of potassium iodide (1.277 g, 7.70 mmol) was added to the solution and heated again under reflux for 18 hours. The solid was filtered, washed with ethanol and water, dried *in vacuo* and recrystallised *via* vapour diffusion in dimethylformamide-diethyl ether giving dark coloured microcrystals.

Yield: 0.194 g, 0.24 mmol, 32%. **μ_{eff}** = 1.79 $\pm$ 0.04 μ_β. **ES+MS** (DMF, m/z): 823.8 [M+H$^+$]. **Analysis Calculated**: C 35.1; H 1.8; N 6.8%. **Analysis found**: C 36.0; H 1.8; N 6.8%. **IR (cm^{-1})**: 3196 (w), 3045 (w), 2868 (b), 1618 (m), 1577 (s), 1543 (s), 1488 (s), 1467 (w), 1351 (m), 1304 (w), 1242 (s), 1174 (s), 1133 (m), 1085 (w), 969 (m), 914 (m), 874 (m), 798 (m), 765 (s), 669 (m), 586 (w), 532 (w), 505 (m), 470 (m), 437 (m)

9.7.6 *Bis*(*N*-2'-chloro-Ph-picolinamide) ruthenium diiodide, $RuC_{24}H_{17}I_2Cl_2N_4O_2$ (4.6)

Ligand **2.6** (0.485 g, 2.09 mmol) was added to a solution of $RuCl_3.3H_2O$ (0.272 g, 1.04 mmol) in ethanol (30 mL), followed by triethylamine (0.106 g, 1.04 mmol). The solution was heated under reflux for 2 hours giving a dark red solution. An excess of potassium iodide (1.730 g, 10.42 mmol) was added to the solution and heated again under reflux for 18 hours. The solid was filtered, washed with ethanol and water, dried *in vacuo* and recrystallised *via* vapour diffusion in dimethylformamide-diethyl ether giving dark coloured microcrystals.

Yield: 0.292 g, 0.36 mmol, 34%. **μ$_{eff}$** = 1.77 ± 0.03 $μ_β$. **ES+MS** (DMF, m/z): 819.8 [M$^+$]. **Analysis Calculated**: C 36.1; H 2.7; N 6.5%. **Analysis found** (with 0.5 molecules of C_2H_6O): C 37.1; H 2.2; N 7.1%. **IR (cm^{-1})**: 3215 (w), 3018 (w), 2861 (w), 1557 (s), 1467 (m), 1441 (m), 1358 (m), 1304 (w), 1256 (w), 1146 (w), 1051 (w), 962 (w), 914 (s), 798 (w), 689 (m), 593 (w), 532 (w), 498 (m), 457 (m)

9.7.7 *Bis*(*N*-3'-chloro-Ph-picolinamide) ruthenium diiodide, $RuC_{24}H_{17}I_2Cl_2N_4O_2$ (4.7)

Ligand **2.7** (0.293 g, 1.26 mmol) was added to a solution of $RuCl_3.3H_2O$ (0.161 g, 0.62 mmol) in ethanol (30 mL), followed by triethylamine (0.061 g, 0.61 mmol). The solution was heated under reflux for 2 hours giving a dark red-brown solution. An excess of potassium iodide (1.029 g, 6.20 mmol) was added to the solution and heated again under reflux for 18 hours. The solid was filtered, washed with ethanol and water, dried *in vacuo* and recrystallised *via* vapour diffusion in dimethylformamide-diethyl ether giving dark coloured microcrystals.

Yield: 0.313 g, 0.38 mmol, 62%. **μ$_{eff}$** = 1.60 ± 0.09 $μ_β$. **ES+MS** (DMF, m/z): 841.8 [M+Na$^+$]. **Analysis Calculated**: C 35.2; H 2.1; N 6.8%. **Analysis found**: C 34.8; H 2.1; N 6.7%. **IR** (cm^{-1}): 3038 (b), 2908 (w), 2847 (w), 1563 (s), 1467 (m), 1420 (w), 1365 (m), 1331 (m), 1297 (w), 1256 (m), 1146 (m), 1072 (m), 983 (w), 935 (w), 874 (m), 758 (s), 676 (s), 586 (w), 560 (w), 491 (m), 444 (m), 416 (w)

9.7.8 *Bis*(*N*-4'-chloro-Ph-picolinamide) ruthenium diiodide, RuC$_{24}$H$_{17}$I$_2$Cl$_2$N$_4$O$_2$ (4.8)

Ligand **2.8** (0.261 g, 1.21 mmol) was added to a solution of RuCl$_3$.3H$_2$O (0.157 g, 0.60 mmol) in ethanol (30 mL), followed by triethylamine (0.061 g, 0.60 mmol). The solution was heated under reflux for 2 hours giving a red-brown solution. An excess of potassium iodide (1.002 g, 6.03 mmol) was added to the solution and heated again under reflux for 18 hours. The solid was filtered, washed with ethanol and water, dried *in vacuo* and recrystallised *via* vapour diffusion in dimethylformamide-diethyl ether giving dark coloured microcrystals.

Yield: 0.293 g, 0.36 mmol, 60%. **μ$_{eff}$** = 1.77 ± 0.02 μ_β. **ES+MS** (DMF, m/z): 819.8 [M$^+$]. **Analysis Calculated**: C 35.2; H 2.1; N 6.8%. **Analysis found**: C 36.0; H 2.1; N 7.1%. **IR** (cm^{-1}): 3120 (w), 3052 (w), 1563 (s), 1536 (s), 1481 (m), 1406 (w), 1358 (m), 1290 (w), 1256 (w), 1229 (w), 1140 (w), 1085 (m), 1010 (m), 969 (w), 921 (w), 819 (s), 765 (s), 723 (m), 689 (m), 505 (s), 470 (m), 437 (m), 416 (m)

9.7.9 *Bis*(*N*-2'4'-dichloro-Ph-picolinamide) ruthenium diiodide, RuC$_{24}$H$_{15}$I$_2$Cl$_4$N$_4$O$_2$ (4.9)

Ligand **2.9** (0.328 g, 1.23 mmol) was added to a solution of RuCl$_3$.3H$_2$O (0.154 g, 0.59 mmol) in ethanol (30 mL), followed by triethylamine (0.061 g, 0.60 mmol). The solution was heated under reflux for 2 hours giving a red-orange solution. An excess of potassium iodide (0.984 g, 5.93 mmol) was added to the solution and heated again under reflux for 18 hours. The solid was filtered, washed with ethanol and water, dried *in vacuo* and recrystallised *via* vapour diffusion in dimethylformamide-diethyl ether giving dark coloured microcrystals.

Yield: 0.231 g, 0.26 mmol, 44%. **μ$_{eff}$** = 1.67 ± 0.08 μ_β. **ES+MS** (DMF, m/z): 889.7 [M+H$^+$]. **Analysis Calculated**: C 32.5; H 1.7; N 6.3%. **Analysis found**: C 32.8; H 1.7; N 6.2%. **IR (cm^{-1})**: 3229 (w), 3073 (w), 1597 (s), 1550 (m), 1460 (m), 1379 (w), 1345 (m), 1249 (w), 1140 (m), 1099 (m), 1051 (m), 969 (w), 914 (w), 888 (w), 853 (s), 819 (m), 798 (m), 765 (s), 669 (m), 546 (m), 505 (s), 444 (s)

9.7.10 *Bis*(*N*-2'5'-dichloro-Ph-picolinamide) ruthenium diiodide,

RuC$_{24}$H$_{15}$I$_2$Cl$_4$N$_4$O$_2$ (4.10)

Ligand **2.10** (0.444 g, 1.66 mmol) was added to a solution of RuCl$_3$.3H$_2$O (0.216 g, 0.82 mmol) in ethanol (30 mL), followed by triethylamine (0.084 g, 0.83 mmol). The solution was heated under reflux for 2 hours giving an orange solution. An excess of potassium iodide (1.370 g, 8.26 mmol) was added to the solution and heated again under reflux for 18 hours. The solid was filtered, washed with ethanol and water, dried *in vacuo* and recrystallised *via* vapour diffusion in dimethylformamide-diethyl ether giving dark coloured microcrystals.

Yield: 0.323 g, 0.36 mmol, 44%. **μ$_{eff}$** = 1.76 ± 0.14 μ_β. **ES+MS** (DMF, m/z): 887.7 [M$^+$]. **Analysis Calculated**: C 32.5; H 1.7; N 6.3%. **Analysis found**: C 33.6; H 1.8; N 6.3%. **IR (cm^{-1})**: 3209 (b), 3052 (w), 2922 (w), 2861 (w), 1583 (s), 1543 (m), 1460 (m), 1393 (m), 1351 (m), 1311 (w), 1256 (w), 1146 (m), 1099 (m), 1051 (m), 962 (m), 935 (m), 881 (m), 805 (m), 751 (s), 682 (m), 593 (m), 560 (m), 512 (m), 451 (m)

9.7.11 *Bis*(*N*-2'-bromo-Ph-picolinamide) ruthenium diiodide,

RuC$_{24}$H$_{15}$I$_2$Br$_4$N$_4$O$_2$ (4.11)

Ligand **2.11** (0.358 g, 1.30 mmol) was added to a solution of RuCl$_3$.3H$_2$O (0.167 g, 0.64 mmol) in ethanol (30 mL), followed by triethylamine (0.068 g, 0.68 mmol). The solution was heated under reflux for 2 hours giving a red-orange solution. An excess of potassium iodide (1.078 g, 6.49 mmol) was added to the solution and heated again under reflux for 18 hours. The solid was filtered, washed with ethanol and water, dried *in vacuo* and recrystallised *via* vapour diffusion in dimethylformamide-diethyl ether giving dark coloured microcrystals.

Yield: 0.304 g, 0.33 mmol, 52%. **μ$_{eff}$** = 1.65 ± 0.09 μ_β. **ES+MS** (DMF, m/z): 909.7 [M+H$^+$]. **Analysis Calculated**: C 31.7; H 1.9; N 6.2%. **Analysis found**: C 31.9; H 2.1; N 6.0%. **IR (cm^{-1})**: 3175 (w), 3045 (w), 1590 (s), 1557 (s), 1467 (m), 1441 (m), 1345 (m), 1297 (m), 1256 (w), 1140 (w), 1051 (m), 1023 (m), 962 (w), 914 (m), 839 (w), 798 (w), 751 (s), 716 (w), 682 (m), 593 (w), 525 (m), 484 (m), 444 (m)

9.7.12 *Bis*(*N*-3'-bromo-Ph-picolinamide) ruthenium diiodide,

RuC$_{24}$H$_{15}$I$_2$Br$_4$N$_4$O$_2$ (4.12)

Ligand **2.12** (0.357 g, 1.29 mmol) was added to a solution of RuCl$_3$.3H$_2$O (0.167 g, 0.64 mmol) in ethanol (30 mL), followed by triethylamine (0.068 g, 0.68 mmol). The solution was heated under reflux for 2 hours giving a dark red-brown solution. An excess of potassium iodide (1.075 g, 6.48 mmol) was added to the solution and heated again under reflux for 18 hours. The solid was filtered, washed with ethanol and water, dried *in vacuo* and recrystallised *via* vapour diffusion in dimethylformamide-diethyl ether giving dark coloured crystals.

Yield: 0.322 g, 0.35 mmol, 55%. **μ$_{eff}$** = 1.81 ± 0.06 μ_β. **ES+MS** (DMF, m/z): 931.7 [M+Na$^+$]. **Analysis Calculated**: C 31.7; H 1.9; N 6.2%. **Analysis found**: C 31.8; H 1.9; N 6.1%. **IR (cm^{-1})**: 3011 (b), 2854 (w), 1557 (s), 1529 (m), 1467 (m), 1413 (w), 1365 (m), 1331 (m), 1297 (w), 1256 (m), 1140 (m), 1065 (m), 969 (w), 928 (w), 867 (m), 758 (s), 669 (s), 586 (w), 546 (w), 491 (m), 437 (m)

9.7.13 *Bis*(*N*-4'-bromo-Ph-picolinamide) ruthenium diiodide,

RuC$_{24}$H$_{15}$I$_2$Br$_4$N$_4$O$_2$ (4.13)

Ligand **2.13** (0.326 g, 1.17 mmol) was added to a solution of RuCl$_3$.3H$_2$O (0.153 g, 0.59 mmol) in ethanol (30 mL), followed by triethylamine (0.061 g, 0.60 mmol). The solution was heated under reflux for 2 hours giving a dark red solution. An excess of potassium iodide (1.060 g, 6.39 mmol) was added to the solution and heated again under reflux for 18 hours. The solid was filtered, washed with ethanol and water, dried *in vacuo* and recrystallised *via* vapour diffusion in dimethylformamide-diethyl ether giving dark coloured crystals.

Yield: 0.295 g, 0.32 mmol, 55%. **μ$_{eff}$** = 1.92 ± 0.05 μ_β. **ES+MS** (DMF, m/z): 909.7 [M+H$^+$]. **Analysis Calculated**: C 31.7; H 1.9; N 6.2%. **Analysis found**: C 31.8; H 1.9; N 5.9%. **IR (cm^{-1})**: 3236 (w), 3059 (w), 2936 (w), 1550 (s), 1488 (m), 1399 (m), 1358 (m), 1260 (w), 1297 (w), 1256 (w), 1133 (m), 1055 (m), 1010 (m), 962 (w), 914 (w), 819 (m), 758 (s), 716 (w), 676 (m), 498 (s), 409 (w)

9.7.14 *Bis*(*N*-2',4'-dibromo-Ph-picolinamide) ruthenium diiodide,

RuC$_{24}$H$_{15}$I$_2$Br$_4$N$_4$O$_2$ (4.14)

Ligand **2.14** (0.436 g, 1.22 mmol) was added to a solution of RuCl$_3$.3H$_2$O (0.156 g, 0.60 mmol) in ethanol (30 mL), followed by triethylamine (0.061 g, 0.60 mmol). The solution was heated under reflux for 2 hours giving a dark red-brown solution. An excess of potassium iodide (1.011 g, 6.08 mmol) was added to the solution and heated again under reflux for 18 hours. The solid was filtered, washed with ethanol and water, dried *in vacuo* and recrystallised *via* vapour diffusion in dimethylformamide-diethyl ether giving dark coloured microcrystals.

Yield: 0.472 g, 0.44 mmol, 74%. **μ$_{eff}$** = 1.68 ± 0.05 μ_β. **ES+MS** (DMF, m/z): 1090.5 [M+Na$^+$+H$^+$]. **Analysis Calculated**: C 27.0; H 1.4; N 5.3%. **Analysis found**: C 28.2; H 1.5; N 5.5%. **IR (cm^{-1})**: 3366 (w), 3209 (w), 3059 (w), 2915 (w), 1583 (s), 1557 (m), 1460 (m), 1345 (m), 1263 (w), 1133 (w), 1079 (w), 1037 (m), 969 (w), 907 (w), 846 (w), 805 (m), 765 (m), 669 (m), 546 (w), 498 (m), 444 (m)

9.7.15 *Bis*(*N*-2',5'-dibromo-Ph-picolinamide) ruthenium diiodide,

RuC$_{24}$H$_{15}$I$_2$Br$_4$N$_4$O$_2$ (4.15)

Ligand **2.15** (0.561 g, 1.58 mmol) was added to a solution of RuCl$_3$.3H$_2$O (0.202 g, 0.77 mmol) in ethanol (30 mL), followed by triethylamine (0.076 g, 0.75 mmol). The solution was heated under reflux for 2 hours giving a red solution. An excess of potassium iodide (1.286 g, 7.75 mmol) was added to the solution and heated again under reflux for 18 hours. The solid was filtered, washed with ethanol and water, dried *in vacuo* and recrystallised *via* vapour diffusion in dimethylformamide-diethyl ether giving dark coloured microcrystals.

Yield: 0.269 g, 0.25 mmol, 33%. **μ$_{eff}$** = 1.85 ± 0.10 μ_β. **ES+MS** (DMF, m/z): 1067.5 [M+H$^+$]. **Analysis Calculated**: C 27.0; H 1.4; N 5.3%. **Analysis found**: C 27.6; H 1.4; N 5.4%. **IR (cm^{-1})**: 3196 (w), 3052 (w), 2840 (b), 1583 (s), 1543 (m), 1454 (m), 1386 (m), 1351 (m), 1297 (w), 1146 (m), 1079 (m), 1023 (s), 962 (m), 928 (m), 867 (m), 798 (s), 758 (s), 682 (s), 600 (m), 505 (s), 451 (s), 409 (w)

9.8   Preparation of *Bis*-picolinamide Rhodium Dihalide Complexes

9.8.1   *Bis*(*N*-3'-fluoro-picolinamide) rhodium dichloride,

$RuC_{24}H_{17}Cl_2F_2N_4O_2$ (5.1)

3'-fluoro-picolinamide ligand (0.218 g, 1.00 mmol) was added to a solution of RhCl$_3$ (0.111 g, 0.47 mmol) in ethanol (30 mL), followed by triethylamine (0.07 g, 0.50 mmol). The solution was heated under reflux for 2 hours giving an orange solution. On adding pentane, the complex precipitated as yellow solid which was then filtered, washed with pentane, dried *in vacuo* and recrystallised *via* vapour diffusion in

methanol-pentane giving orange crystals.

Yield: 0.183 g, 0.23 mmol, 49%. **ES+MS** (CH$_3$OH, m/z): 605.0 [M$^+$]. **Analysis Calculated**: C 47.6; H 2.8; N 9.3, Cl 11.7%. **Analysis found**: C 47.3; H 3.0; N 8.9; Cl 11.4%.

IR (cm^{-1}): 3330 (b), 3079 (w), 1563 (s), 1486 (m), 1475 (m), 1401 (m), 1349 (w), 1305 (w), 1264 (m), 1189 (w), 1120 (w), 1030 (w), 971
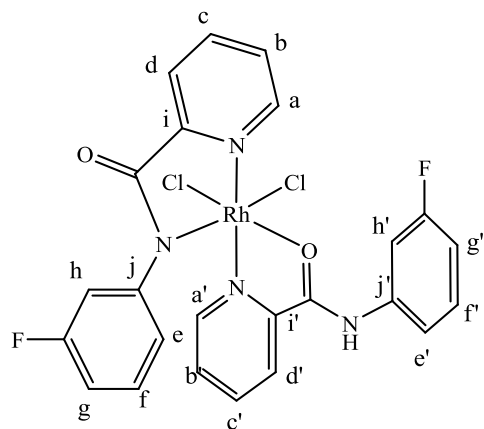
(w), 907 (w), 865 (m), 761 (s), 706 (m), 676 (s), 593 (w), 518 (m), 457 (m), 448 (w)

<u>Major isomer</u>: **^{1}H NMR** (*d*$_4$-MeOD, 300.13 MHz, 300K) δ 9.81 (d, 1H, $^3J_{(H-H)}$ = 5.9 Hz, H$_a$), 9.38 (d, 1H, $^3J_{(H-H)}$ = 5.5 Hz, H$_{a'}$), 8.35 (d, 1H, $^3J_{(H-H)}$ = 7.2 Hz, H$_d$), 8.30 (dd, 1H, $^3J_{(H-H)}$ = 7.7 Hz, $^4J_{(H-H)}$ = 1.5 Hz, H$_{d'}$), 8.19 (m, 2H, H$_{c,c'}$), 7.90 (ddd, $^3J_{(H-H)}$ = 7.6 Hz, $^3J_{(H-H)}$ = 5.8 Hz, $^4J_{(H-H)}$ = 1.6 Hz, H$_b$), 7.81 (t, $^3J_{(H-H)}$ = 6.5(x2) Hz, H$_{b'}$), 7.36 (m, 3H, H$_{e,f,g}$), 7.03 (m, 2H, H$_{h,h'}$), 6.78 (m, 3H, H$_{e',f',g'}$) **^{13}C{^{1}H} NMR** (*d*$_4$-MeOD, 75.47 MHz, 300 K) δ 178.4 (C=O of *(N,N)*-ligand), 174.6 (C=O of *(N,O)*-ligand), 169.7 (C$_a$), 164.4 (C$_i$), 158.8 (C$_{i'}$), 157.3 (C$_j$), 156.1 (C$_{j'}$), 148.9 (C$_c$), 146.2 (C$_{c'}$), 145.0 (C$_f$), 132.9 (C$_{f'}$), 131.5 (C$_b$), 128.4 (C$_d$), 125.2 (C$_{d'}$), 119.2 (C$_{b'}$), 118.8 (C$_e$), 118.3 (C$_g$), 114.8 (C$_{a'}$), 113.8 (C$_h$), 113.4 (C$_{e'}$), 107.2 (C-F of *(N,N)*-ligand), 106.7 (C$_{g'}$), 106.0 (C-F of *(N,O)*-ligand), 97.7 (C$_{h'}$) <u>Minor isomer</u>: **^{1}H NMR** (*d*$_4$-MeOD, 75.47 MHz, 300K) δ 9.69 (d, 1H, $^3J_{(H-H)}$ = 5 Hz, H$_a$), 9.32 (d, 1H, $^3J_{(H-H)}$ = 5.2 Hz, H$_{a'}$), 8.59 (m, 2H, H$_{d,d'}$), 7.59 (br. m, 9H, H$_{b/c/e/f/g/b'/c'/e'/f'/g'}$), 7.19 (d, 2H, $^3J_{(H-H)}$ = 6 Hz, H$_{h,h'}$), 6.70 (br. m, 1H, H$_{g/g'}$). **^{13}C{^{1}H} NMR** (*d*$_4$-MeOD, 75.47 MHz, 300 K) δ 195.8 (C=O of *(N,N)*-ligand,

190.3 (C=O of *(N,O)*-ligand), 187.5 (C_i), 180.7 ($C_{i'}$), 180.4 (C_a), 177.1 (Cj), 172.4 ($C_{j'}$), 170.8 (C_c), 166.1 ($C_{c'}$), 165.3 (C_f), 159.6 ($C_{f'}$), 155.8 (C_b), 151.9 (C_d), 146.3 ($C_{d'}$), 141.3 ($C_{b'}$), 139.6 (C_e), 129.6 (C_g), 124.2 ($C_{a'}$), 117.4 (C_h), 111.9 (C-F of *(N,N)*-ligand), 109.2 (C-F of *(N,O)*-ligand), 105.1 ($C_{e'}$), 94.1 ($C_{g'}$), 90.9 ($C_{h'}$)

9.8.2 *Bis*(*N*-3'-chloro-picolinamide) rhodium dichloride, $RuC_{24}H_{17}Cl_4N_4O_2$ (5.2)

Ligand **2.7** (0.221 g, 0.951 mmol) was added to a solution of $RhCl_3$ (0.112 g, 0.47 mmol) in ethanol (30 mL), followed by triethylamine (0.06 g, 0.48 mmol). The solution was heated under reflux for 2 hours giving a yellow solution. On adding pentane, the complex precipitated as yellow solid which was then filtered, washed with pentane, dried *in vacuo* and recrystallised *via* vapour diffusion in methanol-pentane giving yellow microcrystals.

Yield: 0.185 g, 0.29 mmol, 62%. **ES+MS** (CH_3OH, m/z): 636.9 $[M+H^+]$. **Analysis Calculated**: C 40.7; H 3.0; N 7.9; Cl 25.1%. **Analysis found** (0.33 molecules of H_2O and Cl): C 40.0; H 2.9; N 7.4; Cl 25.5%.
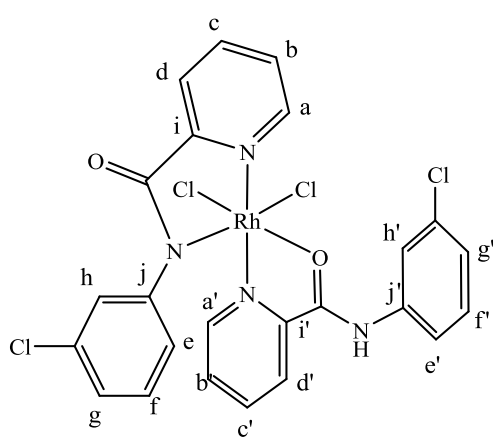
IR (cm^{-1}): 3287 (b), 3086 (w), 1563 (s), 1479 (m), 1428 (w), 1357 (w), 1305 (w), 1297 (w), 1189 (w), 1155 (w), 1098 (w), 1059 (w), 974 (w), 886 (m), 763 (m), 676 (s), 603 (w), 516 (w), 447 (m).

Major isomer: **^{1}H NMR** (d_6-MeOD, 300.13 MHz, 300K) δ 9.69 (d, 1H, $^3J_{(H-H)}$ = 5.7 Hz, H_a), 9.29 (d, 1H, $^3J_{(H-H)}$ = 5.5 Hz, $H_{a'}$), 8.31 (d, 1H, $^3J_{(H-H)}$ = 7.9 Hz, H_d), 8.21 (td, 2H, $^3J_{(H-H)}$ = 7.6 Hz, $^4J_{(H-H)}$ = 1.3, $H_{b',c'}$), 8.14 (m, 1H, $H_{d'}$), 8.09 (m, 2H, $H_{b,c}$), 7.80 (m, 3H, $H_{e,f,g}$), 7.50 (s, 1H, H_h), 7.41 (s, 1H, $H_{h'}$), 6.80 (m, 3H, $H_{e',f',g'}$). **^{13}C{^{1}H} NMR** (d_4-MeOD, 75.47 MHz, 300 K) δ 195.4 (C=O of *(N,N)*-ligand), 194.2 (C=O of *(N,O)*-ligand), 190.4 (C_i), 185.7 (C_j), 185.5 ($C_{j'}$), 179.9 ($C_{i'}$), 178.5 (C_a), 173.7 (C_c), 167.5 (C_f), 157.4 ($C_{c'}$), 154.1 ($C_{f'}$), 151.3 (C_e), 141.5 ($C_{b,d}$), 137.8 (C_g), 135.1 ($C_{b',d'}$), 131.2 ($C_{a'}$), 128.9 (C_h), 128.1 ($C_{e'}$), 126.7 ($C_{g'}$), 124.1 ($C_{h'}$), 119.7 (C-Cl of *(N,N)*-ligand), 117.5 (C-Cl of *(N,O)*-ligand). Minor isomer: **^{1}H NMR** (d_6-MeOD, 300.13 MHz,

300K) δ 9.65 (d, 1H, $^3J_{(H-H)}$ = 5.1 Hz, H$_a$), 9.46 (d, 1H, $^3J_{(H-H)}$ = 5.6 Hz, H$_{a'}$), 8.66 (d, 1H, $^3J_{(H-H)}$ = 7.6 Hz, H$_d$), 8.50 (t, 1H, $^3J_{(H-H)}$ = 7(x2) Hz, H$_c$), 8.39 (t, 1H, $^3J_{(H-H)}$ = 8.4(x2) Hz, H$_b$), 8.01 (d, 1H, $^3J_{(H-H)}$ = 7.6 Hz H$_{d'}$), 7.93 (m, 2H, H$_{b',c'}$), 7.86 (s, 1H, H$_h$), 7.75 (s, 1H, H$_{h'}$), 7.45 (m, 1H, H$_e$), 7.30 (br. m, 2H, H$_{g,f}$), 7.09 (br. m, 2H, H$_{g',f'}$), 6.97 (br. m, 1H, H$_{e'}$). ^{13}C{^{1}H} NMR (d_4-MeOD, 75.47 MHz, 300 K) δ 194.7 (C=O of (N,N)-ligand), 193.3 (C=O of (N,O)-ligand), 188.9 (C$_a$), 184.3 (C$_i$), 181.7 (C$_j$), 175.1 (C$_{i'}$), 174.1 (C$_{j'}$), 168.3 (C$_c$), 165.5 (C$_{c'}$), 163.5 (C$_f$), 160.0 (C$_{f'}$), 154.8 (C$_e$), 153.2 (C$_{a'}$), 148.2 (C$_b$), 140.2 (C$_d$), 133.2 (C$_g$), 129.7 (C$_{b'}$), 125.9 (C$_{d'}$), 123.9 (C$_{g,h}$), 114.7 (C-Cl of (N,N)-ligand), 110.7 (C-Cl of (N,O)-ligand), 107.3 (C$_{g',h'}$).

9.8.3 *Bis*(*N*-3'-bromo-picolinamide) rhodium dichloride, RuC$_{24}$H$_{17}$Cl$_2$Br$_2$N$_4$O$_2$ (5.3)

Ligand **2.12** (0.276 g, 1.00 mmol) was added to a solution of RhCl$_3$ (0.104 g, 0.50 mmol) in ethanol (30 mL), followed by triethylamine (0.05 g, 0.53 mmol). The solution was heated under reflux for 2 hours giving an orange solution. On adding pentane, the complex precipitated as yellow solid which was then filtered, washed with pentane, dried *in vacuo* and recrystallised *via* vapour diffusion in methanol-pentane giving a mixture of red and orange crystals, and yellow microcrystals.

Yield: 0.183 g, 0.25 mmol, 50%. **ES+MS** (CH$_3$OH, m/z): 726.8 [M+H$^+$]. **Analysis Calculated**: C 39.7; H 2.4; N 7.7%. **Analysis found**: C 39.4; H 2.4; N 7.5%.

IR (cm^{-1}): __Red__ 2997 (w), 2915 (w), 2759 (b), 1543 (s), 1467 (m), 1427 (w), 1338 (m), 1297 (w), 1256 (m), 1146 (m), 1058 (m), 969 (m), 928 (w), 860 (m), 778 (m), 751 (m), 682 (s), 593 (w), 567 (w), 512 (m), 484 (m), 437 (m); __Orange__ 3189 (w), 3052 (b), 2980 (w), 1618 (m), 1590 (m), 1562 (s), 1469 (m), 1420 (w), 1389 (w), 1344 (w), 1297 (w), 1229 (m), 1153 (w), 1085 (w), 1058 (w), 983 (m), 907 (w), 860 (m), 758 (s), 672 (s), 600 (w), 553 (w), 512 (m), 470 (w), 430 (w); __Yellow__ 3380 (b), 3209 (b), 3066 (w), 1618 (s), 1598 (s), 1568 (s), 1466 (m), 1433 (w), 1413 (w), 1390 (w), 1340 (w), 1311 (w), 1260 (w), 1151 (w), 1062 (w), 1025 (w), 999 (w), 966 (w), 922 (w), 896 (w), 860 (m), 776 (s), 758 (s), 723 (w), 677 (s), 601 (w), 561 (w), 548 (w), 498 (w), 475 (m), 435 (m), 415 (w).
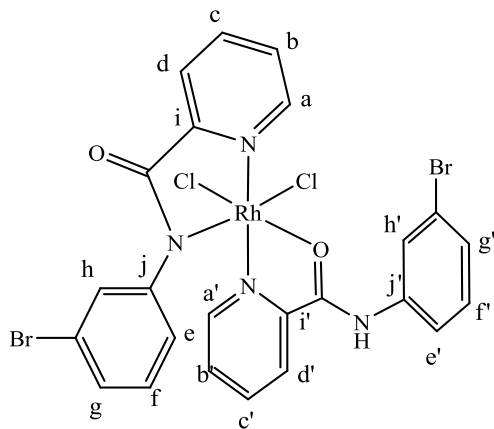
Major isomer: **^{1}H NMR** (d_6-CH$_3$CO, 300.13 MHz, 300K) δ 9.85 (d, 1H, ^{3}J$_{(H-H)}$ = 5.6 Hz, H$_a$), 9.39 (d, 1H, ^{3}J$_{(H-H)}$ = 5.6 Hz, H$_{a'}$), 8.57 (d, 1H, ^{3}J$_{(H-H)}$ = 7.8 Hz, H$_d$), 8.29 (dtd, 2H, ^{3}J$_{(H-H)}$ = 10.4 Hz, ^{3}J$_{(H-H)}$ = 7.8 Hz, ^{4}J$_{(H-H)}$ = 1.5 Hz, H$_{c,c'}$), 8.14 (m, 1H, H$_{d'}$), 7.95 (ddd, 1H, ^{3}J$_{(H-H)}$ = 7.8 Hz, ^{3}J$_{(H-H)}$ = 5.5 Hz, ^{4}J$_{(H-H)}$ = 1.2 Hz, H$_b$), 7.90 (ddd, 1H, ^{3}J$_{(H-H)}$ = 7.6 Hz, ^{3}J$_{(H-H)}$ = 5.7 Hz, ^{4}J$_{(H-H)}$ = 1.6 Hz, H$_{b'}$), 7.83 (t, 1H, ^{3}J$_{(H-H)}$ = 2(x2) Hz, H$_h$), 7.64 (ddd, 1H, ^{3}J$_{(H-H)}$ = 8.1 Hz, ^{3}J$_{(H-H)}$ = 2.1 Hz, ^{4}J$_{(H-H)}$ =0.9 Hz, H$_e$), 7.45 (ddd, 1H, ^{3}J$_{(H-H)}$ = 8.0 Hz, ^{3}J$_{(H-H)}$ = 1.9 Hz, ^{4}J$_{(H-H)}$ = 1 Hz, H$_g$), 7.34 (t, 1H, ^{3}J$_{(H-H)}$ = 8.1(x2) Hz, H$_f$), 7.18 (t, 1H, ^{3}J$_{(H-H)}$ = 1.9(x2) Hz, H$_{h'}$), 7.01 (m, 2H, H$_{e',g'}$), 6.86 (m, 1H, H$_{f'}$). **^{13}C{^{1}H} NMR** (d_6-CH$_3$CO, 75.47 MHz, 300 K) δ 199.2 (C=O of *(N,N)*-ligand), 197.2 (C$_a$), 194.1 (C=O of *(N,O)*-ligand), 188.6 (C$_i$), 168.7 (C$_{i'}$), 153.3 (C$_{a'}$), 152.7 (C$_j$), 151.7 (C$_{j'}$), 139.6 (C$_c$), 139.4 (C$_{c'}$), 130.8 (C$_{b'}$), 130.5 (C$_f$), 130.1 (C$_e$), 129.9 (C$_b$), 129.6 (C$_g$), 129.2 (C$_{g'}$), 126.9 (C$_{e'}$), 126.3 (C$_{f',h'}$), 125.5 (C$_d$), 125.3 (C$_{d'}$), 121.5 (C$_h$), 121.2 (C-Br of *(N,N)*-ligand), 120.8 (C-Br of *(N,O)*-ligand).

Minor isomer 1: **^{1}H NMR** (d_6-CH$_3$CO, 300.13 MHz, 300K) δ 9.46 (d, 1H, ^{3}J$_{(H-H)}$ = 5.6 Hz, H$_a$), 8.91 (d, 1H, ^{3}J$_{(H-H)}$ = 5.2 Hz, H$_{a'}$), 8.04 (dd, 1H, ^{3}J$_{(H-H)}$ = 3.0 Hz, ^{4}J$_{(H-H)}$ = 1.4 Hz, H$_b$), 7.8 (d, 1H, ^{3}J$_{(H-H)}$ = 1.9 Hz, H$_d$), 7.75 (m, 2H, H$_{c,d'}$), 7.73 (m, 1H, H$_{c'}$), 7.68 (ddd, 1H, ^{3}J$_{(H-H)}$ = 7.5 Hz, ^{3}J$_{(H-H)}$ = 5.7 Hz, ^{4}J$_{(H-H)}$ = 1.5 Hz , H$_{b'}$), 7.14 (t, 2H, ^{3}J$_{(H-H)}$ = 1.9(x2) Hz, H$_{f,g}$), 7.12 (m, 1H, H$_e$), 7.05 (m, 2H, H$_{e',g'}$), 6.97 (s, 1H, H$_h$), 6.93 (s, 1H, H$_{h'}$), 6.91 (m, 1H, H$_{f'}$). **^{13}C{^{1}H} NMR** (d_6-CH$_3$CO, 75.47 MHz, 300 K) δ 209.0 (C=O of *(N,N)*-ligand), 201.1 (C=O of *(N,O)*-ligand), 195.4 (C$_a$), 192.2 (C$_{a'}$), 161.2 (C$_c$), 159.5 (C$_i$), 156.8 (C$_{i'}$), 155.7 (C$_{c'}$), 149.7 (C$_j$), 146.1 (C$_{j'}$), 143.6 (C$_b$), 141.6 (C$_f$), 138.5 (C$_e$), 136.2 (C$_{b'}$), 134.0 (C$_g$), 133.3 (C$_{g'}$), 132.7 (C$_e$), 131.7 (C$_h$), 127.2 (C$_{f'}$), 123.6 (C$_d$), 120.7 (C-Br of *(N,N)*-ligand), 120.3 (C$_{d'}$) 118.4 (C-Br of *(N,O)*-ligand), 115.4 (C$_{h'}$). Minor isomer 2: **^{1}H NMR** (d_6-CH$_3$CO, 300.13 MHz, 300K) δ 9.70 (d, 1H, ^{3}J$_{(H-H)}$ = 5.4 Hz, H$_a$), 9.50 (d, 1H, ^{3}J$_{(H-H)}$ = 5.8 Hz, H$_{a'}$), 8.72 (d, 1H, ^{3}J$_{(H-H)}$ = 8.6 Hz, H$_d$), 8.39 (m, 1H, H$_c$), 8.09 (m, 1H, H$_b$), 8.05 (dd, 1H, ^{3}J$_{(H-H)}$ = 3.1 Hz, ^{4}J$_{(H-H)}$ = 1.4 Hz, H$_{b'/c'}$), 8.02 (dd, 1H, ^{3}J$_{(H-H)}$ = 3.1 Hz, ^{4}J$_{(H-H)}$ = 1.4 Hz, H$_{b'/c'}$), 7.99 (d, 1H, ^{3}J$_{(H-H)}$ = 7.3 Hz, H$_{d'}$), 7.86 (m, 1H, H$_g$), 7.78 (d, 1H, ^{3}J$_{(H-H)}$ = 1.5 Hz, H$_h$), 7.55 (m, 1H, H$_e$), 7.51 (m,

1H, H$_f$), 7.39 (t, 1H, $^3J_{(H-H)}$ = 1.9(x2) Hz, H$_{h'}$), 7.37 (t, 1H, $^3J_{(H-H)}$ = 2(x2) Hz, H$_{g'}$), 7.15 (m, 1H, H$_{f'}$), 7.07 (dd, 1H, $^3J_{(H-H)}$ = 1.9 Hz, $^4J_{(H-H)}$ = 1.1 Hz, H$_{e'}$). ^{13}C{^{1}H} NMR (d_6-CH$_3$CO, 75.47 MHz, 300 K) δ 203.2 (C=O of *(N,N)*-ligand), 196.5 (C=O of *(N,O)*-ligand), 190.4 (C$_a$), 186.6 (C$_{a'}$), 183.6 (C$_i$), 156.1 (C$_j$), 154.0 (C$_c$), 147 (C$_{i'}$), 145.7 (C$_{c'}$), 143.3 (C$_{j'}$), 137.8 (C$_b$), 135.8 (C$_f$), 134.5 (C$_e$), 131.1 (C$_{f'}$), 127.9 (C$_{e'}$), 125.0 (C$_{b'}$), 119.3 (C$_d$), 117.6 (C$_g$), 116.5 (C$_{d'}$), 115.7 (C$_{g'}$), 114.3 (C-Br of *(N,N)*-ligand), 112.8 (C$_h$), 110.9 (C-Br of *(N,O)*-ligand), 109.3 (C$_{h'}$)

9.8.4 *Bis*(*N*-3'-iodo-picolinamide) rhodium dichloride, RuC$_{24}$H$_{17}$Cl$_2$I$_2$N$_4$O$_2$ (5.4)

3'-Iodo-picolinamide (0.322 g, 1.00 mmol) was added to a solution of RhCl$_3$ (0.117 g, 0.49 mmol) in ethanol (30 mL), followed by triethylamine (0.07 g, 0.50 mmol). The solution heated under reflux for 2 hours giving a yellow solution. On adding pentane, the complex precipitated as yellow solid which was then filtered, washed with pentane, dried *in vacuo* and recrystallised *via* vapour diffusion in methanol-pentane giving red crystals.
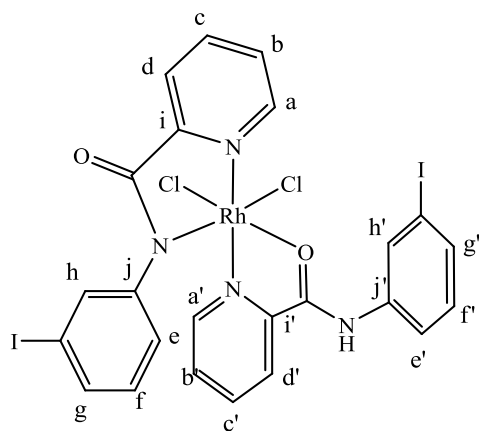
Yield: 0.294 g, 0.36 mmol, 73%. **ES+MS** (CH$_3$OH, m/z): 820.8 [M+H$^+$]. **Analysis Calculated**: C 34.4; H 2.3; N 6.7%. **Analysis found** (with 0.5 molecules of H$_2$O): C 34.0; H 2.2; N 6.3%.

IR (cm^{-1}): 3236 (b), 3091 (w), 1564 (s), 1469 (m), 1418 (w), 1302 (w), 1270 (w), 1155 (w), 1063 (w), 1028 (w), 995 (w), 860 (w), 764 (m), 681 (s), 601 (w), 515 (w), 437 (w)

<u>Major isomer</u>: ^{1}H NMR (d_4-MeOD, 300.13 MHz, 300K) δ 9.83 (d, 1H, $^3J_{(H-H)}$ = 5.6 Hz, H$_a$), 9.42 (d, 1H, $^3J_{(H-H)}$ = 5.2 Hz, H$_{a'}$), 8.43 (d, 1H, $^3J_{(H-H)}$ = 8.7 Hz, H$_d$), 8.35 (d, 1H, $^3J_{(H-H)}$ = 8.7 Hz, H$_{d'}$), 8.28 (td, 1H, $^3J_{(H-H)}$ = 8.0(x2) Hz, $^4J_{(H-H)}$ = 1 Hz, H$_c$), 8.01 (dd, 2H, $^3J_{(H-H)}$ = 8.4(x2) Hz, $^3J_{(H-H)}$ = 1.5 Hz, H$_{b,b'}$), 7.94 (m, 1H, H$_{c'}$), 7.79 (m, 1H, H$_f$), 7.71 (m, 2H, H$_{e,g}$), 7.37 (s, 1H, H$_h$), 7.19 (m, 3H, H$_{e',f',g'}$), 6.83 (s, 1H, H$_{h'}$). ^{13}C{^{1}H} NMR (d_4-MeOD, 75.47 MHz, 300 K) δ 192.0 (C=O of *(N,N)*-ligand), 190.2 (C$_a$), 188.50 (C=O of *(N,O)*-ligand), 173.6 (C$_{a'}$), 158.0 (C$_i$), 155.7 (C$_j$), 154.7 (C$_{b,c}$),

141.6 ($C_{i'}$), 139.7 ($C_{j'}$), 137.6 ($C_{c'}$), 137.4 ($C_{b'}$), 135.8 (C_f), 135.3 (C_e), 134.7 ($C_{f'}$), 133.1 (C_g), 132.3 ($C_{g'}$), 131.6 ($C_{e'}$), 130.1 (C_d), 126.4 (C_h), 124.9 ($C_{d'}$), 121.4 (C-I of *(N,N)*-ligand), 118.6 (C-I of *(N,O)*-ligand), 112.9 ($C_{h'}$). <u>Minor isomer</u>: **^{1}H NMR** (d_4-MeOD, 300.13 MHz, 300K) δ 9.16 (d, 1H, $^3J_{(H-H)}$ = 5.3 Hz, H_a), 9.03 (d, 1H, $^3J_{(H-H)}$ = 5.2 Hz, $H_{a'}$), 8.29 (dd, 2H, $^3J_{(H-H)}$ = 7.8 Hz, $^4J_{(H-H)}$ = 1.6 Hz, $H_{b,b'}$), 8.08 (d, 1H, $^3J_{(H-H)}$ = 8.3 Hz, H_d), 7.81 (m, 2H, $H_{c,c'}$), 7.73 (d, 1H, $^3J_{(H-H)}$ = 6.2 Hz, $H_{d'}$), 7.69 (br. m, 3H, $H_{e,f,g}$), 7.45 (s, 1H, H_h), 7.32 (d, 1H, $^3J_{(H-H)}$ = 7.1 Hz, $H_{e'}$), 7.21 (d, 1H, $^3J_{(H-H)}$ = 7.7 Hz, $H_{g'}$), 7.00 (s, 1H, $H_{h'}$), 6.95 (br. m, 1H, $H_{f'}$). **^{13}C{^{1}H} NMR** (d_4-MeOD, 75.47 MHz, 300 K) δ 178.6 (C=O of *(N,N)*-ligand), 178.3 (C_a), 177.6 (C=O of *(N,O)*-ligand), 176.1 (C_i), 174.6 (C_j), 157.6 ($C_{a'}$), 144.3 (C_i), 143.5 ($C_{j'}$), 140.4 (C_b), 139.3 ($C_{c'}$), 139.0 ($C_{b'}$), 136.2 (C_f), 136.1 (C_e), 135.2 ($C_{f'}$), 133.7 (C_g), 132.8 ($C_{g'}$), 127.0 (C_e), 126.3 (C_f), 125.5 (C_h), 122.8 (C_d), 122.0 ($C_{d'}$), 117.8 (C-I of *(N,N)*-ligand), 117.6 (C_h), 116.0 (C-I of *(N,O)*-ligand)

9.8.5 *Bis*(*N*-3'-chloro-picolinamide) rhodium diiodide, $RuC_{24}H_{17}I_2Cl_2N_4O_2$ (5.5)

Ligand **2.7** (0.213 g, 0.92 mmol) was added to a solution of RhCl$_3$ (0.103 g, 0.43 mmol) in ethanol (30 mL), followed by triethylamine (0.06 g, 0.46 mmol). The solution was heated under reflux for 2 hours giving a yellow solution. An excess of potassium iodide (0.721 g, 4.35 mmol) was added to the solution and heated again under reflux for 18 hours. The dark brown solid was filtered, washed with ethanol and water, dried *in vacuo* and recrystallised *via* vapour diffusion in dimethylformamide-diethyl ether giving red crystals.
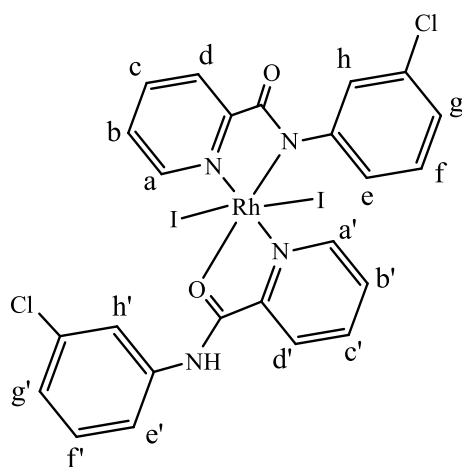
Yield: 0.160 g, 0.19 mmol, 45%. **ES+MS** (DMF, m/z): 820.8 [M+H$^+$]. **Analysis Calculated**: C 36.2; H 2.9; N 7.8%. **Analysis found** (with 0.33 molecules of DMF and H$_2$O) : C 36.2; H 2.6; N 7.7%.

IR (cm^{-1}): 3054 (b), 2865 (w), 1567 (s), 1471 (m), 1427 (w), 1343 (m), 1305 (m), 1258 (m), 1155 (m), 1074 (m), 981 (w), 875 (m), 760 (s),

676 (m), 613 (w), 497 (m), 440 (m)

¹H NMR (d_4-MeOD, 300.13 MHz, 300K) δ 9.62 (d, 1H, $^3J_{(H-H)}$ = 5.6 Hz, H_a), 8.45 (d, 1H, $^3J_{(H-H)}$ = 4.9 Hz, $H_{a'}$), 7.77 (td, 1H, $^3J_{(H-H)}$ = 7.8(x2) Hz, H_b), 7.71 (m, 1H, H_c), 7.66 (m, 1H, H_d), 7.42 (dd, 1H, $^3J_{(H-H)}$ = 8.2 Hz, $^3J_{(H-H)}$ = 1.4 Hz, $H_{d'}$), 7.36 (m, 1H, $H_{c'}$), 7.29 (ddd, 1H $^3J_{(H-H)}$ = 7.4 Hz, $^3J_{(H-H)}$ = 5.8 Hz, $^4J_{(H-H)}$ = 2 Hz, $H_{b'}$), 7.00 (s, 1H, H_h), 6.87 (t, 1H, $^3J_{(H-H)}$ = 7.1(x2) Hz, H_f), 6.7 (m, 5H, $H_{e,g,e',f',g'}$), 6.6 (s, 1H, $H_{h'}$). **¹³C{¹H} NMR** (d_4-MeOD, 75.47 MHz, 300 K) δ 194.2 (C=O of *(N,N)*-ligand), 192.50 (C=O of *(N,O)*-ligand), 191.6 (C_a), 174.2 ($C_{a'}$), 172.8 (C_i), 167.9 (C_j), 159.9 ($C_{i'}$), 157.6 ($C_{j'}$), 147.6 (C_c), 147.1 ($C_{c'}$), 135.7 (C_b), 133.4 (C_f), 132.3 (C_e), 130.5 ($C_{b'}$), 129.1 (C_g), 128.7 ($C_{g'}$), 128.1 (C_e), 127.0 ($C_{h'}$), 125.3 ($C_{f'}$), 122.0 (C_d), 118.8 (C-Cl of *(N,N)*-ligand), 117.5 ($C_{d'}$), 117.3 (C_h), 116.5 (C-Cl of *(N,O)*-ligand).

9.8.6 *Bis*(*N*-3'-bromo-picolinamide) rhodium diiodide, $RuC_{24}H_{17}I_2Br_2N_4O_2$ (5.6)

Ligand **2.12** (0.254 g, 0.91 mmol) was added to a solution of $RhCl_3$ (0.115 g, 0.48 mmol) in ethanol (30 mL), followed by triethylamine (0.06 g, 0.46 mmol). The solution heated under reflux for 2 hours giving an orange solution. An excess of potassium iodide (0.819 g, 4.93 mmol) was added to the solution and heated again under reflux for 18 hours. The dark brown solid was filtered, washed with ethanol and water, dried *in vacuo* and recrystallised *via* vapour diffusion in dimethylformamide-diethyl ether giving dark coloured microcrystals.
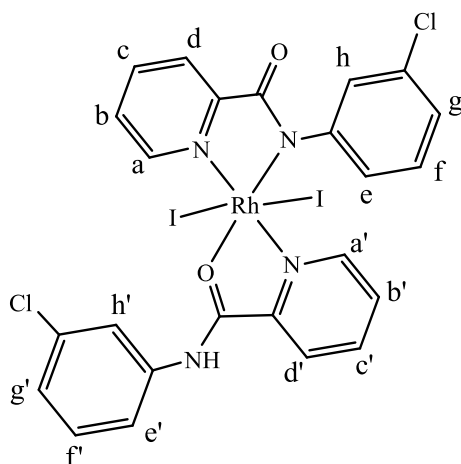
Yield: 0.156 g, 0.17 mmol, 36%. **ES+MS** (DMF, m/z): 908.7 [M+H⁺]. **Analysis Calculated**: C 26.8; H 1.6; N 5.2%. **Analysis found** (0.5 molecules of KI): C 27.2; H 1.7; N 5.0%.

IR (cm⁻¹): 3044 (b), 2919 (w), 1544 (s), 1468 (m), 1430 (w), 1343 (m), 1298 (m), 1263 (m), 1148 (m), 1059 (w), 996 (w), 924 (w), 862 (m), 783 (m), 778 (m), 678 (s), 600 (w), 562 (w), 516 (m), 514 (m), 437 (m)

^{1}H NMR (d_4-MeOD, 300.13 MHz, 300K) δ 9.96 (d, 1H, $^3J_{(H-H)}$ = 5.3 Hz, H_a), 9.62 (d, 1H, $^3J_{(H-H)}$ = 5.0 Hz, $H_{a'}$), 8.41 (d, 1H, $^3J_{(H-H)}$ = 7.6 Hz, H_d), 8.09 (m, 1H, H_b), 7.92 (d, 1H, $^3J_{(H-H)}$ = 7.9 Hz, $H_{d'}$), 7.73 (td, 1H, $^3J_{(H-H)}$ = 7.6(x2) Hz, $^4J_{(H-H)}$ = 1.8 Hz, $H_{b'}$), 7.42 (m, 2H, $H_{c,c'}$), 7.31 (dd, 1H, $^3J_{(H-H)}$ = 6.5 Hz, $^4J_{(H-H)}$ = 4.8 Hz, H_h), 7.18 (t, 1H, $^3J_{(H-H)}$ = 8.5(x2) Hz, H_f), 7.01 (m, 2H, $H_{e,g}$), 6.91 (d, 1H, $^3J_{(H-H)}$ = 8.3 Hz, $H_{e'}$). 6.87 (m, 2H, $H_{f',g'}$), 6.76 (s, 1H, $H_{h'}$). **^{13}C{^{1}H} NMR** (d_4-MeOD, 75.47 MHz, 300 K) δ 193.7 (C=O of *(N,N)*-ligand), 192.3 (C_a), 192.0 (C=O of *(N,O)*-ligand), 188.3 (C_i), 179.2 ($C_{a'}$), 173.4 (C_j), 163.0 ($C_{i'}$), 147.9 ($C_{j'}$), 142.5 (C_b), 138.9 ($C_{b',c'}$), 138.3 (C_c), 136.8 (C_f), 130.8 (C_e), 130.2 (C_g), 129.8 ($C_{f'}$), 128.9 ($C_{g'}$), 128.2 ($C_{e'}$), 126.7 (C_h), 124.2 (C_d), 123.4 ($C_{d'}$), 122.0 (C-Br of *(N,N)*-ligand), 117.4 ($C_{h'}$), 116.6 (C-Br of *(N,O)*-ligand)

9.9 Preparation of *Bis*(*N*-3'-bromo-Ph-picolinamide) ruthenium diaqua, $RuC_{24}H_{21}Br_2N_4O_4[2SbF_6]$ (8.1)

A solution of $AgSbF_6$ (0.110 g, 0.320 mmol) in acetone (1 mL) was added to a solution of complex **3.12** (0.102 g, 0.141 mmol) in dichloromethane (25 mL). The suspension was stirred overnight in the dark, and the AgCl formed was filtered off. The resulting solution was evaporated to dryness to obtain an oily residue which was recrystallised by stirring with diethyl ether.

Yield: 0.098 g, 0.08 mmol, 60%. **ES+MS** (CH_3OH, m/z): 689.8 [M+H$^+$]. **Analysis Calculated**: C 24.8; H 1.8; N 4.8%. **Analysis found**: C 24.6; H 1.9; N 4.2%. **IR (cm^{-1})**: 3284 (w), 3073 (w), 2950 (w), 1557 (s), 1467 (m), 1427 (w), 1338 (w), 1263 (w), 1229 (w), 1153 (w), 1120 (w), 1065 (w), 1030 (w), 976 (w), 765 (s), 669 (m), 593 (m), 430 (m)

9.10 Cell Culture Work

9.10.1 General Experimental Procedures

The *in vitro* tests were performed at the Institute of Cancer Therapeutics, Bradford, on A2780 (human ovarian adenocarcinoma), A2780cis (human ovarian cisplatin resistant adenocarcinoma) and HT-29 (human colon adenocarcinoma) cell lines. Standard sterile techniques were used throughout this work. Chemicals were purchased through Sigma Aldrich and were used as supplied. The stock cultures were grown in T-75 flasks containing RPMI-1640 complete cell medium (20 mL) and incubated at 37 °C

with 5.0 % CO_2. The complete media was prepared from RPMI-1640 Incomplete Media (500 mL), sodium pyruvate (5 mL, 0.5 mmol), L-glutamine (5 mL, 1.0 mmol) and foetal bovine serum (50 mL). HANKS Balanced Salt Solution was used to wash the cells, and 0.25 % Trypsin-EDTA solution was used to detach the rest of the cells from the flask. RPMI-1640 incomplete media, RPMI-1640 complete media, sodium pyruvate, MTT and MTT stock solutions were all stored at 4 °C. L-glutamine, foetal bovine serum and 0.25 % trypsin-EDTA solution were all stored at -20 °C. All chemicals except the MTT stock solution were incubated at 37 °C prior to use.

9.10.2 Cell Passaging

Cells were washed with HANKS Balanced Salt Solution (3 x 10 mL), and were carefully removed so no salt solution remained in the flask. 0.25 % Trypsin-EDTA solution (5 mL) was added and the T-75 flask was incubated at 37 °C for 5 minutes. When the cells were lifted and become detached from the flask wall, cell media (10 mL) was added. Two new flasks were prepared with cell suspension (0.5 mL) and cell media (20 mL) added to each. The lids of the flask were cracked and transferred into the incubator.

9.10.3 Cell Counting

After cells were trypsinised, each cell suspension (10 μL) was transferred to a haemocytometer, onto each side of the glass slide. Cells were counted under the microscope in five squares of the haemocytometer and an average was taken with units of 10^4 cells/mL.

9.10.4 MTT Solution

The MTT stock solution (5 mg/mL) was prepared by dissolving MTT (3-(4,5-dimethylthiazol-2-yl)-2,5-diphenyl tetrazolium bromide) (250 mg) in distilled water (50 mL), then passing through a 0.2 μm sterile filter.

9.10.5 The 5-day Cytotoxic Study (Normoxic Conditions)

The cell suspension was diluted with RPMI-1640 complete media to give a concentration of 2×10^4 cells/mL. A 96-well plate was used and 100 μL of cell media was added to lane one, to serve as a blank. 100 μL of the diluted cell suspension was then added to lanes 2 to 12, and were incubated for 24 hours at 37°C in an atmosphere of 5.0% CO_2 prior to drug exposure. The drugs to be tested were dissolved in dimethylsulfoxide and diluted further with media to obtain drug solutions ranging from 250 to 0.49 μM. The final dimethylsulfoxide concentration was 0.1% (v/v) which is non-toxic to cells. Drug solutions were applied to cells and incubated for five days at 37 °C in an atmosphere of 5% CO_2. Cell survival was determined using the MTT assay and MTT (20 μL of a 5mg/ml stock) was added to each well and incubated for 3 hours at 37°C in an atmosphere of 5% CO_2. The solutions were then removed and 150 μL of dimethylsulfoxide was added to each well to dissolve the purple formazan crystals.

9.10.6 Data Analysis

A Thermo Scientific Multiskan EX microplate photometer was used to measure the absorbance at 540 nm. Lanes containing medium only and cells in medium (no drug) were used as blanks and 100% cell survival respectively. Cell survival was determined as the absorbance of treated cells divided by the absorbance of controls and expressed as a percentage. The IC_{50} values were determined from plots of % survival against drug concentration. Each experiment was repeated three times, to give the mean of IC_{50} values and standard deviations.

9.11 The 5-day Cytotoxic Study (Hypoxic Conditions)

The hypoxic studies were carried out in a Don Whitley Scientific H35 Hypoxystation, with the oxygen level set at 0.1%, on HT-29 (human colon adenocarcinoma) cell lines. RPMI-1640 complete media was conditioned for at least 24 hours in 0.1% O_2 atmosphere prior to start of the experiment. HT-29 colon cancer cells were cultured in a 96-well plate and incubated overnight at 37 °C with 0.1% O_2 atmosphere. The cells were then exposed to different concentrations of the drugs to be tested, with a range from 250 μM to 0.49 μM, and incubated for five days at 37 °C with 0.1% O_2

atmosphere. Cell survival was then determined using the MTT assay as described previously.

9.12 Mechanistic studies

9.12.1 Hydrolysis studies

A calibration curve was prepared for each complex by dissolving in either 10% of methanol or DMF, and diluting it further with deionised water. The concentrations used were 100, 80, 60, 40 and 20 μM. The maximum absorbance (λ_{max}) was taken to plot the calibration curve of concentration against absorbance. Hydrolysis samples were prepared by dissolving complexes **3.3**, **3.5**, **3.7**, **3.10**, **3.12** and **3.14** in 10% methanol for $RuCl_2L_2$ complexes, and complexes **4.7**, **4.10**, **4.11** and **4.12** in 10% DMF for RuI_2L_2 complexes, followed by the addition of 90% deionised water to give a final concentration of 50 μM. These aqueous solutions were scanned every 24 hours by UV-Visible Spectrophotoscopy over five days at 293 K. The concentration of each complex every 24 hours was determined using its individual calibration curve. The following formula is used to calculate the percentage of hydrolysed complex,

$$\% \ hydrolysed \ complex = \left(\frac{[C]_{initial} - [C]_{final}}{[C]_{initial}} \right) x \ 100\%$$

9.12.2 Hydrophobicity tests

A calibration curve was prepared for each complex by dissolving the complexes in octanol, and diluting it further to obtain the concentrations of 100, 80, 60, 40 and 20 μM. The maximum absorbance (λ_{max}) was taken to plot the calibration curve of concentration against absorbance. Equal amounts of octanol and deionised water (containing 300mM NaCl to prevent complexes from undergoing hydrolysis) were stirred overnight for saturation and separated to obtain water-saturated octanol and octanol-saturated water solutions. Approximately 1 mg of complexes **3.2**, **3.3**, **3.5**, **3.7**, **3.10**, **3.11**, **3.12**, **3.13** and **3.14** were dissolved in 25 ml of water-saturated octanol as stock solution, and sonicated for complete dissolution. Six independent samples were prepared for each complex by adding 2 ml of octanol-saturated water, followed by 2 ml of the stock solution containing ruthenium complexes in each labelled 15 ml Falcon tubes. The samples were then shaken using the IKA Vibrax VXC basic shaker at 500

g/min for 4 hours. Organic (octanol) layer of the stock solution and from the six independent samples were taken for analysis on UV-Visible spectrophotometry. The concentration of each complex was determined using its individual calibration curve. The following formula is used to calculate the partition coefficient of the complexes (Log P),

$$Log\ P = Log\ \left(\frac{[C]_{org}}{[C]_{aq}}\right)$$

$$[C]_{aq} = [C]_{org}\ stock - [C]_{org}\ final$$

9.13 Catalytic Benzaldehyde Reduction

Isopropanol (10 ml) was added to the selected complexes (0.01 mmol Ru/Rh) in a carousel tube, followed by the addition of triethylamine (0.01 ml, 0.08 mmol). The mixture was stirred at reflux for 30 mins in order to pre-activate the catalyst. Benzaldehyde (0.1 ml, 1 mmol) was then added and the reaction was left to stir at reflux for 24 hours. Where monitoring of reaction was performed, 250 µl of the reaction sample was taken at 1, 3, 5, 7, 9 and 24 hours while maintaining the reflux. A stock solution of acetonitrile containing 0.1 mmol external standard, *n*-decane, was prepared. The samples taken from the reaction were dissolved in 1.5 ml of the acetonitrile stock solution for gas chromatography analysis.

Prior to GC analysis of the samples, benzaldehyde (0.1 ml, 1 mmol) and benzylalcohol (0.1 ml, 1 mmol) in 1.5ml of acetonitrile stock solution were run to obtain the response factor using the following formula,

$$Response\ factor = \left(\frac{area\ of\ ext.std.x\ amt.of\ substrate}{amt.of\ ext.std.x\ area\ of\ substrate}\right)$$

The retention times for benzaldehyde, *n*-decane and benzylalcohol was 4.13, 4.40 and 4.71 minutes respectively, and the response factors for benzaldehyde and benzylalcohol were 1.91 and 1.10 respectively. The following formula was used for the calculation of percentage conversion,

$$\%\ conv. = (Initial\ amt.\ of\ substrate - final\ amt.of\ substrate)\ x\ 100\%$$

9.14 Attempted Techniques for Separation of Pure Isomers

9.14.1 Column Chromatography

Recrystallised product of Ru complex was dissolved in methanol and subjected to column chromatography containing silica (10g) packed with the respective apolar solvent. Orange, dark red, light brown and light red bands were collected separately. The extracts were evaporated giving very low yield of coloured precipitates. The precipitates were recrystallised in methanol, however, a mixture of different shapes and colours of the few crystals were still obtained. The following is a list for the combination of apolar and polar solvents used with different ratios, after separation of few spots was seen on a TLC plate.

Apolar solvent	Polar solvent	Ratio (apolar:polar)
CHCl$_3$	-	-
CHCl$_3$	CH$_3$CN	1:9, 1:4, 3:1
-	CH$_3$CN	-
-	EtOAc	-
Hexane	EtOAc	1:9, 1:4, 3:1, 2:3, 1:1
C$_6$H$_6$	CH$_3$CN	1:1
Diethyl ether	-	-
Diethyl ether	CHCl$_3$	1:9, 1:4, 3:1, 2:3, 1:1

9.14.2 Syntheses following Krause and Krause Procedure

The attempted syntheses were followed using the same synthetic route of the published procedure by Krause and Krause.[19]

<u>**Isomer 1**</u>

Ligand **2.12** (0.346 g, 1.25 mmol) was added to a solution of $RuCl_3.3H_2O$ (0.160 g, 0.61 mmol) in ethanol (30 mL), followed by triethylamine (0.08 g, 0.63 mmol). The solution was heated under reflux for 2 hours giving a dark red solution. After cooling of the mixture, the red-orange precipitate was filtered and washed with ethanol and diethyl ether, and dried *in vacuo*. 0.1 g of the precipitate was finely ground, mixed with toluene and heated under reflux (30 mL) for 1 hour. The dark red precipitate was filtered hot, washed with diethyl ether, and dried *in vacuo*. Few spots were observed on TLC plate.

Yield: 0.134 g, 0.19 mmol, 30%. **ES+MS** (DMSO, m/z): 725.82 [M^+].

IR (cm^{-1}): 3067 (b), 2887 (w), 1608 (s), 1472 (m), 1414 (w), 1340 (m), 1298 (w), 1258 (m), 1134 (m), 1084 (w), 969 (w), 921 (w), 860 (s), 780 (s), 674 (s), 598 (w), 470 (m)

<u>**Isomer 2**</u>

Ligand **2.12** (0.189 g, 0.68 mmol) was added to a solution of $RuCl_2(DMSO)_4$ (0.164 g, 0.34 mmol) in acetone (30 mL). The solution was heated under reflux for 18 hours giving a dark coloured solution. Upon cooling of the mixture, the orange precipitate was filtered, washed with acetone and dried *in vacuo*. **Product expected**: $RuCl_2L_2$. **Product obtained**: $RuCl_2L(DMSO)_2$

Yield: 0.053 g, 0.09 mmol, 26%. **ES+MS** (DMSO, m/z): 606.9 [$M+H^+$]. **Analysis Calculated**: C 31.7; H 3.5; N 4.6%. **Analysis found**: C 31.9; H 3.5; N 4.5%.

IR (cm^{-1}): 3016 (b), 2891 (w), 1600 (m), 1575 (m), 1546 (m), 1479 (m), 1430 (m), 1336 (w), 1302 (w), 1287 (w), 1260 (w), 1236 (w), 1195 (w), 1165 (w), 1135 (w), 1086 (s), 1057 (w), 1008 (m), 961 (w), 924 (w), 866 (w), 804 (w), 790 (m), 757 (m), 712 (w), 679 (m), 591 (m), 547 (m), 446 (w), 424 (w).

^{1}H NMR (d_6-DMSO, 300.13 MHz, 300K) δ 11.95 (br. s, 1H, NH), 10.34 (d, 1H, $^3J_{(H-H)}$ = 5.5 Hz, pyridyl CH *ortho* to N), 8.73 (d, 1H, $^3J_{(H-H)}$ = 8.0 Hz, pyridyl H *meta* to N, *ortho* to amide), 8.34 (t, 1H, $^3J_{(H-H)}$ = 7.2(x2) Hz, pyridyl CH *para* to N), 7.98 (t, 1H, $^3J_{(H-H)}$ = 6.5(x2) Hz, pyridyl CH *para* to amide), 7.93 (s, 1H, CH *ortho* to Br and

CONH), 7.63 (d, 1H, $^3J_{(H-H)}$ = 8.2 Hz, CH *ortho* to CONH), 7.58 (m, 1H, CH *meta* to CONH), 7.53 (m, 1H, CH *para* to CONH), 3.37 (s, 6H, 2CH₃ of DMSO ligand), 3.31 (s, 6H, 2CH₃ of DMSO ligand)

Isomer 3

Product obtained from 'Isomer 2' (0.0814 g, 0.13 mmol) was mixed with 30 ml of xylenes and heated under reflux for 3 hours. When the reaction is cooled, the brown precipitate was filtered, washed with diethyl ether and dried *in vacuo*.

Product expected: $RuCl_2L_2$. **Product obtained**: $RuCl_2L(DMSO)_2$

Yield: 0.037 g, 0.06 mmol, 47%. **ES+MS** (DMSO, m/z): 606.9 [M+H⁺].

IR (cm⁻¹): 3023 (b), 2885 (w), 1592 (w), 1472 (w), 14156 (w), 1369 (w), 1196 (w), 1134 (w), 1086 (s), 995 (w), 926 (w), 868 (w), 788 (m), 757 (m), 679 (m), 590 (w), 546 (w), 429 (w).

¹H NMR (d_6-DMSO, 300.13 MHz, 300K) δ 11.94 (br. s, 1H, NH), 10.33 (d, 1H, $^3J_{(H-H)}$ = 5.5 Hz, pyridyl CH *ortho* to N), 8.72 (d, 1H, $^3J_{(H-H)}$ = 8.0 Hz, pyridyl H *meta* to N, *ortho* to amide), 8.33 (t, 1H, $^3J_{(H-H)}$ = 7.2(x2) Hz, pyridyl CH *para* to N), 7.98 (t, 1H, $^3J_{(H-H)}$ = 6.5(x2) Hz, pyridyl CH *para* to amide), 7.92 (s, 1H, CH *ortho* to Br and CONH), 7.62 (d, 1H, $^3J_{(H-H)}$ = 8.2 Hz, CH *ortho* to CONH), 7.54 (m, 2H, CH *meta* to CONH & CH *para* to CONH), 3.36 (s, 6H, 2CH₃ of DMSO ligand), 3.30 (s, 6H, 2CH₃ of DMSO ligand)

9.14.3 Extraction with Solvents

To several fractions of the Ru product, were washed with a range of solvents to obtain coloured filtrates, which were then evaporated to obtain coloured precipitates. The products were recrystallised *via* vapour diffusion in methanol/pentane to obtain crystals. The following is the list of solvents used for the attempted technique.

Solvents	Observation (colour of filtrate; precipitate; recystallised product)
Diethyl ether	Colourless filtrate
Pentane	Colourless filtrate
Petrol	Colourless filtrate
Toluene	Slightly yellow filtrate; No precipitate obtained.
Dichloromethane	Orange filtrate; Red-orange precipitate; No product obtained after recrystallisation.
Chloroform	Orange filtrate; Red precipitate; Red-orange precipitate after recrystallisation; Few spots were observed on TLC
Ethanol	Red-orange filtrate; Red-orange precipitate; Mixture of red block and orange microcrystals after recrystallisation
Ethyl Acetate	Light orange filtrate; No precipitate obtained
THF	Light orange filtrate; Dark coloured precipitate; Very low yield after recrystallisation
Acetone	Orange filtrate; No precipitate obtained

9.15 References

1.   Bruker, *OPUS Software*, 2011.

2.   Agilent, *Cary WinUV*, 2011.

3.   J. Cosier and A. M. Glazer, *J. Appl. Crystallogr.*, 1986, **19**, 105-107.

4.   Z. Otwinowski and W. Minor, *Methods Enzymol.*, ed. Charles W. Carter, Jr., Academic Press, 1997, pp. 307-326.

5.   G. M. Sheldrick, *Crystallographic Computing 3: Data Collection, Structure Determination, Proteins, and Databases*, Clarendon Press Oxford, UK, 1986.

6.   A. Altomare, G. Cascarano, C. Giacovazzo and A. Guagliardi, *J. Appl. Crystallogr.*, 1993, **26**, 343-350.

7.   A. Altomare, M. C. Burla, M. Camalli, G. L. Cascarano, C. Giacovazzo, A. Guagliardi, A. G. G. Moliterni, G. Polidori and R. Spagna, *J. Appl. Crystallogr.*, 1999, **32**, 115-119.

8.   G. M. Sheldrick and T. R. Schneider, *Methods Enzymol.*, ed. R. M. S. Charles W. Carter Jr, Academic Press, 1997, pp. 319-343.

9.   L. J. Barbour, *XSeed*, 1999.

10.   M. Thornton-Pett, *WC*, 2000.

11.   A. Spek, *J. Appl. Crystallogr.*, 2003, **36**, 7-13.

12.   O. V. Dolomanov, L. J. Bourhis, R. J. Gildea, J. A. K. Howard and H. Puschmann, *J. Appl. Crystallogr.*, 2009, **42**, 339-341.

13.   P. van der Sluis and A. L. Spek, *Acta Crystallogr., Sect. A: Found. Crystallogr.*, 1990, **46**, 194-201.

14.   Bruker AXS, *DiffracEva Suite*, 2009.

15.   J. Laugier and B. Bochu, *Chekcell*, 2004.

16.   C.C.D.C, *Mercury*, 2011.

17.   S. Dutta, S. Pal and P. K. Bhattacharya, *Polyhedron*, 1999, **18**, 2157-2162.

18.   Z. Almodares, S. J. Lucas, B. D. Crossley, A. M. Basri, C. M. Pask, A. J. Hebden, R. M. Phillips and P. C. McGowan, *Inorg. Chem.*, 2014, **53**, 727-736.

19.   R. A. Krause and K. Krause, *Inorg. Chem.*, 1980, **19**, 2600-2603.

CHAPTER 10

Conclusions and Future Work

10 Conclusions and Future Work

10.1 Conclusions

The peptide chemistry of amide ligands is of importance due to their biological role that includes protein construction and maintenance. Five novel functionalised picolinamide ligands have been synthesised using the general procedure from picolinic acid and substituted anilines. These ligands have been fully characterised by IR, NMR, mass spectrometry and elemental analysis, and where suitable crystals were obtained, analysed for x-ray crystallography, as described in Chapter 2. Their crystal structures have shown that these ligands adopt an almost planar configuration with a twist between the two planes of pyridyl ring and the aniline ring, giving a degree of flexibility to incorporate with metal centres either by *N,N-* or *N,O-* coordination.

A library of novel functionalised *bis*-picolinamide ruthenium (III) dichloride complexes have been successfully synthesised and fully characterised using IR, ES-MS, elemental analysis and single crystal X-Ray diffraction, where suitable crystals were obtained, as described in Chapter 3. These complexes were all prepared by using the same procedure and recrystallised by vapour diffusion, either from methanol/hexane or methanol/pentane. Three different types of structural isomers, which are the *cis-cis-cis, cis-trans-cis* and *trans-trans-trans* structural isomers were obtained, and have shown a distorted octahedral geometry about the ruthenium metal centre. Isomerisation studies on complex **3.7** showed insignificant changes over time and within a range of temperature. Powder diffraction patterns of complex **3.7** did not match between the bulk powder samples and crystal structures. There have been many attempts to separate the pure isomers, however has been unsuccessful. Despite the different structural isomers obtained, complex **3.1** - **3.16** have been tested against various cancer cell lines for an indication as potential anti-cancer agents, reported in Chapter 6. Selected Ru dichloride complexes were also tested as catalysts in benzaldehyde reduction, described in Chapter 8.

There have been few studies in investigating the effects of *trans* geometry, also when changing the leaving group of metal complexes towards biological activities. The diiodide analogues of *bis*-picolinamide ruthenium (III) dichloride complexes have been synthesised, by a halide exchange reaction with an excess of solid potassium iodide. They were characterised using IR, ES-MS, elemental analysis, and x-ray diffraction. Two different types of structural isomers were found for the ruthenium diiodide analogue, which are the *trans-trans-trans* and *trans-cis-cis* structural isomers. *Bis*-picolinamide Ru diiodide complexes have been studied for isomerisation in DMF solution by UV-Vis spectrophotometry, and as powder samples by powder diffraction. No changes were observed in their uv-vis spectra over a period of time and also, when decreasing temperature from 100°C to 0°C. Comparison between a diffractogram simulated from single crystal data of the ruthenium diiodide complex and a diffractogram recorded from its powder sample have also shown no differences in their peaks, and very well matches the unit cell between both data, showing the evidence of stability for *trans*-ruthenium diiodide complexes both in solution and powder. These complexes are tested against A2780 and HT-29 cancer cell lines for cytotoxicity to determine their potential as anti-cancer agents (Chapter 6), as well as, their application as catalysts in benzaldehyde reduction (Chapter 8).

Novel *bis*-picolinamide rhodium (III) dihalide complexes with *meta*-functionalisation on the phenyl ring of the picolinamide ligands were also synthesised and characterised in Chapter 5. These complexes are the analogues of the *bis*-picolinamide ruthenium dihalide complexes and were prepared to specifically study the possible isomerisation of the complex, both in solid state and in solution. The rhodium complexes were synthesised following the same procedure as the preparation of the ruthenium analogues, and were crystallised either with methanol/pentane or dimethylformamide/ether. Two different types of structural isomers were obtained, which are the *cis-trans-cis* for the rhodium dichloride complexes, and *trans-trans-trans* for the rhodium diiodide complexes. The ^{1}H NMR studies of the rhodium dichloride complex **5.3** have shown to have a mixture of isomers with different ratios when in solution. The highest ratio obtained is that of the *cis-trans-cis* complex. These

isomers are found to be stable and do not undergo any structural changes over days at room temperature. The changes of shifts and signals seen in the NMR temperature-dependant study were the possible stacking of the complex molecules. The signals showed broad peaks when at low temperature and sharpens when the temperature is increased, as the molecules became separated from each other. The ^{1}H NMR spectrum of complex **5.3** is in contrast with the rhodium diiodide complex **5.5** which has only shown one possible structure in solution, which is the *trans-trans-trans*. Powder diffraction studies on both complexes **5.3** and **5.5**, however, were inconclusive as to insufficient data obtained. Although, the diffractograms of complex **5.5** have shown a similar pattern and may possibly have only one structural geometry both in the powder sample and in solution. *Bis*-picolinamide rhodium complexes **5.1** - **5.6** were tested for their catalytic applications in benzaldehyde reduction with comparison to the ruthenium analogues, and these are reported in Chapter 8. Due to limited access to perform cell culture studies at Institute Cancer Therapeutics, Bradford, rhodium dihalide complexes were not tested for cytotoxicity in this thesis.

A series of functionalised *bis*-picolinamide ruthenium dihalide complexes were tested for cytotoxicity against three different cancer cell lines, A2780 ovarian, A2780cis ovarian cisplatin-resistant and HT-29 colon cancer cell lines. Their cytotoxicity was determined following the general procedure used at the cell culture lab, which is a 5-day drug exposure MTT assay. Shorter incubation times often shows a very low potency of the drug, hence 5-day incubation time was used in the assay. This assay allowed the IC_{50} values of the drugs to be calculated. The cytotoxicity of *bis*-picolinamide ruthenium dihalide complexes is affected by the halide ligands that are bonded to the ruthenium metal centre, as most of the ruthenium diiodide complexes are seen to be highly potent than their chloride analogues. The different halide substituents attached on the phenyl ring of the picolinamide ligands are dependent on their position on the ring. Complexes with *meta* or *para* chloro and bromo substituents are more cytotoxic when compared with other functionalised complexes in the series. The complexes are also seen to be selective in different cancer cell lines. Some of the complexes have increased in their anti-cancer activity when in the HT-29 cell line,

suggesting that they are specific for targeting cancer cells. From the hypoxic cytotoxicity studies, the activities of the complexes are seen to be comparable to cisplatin and TPZ. They are also potent under both normoxic and hypoxic conditions, suggesting that they are independent towards the hypoxic environment. Complexes **4.8** and **4.13** are the two most promising anti-cancer complexes in the series of *bis*-picolinamide ruthenium dihalide complexes.

Following the cytotoxicity studies on *bis*-picolinamide ruthenium dihalide complexes against A2780 ovarian and HT-29 colon cancer cell lines, selected complexes from this series were examined for further structural-activity relationship studies. Hydrolysis and hydrophobicity tests have been conducted for the selected complexes with interesting results and observations. The UV-Vis hydrolysis study taken over a period of five days showed changes of peak intensity and absorbances, indicating that substitution reactions have taken place between the monosubstituted halide ligands attached on the ruthenium metal centre of the neutral complex and water molecules from the aqueous sample solution. The exchange of ligands was confirmed by ESI-MS analysis at day 5 which has shown the presence of di-aqua and mono-aqua ruthenium complexes. Their fitted kinetic curve between time and percentage of hydrolysed complex have shown that the ruthenium dichloride complexes are very well correlated with their cytotoxic activity whereby the most cytotoxic complex hydrolyses more and undergoes the fastest hydrolysis. This is in contrast with the ruthenium diiodide complexes which have shown the opposite correlation, by which the most cytotoxic complex undergoes the least hydrolysis after five days. These results suggest that hydrolysis may be one of the major mechanisms in anti-cancer activity for ruthenium dichloride complexes, but may not be for the diiodide analogues. Ruthenium dichloride complexes have shown to have hydrophobic properties with acceptable log P values according to Lipinski's rule of five and Hansch's principle of minimum hydrophobicity, suggesting that these complexes may possibly enter the cells by passive diffusion. Although, there are very few correlations observed between the cytotoxicity and log P values of the ruthenium dichloride complexes, which are not as comparable as the platinum complexes that have shown their cytotoxicity increases

with increasing hydrophobicity. This could also suggest that the cell uptake mechanism of *bis*-picolinamide ruthenium dichloride complexes may not relate to their cytotoxic anti-cancer activities. The potential for the complexes to bind with specific transporters within the cell membrane may contribute to their cell uptake mechanism that could also relate to their cytotoxic activity.

Several *bis*-picolinamide metal dihalide complexes have been studied as catalysts in the reduction of benzaldehyde. The reactions were performed in an excess of isopropanol in the presence of a base, Et_3N, and heated under reflux for 24 hours. The complexes that were selected for the studies have several components that can be used to investigate their structural-activity relationship in catalytic benzaldehyde reductions. Both the starting materials, $RuCl_3.3H_2O$ and $RuCl_3.3H_2O$ have showed no activities in the reaction. Whereas, when picolinamide ligands are coordinated to the metal centre, their catalytic activities increase depending on the halide ligands that are attached to the metal centre, and the halide substituents that are attached on the phenyl ring of the picolinamide ligands. In general, the diiodide analogues of the catalysts are more active than the dichloride analogues. In combination of the dihalide ligands with the appropriate functionalised picolinamide ligands can improve their catalytic activities. However, having a halide substituent at the *meta* position on the phenyl ring of the picolinamide ligands only showed low to moderate catalytic activities. The highest percentage conversion is seen for complex **4.9** that consists of diiodide ligands and *bis*-2',4'dichloro picolinamide ligands coordinated to the Ru metal centre. There is a contrasting activity seen between Ru and Rh catalysts, whereby their catalytic activities are affected by different components of the catalysts. Ru catalyst may be largely affected by the different functionalised picolinamide ligands (**Figure 8.6**), whereas Rh catalysts have showed more difference when changing the X ligands (**Figure 8.10**).

10.2   Future Work

Further analysis for the structural isomers of *bis*-picolinamide ruthenium dihalide complexes will include variable-dependant solution studies by Electron Paramagnetic Resonance (EPR) spectroscopy. This is to investigate whether the complexes undergo isomerisation when in solution over time and temperature. Further attempts to separate the mixtures of isomers are necessary to obtain pure products of each isomer for further study in structural characterisation. As for *bis*-picolinamide rhodium dihalide complexes, the attempt to obtain single crystals of different molecular structural isomers can give more data in comparison with the collected data for ^{1}H NMR characterisation and PXRD powder diffraction studies. Cytotoxicity studies on *bis*-picolinamide rhodium dihalide complexes will also be added as future work for studies as comparison with its ruthenium analogue.

Bis-picolinamide ruthenium dihalide complexes are novel and little is known about ruthenium complexes with *trans*-dihalide ligands that are potent both in normoxic and hypoxic conditions. Further studies on *bis*-picolinamide ruthenium dihalide complexes can develop towards a better understanding on their structural-activity relationships as potential anti-cancer drugs. The studies may include isolating the ruthenium aqua complex, followed by cytotoxicity study, to further prove that hydrolysis is one of its anti-cancer mechanisms. Also, time-dependant cell uptake studies in order to measure the pharmacokinetics of the drug by measuring the intracellular concentration for prolonged incubation time. Temperature-dependant cell uptake studies is also important to indicate the transport mechanism of the drug into the cells, either passive diffusion or active transport. Another study that will be helpful is cell fractionation study, in order to determine the major drug distribution within the cells that could relate to its anti-cancer activity: cytoplasm (e.g. mitochondria), cell membrane (e.g. protein receptor), nucleus (e.g. DNA binding) and cytoskeleton (e.g. tubulin polymerisation). *In vivo* drug accumulation in an experimental model is also an important study to aim for clinical potential anti-cancer drugs, especially for complex **4.13** which is the most potent in the series of *bis*-picolinamide ruthenium dihalide complexes.

Catalytic work on the ruthenium and rhodium dihalide complexes is the initial step of *bis*-picolinamide Ru and Rh complexes towards catalytic applications. In order to extend this work further, various studies could include catalytic screening for a larger library of *bis*-picolinamide Ru and Rh catalysts in order to have a better understanding in the correlation between the structure and activity. As well as, catalytic study of different transfer hydrogenation reactions, for example reductions in acetophenone, or redox neutral alkylation of *tert*-butylamine

APPENDIX

Crystal data and structure refinement for Ligand **2.13**

Formula	$C_{12}H_9BrN_2O$
Formula weight	277.12
Size	0.27 x 0.24 x 0.06 mm
Crystal morphology	Colourless Prism
Temperature	150(2) K
Wavelength	0.71073 Å [Mo-K_α]
Crystal system	Triclinic
Space group	$P\ \bar{1}$
Unit cell dimensions	$a = 6.3232(10)$ Å $\quad \alpha = 89.585(10)°$
	$b = 8.2665(15)$ Å $\quad \beta = 87.599(9)°$
	$c = 11.1055(19)$ Å $\quad \gamma = 78.366(10)°$
Volume	568.07(17) Å^3
Z	2
Density (calculated)	1.62 Mg/m^3
Absorption coefficient	3.597 mm^{-1}
$F(000)$	276
Data collection range	$1.84 \leq \theta \leq 30.22°$
Index ranges	$-8 \leq h \leq 8,\ -11 \leq k \leq 11,\ -15 \leq l \leq 15$
Reflections collected	19736
Independent reflections	3323 [$R(\text{int}) = 0.1295$]
Observed reflections	1653 [$I > 2\sigma(I)$]
Absorption correction	none
Max. and min. transmission	0.8131 and 0.4435
Refinement method	Full
Data / restraints / parameters	3323 / 0 / 145
Goodness of fit	1.045
Final R indices [$I > 2\sigma(I)$]	$R_1 = 0.0953,\ wR_2 = 0.2291$
R indices (all data)	$R_1 = 0.1859,\ wR_2 = 0.287$
Largest diff. peak and hole	2.096 and -1.586e.Å^{-3}

Crystal data and structure refinement for Ligand **2.15**

Formula	$C_{12}H_8Br_2N_2O$
Formula weight	356.02
Size	0.25 x 0.06 x 0.03 mm
Crystal morphology	Colourless Needle
Temperature	150(2) K
Wavelength	0.71073 Å [Mo-K_α]
Crystal system	Monoclinic
Space group	$P2_1/c$
Unit cell dimensions	$a = 4.3255(10)$ Å $\quad \alpha = 90°$
	$b = 20.510(6)$ Å $\quad \beta = 106.851(12)°$
	$c = 14.314(4)$ Å $\quad \gamma = 90°$
Volume	1215.4(6) Å^3
Z	4
Density (calculated)	1.946 Mg/m^3
Absorption coefficient	6.653 mm^{-1}
$F(000)$	688
Data collection range	$2.48 \leq \theta \leq 18.663°$
Index ranges	$-5 \leq h \leq 5, \ -29 \leq k \leq 29, \ -20 \leq l \leq 20$
Reflections collected	13083
Independent reflections	8192 [R(int) = 0.2137]
Observed reflections	1402 [$I > 2\sigma(I)$]
Absorption correction	multi-scan
Max. and min. transmission	0.8254 and 0.2871
Refinement method	Full
Data / restraints / parameters	3125 / 0 / 154
Goodness of fit	0.959
Final R indices [$I > 2\sigma(I)$]	$R_1 = 0.0847, wR_2 = 0.1825$
R indices (all data)	$R_1 = 0.1974, wR_2 = 0.2781$
Largest diff. peak and hole	1.751 and -1.185e.Å^{-3}

Crystal data and structure refinement for Complex **3.1a**

Formula	$C_{25}H_{23}Cl_2N_4O_3Ru$
Formula weight	599.44
Size	0.3255 x 0.0394 x 0.0296 mm
Crystal morphology	Red needle
Temperature	100.01(10) K
Wavelength	0.7107 Å [Mo -K_α]
Crystal system	Monoclinic
Space group	$P2_1/c$
Unit cell dimensions	$a = 15.7095(6)$ Å $\quad \alpha = 90°$
	$b = 8.3304(3)$ Å $\quad \beta = 93.397(3)°$
	$c = 18.7473(6)$ Å $\quad \gamma = 90°$
Volume	2449.08(15) Å^3
Z	4
Density (calculated)	1.626 Mg/m^3
Absorption coefficient	0.894 mm^{-1}
F(000)	1212
Data collection range	$2.18 \leq \theta \leq 29.76°$
Index ranges	$-20 \leq h \leq 20$, $-10 \leq k \leq 11$, $-24 \leq l \leq 24$
Reflections collected	28232
Independent reflections	6313 [R(int) = 0.0706]
Observed reflections	5118 [$I > 2\sigma(I)$]
Absorption correction	multi-scan
Max. and min. transmission	1 and 0.60303
Refinement method	Full
Data / restraints / parameters	6313 / 0 / 317
Goodness of fit	1.143
Final R indices [$I > 2\sigma(I)$]	$R_1 = 0.0681$, $wR_2 = 0.1319$
R indices (all data)	$R_1 = 0.0881$, $wR_2 = 0.1403$
Largest diff. peak and hole	2.021 and -0.865e.Å^{-3}

Crystal data and structure refinement for Complex **3.1b**

Formula	$C_{25}H_{23}Cl_2N_4O_3Ru$
Formula weight	599.44
Size	0.3255 x 0.0394 x 0.0296 mm
Crystal morphology	Red needle
Temperature	100.01(10) K
Wavelength	0.7107 Å [Mo -K_α]
Crystal system	Monoclinic
Space group	$P2_1/c$
Unit cell dimensions	$a = 15.7095(6)$ Å $\alpha = 90°$
	$b = 8.3304(3)$ Å $\beta = 93.397(3)°$
	$c = 18.7473(6)$ Å $\gamma = 90°$
Volume	2449.08(15) Å^3
Z	4
Density (calculated)	1.626 Mg/m^3
Absorption coefficient	0.894 mm^{-1}
F(000)	1212
Data collection range	$2.18 \leq \theta \leq 29.76°$
Index ranges	$-20 \leq h \leq 20,\ -10 \leq k \leq 11,\ -24 \leq l \leq 24$
Reflections collected	28232
Independent reflections	6313 [R(int) = 0.0706]
Observed reflections	5118 [$I > 2\sigma(I)$]
Absorption correction	multi-scan
Max. and min. transmission	1 and 0.60303
Refinement method	Full
Data / restraints / parameters	6313 / 0 / 317
Goodness of fit	1.143
Final R indices [$I > 2\sigma(I)$]	$R_1 = 0.0681, wR_2 = 0.1319$
R indices (all data)	$R_1 = 0.0881, wR_2 = 0.1403$
Largest diff. peak and hole	2.021 and -0.865e.Å^{-3}

Crystal data and structure refinement for Complex **3.3**

Formula	$C_{24}H_{17}Cl_2F_2N_4O_2Ru$
Formula weight	603.39
Size	0.08 x 0.07 x 0.03 mm
Crystal morphology	Red prism
Temperature	100.01(10) K
Wavelength	0.7107 Å [Mo -K_α]
Crystal system	Monoclinic
Space group	$P2_1/n$
Unit cell dimensions	$a = 10.1863(5)$ Å $\quad \alpha = 90°$
	$b = 12.7202(6)$ Å $\quad \beta = 95.399(5)°$
	$c = 17.8694(10)$ Å $\quad \gamma = 90°$
Volume	2305.1(2) Å^3
Z	4
Density (calculated)	1.739 Mg/m^3
Absorption coefficient	0.959 mm^{-1}
F(000)	1204
Data collection range	$1.97 \le \theta \le 26.37°$
Index ranges	$-12 \le h \le 9, \; -12 \le k \le 15, \; -22 \le l \le 20$
Reflections collected	10765
Independent reflections	4718 [R(int) = 0.0501]
Observed reflections	3653 [$I > 2\sigma(I)$]
Absorption correction	multi-scan
Max. and min. transmission	1 and 0.79922
Refinement method	Full
Data / restraints / parameters	4718 / 0 / 316
Goodness of fit	1.021
Final R indices [$I > 2\sigma(I)$]	$R_1 = 0.0484, wR_2 = 0.0993$
R indices (all data)	$R_1 = 0.0688, wR_2 = 0.1116$
Largest diff. peak and hole	0.911 and -0.903e.Å^{-3}

Crystal data and structure refinement for Complex **3.5**

Formula	$C_{25}H_{19}Cl_2F_4N_4O_3Ru$
Formula weight	671.41
Size	0.45 x 0.09 x 0.02 mm
Crystal morphology	Red Plate
Temperature	150(2) K
Wavelength	0.71073 Å [Mo-K_α]
Crystal system	Triclinic
Space group	$P\ \bar{1}$
Unit cell dimensions	$a = 8.5290(11)$ Å $\quad \alpha = 89.670(5)°$
	$b = 8.6964(14)$ Å $\quad \beta = 78.981(5)°$
	$c = 17.728(3)$ Å $\quad \gamma = 89.770(5)°$
Volume	1290.6(3) Å^3
Z	2
Density (calculated)	1.728 Mg/m^3
Absorption coefficient	0.88 mm^{-1}
$F(000)$	670
Data collection range	$2.61 \le \theta \le 30.42°$
Index ranges	$-10 \le h \le 8,\ -12 \le k \le 12,\ -25 \le l \le 24$
Reflections collected	13034
Independent reflections	6035 [R(int) = 0.0438]
Observed reflections	4950 [$I > 2\sigma(I)$]
Absorption correction	multi-scan
Max. and min. transmission	0.9826 and 0.909
Refinement method	Full
Data / restraints / parameters	6035 / 0 / 354
Goodness of fit	1.101
Final R indices [$I > 2\sigma(I)$]	$R_1 = 0.0452, wR_2 = 0.1261$
R indices (all data)	$R_1 = 0.0611, wR_2 = 0.1368$
Largest diff. peak and hole	0.949 and -2.055e.Å^{-3}

Crystal data and structure refinement for Complex **3.6**

Formula	$C_{49.25}H_{39}Cl_8N_8O_{5.25}Ru_2$
Formula weight	1312.62
Size	0.71 x 0.71 x 0.24 mm
Crystal morphology	Red Fragment
Temperature	150.15 K
Wavelength	0.71073 Å [Mo-K_α]
Crystal system	Monoclinic
Space group	$P2_1/c$
Unit cell dimensions	$a = 20.4382(12)$ Å $\quad \alpha = 90°$
	$b = 15.1424(8)$ Å $\quad \beta = 113.339(3)°$
	$c = 19.7673(11)$ Å $\quad \gamma = 90°$
Volume	5617.1(5) Å^3
Z	4
Density (calculated)	1.552 Mg/m^3
Absorption coefficient	0.97 mm^{-1}
$F(000)$	2626
Data collection range	$1.75 \leq \theta \leq 26.39°$
Index ranges	$-25 \leq h \leq 25, \ -14 \leq k \leq 18, \ -24 \leq l \leq 24$
Reflections collected	52269
Independent reflections	11441 [R(int) = 0.0715]
Observed reflections	7153 [$I > 2\sigma(I)$]
Absorption correction	multi-scan
Max. and min. transmission	0.8006 and 0.5459
Refinement method	Full
Data / restraints / parameters	11441 / 14 / 624
Goodness of fit	1.005
Final R indices [$I > 2\sigma(I)$]	$R_1 = 0.0535, wR_2 = 0.1271$
R indices (all data)	$R_1 = 0.1071, wR_2 = 0.1524$
Largest diff. peak and hole	1.389 and -0.997e.Å^{-3}

Crystal data and structure refinement for Complex **3.7a**

Formula	$C_{25}H_{21}Cl_4N_4O_3Ru$
Formula weight	668.33
Size	0.1155 x 0.0697 x 0.0438 mm
Crystal morphology	Red needle
Temperature	100.00(10) K
Wavelength	0.7107 Å [Mo -K_α]
Crystal system	Triclinic
Space group	$P\ \bar{1}$
Unit cell dimensions	$a = 8.5066(5)$ Å $\alpha = 88.281(5)°$
	$b = 10.1491(6)$ Å $\beta = 86.551(5)°$
	$c = 15.1443(9)$ Å $\gamma = 83.546(5)°$
Volume	1296.48(13) Å^3
Z	2
Density (calculated)	1.712 Mg/m^3
Absorption coefficient	1.053 mm^{-1}
F(000)	670
Data collection range	$2.02 \le \theta \le 26.37°$
Index ranges	$-9 \le h \le 10,\ -12 \le k \le 12,\ -18 \le l \le 13$
Reflections collected	10188
Independent reflections	5316 [R(int) = 0.0406]
Observed reflections	4258 [$I > 2\sigma(I)$]
Absorption correction	multi-scan
Max. and min. transmission	1 and 0.89396
Refinement method	Full
Data / restraints / parameters	5316 / 0 / 336
Goodness of fit	1.038
Final R indices [$I > 2\sigma(I)$]	$R_1 = 0.0419$, $wR_2 = 0.0718$
R indices (all data)	$R_1 = 0.0573$, $wR_2 = 0.0815$
Largest diff. peak and hole	0.491 and -0.478e.Å^{-3}

Crystal data and structure refinement for Complex **3.7b**

Formula	$C_{24}H_{17}Cl_4N_4O_2Ru$
Formula weight	636.29
Size	0.35 x 0.3 x 0.09 mm
Crystal morphology	Red Prism
Temperature	150(2) K
Wavelength	0.71073 Å [Mo-K_α]
Crystal system	Monoclinic
Space group	$P2_1/n$
Unit cell dimensions	$a = 7.9504(11)$ Å $\alpha = 90°$
	$b = 16.070(2)$ Å $\beta = 95.268(7)°$
	$c = 24.526(3)$ Å $\gamma = 90°$
Volume	3120.2(7) Å^3
Z	4
Density (calculated)	1.354 Mg/m^3
Absorption coefficient	0.869 mm^{-1}
$F(000)$	1268
Data collection range	$2.09 \leq \theta \leq 30.42°$
Index ranges	$-11 \leq h \leq 11, \ 0 \leq k \leq 22, \ 0 \leq l \leq 34$
Reflections collected	9430
Independent reflections	9430
Observed reflections	8291 [$I > 2\sigma(I)$]
Absorption correction	multi-scan
Max. and min. transmission	0.9259 and 0.7506
Refinement method	Full
Data / restraints / parameters	9430 / 0 / 316
Goodness of fit	1.105
Final R indices [$I > 2\sigma(I)$]	$R_1 = 0.0315, \ wR_2 = 0.0809$
R indices (all data)	$R_1 = 0.038, \ wR_2 = 0.084$
Largest diff. peak and hole	1.178 and -0.583e.Å^{-3}

Crystal data and structure refinement for Complex **3.9**

Formula	$C_{25}H_{19}Cl_6N_4O_3Ru$
Formula weight	737.21
Size	0.18 x 0.11 x 0.04 mm
Crystal morphology	Red Cuboid
Temperature	150(2) K
Wavelength	0.71073 Å [Mo-K_α]
Crystal system	Triclinic
Space group	$P\ \bar{1}$
Unit cell dimensions	$a = 9.3548(12)$ Å $\quad \alpha = 104.592(5)°$
	$b = 12.7693(15)$ Å $\quad \beta = 98.755(5)°$
	$c = 13.3128(15)$ Å $\quad \gamma = 100.683(5)°$
Volume	1478.8(3) $Å^3$
Z	2
Density (calculated)	1.656 Mg/m^3
Absorption coefficient	1.107 mm^{-1}
$F(000)$	734
Data collection range	$1.62 \le \theta \le 37.62°$
Index ranges	$-15 \le h \le 15,\ -20 \le k \le 21,\ -22 \le l \le 22$
Reflections collected	49310
Independent reflections	14172 [R(int) = 0.0361]
Observed reflections	10930 [$I > 2\sigma(I)$]
Absorption correction	multi-scan
Max. and min. transmission	0.9571 and 0.8257
Refinement method	Full
Data / restraints / parameters	14172 / 0 / 354
Goodness of fit	1.029
Final R indices [$I > 2\sigma(I)$]	$R_1 = 0.0394$, $wR_2 = 0.0944$
R indices (all data)	$R_1 = 0.0603$, $wR_2 = 0.1036$
Largest diff. peak and hole	1.477 and -1.38e.$Å^{-3}$

Crystal data and structure refinement for Complex **3.11**

Formula	$C_{25}H_{21}Br_2Cl_2N_4O_3Ru$
Formula weight	757.25
Size	0.32 x 0.18 x 0.09 mm
Crystal morphology	Red Fragment
Temperature	150(2) K
Wavelength	0.71073 Å [Mo-K_α]
Crystal system	Monoclinic
Space group	$P2_1/c$
Unit cell dimensions	$a = 8.6661(9)$ Å $\quad$ $\alpha = 90°$
	$b = 18.3450(17)$ Å $\quad$ $\beta = 114.132(6)°$
	$c = 19.1648(18)$ Å $\quad$ $\gamma = 90°$
Volume	2780.5(5) Å^3
Z	4
Density (calculated)	1.809 Mg/m^3
Absorption coefficient	3.664 mm^{-1}
$F(000)$	1484
Data collection range	$1.61 \leq \theta \leq 31.8°$
Index ranges	$-12 \leq h \leq 12,\ -26 \leq k \leq 27,\ -28 \leq l \leq 28$
Reflections collected	106652
Independent reflections	9463 [R(int) = 0.0451]
Observed reflections	7657 [$I > 2\sigma(I)$]
Absorption correction	multi-scan
Max. and min. transmission	0.7339 and 0.3868
Refinement method	Full
Data / restraints / parameters	9463 / 0 / 336
Goodness of fit	1.147
Final R indices $[I > 2\sigma(I)]$	$R_1 = 0.0427$, $wR_2 = 0.1033$
R indices (all data)	$R_1 = 0.0594$, $wR_2 = 0.111$
Largest diff. peak and hole	1.659 and -1.494e.Å^{-3}

Crystal data and structure refinement for Complex **3.12**

Formula	$C_{24}H_{17}Br_2Cl_2N_4O_2Ru$
Formula weight	725.21
Size	0.18 x 0.1 x 0.01 mm
Crystal morphology	Red Cuboid
Temperature	150(2) K
Wavelength	0.71073 Å [Mo-K_α]
Crystal system	Monoclinic
Space group	$P2_1/n$
Unit cell dimensions	$a = 8.0068(6)$ Å $\alpha = 90°$
	$b = 16.0313(11)$ Å $\beta = 93.717(4)°$
	$c = 24.677(2)$ Å $\gamma = 90°$
Volume	3160.9(4) Å^3
Z	4
Density (calculated)	1.524 Mg/m^3
Absorption coefficient	3.218 mm^{-1}
$F(000)$	1412
Data collection range	$2.09 \leq \theta \leq 30.42°$
Index ranges	$-11 \leq h \leq 11$, $-21 \leq k \leq 22$, $-35 \leq l \leq 35$
Reflections collected	55509
Independent reflections	9479 [R(int) = 0.0927]
Observed reflections	7580 [$I > 2\sigma(I)$]
Absorption correction	multi-scan
Max. and min. transmission	0.9624 and 0.5951
Refinement method	Full
Data / restraints / parameters	9479 / 0 / 316
Goodness of fit	1.048
Final R indices [$I > 2\sigma(I)$]	$R_1 = 0.0399$, $wR_2 = 0.0945$
R indices (all data)	$R_1 = 0.0535$, $wR_2 = 0.1009$
Largest diff. peak and hole	1.343 and -0.997e.Å^{-3}

Crystal data and structure refinement for Complex **3.13**

Formula	$C_{25}H_{20}Br_2Cl_2N_4O_3Ru$
Formula weight	756.24
Size	0.1505 x 0.0675 x 0.0396 mm
Crystal morphology	Orange needle
Temperature	100.01(10) K
Wavelength	0.7107 Å [Mo -K_α]
Crystal system	Triclinic
Space group	$P\ \bar{1}$
Unit cell dimensions	$a = 11.1486(11)$ Å $\alpha = 103.937(9)°$
	$b = 11.3608(13)$ Å $\beta = 108.713(9)°$
	$c = 12.3471(12)$ Å $\gamma = 103.653(9)°$
Volume	1351.5(2) Å^3
Z	2
Density (calculated)	1.858 Mg/m^3
Absorption coefficient	3.769 mm^{-1}
$F(000)$	740
Data collection range	$1.85 \le \theta \le 29.83°$
Index ranges	$-15 \le h \le 15,\ -14 \le k \le 12,\ -15 \le l \le 17$
Reflections collected	13453
Independent reflections	6362 [R(int) = 0.0686]
Observed reflections	4245 [$I > 2\sigma(I)$]
Absorption correction	multi-scan
Max. and min. transmission	1 and 0.94213
Refinement method	Full
Data / restraints / parameters	6362 / 0 / 336
Goodness of fit	1.01
Final R indices [$I > 2\sigma(I)$]	$R_1 = 0.0617, wR_2 = 0.0819$
R indices (all data)	$R_1 = 0.109, wR_2 = 0.0938$
Largest diff. peak and hole	0.828 and -0.886e.Å^{-3}

Crystal data and structure refinement for Complex **3.15**

Formula	$C_{26}H_{23}Br_4Cl_2N_4O_4Ru$
Formula weight	947.09
Size	0.18 x 0.14 x 0.09 mm
Crystal morphology	Red Fragment
Temperature	150(2) K
Wavelength	0.71073 Å [Mo-K_α]
Crystal system	Monoclinic
Space group	$P2_1/c$
Unit cell dimensions	$a = 14.508(3)$ Å $\quad \alpha = 90°$
	$b = 17.366(3)$ Å $\quad \beta = 116.143(6)°$
	$c = 14.786(3)$ Å $\quad \gamma = 90°$
Volume	3344.2(11) Å^3
Z	4
Density (calculated)	1.881 Mg/m^3
Absorption coefficient	5.444 mm^{-1}
$F(000)$	1828
Data collection range	$1.56 \leq \theta \leq 29.61°$
Index ranges	$-20 \leq h \leq 20, \ -23 \leq k \leq 24, \ -20 \leq l \leq 20$
Reflections collected	55567
Independent reflections	9366 [R(int) = 0.0621]
Observed reflections	6995 [$I > 2\sigma(I)$]
Absorption correction	multi-scan
Max. and min. transmission	0.64 and 0.4407
Refinement method	Full
Data / restraints / parameters	9366 / 0 / 374
Goodness of fit	1.033
Final R indices [$I > 2\sigma(I)$]	$R_1 = 0.0392, wR_2 = 0.1002$
R indices (all data)	$R_1 = 0.0611, wR_2 = 0.1082$
Largest diff. peak and hole	1.306 and -0.957e.Å^{-3}

Crystal data and structure refinement for Complex **3.16a**

Formula	$C_{25}H_{21}Cl_2I_2N_4O_3Ru$
Formula weight	851.23
Size	0.1 x 0.07 x 0.02 mm
Crystal morphology	Red block
Temperature	100.00(10) K
Wavelength	1.5418 Å [Cu -K_α]
Crystal system	Orthorhombic
Space group	$P2_12_12_1$
Unit cell dimensions	$a = 8.4296(8)$ Å $\alpha = 90°$
	$b = 17.8286(11)$ Å $\beta = 90°$
	$c = 18.1388(11)$ Å $\gamma = 90°$
Volume	2726.1(3) Å^3
Z	4
Density (calculated)	2.074 Mg/m^3
Absorption coefficient	24.54 mm^{-1}
$F(000)$	1628
Data collection range	$3.48 \le \theta \le 74.15°$
Index ranges	$-9 \le h \le 10$, $-20 \le k \le 21$, $-22 \le l \le 15$
Reflections collected	7629
Independent reflections	4785 [R(int) = 0.0631]
Observed reflections	4012 [$I > 2\sigma(I)$]
Absorption correction	multi-scan
Max. and min. transmission	1 and 0.87282
Refinement method	Full
Data / restraints / parameters	4785 / 0 / 337
Goodness of fit	1.036
Final R indices [$I > 2\sigma(I)$]	$R_1 = 0.0618$, $wR_2 = 0.1391$
R indices (all data)	$R_1 = 0.0766$, $wR_2 = 0.1491$
Largest diff. peak and hole	1.82 and -1.6e.Å^{-3}

Crystal data and structure refinement for Complex **3.16b**

Formula	$C_{24}H_{17}Cl_2I_2N_4O_2Ru$
Formula weight	819.19
Size	0.02 x 0.008 x 0.008 mm
Crystal morphology	Orange needle
Temperature	100.00(10) K
Wavelength	0.7107 Å [Mo -K_α]
Crystal system	Monoclinic
Space group	$P2_1/n$
Unit cell dimensions	$a = 12.1869(4)$ Å $\quad \alpha = 90°$
	$b = 16.5955(5)$ Å $\quad \beta = 93.836(3)°$
	$c = 12.6592(4)$ Å $\quad \gamma = 90°$
Volume	2554.56(14) Å^3
Z	4
Density (calculated)	2.13 Mg/m^3
Absorption coefficient	3.27 mm^{-1}
F(000)	1556
Data collection range	$2.03 \leq \theta \leq 25.03°$
Index ranges	$-13 \leq h \leq 14, \ -17 \leq k \leq 19, \ -14 \leq l \leq 15$
Reflections collected	11805
Independent reflections	4510 [R(int) = 0.0405]
Observed reflections	3703 [$I > 2\sigma(I)$]
Absorption correction	multi-scan
Max. and min. transmission	1 and 0.75701
Refinement method	Full
Data / restraints / parameters	4510 / 95 / 326
Goodness of fit	1.039
Final R indices [$I > 2\sigma(I)$]	$R_1 = 0.0344, wR_2 = 0.0619$
R indices (all data)	$R_1 = 0.0483, wR_2 = 0.0679$
Largest diff. peak and hole	0.875 and -0.682e.Å^{-3}

Crystal data and structure refinement for Complex **4.2**

Formula	$C_{24}H_{16}F_2I_2N_4O_2Ru$
Formula weight	785.28
Size	0.24 x 0.22 x 0.19 mm
Crystal morphology	Black block
Temperature	100.01(10) K
Wavelength	0.71073 Å [Mo-K_α]
Crystal system	Orthorhombic
Space group	$Pna2_1$
Unit cell dimensions	$a = 19.4788(15)$ Å $\quad \alpha = 90°$
	$b = 10.3583(11)$ Å $\quad \beta = 90°$
	$c = 12.0324(12)$ Å $\quad \gamma = 90°$
Volume	2427.7(4) $Å^3$
Z	4
Density (calculated)	2.148 Mg/m^3
Absorption coefficient	3.235 mm^{-1}
$F(000)$	1488
Data collection range	$2.09 \leq \theta \leq 25.02°$
Index ranges	$-18 \leq h \leq 23, \; -7 \leq k \leq 12, \; -14 \leq l \leq 7$
Reflections collected	6768
Independent reflections	3133 [R(int) = 0.0471]
Observed reflections	2441 [$I > 2\sigma(I)$]
Absorption correction	multi-scan
Max. and min. transmission	1 and 0.60303
Refinement method	Full
Data / restraints / parameters	3133 / 1 / 296
Goodness of fit	1.029
Final R indices [$I > 2\sigma(I)$]	$R_1 = 0.0624$, $wR_2 = 0.1652$
R indices (all data)	$R_1 = 0.0798$, $wR_2 = 0.1805$
Largest diff. peak and hole	1.525 and -1.171e.$Å^{-3}$

Crystal data and structure refinement for Complex **4.3**

Formula	$C_{24}H_{17}F_2I_2N_4O_2Ru$
Formula weight	786.29
Size	0.14 x 0.13 x 0.02 mm
Crystal morphology	Green irregular
Temperature	100.01(10) K
Wavelength	0.71073 Å [Mo-K_α]
Crystal system	Orthorhombic
Space group	$Pna2_1$
Unit cell dimensions	$a = 19.483(2)$ Å $\alpha = 90°$
	$b = 10.2433(9)$ Å $\beta = 90°$
	$c = 12.4461(11)$ Å $\gamma = 90°$
Volume	2483.9(4) Å^3
Z	4
Density (calculated)	2.103 Mg/m^3
Absorption coefficient	3.162 mm^{-1}
F(000)	1492
Data collection range	$2.09 \leq \theta \leq 30.77°$
Index ranges	$-27 \leq h \leq 27,\ -14 \leq k \leq 14,\ -16 \leq l \leq 17$
Reflections collected	27470
Independent reflections	7404 [R(int) = 0.0474]
Observed reflections	6135 [$I > 2\sigma(I)$]
Absorption correction	multi-scan
Max. and min. transmission	1 and 0.60303
Refinement method	Full
Data / restraints / parameters	7404 / 1 / 311
Goodness of fit	1.066
Final R indices [$I > 2\sigma(I)$]	$R_1 = 0.0519, wR_2 = 0.141$
R indices (all data)	$R_1 = 0.0673, wR_2 = 0.1523$
Largest diff. peak and hole	2.485 and -2.642e.Å^{-3}

Crystal data and structure refinement for Complex **4.12**

Formula	$C_{27}H_{24}Br_2I_2N_5O_3Ru$
Formula weight	981.2
Size	0.19 x 0.18 x 0.12 mm
Crystal morphology	Black prism
Temperature	120(2) K
Wavelength	0.71073 Å [Mo-K_α]
Crystal system	Monoclinic
Space group	*Cc*
Unit cell dimensions	$a = 15.7434(14)$ Å $\alpha = 90°$
	$b = 9.3052(9)$ Å $\beta = 95.791(4)°$
	$c = 21.721(2)$ Å $\gamma = 90°$
Volume	3165.7(5) Å^3
Z	4
Density (calculated)	2.059 Mg/m^3
Absorption coefficient	5.006 mm^{-1}
F(000)	1860
Data collection range	$1.88 \leq \theta \leq 25.03°$
Index ranges	$-18 \leq h \leq 18,\ -10 \leq k \leq 11,\ -25 \leq l \leq 25$
Reflections collected	26603
Independent reflections	5403 [R(int) = 0.0202]
Observed reflections	5351 [$I > 2\sigma(I)$]
Absorption correction	multi-scan
Max. and min. transmission	0.7461 and 0.5098
Refinement method	Full
Data / restraints / parameters	5403 / 8 / 363
Goodness of fit	1.123
Final *R* indices [$I > 2\sigma(I)$]	$R_1 = 0.0174$, $wR_2 = 0.0475$
R indices (all data)	$R_1 = 0.0177$, $wR_2 = 0.0476$
Largest diff. peak and hole	0.809 and -0.589e.Å^{-3}

Crystal data and structure refinement for Complex **4.13**

Formula	$C_{27}H_{24}Br_2I_2N_5O_3Ru$
Formula weight	981.2
Size	0.08 x 0.02 x 0.02 mm
Crystal morphology	Black plank
Temperature	100.01(10) K
Wavelength	0.71073 Å [Mo-K_α]
Crystal system	Monoclinic
Space group	$P2_1/n$
Unit cell dimensions	$a = 11.5135(11)$ Å $\quad \alpha = 90°$
	$b = 18.5582(18)$ Å $\quad \beta = 99.770(4)°$
	$c = 14.3455(12)$ Å $\quad \gamma = 90°$
Volume	3020.7(5) Å^3
Z	4
Density (calculated)	2.158 Mg/m^3
Absorption coefficient	5.247 mm^{-1}
$F(000)$	1860
Data collection range	$2.1 \leq \theta \leq 26.36°$
Index ranges	$-14 \leq h \leq 13, \ -22 \leq k \leq 23, \ -10 \leq l \leq 17$
Reflections collected	20606
Independent reflections	6131 [R(int) = 0.1072]
Observed reflections	3401 [$I > 2\sigma(I)$]
Absorption correction	multi-scan
Max. and min. transmission	1 and 0.60303
Refinement method	Full
Data / restraints / parameters	6131 / 30 / 363
Goodness of fit	0.96
Final R indices [$I > 2\sigma(I)$]	$R_1 = 0.0554, \ wR_2 = 0.0906$
R indices (all data)	$R_1 = 0.133, \ wR_2 = 0.1118$
Largest diff. peak and hole	1.196 and -1.074e.Å^{-3}

Crystal data and structure refinement for Complex **5.1**

Formula	$C_{24}H_{17}F_2Cl_2N_4O_2Rh$
Formula weight	605.2
Size	0.48 x 0.20 x 0.13 mm
Crystal morphology	Orange block
Temperature	100.01(4) K
Wavelength	0.71073 Å [Mo-K_α]
Crystal system	Orthorhombic
Space group	$P2_12_12_1$
Unit cell dimensions	$a = 10.5456(3)$ Å $\quad \alpha = 90°$
	$b = 12.0060(4)$ Å $\quad \beta = 90°$
	$c = 19.5775(7)$ Å $\quad \gamma = 90°$
Volume	2478.72(14) Å^3
Z	4
Density (calculated)	1.622 Mg/m^3
Absorption coefficient	0.949 mm^{-1}
$F(000)$	1208
Data collection range	$6.62 \leq \theta \leq 59.08°$
Index ranges	$-14 \leq h \leq 10, \ -15 \leq k \leq 15, \ -19 \leq l \leq 27$
Reflections collected	9366
Independent reflections	5515 [R(int) = 0.0438]
Observed reflections	4829 [$I > 2\sigma(I)$]
Absorption correction	multi-scan
Max. and min. transmission	1 and 0.86114
Refinement method	Full
Data / restraints / parameters	5515 / 0 / 336
Goodness of fit	1.047
Final R indices $[I > 2\sigma(I)]$	$R_1 = 0.0524, wR_2 = 0.1084$
R indices (all data)	$R_1 = 0.0636, wR_2 = 0.1159$
Largest diff. peak and hole	1.24 and -0.73e.Å^{-3}

Crystal data and structure refinement for Complex **5.3**

Formula	$C_{24}H_{17}Cl_2Br_2N_4O_2Rh$
Formula weight	727.05
Size	0.06 x 0.054 x 0.017 mm
Crystal morphology	Red Plate
Temperature	100.01(10) K
Wavelength	0.71073 Å [Mo-K_α]
Crystal system	Monoclinic
Space group	*Cc*
Unit cell dimensions	$a = 9.3722(6)$ Å $\alpha = 90°$
	$b = 23.9103(17)$ Å $\beta = 100.609(7)°$
	$c = 11.5081(7)$ Å $\gamma = 90°$
Volume	2534.8(3) Å^3
Z	4
Density (calculated)	1.905 Mg/m^3
Absorption coefficient	4.068 mm^{-1}
F(000)	1416
Data collection range	$6.76 \leq \theta \leq 62°$
Index ranges	$-13 \leq h \leq 11$, $-33 \leq k \leq 21$, $-15 \leq l \leq 19$
Reflections collected	5735
Independent reflections	4369 [*R*(int) = 0.0419]
Observed reflections	4012 [$I > 2\sigma(I)$]
Absorption correction	multi-scan
Max. and min. transmission	1 and 0.91409
Refinement method	Full
Data / restraints / parameters	4369 / 2 / 316
Goodness of fit	1.011
Final *R* indices [$I > 2\sigma(I)$]	$R_1 = 0.0378$, $wR_2 = 0.0811$
R indices (all data)	$R_1 = 0.0434$, $wR_2 = 0.0841$
Largest diff. peak and hole	0.92 and -0.84e.Å^{-3}

Crystal data and structure refinement for Complex **5.4**

Formula	$C_{26}H_{25}Cl_2I_2N_4O_4Rh$
Formula weight	885.11
Size	0.41 x 0.37 x 0.32 mm
Crystal morphology	Red Plate
Temperature	100.2(4) K
Wavelength	0.71073 Å [Mo-K_α]
Crystal system	Monoclinic
Space group	$P2_1/c$
Unit cell dimensions	$a = 17.9801(8)$ Å $\alpha = 90°$
	$b = 10.3200(4)$ Å $\beta = 115.036(6)°$
	$c = 17.7408(9)$ Å $\gamma = 90°$
Volume	2982.6(2) Å^3
Z	5
Density (calculated)	2.464 Mg/m^3
Absorption coefficient	3.576 mm^{-1}
$F(000)$	2130
Data collection range	$6.38 \leq \theta \leq 59.06°$
Index ranges	$-24 \leq h \leq 20$, $-13 \leq k \leq 14$, $-24 \leq l \leq 24$
Reflections collected	19498
Independent reflections	7240 [R(int) = 0.0499]
Observed reflections	5836 [$I > 2\sigma(I)$]
Absorption correction	multi-scan
Max. and min. transmission	1 and 0.74238
Refinement method	Full
Data / restraints / parameters	7240 / 0 / 356
Goodness of fit	1.081
Final R indices [$I > 2\sigma(I)$]	$R_1 = 0.0499$, $wR_2 = 0.0963$
R indices (all data)	$R_1 = 0.0667$, $wR_2 = 0.1047$
Largest diff. peak and hole	2.73 and -1.95e.Å^{-3}

Crystal data and structure refinement for Complex **5.5**

Formula	$C_{27}H_{23}Cl_2I_2N_5O_3Rh$
Formula weight	893.11
Size	0.12 x 0.11 x 0.03 mm
Crystal morphology	Red Plate
Temperature	100.0(3) K
Wavelength	0.71073 Å [Mo-K_α]
Crystal system	Monoclinic
Space group	*Cc*
Unit cell dimensions	$a = 15.4740(11)$ Å $\quad \alpha = 90°$
	$b = 9.1361(6)$ Å $\quad \beta = 95.700(6)°$
	$c = 21.4115(13)$ Å $\quad \gamma = 90°$
Volume	3012.0(3) Å^3
Z	4
Density (calculated)	1.970 Mg/m^3
Absorption coefficient	2.832 mm^{-1}
F(000)	1716
Data collection range	$6.22 \leq \theta \leq 52.74°$
Index ranges	$-16 \leq h \leq 19,\ -11 \leq k \leq 9,\ -26 \leq l \leq 21$
Reflections collected	9196
Independent reflections	4805 [*R*(int) = 0.0675]
Observed reflections	3986 [$I > 2\sigma(I)$]
Absorption correction	multi-scan
Max. and min. transmission	0.9973 and 0.7721
Refinement method	Full
Data / restraints / parameters	4805 / 2 / 361
Goodness of fit	1.046
Final *R* indices [$I > 2\sigma(I)$]	$R_1 = 0.0524, wR_2 = 0.1030$
R indices (all data)	$R_1 = 0.0689, wR_2 = 0.1149$
Largest diff. peak and hole	1.22 and -0.82e.Å^{-3}